POLITECNICO DI TORINO

PhD Degree in Mechanics

Advanced methods for rock discontinuities estimation in tunneling

Andrea Bellino

Supervisors:

prof. Luigi Garibaldi

prof. Alberto Godio

Cycle XXV

Acknowledgements

First of all, I want to thank my supervisors, Prof. Luigi Garibaldi and Prof. Alberto Godio, for the support during the three-years work. In particular, prof. Garibaldi was more concentrated in the work organization, while prof. Godio was fundamental during the numerical simulations and for the tuning of the methods proposed in this thesis.
Then, true thanks to the company Gd Test S.r.l. which gave me the possibility to obtain the doctorate by proposing this project to the Politecnico di Torino. In particular, I appreciated the management work done by Eng. Alberto Morino, the practical coordination of Dr. Andrea Geuna and the constant support of Eng. Alessandro Viglietti during the experimental tests in the Brennero tunnel. Moreover, the help provided by Eng. Marco Cauduro has been very useful for the data interpretation.

Abstract

The thesis is the summary of the three-years work done at the Department of Mechanics at the Politecnico di Torino, from January 2010 to December 2012, under the supervision of professor Luigi Garibaldi (Dipartimento di Ingegneria Meccanica e Aerospaziale) and professor Alberto Godio (Dipartimento di Ingegneria Ambientale, del Territorio e delle Infrastrutture).

The subject of the thesis has been chosen in collaboration with *Gd Test S.r.l.*, a company operating in the field of environmental engineering, based in Torino, relatively close to the Politecnico. During the three years, the company cooperated with me and the professors, in particular by giving an important help for the experimental tests.

The topic is the prediction of lithological discontinuities ahead of a tunnel face, in a tunnel under construction, i.e. the identification of whatever type of zone producing a reflection of the seismic waves generated in a source point. Typical excitations are the blasting, the hammer or magneto-strictive sources. Moreover, the procedures can be improved to be applied in presence of the Tunnel Boring Machine, by exploiting the noise produced by its cutter head.

The main objective of the work is duplex: to reduce the risk for people and machinery and to reduce the excavation cost by setting the excavation based on the rock configuration that has been predicted.

The theme is a modification of the classical reflection seismology techniques, in order to be applied in tunnels. Indeed, the particular configuration of sources and receivers in a tunnel obliges to develop *ad hoc* methods for the analysis of the seismic data.

The thesis proposes two methods for the identification of the discontinuities ahead of a tunnel face: the first comes directly from the concept of ellipsoids, fundamental in the reflection seismology, and the second is a backward method, able to provide an automatic prediction without extracting the time arrivals corresponding to the reflected waves. To run, this procedure needs only the coordinates of sources and receivers, together with the acquisition data parameters, and then it allows: i) to estimate an average value of the wave velocity; ii) to detect the discontinuities for each source; iii) to analyze and plot the number of superposing estimations for each node of the selected space domain.

The final result can be interpreted as the probability to detect a discontinuity at a certain distance from the tunnel face.

The thesis first describes the fundamental relationships in tunneling seismology, then it proposes a direct technique for the reflectors detection. Since it is demonstrated to be not too reliable in presence of low signal-to-noise ratio, the automatic method is presented.

This procedure has been tested on synthetic and real data coming from the new Brennero tunnel under construction, which will be one of the longest tunnel in the world. The results indicate that the method runs very fast and it is reliable in the identification of lithological changes and discontinuities, up to more than one hundred meters ahead the tunnel face. Moreover, it can be used in every kind of tunnels, without any detailed knowledge of the soil and rocks around the tunnel, and with different excitations.

The thesis deals also with another important issue during the tunnel construction: the monitoring of the rockburst phenomenon, a small seismic event caused by the rock alteration during the excavation. For this purpose, a specific procedure has been created, able to estimate the position of the source point.

Contents

Acknowledgements ..... **i**
Abstract ..... **iii**
Contents ..... **v**

Chapter 1: Introduction **1**
1.1. Motivation 1
1.2. Objectives of the thesis 2
1.3. State of the art 3
1.4. Work organization 5

Chapter 2: Geophysics and seismic monitoring in tunnelling **7**
2.1. Seismic waves 7
2.1.1. Body waves 7
2.1.2. Wave equation 9
2.1.3. Surface waves 11
2.2. Reflection coefficient 11
2.3. Classical reflection seismology 14
2.3.1. The reflected times 14
2.3.2. Data acquisition 16
2.3.3. Data elaboration 16
2.3.4. Differences respect to classical seismic reflection 18
2.4. The monitoring in tunnels 19
2.4.1. Methods of excavation in tunnels 21
2.4.2. Seismic methods in tunneling 24
2.4.3. TRT 24
2.4.4. TRUST 26
2.4.5. TSWD 28
2.4.6. The Potsdam approach 29
2.4.7. Monitoring of the rockburst 29

Chapter 3: Modelling of reflections 33
3.1. General idea 33
3.2. Geometric idea 34
3.2.1. 2D representation 34
3.2.2. Relationships among the parameters in the 2D case 35
3.2.3. 3D representation 38
3.2.4. Characterization of the discontinuity 39
3.3. Construction of the ellipsoids 40
3.3.1. Sensors aligned with the source 42
3.3.2. Sensors not aligned with the source 43
3.3.3. How to do in a real investigation? 45
3.4. Characterization of the discontinuity 46
3.4.1. Tangent plane 47
3.4.2. Generic discontinuity 48
3.4.3. Source and receiver position 49
3.5. Relationships among the receivers and reflection point 51
3.5.1. Receiver position once given the reflection point 53
3.5.2. Reflection point once given the receiver position 54
3.6. A case study: frontal discontinuity 55
3.6.1. Reflection angle 55
3.6.2. Investigation on the reflection point 56
3.6.3. Time arrivals 58

Chapter 4: The ellipsoid method for the estimation of discontinuities 63
4.1. The meaning 63
4.2. The ellipsoid method 64
4.2.1. Construction of the ellipsoids 64
4.2.2. Search of the reflection point 65
4.2.3. Calculation of the tangent plane 67
4.2.4. Estimation of the discontinuity 68
4.3. Numerical simulations in Matlab® 70
4.4. A numerical simulation in Reflex 72
4.4.1. Physical description 73
4.4.2. Identification of the wave phenomena 74
4.4.3. Estimation of the velocity 75
4.4.4. Reflected waves 76
4.4.5. Discontinuity estimation 77

4.5. Simulations in 3D 80
4.6. Multiple ellipsoid method 82
4.7. Limitations of the forward methods 84

Chapter 5: The backward method 85
5.1. The concept 85
5.2. Pre-processing 88
5.3. Velocity estimation 90
5.3.1. Spectral analysis 91
5.3.2. The method of successive eliminations 91
5.3.3. Estimation of velocity and delay time 93
5.3.4. The admissible times 93
5.3.5. Summary of the first part 94
5.4. Single estimation of the discontinuities 95
5.4.1. Choice of the domain 95
5.4.2. Calculation of the reflection points 96
5.4.3. Summary of the second part 98
5.5. Common discontinuity estimation 98
5.5.1. Change of coordinates 98
5.5.2. Visualization of common points 99
5.5.3. Summary of the third part 101
5.6. Interpretation and final visualization 101

Chapter 6: Numerical simulations 103
6.1. A tutorial example 103
6.1.1. The configuration 103
6.1.2. Velocity estimation 105
6.1.3. Single estimates of the discontinuities 106
6.1.4. Final representation 109
6.1.5. Observations 110
6.1.6. Interpretation of the results 111
6.2. Simulation in Comsol Multiphysics® 112
6.2.1. The configuration 113
6.2.2. The signals and the velocity estimation 116
6.2.3. The estimation of discontinuities 116

Chapter 7: Experimental tests in the Brenner Base Tunnel 119
7.1. The Brenner Base Tunnel 119
7.1.1. The project 119
7.1.2. The Mules site 120
7.2. The experimental survey 122
7.2.1. TRT scheme 122
7.2.2. The TRUST scheme 124
7.2.3. Evaluation of the results 126
7.3. First test 127
7.3.1. Signals and spectra 127
7.3.2. Estimation of the discontinuities 129
7.3.3. Final interpretation and evaluation of the results 132
7.4. Second test 134
7.5. Third test 136
7.6. Identification of the Periadriatic seam 141
7.6.1. Planning of the survey 141
7.6.2. Results about the Periadriatic seam 142
7.7. Final observations 145
7.7.1. Computational time 145
7.7.2. Differences between TRT and TRUST approach 145

Chapter 8: Rockburst monitoring 147
8.1. Estimation of the rockburst source 147
8.1.1. The idea 147
8.1.2. The problem 148
8.1.3. 4CM method 149
8.1.4. 3CM method 151
8.1.5. 3CMM method 152
8.1.6. Iterative method 153
8.2. Condition number and optimal sensor configuration 154
8.2.1. Estimation of the x-coordinate 155
8.2.2. Estimation of the other coordinates 156
8.2.3. Minimization of the condition number 159
8.2.4. Optimal configuration of sensors 161
8.3. Procedure of analysis 161
8.3.1. Sensor placement 161
8.3.2. Estimation of the source location 163

8.3.3. Estimation of the intensity 164
8.3.4. Frequency of the event 166
8.3.5. Scheme of the analysis 166
8.4. Numerical example 166
8.4.1. First simulation 166
8.4.2. Second simulation 170
8.4.3. Reliability of the estimation 172
8.5. Test in the Brennero tunnel 173
8.5.1. The acquisition 173
8.5.2. The data analysis 174

Chapter 9: Conclusions and future works 177
9.1. Final comments 177
9.2. Improvements of the automatic method 178
9.2.1. Reflection not in a single node 178
9.2.2. Velocity in the domain 179
9.2.3. Application in the case of excavation with TBM 179
9.2.4. Characterization of the discontinuities 180
9.3. Backward method for the rockburst 181

Appendix A: The ellipsoid 183
Appendix B: The condition number 185

References 187

Vita 193

Chapter 1

Introduction

1.1. Motivation

In the last years, many tunnels have been constructed all around the world, and in particular long tunnels are one of the most important issues in the field of the civil engineering, because of their advantage of connecting two or more cities that are geographically separated by seas or mountains. In particular, in Europe, a big increment of the main railway and highway connections is expected and this needs the crossing of the principal mountains (Alps, Pyrenees, Apennines, ecc…).

Considering the submarine tunnels, the principal examples are the Channel Tunnel, connecting France and England, 50 km long, and the Seikan Tunnel, in Japan, 53.8 km long.

On the contrary, the most significant tunnel excavated within the mountains is the Gotthard Base Tunnel, in Switzerland, expected to open in 2016 with a length of 57 km. Other long tunnels under construction are the Torino–Lyon high-speed railway (57 km), between Italy and France, and the Brennero Basis Tunnel (55 km), connecting Italy with Austria. The latter is the subject of the experimental applications presented in the thesis.

All the cited tunnels are built for railways; if considering only car tunnels, the most important ones are the Lærdal Tunnel, in Norway, 24.5 km long and the Zhongnanshan Tunnel, in China, 18 km long.

The construction of long tunnels usually requires many years, and then a constant monitoring of the site is necessary, to predict the geological risks during tunnel excavation. This is not useful only for technical aspects, as for example for choosing the appropriate excavation technique, but also for the safety purposes, especially of the workers, which spend lot of time inside the tunnel, and of the machinery.

This facts lead to monitor the stability of the built part, the variation of the rock stress near the tunnel, the small seismic events caused by the altered rock configuration (rockburst) and the discontinuities ahead of the tunnel face. In particular, the thesis is concentrated on the last topic, with an entire chapter dedicated also to the rockburst monitoring.

1.2. Objectives of the thesis

Within the geophysical techniques, the seismic methods are one of the most important categories because of their high penetration depth and good resolution in estimating the discontinuities present in the soil.

Seismic methods can be divided in two categories: invasive tests and non-invasive tests. The first ones are characterized by the presence of boreholes, while the second ones are conducted from the free surface. Within the non-invasive tests, the seismic reflection methods are the only techniques that can be used profitably in a tunnel investigation.

However, since the configuration of sources and receivers cannot be placed analogously to the classical seismic reflection surveys, *ad hoc* methods must be created. Indeed, the particular geometry obliges to place the sensors and the source points on the tunnel walls or in the tunnel face.

Despite these problems, some methodologies have been developed during the last years, trying to the give an indication of the discontinuities ahead of the tunnel face. A discontinuity is a change of impedance, i.e. a change of the product of the velocity and the density.

Almost all the methods proposed do not come exclusively from academic studies: they are developed entirely or in collaboration with important companies in the field of seismic monitoring. This is indicative of two facts:

- the application of the seismic reflection in tunneling is not straightforward and needs capacity both on the theoretical and on the experimental point of view
- there is not a methodology which has been demonstrated to be much better than the others.

The first point indicates that both theoretical study and practical skills are useful to find an optimal configuration, for example about the sensor placement, the coupling rock-receivers, the choice and the location of the excitations and the data interpretation.

The second point highlights that there are many different methods existing in the literature but there is not a reference one, therefore this is actually an interesting challenge for the thesis.

The objective is then to propose a new method for the interpretation of seismic data coming from a tunnel survey. In particular, the real target is to create an algorithm able

to analyze the data in a completely automatic way, without any human intervention for the selection of the peaks due to the reflection events. The algorithm should work for different sources-sensors configurations and for different types of excitations.

1.3. State of the art

In the last decades, different methods have been proposed for the estimation of geological faults during a tunnel construction (e.g Sattel et *al.*, 1992; Kneib et *al.*, 2000; Kneib *et al.* 2004)

Chang and Yu (2005) discussed several methods for geological explorations in tunnel when using a TBM. Some examples of non-seismic methods, of are:

- Probe Hole: some hole probes are realized beside the TBM, in order to acquire some information about the ground. Sometimes, this method can interfere with the TBM and moreover it not so representative of the ground because only a small section is analyzed.
- Pilot drilling: a pilot hole is drilled in a certain zone of the excavation front. It is able to advance for 30 meters in two hours. Analogously to the Probe Hole technique, this technique allows to have only some punctual information about the rock typology.
- Long distance horizontal drilling (LDHD): there is a direct rock inspection of the rock cores, but it is very expensive and it needs a long stopping of the TBM activity.
- GPR (Ground Penetrating Radar): a Radar, mounted on the rotating head, which allows identifying the obstacles in front of the TBM for 2-3 meters.
- Horizontal sonic logs: they are placed in small diameters boreholes, drilled ahead the tunnel front, are a good compromise between the need to reduce the time of no activity and reliability in detection faults and discontinuities (Godio and Dall'Ara, 2012).

Most of the methods present in literature are however based on seismic investigations of the rock ahead of the tunnel face; substantial differences among the methods consist to perform the geophysical survey in tunneling with TBM or with conventional work using explosives.

Differently from the survey in open field, the prediction of lithological changes or rock discontinuities in a tunnel is a critical problem, mainly because the sensors and the sources cannot have a large spatial coverage. Therefore, *ad hoc* techniques must be developed.

The major part of the methods are based on the concept of ellipsoids (Ashida and Koichi, 1993; Ashida *et al.*,2001), built starting from a source-receiver pair, which

forms the two foci of the quadric surface. This is fundamental for the identification of reflectors, which are defined as the tangent planes to all the ellipsoids.

Some methods are based on the tomography approach to characterize the rock volume around the tunnel using seismic attributes, like the wave velocity or the reflectivity (Tzavaras *et al.*, 2012; Yamamoto *et al.*, 2006). Basically, in the travel-time tomography a velocity model is assumed, then all the possible ray-paths between the sources and the receivers are calculated, after having discretized the space domain in pixels or voxels according to the expected resolution. The inversion problem is usually solved by iterative algorithm, where the whole space domain is evaluated, trying to minimize an objective function of the synthetic and experimental travel-times. The maximum reliable imaging distance is dependent on the attenuation of the rocks encountered (hard rock corresponds to low attenuation).

One of the most famous techniques is the TSP (Tunnel Seismic Prediction), proposed by the Amber Measuring Technique society. It is a direct consequence of Vertical Seismic Profiling, and it is based on the recording of seismic waves produced by charges of explosive. The data processing method is an advanced migration imaging technique making full use of both kinetic and dynamic characteristics of seismic waves, that is, both travel time and amplitude (Baldi *et al*., 2006; Klose, 2002).

More recently, Tzavaras *et al.* (2008, 2012) processed the data acquired in the Gotthard base tunnel by using the 3D versions of the KPSDM (Kirchhoff Pre-Stack Depth Migration), the FVM (Fresnel Volume Migration) and the RIS (Reflection Image Spectroscopy).

The SIST is a method proposed by Cosma C. and Enescu N. (2001), which is a viable solution for high-resolution surveys in hard rocks. The method is a combination of the Vibroesis swept frequency and the Mini-Sosie multi impact ideas. The SIST technique is based on a low-power impact source, which is simple and easy to transport. There are considerable benefits in increasing the impact frequency as much as possible.

The Tunnel Seismic Tomography (TST) is a tunnel seismic prediction technology developed by the Chinese Academy of Sciences (Yonggui *et al.*, 2006). Data processing integrates seismic migration imaging, velocity scanning structural grain analysis and travel time inversion imaging. The seismic migration imaging obtains the positions of the reflection planes in front of the tunnel face, the reflection strength and the velocity distribution.

Another approach is the Three-dimensional Reflection Tracing (TRT), which uses advanced algorithms for rapidly imaging subsurface cavities and structures that exhibit significant changes in velocity or attenuation, based on the reflected waves. The

excitation is produced by sledgehammer strokes or by a magneto-strictive source driven by a swept frequency signal (Yamamoto *et al.*, 2006; Yamamoto *et al.*, 2008).
Contrarily to TRT, the True Reflection Underground Seismic Technique (TRUST) uses detonations from small boreholes in the tunnel face or side wall (Benecke *et al.*, 2008). The sensors are placed in "listening boreholes" drilled into the rock at about every 50 meters.
In addition to the methods just presented, other methods are specific when TBM is used as seismic source. Swinnen *et al.* (2007) propose a technique for the seismic imaging from a TBM by using a method based on short focusing operators optimized in a least-square sense.
The SSP (Sonic Soft-ground Probing) is based on a Vibroesis (trademark name) source at high frequency and on a series of accelerometers placed on the head of the TBM (Kneib et al., 2000). The source is a seismic vibrator propagating energy signals over an extended period of time as opposed to the near instantaneous energy provided by impulsive sources. The data recorded must be correlated to convert the extended source signal into an impulse. The source signal using this method was originally generated by a servo-controlled hydraulic vibrator or shaker unit mounted on a mobile base unit, but electro-mechanical versions have also been developed.
The TSWD (Tunnel Seismic While Drilling) makes use of the vibrations produced by the cutting head of the TBM as seismic source (Petronio and Poletto, 2002; Poletto et al., 2007; Bruckl et al., 2008). The process includes the noise separation in remote seismic data and the cross-correlation between the pilot signal and the data acquired by sensors, in order to have interpretable seismic data. The main advantages respect to the previous methods are the acquisition of real-time information about the rock characteristics ahead of the TBM, without excavation interruption.

1.4. Work organization

The thesis starts with an overview of the seismic waves, focusing on fundamental concepts as the reflection coefficient and on the differences between the classical seismic reflection surveys and the tunnel investigations; successively, the most important methods for the prediction of discontinuities in tunneling, just cited in the previous subsection, are described.
In the third chapter, the geometrical representation of the problem under study is analyzed, together with the principal relationships among the parameters, with a particular attention to the concept of ellipsoids.
Then, the ellipsoid method, descending directly from the extracted relationships, is presented together with some numerical examples.

The real core of the thesis is concentrated on the fifth chapter, where the automatic backward method for the estimation of rock discontinuities is described. The approach is a fully automatic method based on an automatic picking of all the possible reflection events recorded in an array of sensors when several sources are used. The space domain in front of the tunnel is subdivided in pixels and the main clusters back-projected in the space domain reflect the zone of higher probability to detect a change of impedance, which can be related to rock failures or lithological changes. The velocity model is based on a simple regression analysis of the wave velocity of the travel-times of the direct wave.

In order to check the method efficiency, in the sixth chapter the results on 2D synthetic models are discussed, generated using commercial programs.

Successively, some seismic investigations conducted in the Brennero tunnel under construction are analyzed to point out the performances of the methodology, in different configurations and with different excitations.

The last chapter is dedicated to the conclusions and the proposals for further improvements of the method.

Chapter 2

Geophysics and seismic monitoring in tunnelling

In every tunnel under construction, it is important to keep different parameters under monitoring, to ensure safety for the working people and for the machinery. One of these topics is related to the seismic surveys, which are discussed in this chapter, starting from the principles of geophysics and then showing the differences between the classical seismic reflection analyses and those in tunnels. At the end, the main methods used for the characterization of the rocks ahead of a tunnel face are presented.

2.1. Seismic waves

The geophysics is the general field of study involved in this work. Its name comes from the ancient Greek and means “physics of the Earth”, referring to the fact that it includes all the physical methods for the study of the Earth.
Within the geophysics, our attention is focused on the seismology, and consequently the study of the propagation of the seismic waves in the ground. More precisely, there are two types of waves travelling in the ground:

- Body waves
- Surface waves

2.1.1. Body waves

Within the body waves, the P-waves and the S-waves are distinguished. The P-waves name stands for Primary waves, since they are the quickest wave travelling in the ground. They are also called pressure waves because they are formed from alternating compressions and rarefactions.

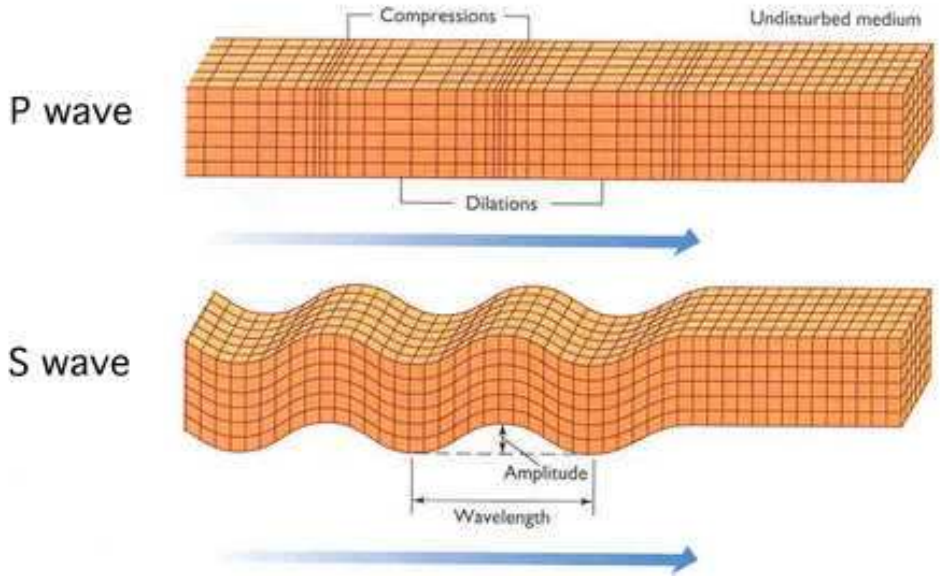

Figure 2.1. Particle motion associated to the body waves propagation (Font: earth.northwestern.edu)

The mode of propagation of a P-wave is always longitudinal: the particles in the solid have vibrations along the travel direction of the wave energy.

The name of S-waves, on the contrary, are called Secondary waves, coming from the fact that they are slower than the P-waves. They are also called shear waves because their motion is perpendicular to the direction of wave propagation.

The propagation of the body waves is depicted in Figure 2.1.

The velocities of Primary and Secondary waves are defined by

$$v_P = \sqrt{\frac{\lambda + 2\mu}{\rho}} \tag{2.1}$$

$$v_S = \sqrt{\frac{\mu}{\rho}} \tag{2.2}$$

where ρ is the density of the material in which the wave propagates, while λ and μ are the Lamé parameters in the stress-strain relationship for an isotropic solid in Einstein notation:

$$\tau_{ij} = \lambda \delta_{ij} e_{kk} + 2\mu e_{ij} \tag{2.3}$$

where τ is the stress, δ_{ij} is the Kronecker Delta and e is the strain tensor.

Eq. (2.1) can be also re-written as:

$$v_P = \sqrt{\frac{K + \frac{4}{3}\mu}{\rho}} \tag{2.4}$$

in order to evidence K, which is called bulk modulus or modulus of incompressibility. The constant μ is also called shear modulus or modulus of rigidity.

The ratio γ between the velocities of P- and S-waves depends only on the Poisson ration $\nu = \frac{\lambda}{2(\lambda + \mu)}$:

$$\gamma = \frac{v_P}{v_S} = \sqrt{\frac{\lambda + 2\mu}{\mu}} = \sqrt{\frac{1 - 2\nu}{2(1 - \nu)}} \tag{2.5}$$

Since for real media $0 \le \nu \le 0.5$, then $v_P > v_S$. This is also evident from Eq. (2.1) and (2.2).

2.1.2. Wave equation

Let's now consider the equation for the one-dimensional case along the direction x, for the shear wave. The equation of motion is given by:

$$\frac{\partial^2 u}{\partial x^2} = \frac{1}{v_S^2}\frac{\partial^2 u}{\partial t^2} \tag{2.6}$$

The solution is assumed in the following form:

$$u = f(x)e^{-i\omega t} \tag{2.7}$$

Then, by inserting Eq. (2.7) in Eq. (2.6),

$$\frac{d^2 f(x)}{\partial x^2} + \frac{\omega^2}{v_S^2} f(x) = 0 \tag{2.8}$$

This ordinary differential equation has a harmonic solution that, combined with Eq. (2.7), gives the general solution for a harmonic wave propagating in the x direction:

$$u(x,t) = Ae^{i(kx-\omega t)} \tag{2.9}$$

where A is the wave amplitude, $k = \frac{\omega}{v_S}$ is the wavenumber and the phase can be written as

$$\phi = kx - \omega t = k\left(x - v_S t\right) \tag{2.10}$$

The wavelength is defined as the distance between two successive points in space having equal phase:

$$\lambda = \frac{2\pi}{k} \tag{2.11}$$

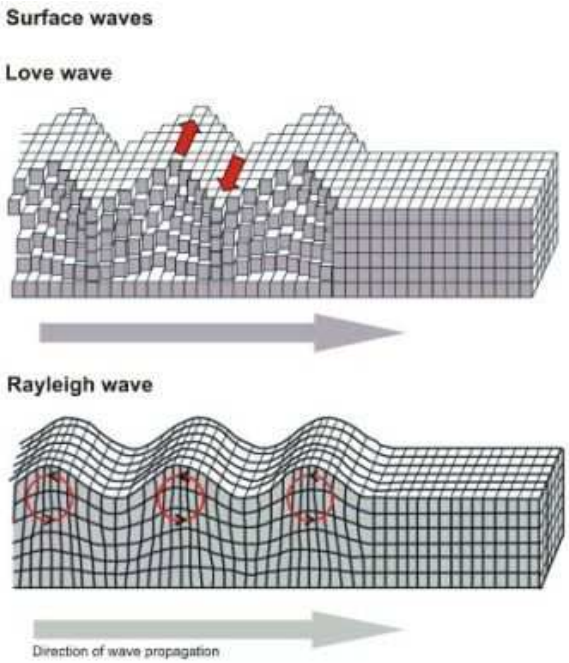

Figure 2.2. Particle motion associated to the surface waves propagation (Font: division1frankwproject.wikispaces.com)

2.1.3. Surface waves

The superficial waves travel in a very shallow zone close to the free surface of an half-space. There are two principal types:

- Love waves
- Rayleigh waves

Love waves can exist only in presence of a soft superficial layer over a stiffer half-space. Rayleigh waves are always generated in presence of a free surface in a continuous body.

The range of variation of the velocity of the Rayleigh waves v_R is given by

$$0.87 < \frac{v_R}{v_S} < 0.96 \tag{2.12}$$

Therefore, they are slightly slower than the shear waves.

2.2. Reflection coefficient

Within the seismology, one of the most important topics is the reflection seismology, i.e. the characterization of the soil by taking into account the waves reflected back by a layer which is simply called reflector. In simple terms, a wave is reflected when there is a change of impedance (product of velocity and density). Moreover, a part of the wave energy is reflected at the boundary while the remaining part is transmitted through the second material.

The amplitude of the reflected wave is obtained by multiplying the energy of the incoming wave by a the reflection coefficient R, which is defined by the impedances of the two media:

$$R = \frac{v_2\rho_2 - v_1\rho_1}{v_2\rho_2 + v_1\rho_1} \tag{2.13}$$

where v indicates the velocity, ρ the density and the subscripts are referred to the first and the second material. If R is equal to zero, then the two media have the same impedance and no reflections can appear.

The phenomenon just described is represented in Figure 2.3, showing that the reflection coefficient plays the role of amplitude modulator.

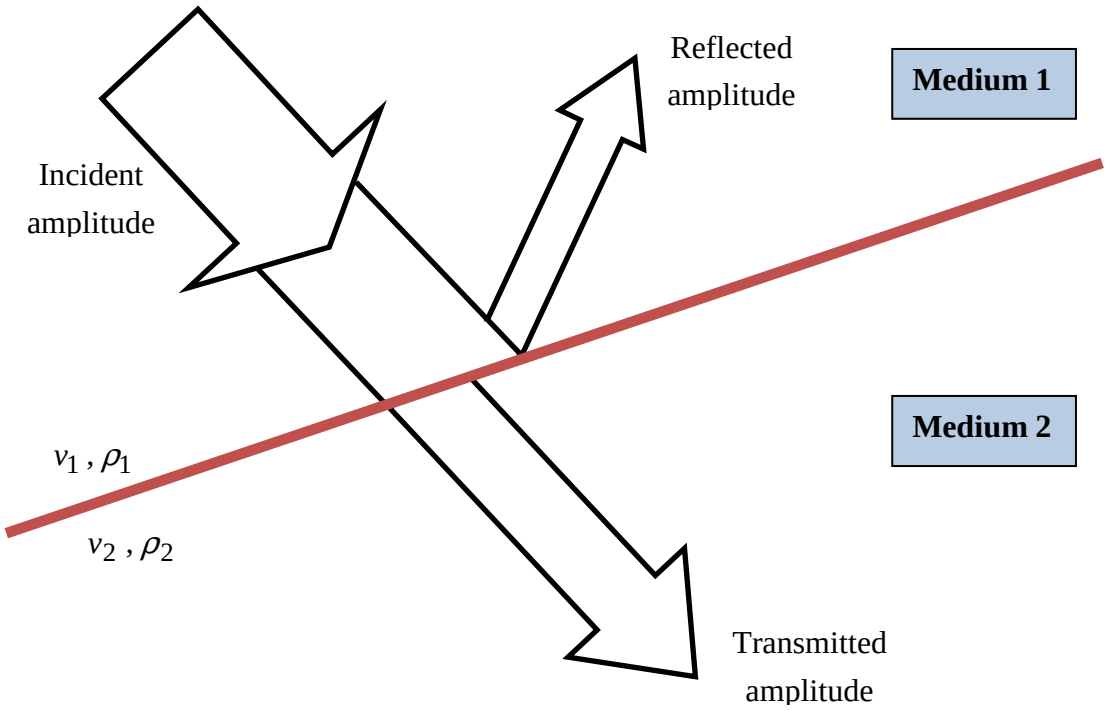

Figure 2.3. Scheme of the reflection in presence of two media with different impedances. The amplitude of the incident wave is split in the reflected amplitude and in the transmitted amplitude, according to the reflection coefficient.

Together with the considerations just expressed, there are some assumptions coming from the geometrical optics, if the reflection happens quite far from the source (far-field condition):

- the reflection angle is equal to the incident angle
- the ray of the amplitude wave and that of the incident wave are on the same plane
- the amplitude of the reflected wave is dependent on the reflection coefficient

When crossing many media, the final amplitude value of the transmitted wave is proportional to the product of all the transmission coefficients, each of them defined by:

$$T = \frac{2v_1\rho_1}{v_2\rho_2 + v_1\rho_1} \tag{2.14}$$

It is clear that the following relationship is valid:

$$T = 1 - R \tag{2.15}$$

A sequence of reflection coefficients $R(t)$ can be used to generate a seismic trace $s(t)$ through the convolution, starting from a source signal $w(t)$:

$$s(t) = R(t) * w(t) + n(t) \tag{2.16}$$

where $n(t)$ is a generic random noise.

In Figure 2.4, a simple example is represented: the source is defined by a Ricker wavelet with frequency equal to 100 Hz, and a seismic trace is obtained by convoluting the source signal with the sequence of reflection coefficients given in Figure 2.4b. No noise is added to the signals.

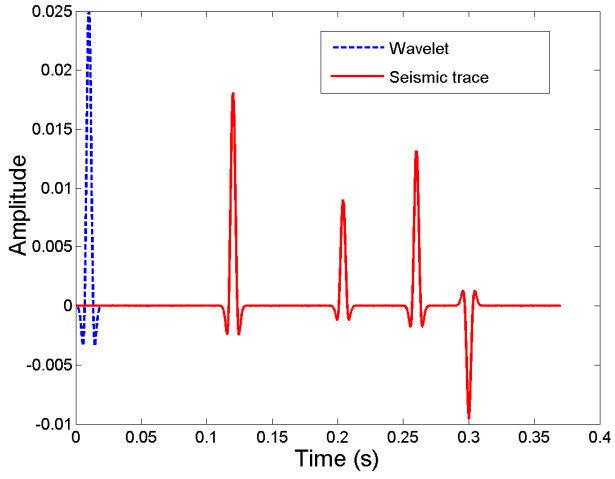

a)

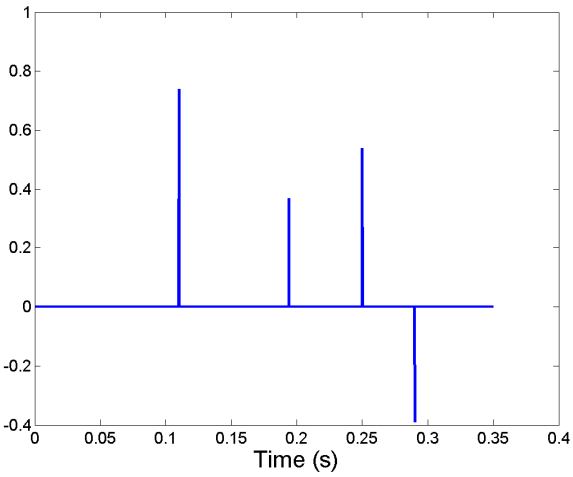

b)

Figure 2.4. Convolutive model in the time domain to obtain a seismic trace from a wavelet representing the source signal (a) by means of the reflectivity (b).

2.3. Classical reflection seismology

The term classical reflection seismology is here adopted to define the methodologies used for the soil characterization by means of sensors (usually geophones) placed on the ground surface. Larger the number of sensors, more accurate are the results.
Nowadays, this technique is not only used for the detection of discontinuities in the ground, but also to have information about the soil lithology and to investigate on the presence of hydrocarbons.

2.3.1. The reflected times

The typical configuration on a single sensor line is proposed in Figure 2.5. A seismic wave is generated in the source point S, and it can be either reflected back to a receiver A or transmitted until to the third medium, where a new boundary is found and a new reflection is produced (recorded by B).
For simplicity, let's analyze the first reflection with the discontinuity parallel to the ground surface. The total time t_r from S to A is equal to:

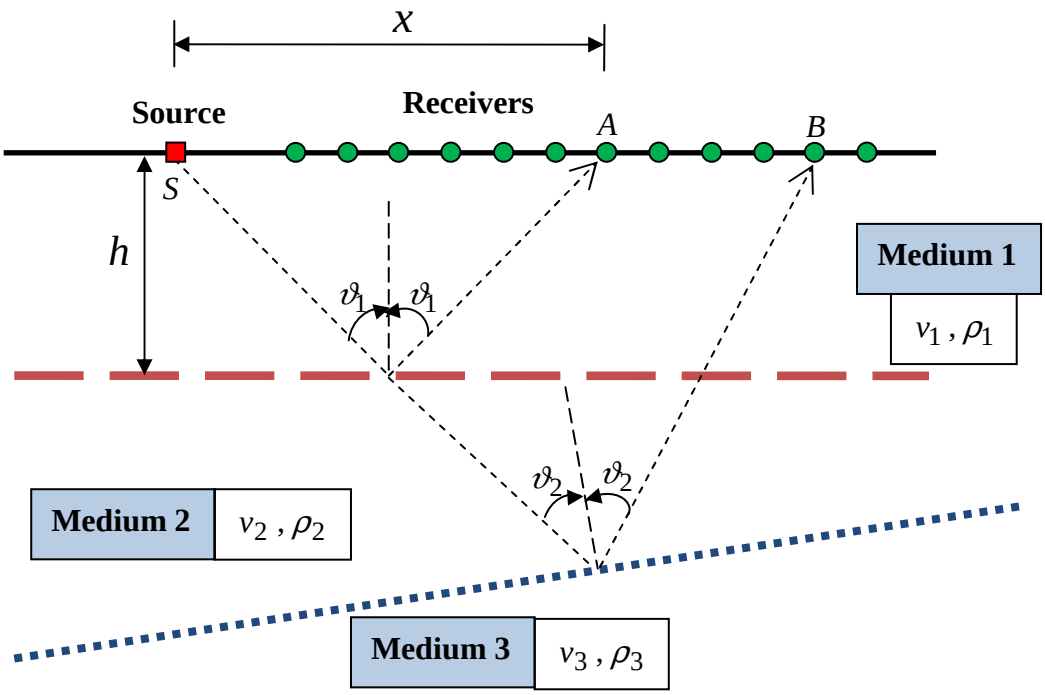

Figure 2.5. Configuration of a reflection seismology for the soil characterization, together with the most important parameters involved in the relationships.

$$t_r = \frac{2 \cdot \sqrt{(x/2)^2 + h^2}}{v_1} \tag{2.17}$$

where x is the distance source-receiver, h is the layer thickness and v_1 is the velocity of the direct wave of the first medium.
If manipulating the equation, then it is possible to obtain an hyperbole:

$$t_r^2 - \frac{x^2}{v_1^2} = \frac{4h^2}{v_1^2} \tag{2.18}$$

At the same time, the time t_d due to the direct wave from S to A is simply given by

$$t_d = \frac{x}{v_1} \tag{2.19}$$

In Figure 2.6 the hyperbole due to reflection is compared to the lines due to the direct waves. The figure has been generated by considering the medium velocity equal to $v = 3000$ m/s, a layer with thickness $h = 50$ m and sensors distributed over a line 500 meters long, symmetric respect to the zero where the source is located.

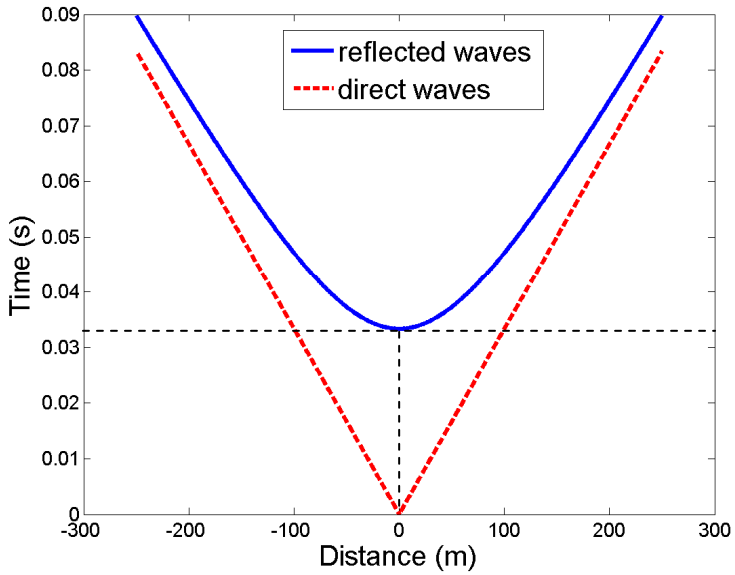

Figure 2.6. Comparison between the time arrivals of the direct waves and those of the reflected waves, for a simple numerical example.

In the hypothetic case that a sensor is placed on the same position of the source, here located in the origin of the axes, the corresponding time is

$$t_0 = \frac{2h}{v} \tag{2.20}$$

the thickness of the layer can be easily found:

$$h = \frac{v \cdot t_0}{2} \tag{2.21}$$

The hyperbole, for receivers far from the source, tends to the line determined by the times of the direct waves.

2.3.2. Data acquisition

During the acquisition of the signals, it is important to have a good coupling between sensors and the ground/rock analyzed. Moreover, in order to contrast the amplitude decay due to the geometric dispersion and to the intrinsic attenuation, the signals are progressively amplified.

In these seismic reflection surveys, two main assumptions are done:

1. Reflection with “small angles”: the distance (offset) between each source-receiver pair is smaller than the depth of the reflecting layer
2. Vertical resolution: the wavelength of the seismic signal must be significantly smaller than the depth of the reflecting layer.

In real applications, the number of sensors is chosen as large as possible, related to the capacity of the seismogram. Typical configurations for the data analysis are:

- common shot gather → all the traces with the same source
- common receiver gather → all the traces with the same receiver
- common offset gather → all the traces with equal distance source-receiver
- common midpoint gather → all the traces with source and receiver symmetric respect to their middle point.

2.3.3. Data elaboration

The process of data elaboration is quite long because many different operations must be performed. In Figure 2.7, a typical processing flow is presented, together with a brief description of the procedures.

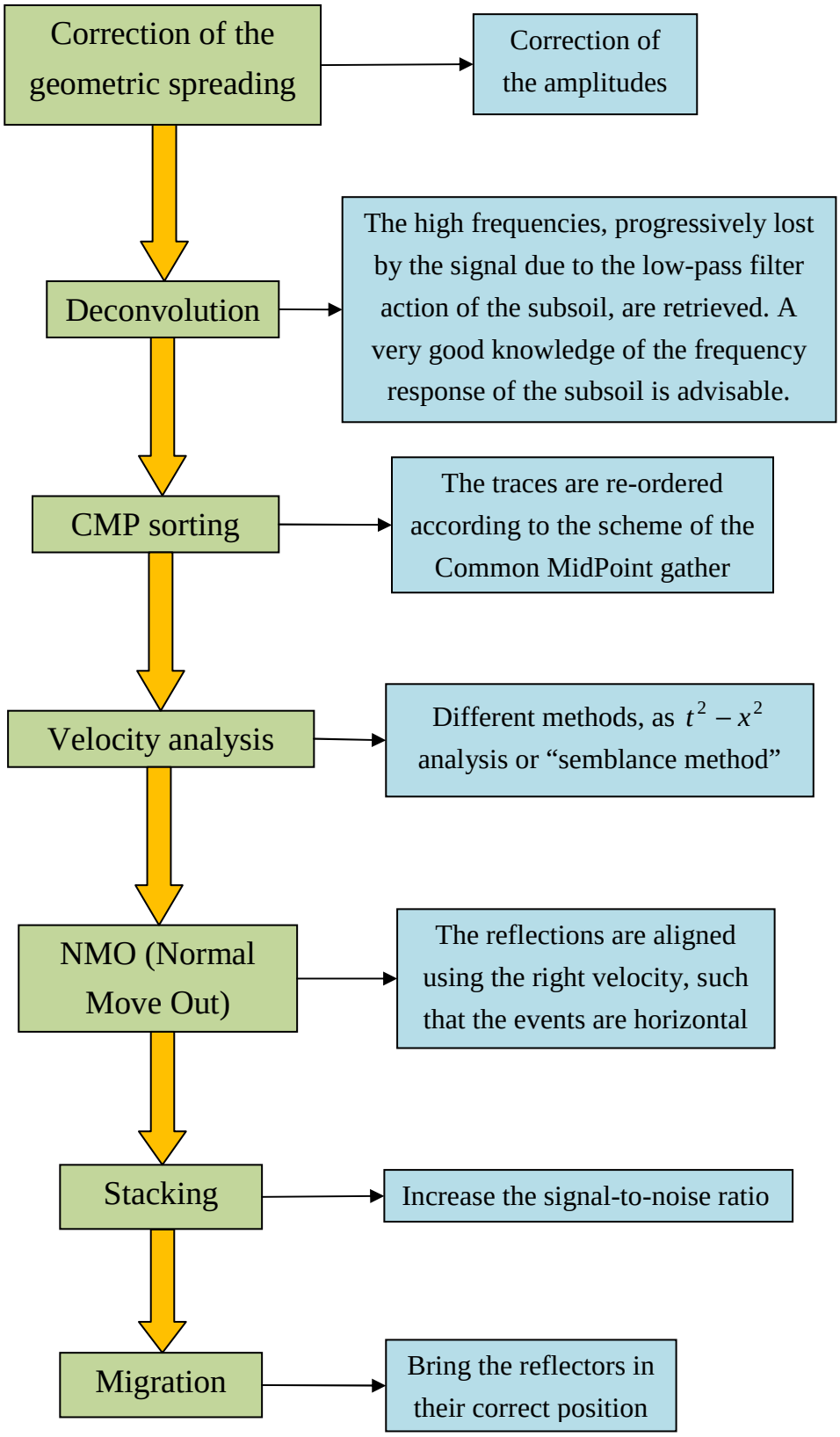

Figure 2.7. Flow chart for the processing procedure for a classical investigation based on the seismic reflection, and descriptions of each procedure.

2.3.4. Differences respect to classical seismic reflection

The objective of the thesis is to present a method for the interpretation of seismic data in tunnelling. In general, the tunnel-seismology applies the seismology techniques in a tunnel and the aim is to predict elastic ground properties ahead and around the tunnel.

First of all, it is important to note that the seismic reflection in tunnels is different from the classical one, because the configuration of sources and receivers is strongly conditioned by the geometry of the tunnel; therefore they have to be confined on the tunnel walls and cannot be placed everywhere on the space.

Figure 2.8 gives a graphical representation of this sentence, showing two waves generated in a source point reflected back and recorded by the first and the last receiver. The points on the discontinuities where the reflected waves are generated are called reflection points. The distance from the two farther of them picks out the identifiable zone, which is quite limited. This is a typical situation in a tunnel configuration and therefore the methods should be as accurate as possible.

Moreover, no information is given about the point D, which represents the point in which the tunnel will cross the discontinuity. Therefore, the unique possibility is to detect all the identifiable zone and then to continue the line until to cross the line given by the tunnel axis.

On the contrary, if the configuration would be analogous to the classical seismic surveys, then it would be like in Figure 2.9.

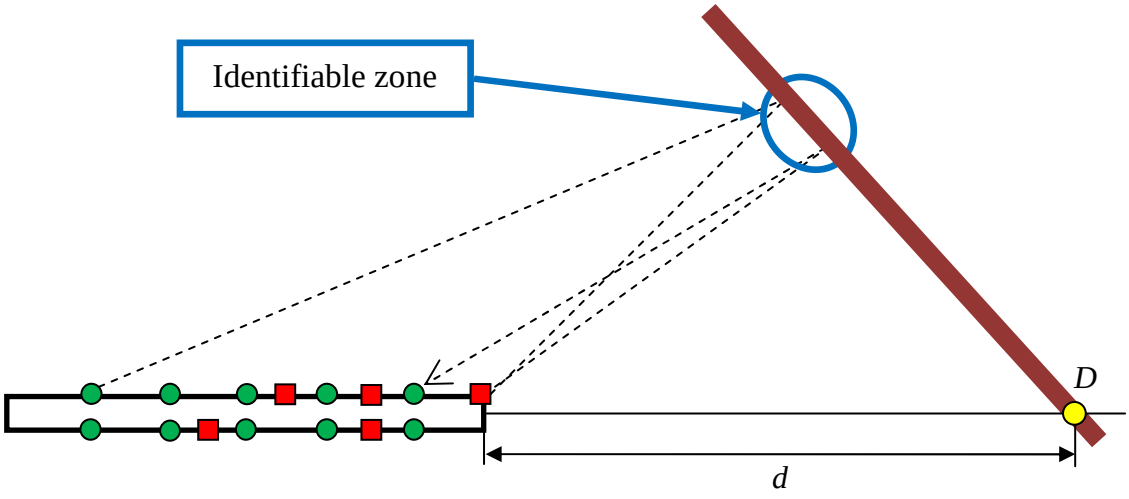

Figure 2.8. Typical configuration of sources and receivers in a tunnel, with the identifiable zone in evidence. The red squares indicate the sources, the green circles represent the receivers.

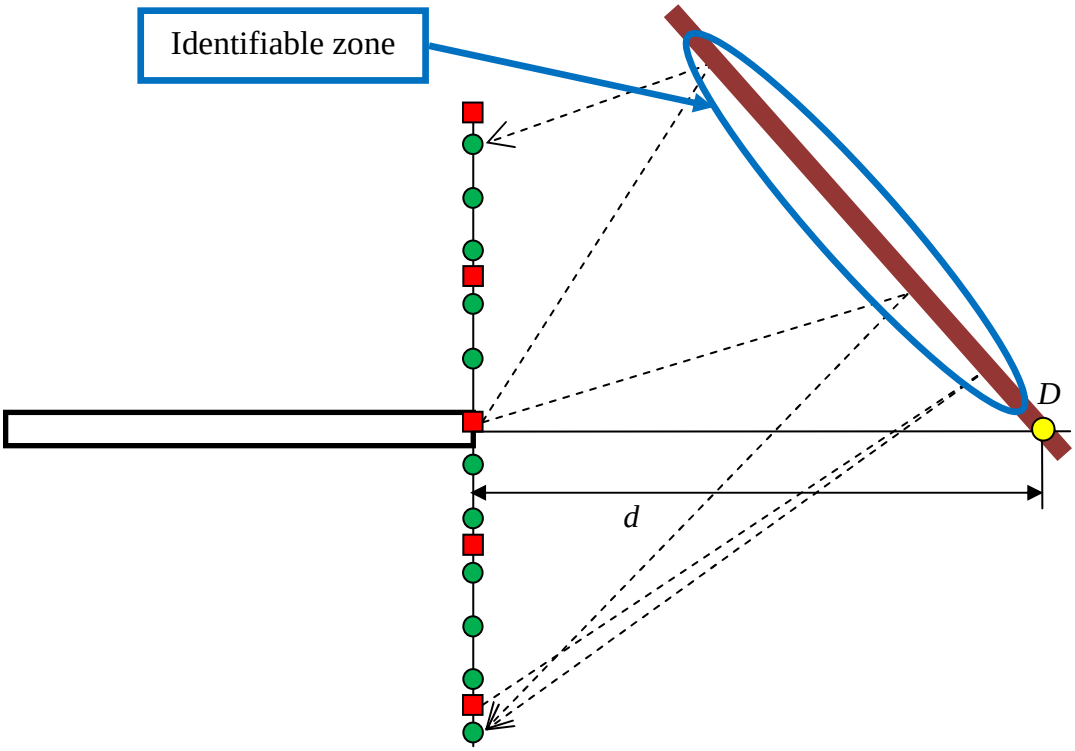

Figure 2.9. Hypothetical ideal configuration of sources and receivers in a tunnel, created analogously to the classical seismic reflection surveys, with the identifiable zone in evidence. The red squares indicate the sources, the green circles represent the receivers.

In this hypothetical ideal case the sources and the sensors are placed laterally respect to the tunnel face, and the identifiable zone is much larger respect to the previous case. Furthermore, the point D is easily estimated since the identifiable zone can be on or very close to it. This configuration is obviously ideal because in a real test it is very complicated to excavate long holes laterally and/or below and above the tunnel; and it would be also very difficult to place the sensors and to produce an efficient excitation.

2.4. The monitoring in tunnels

The monitoring during the construction or for the maintenance of a certain structure is essential to limit the risks for the workers and for the machinery utilized. This is particularly important during a tunnel construction, where it is necessary to study the rocks that will be crossed (prediction methods) and to monitor the seismic events caused by rock alteration (rockburst investigations).

Here, firstly the excavation techniques are presented, then the principal methods for the estimation of discontinuities are described, and finally the monitoring of the rockburst phenomenon is treated.

Figure 2.10. Drill operation done by the jumbo for the excavation of small holes in which the explosives will be inserted, in the Brennero tunnel under construction.

Figure 2.11. Tunnel face ready for the blast operation (Font: ec.europa.eu).

2.4.1. Methods of excavation in tunnels

The monitoring of discontinuities is important to decide which is the most suitable excavation method in a certain zone or which are the parameters to set to optimize the drilling operations. The most important techniques are:

- drilling and blasting (D&B)
- TBM (Tunnel Boring Machine)

The drilling and blasting methods, adopted for many years, are divided into two phases:

1. DRILLING: a drilling jumbo is used to drill a predetermined pattern of holes in the tunnel face (see Figure 2.10).
2. BLASTING: The drilled holes are filled with explosives and then the charges are detonated (see Figure 2.11).

One of the disadvantages of the method is the risk for workers, because the fumes and gases generated from detonating explosives are toxic. Moreover, a high quantity of dust is produced. This is the reason why the air always has to be circulated through some types of ventilation duct. Another risks are undetonated explosives.

During the last years, a new excavation technique is born, based on the Tunnel Boring Machine (TBM), also named "mole". It is a machine used to excavate tunnels with a circular cross section in very different soils and rocks, as for example hard rock, sand, and almost everything in between.

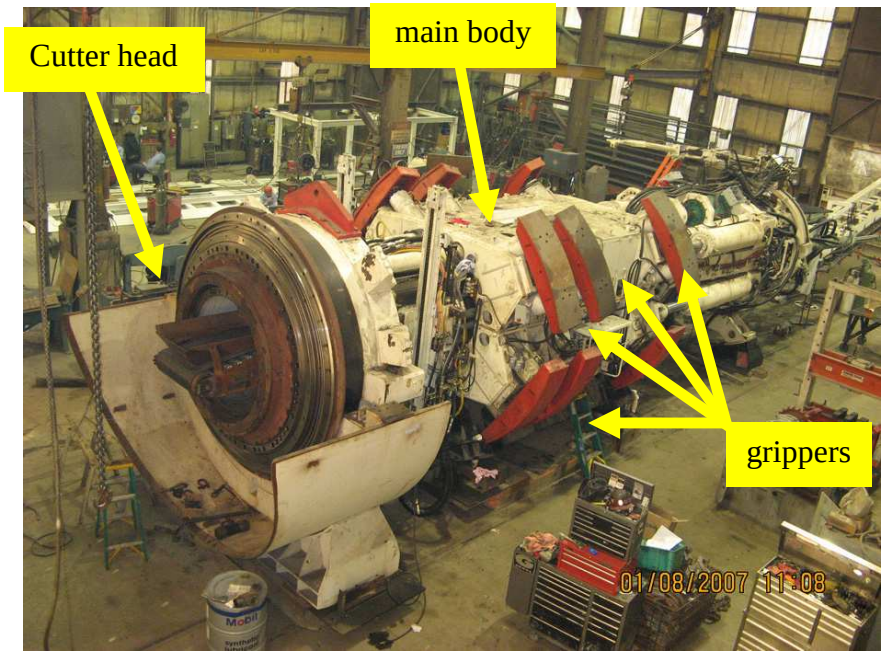

Figure 2.12. Disassembled TBM with the most important parts in evidence (Font: tunneltalk.com).

Figure 2.13. Example of a cutter head of a TBM (Font: tunneltalk.com).

The tunnel diameters can range from a metre (micro-TBMs) to almost 16 metres.
A TBM, under the mechanical point of view, is composed mainly by three elements:

- the main body
- some grippers, to fix the machine to the tunnel walls during the drilling phase
- the cutter head, composed by many roller bits.

The different components of the TBM can be seen in Figure 2.12, while the composition of the cutter head is well shown in Figure 2.13.
In the latter one, it is possible to see that the hardened steel roller bits are disposed in a way that, during the rotation of the cutter head, they can destroy all the rock wall ahead of the TBM. The type, number and geometry pattern of the cutter head depend on the rock characteristics and planned rate of penetration (from 5 to 50 m/day, but typically about 15-20). Harder is the rock, larger the penetration rate.
The TBM repeats cyclically some operations:

1. The grippers are coupled with the tunnel wall.
2. The cutter head is moved against the tunnel front and the drilling phase begins.
3. The drilling phase ends when the cutter head has reached the maximum elongation.
4. The grippers are retracted.
5. The main body moves forward.

The drilling cycle is said to correspond of about 1.2 m of advancement.
Tunnel boring machines are used as an alternative to the classical drilling and blasting methods. They have the advantages of limiting the disturbance to the surrounding

ground and producing a smooth tunnel wall, therefore their use is advisable in heavily urbanized areas.

On the contrary, the major disadvantage of TBMs is the cost of both construction and transport. However, as modern tunnels become longer, the tunnel boring machines result more convenient respect to drilling and blasting technique, because the excavation with TBMs is much more efficient and needs a shorter project. Moreover, in soft grounds and in presence of critical zones (from a geological point of view) the drilling and blasting technique is still very used.

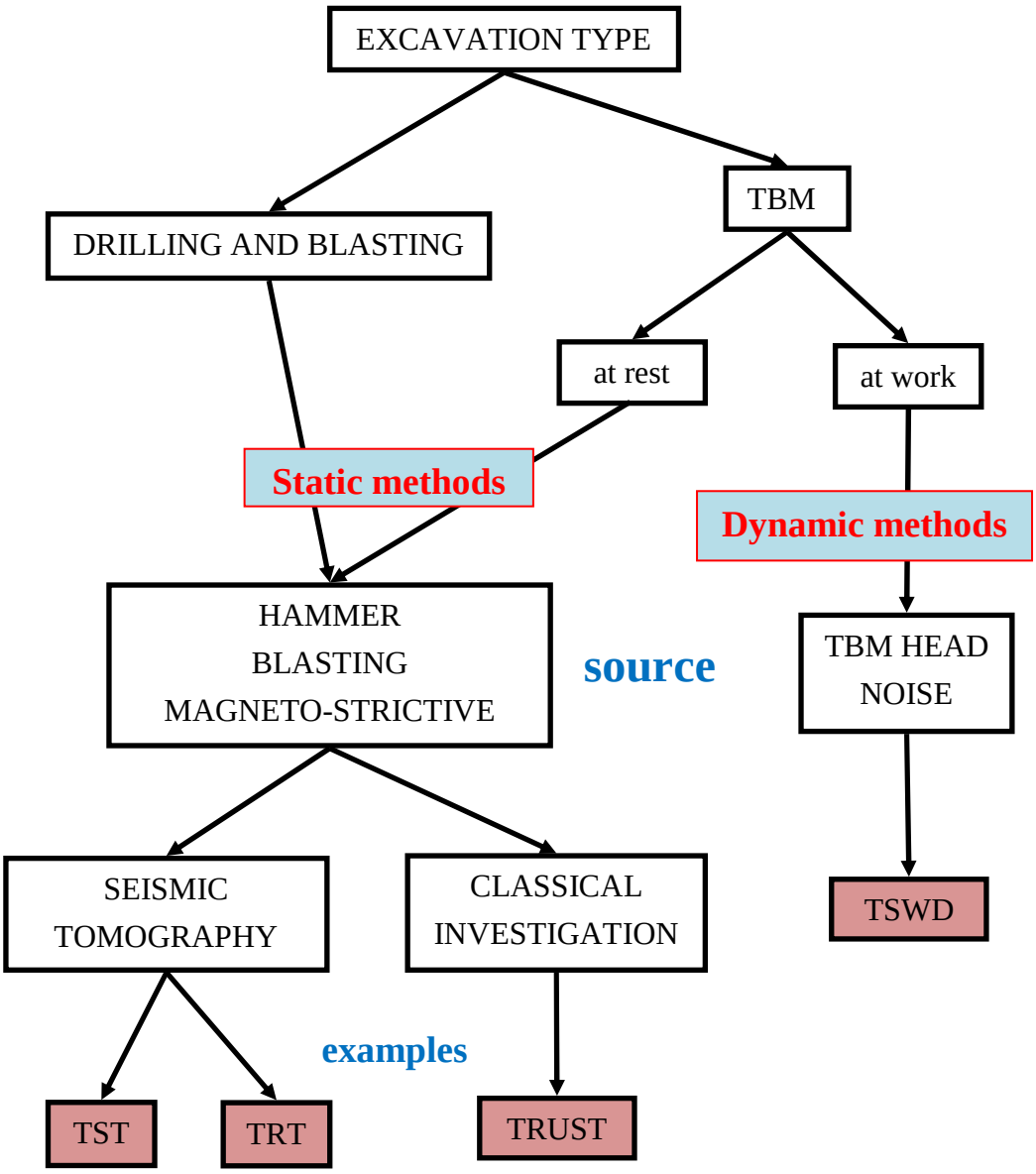

Figure 2.14. Scheme of the seismic methods for the prediction of discontinuities in a tunnel investigation. They are classified starting from the type of excavation adopted.

2.4.2. Seismic methods in tunneling

As explained in the introduction, there exist some methods for the prediction of the lithological discontinuities in tunnelling. The most important ones are depicted in the scheme of Figure 2.14, where the distinction is based mainly on the excavation type used for the tunnel construction. In particular the main division among the techniques is the following:

- dynamic methods: they are used while the TBM is working
- static methods: they are used during a TBM pause or if the tunnel is excavated with the traditional drilling and blasting procedure.

Consequently, each of both the typology is based on a specific class of excitations. For the dynamic methods, the TBM is not stopped during the lithological study and the noise produced by its cutter head is considered as the excitation. On the contrary, for a static method, since no excavation operations are ongoing, the excitation can be freely chosen; in particular the most important ones are:

- blasting
- hammer strokes
- magneto-strictive sources

Each of the method highlighted at the end of Figure 2.14 are the most used in seismic surveys in tunnelling. In the following, the TRT, the TRUST and the TSWD are described more deeply than in the introduction, by focusing on the different configurations and peculiarities.

2.4.3. TRT

The TRT method (Tunnel Reflector Tracing or Three-dimensional Reflector Tracing) was invented in Japan in 1999, and it was improved during the successive years (Descour *et al.*, 2012; Aoki K. *et al.*, 2007; Yamamoto et al., 2006) until the present days. It is a non-intrusive and “near-real time” approach, able to predict the rock condition up to 100-150 m ahead and 30 meters around the tunnel. The method is relatively cheap and quick, because it is based on excitations produced by sledgehammer strikes or magneto-strictive sources (driven by a swept frequency signal) against the tunnel walls, while the accelerometers are directly attached to the tunnel walls.

A typical configuration of sensors and sources is represented in Figure 2.15. There are 12 sources disposed on two different sections and ten receivers distributed over four rings, alternating two and three sensors per each section. It is important to note that sensors and sources are quite close each other, since the maximum distance among them is about 30 meters.

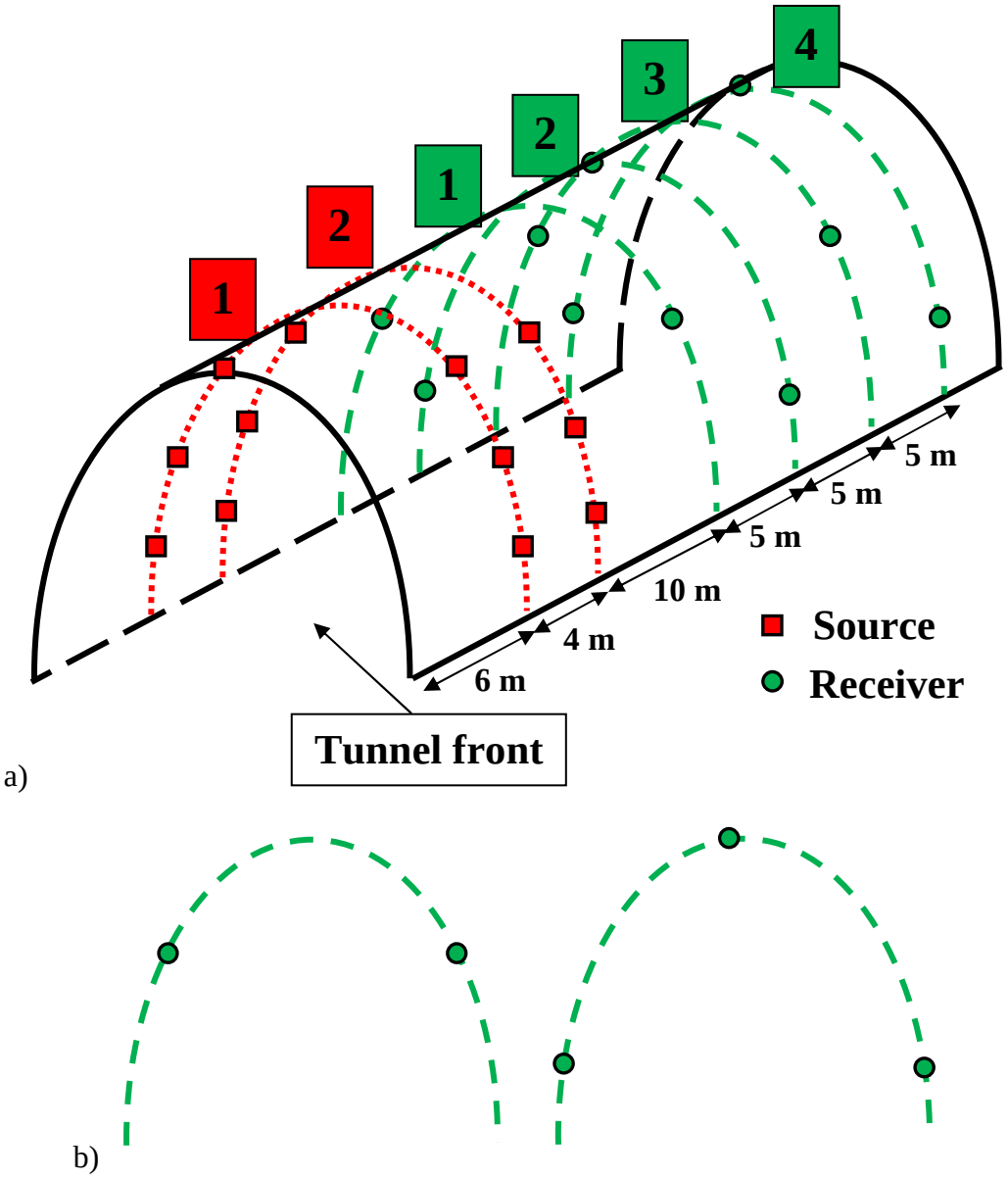

Figure 2.15. Configuration of source points and accelerometers on the tunnel for the TRT scheme: a) the general scheme; b) the alternating sections for the receivers location. Source points are indicated with red squares, receivers with green circles.

The processing technique is composed by 8 steps:

1. collect the information about the positions of sources and receivers;
2. define the three-dimensional domain of investigation, in respect to the fact that the resolution is inversely proportional to the distance from the array and directly proportional to the shortest detectable wavelength;
3. set the frequency filter to compensate the amplitude decay;
4. detect the time arrivals of direct waves and then the velocity;

5. construct seismic velocity model which is assigned to all the volume;
6. set filters for data processing and calculate the reflectogram by means of the ellipsoids;
7. run data processing repeating steps 3-4-5-6 until the results are balanced (reflectogram is stable) and noise is sufficiently suppressed;
8. set background (scale, color code) for displaying the results;

The results are visualized in terms of reflection number. The extent and hardness of reflecting boundaries is measured by normalized Reflection Magnitude, defined as ratio between the average level of amplitude of reflected waves and those of direct waves. It is proportional to the reflection coefficient and it allows to distinguish high impedance from low impedance.

The total calculation time is about 3 hours per each survey on a common laptop.

Yamamoto *et al.* (2008) improved the methodology by introducing the wireless TRT, based on radio communication, without using any cable. This system is very efficacious in tunnel with a large cross-section, but it has some problems due to interferences especially for small cross-section tunnels.

2.4.4. TRUST

The TRUST (True Reflection Underground Seismic Technique) has been invented in Germany by DTM, in Essen. The substantial difference respect to the TRT method is the use of blasting, therefore the total time of the investigation and the costs are slightly higher.

In details, the sources are small explosives detonated from small boreholes in the tunnel face or side wall. Usually, series of 20-30 single blasts starting from the tunnel face along the tunnel axis are performed. Their characteristics are:

- Electric triggered zero-delay detonators
- Explosive material of 100-150 g per single shot
- Explosives with detonation velocity > 6000 m/s
- Packer/fill material (water tubes) to fill the borehole

The frequency range of the signal varies from 20 Hz to 1000 Hz.

The receivers are typically three-component geophones mounted in separated “listening boreholes”, drilled radial into the rock. Usually, there are some rings with 3-4 borehole geophones each, placed about every 50 m.

An exemplar configuration is proposed in Figure 2.16, where it can be seen that the sources are normally on the same tunnel side, and the receivers have two preferable schemes: with two elements at 4- and 8-hours respectively and the third either at 10- or 12-hours.

The processing technique is based on classical seismic reflection techniques while the results are much less fine respect to TRT. Moreover, the calculus time is higher: about 24 hours to obtain a final representation of the discontinuities on a common laptop.
In case of problematic excavation zones, additional techniques are used, as exploration boreholes, radar boreholes or Shuttle boreholes (wireless).

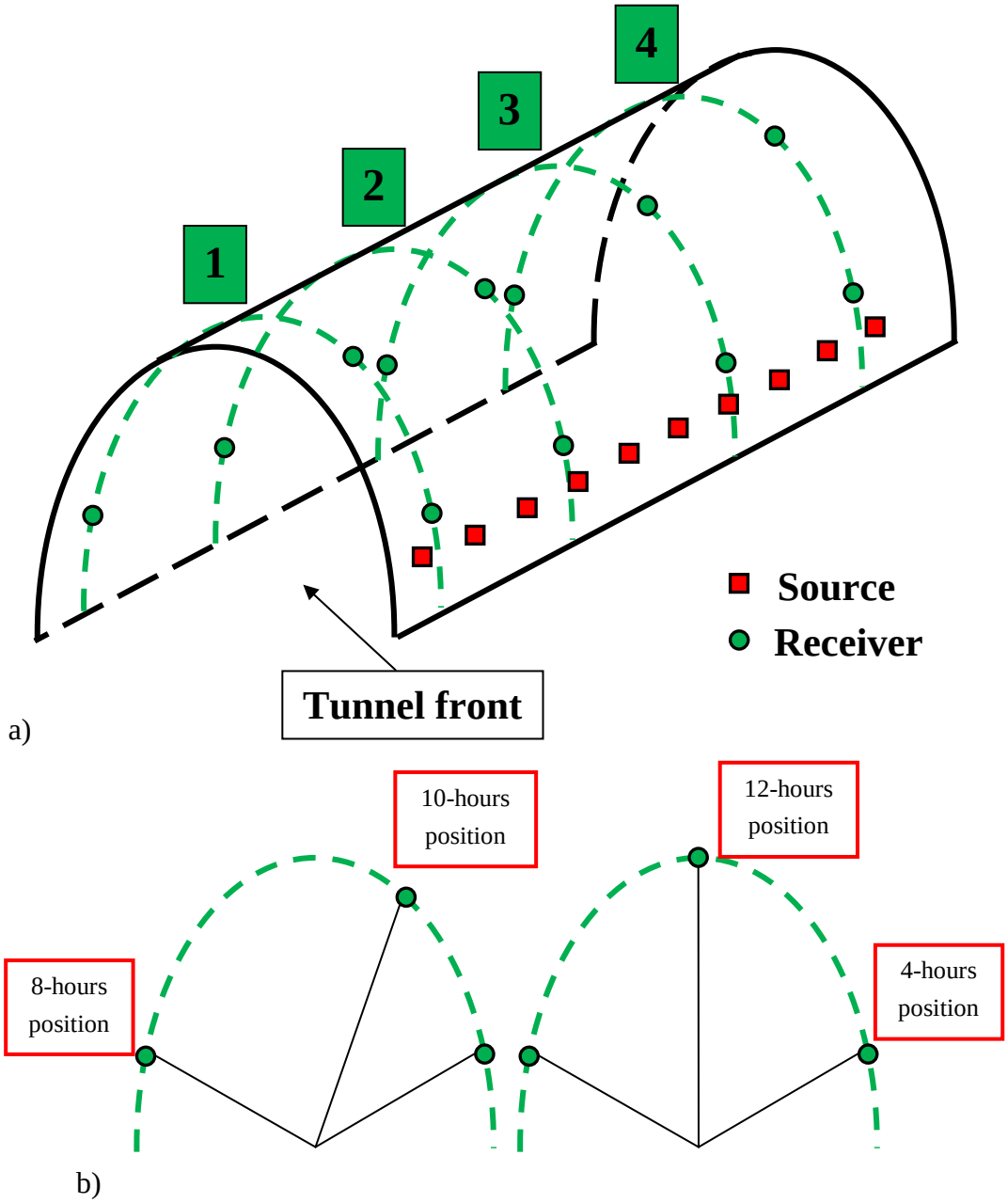

Figure 2.16. Configuration of source points and accelerometers on the tunnel for the TRUST scheme: a) the general scheme; b) possible section for the receivers location. Source points are indicated with red squares, receivers with green circles.

2.4.5. TSWD

The TSWD (Tunnel Seismic While Drilling) is a methodology born about ten years ago in Trieste, at the OGS (Istituto Nazionale di Oceanografia e geofisica sperimentale), thanks to the work of two scientists: Lorenzo Petronio and Flavio Poletto. The first article produced by the two authors is “Seismic-while-drilling by using tunnel boring machine noise” (Petronio L., Poletto F., 2002) while other fundamental works have been developed later (Poletto and Petronio, 2006; Petronio *et al.*, 2007).

The Poletto and Petronio’s idea is to create a new method for the prediction of discontinuities ahead of a TBM, without stopping the machine, contrarily to the static methods. Indeed, the latter ones are not convenient because the cost of stopping and restarting the TBM is very large. The realization of a reliable dynamic method will permit to save a lot of money and to conclude the tunnels in less time.

The seismic-while-drilling (SWD) techniques (T. Yokota *et al.*, 2004) have been very frequently adopted in many fields, such as the petroleum engineer, the geophysical surveys of the ground and the exploration of geothermal fields. The main peculiarity is the use of the noise produced by a certain drilling source as a seismic source, which is inserted in a borehole. The most classical procedures for the data analysis are to gather the first time arrivals of the seismic waves, both direct waves and reflected waves, and then cross-correlate the signals coming from the pilot sensor (reproducing the source signal) and from the geophones.

The TSWD method uses accelerometers mounted on the cutter head of the TBM (called pilot sensors) and geophones located along and outside the tunnel. The central idea is to consider the noise produced by the working TBM as a seismic source. In this way, the cross-correlation between the signals coming from the pilot sensors and those coming from the geophones gives information about the velocity of the seismic waves and consequently about the rock characterization. The typical results of this analysis are strong coherent events, corresponding to P and S arrivals.

Actually, the TBM produces other types of vibrations because, during the drilling phase, it is coupled with the tunnel walls by means of the grippers. These signals can be considered as noise added to the system. Moreover, the TBM train can be hundred of meters long, and the vibrations produced in the farthest points of the machinery may add up many milliseconds of relative delay.

The most innovative peculiarity is the real-time identification of the rock discontinuities and consequently the setting of the drilling parameters. For this reason, the process can reduce significantly the project costs and the number of working days.

With this dynamic method, the most critical problem is connected with the source, because it has a low energy level and because the machine produces also a different

noise caused by the coupling of the grippers with the tunnel wall. The first problem may be solved by modifying the source, for example by adding other excitations. The second problem can be solved by means of methods for the separation of the sources, as the Blind Source Separation and Blind Component separation (Antoni, 2005).
Petronio and Poletto proposed a simple method to decompose the signal recorded at the beginning and at the end of the tunnel, in order to distinguish the cutter head noise (called $S(\omega)$) from the noise due to the coupling ($N(\omega)$). This operation has been done by calculating the total paths travelled by the waves.

2.4.6. The Potsdam approach

Instead of considering the noise produced by the cutter head, a seismic reflection method can be also conducted when the TBM is at rest or between two consecutive drilling cycles. Within this topic, some promising works have been done by the GFZ Potsdam in Germany, where Luth et al. (2008) tried to applied a seismic method by considering two types of sources:

1. A pneumatic impact hammer, constituted by a moving mass of 5 kg accelerated onto a shock plate generating an impact of approximately 1 ms duration, by generating frequencies up to 2 kHz.
2. A magneto-strictive vibrator able to generate sweep signals within a frequency range of 10 Hz with a dynamic force of 22kN.

The sources are placed on the grippers of the TBM, while the sensors are placed where the TBM is open and the rock is easy to reach. For this particular application, the sensors must be wireless, to avoid the difficult wiring operations with the presence of the TBM.

2.4.7. Monitoring of the rockburst

Another aspect, parallel to the prediction of discontinuities ahead of the tunnel face, is the monitoring of the rockburst, a small seismic event caused by the alteration of the rock configuration due to the excavation. These phenomenon is frequent especially in deep mines. It is due to the fact that the tunnel construction breaks the equilibrium state of stress, which is immediately redistributed when advancing. Stronger rock corresponds to higher stored energy (larger risk in granite and volcanic rock, lower in weak rocks). Rockbursts occur due to violent release of this energy.
The rockburst is very dangerous both for the workers and for the tunnel excavation, as can be seen in Figure 2.17, where an example of its effects is proposed. In this case, the magnitude of seismic event is 2.7 of the Richter scale, but a significant collapse happened.

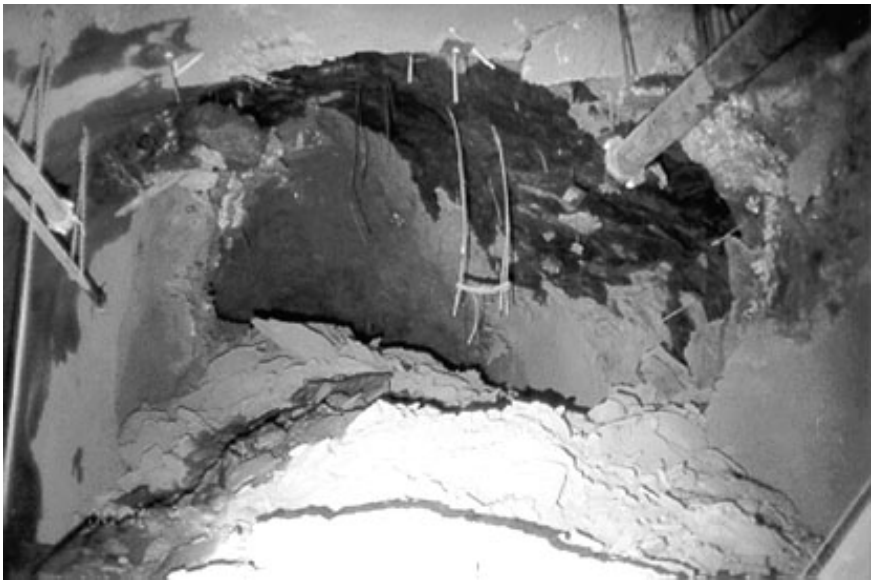

Figure 2.17. Example of a collapse in a tunnel due to the rockburst phenomenon (Font: accessscience.com).

Even if many researchers deeply studied the phenomenon, there is no comprehensive and rational explanation for its cause. Moreover, the prevention to rockburst depends primarily on practical experience.

The rockburst mainly occurs in two forms (Zhu *et al.*, 2009):

- tension fracture on the surface of surrounding rock parallel to the tunnel wall
- shear failure at an angle from 15º to 40º to the tunnel wall, which forms a step-like triangular damage area on the wall.

To reduce the severity of rockbursts, some preconditioning techniques have been developed:

- to detonate explosives in the confined rock mass ahead of the mining face, thereby transferring the stresses further away and effectively de-stressing the immediate face area;
- a large diameter (about 50 mm) hole is drilled parallel to excavation 5 m ahead of the mining face (face parallel method)
- long holes (3 m) are drilled at the same time as the normal 1-1.2 m long production holes (face perpendicular method).

Grodner (2001) investigated the gold mines of the Witwatersrand Basin, South Africa, one of deepest excavations in the world. His work was mainly concentrated in reducing the severity of the rockburst by preconditioning, in particular with the Ground Penetrating Radar (GPR), which maps the fracture density and pattern around deep

excavations, quantifies the change in fracture pattern ahead of mining (e.g. with preconditioning) and delineates new fractures.

Zhu *et al.*, 2009 proposed a numerical study, based on the classical elasto-plastic theory, to prevent rockburst by means of guide holes drilled during tunnel excavation. The results showed that the stress field around the guide holes severely changed. This fact caused the formation of an X-shaped area of plastic deformation, which prevented the rockburst.

Significant studies about the rockburst have been also done by Tang et al. (2010) and by Liu *et al.* (2011), about a hydropower station in Southwest China, where many rockburst events were recorded in the transportation tunnel and in the drainage tunnel, and by Khanlari and Ghaderi-Meybodi (2011), about the Karaj-Tehran Water Supply Tunnel in Iran, finding that zones with high overburden have high possibility of rockburst.

Chapter 3

Modelling of reflections

Before presenting the methods for the estimation of the discontinuities ahead of the tunnel face, it is important to give an idea about the geometrical representation of the problem under study, with a particular attention to the concept of ellipsoids. Moreover, the most important relationships among the variables are extracted.

3.1. General idea

Simply speaking, it is easy to imagine that the seismic waves are generated in a certain point and they propagate in all the directions, according to the properties of the rock that they cross. However, the waves can meet some irregularities and this might produce a reflection, i.e. an amount of the total wave amplitude is pushed back according with the inclination of the reflector.

As already stated in Subsection 2.3.4, a seismic investigation in a tunnel is similar to the classical survey based on the seismic reflection, but with the substantial difference that the zone in which the sensors are located is very limited, usually close to the tunnel face. Indeed, they are placed on tunnel walls, in order to detect the waves that have been generated in the source point and have been reflected back by discontinuity, considered as a region characterized by a contrast of impedance with respect to the embedded material.

A typical configuration of sources/receivers is shown in Figure 3.1.

Since the wave arrivals can be detected by accelerometers or geophones placed behind the tunnel front, then it is possible to construct simple geometric relationships.

Since the sensors can be distributed everywhere on the tunnel walls, the reflections are not generated in a single point but they cluster in a reflection zone.

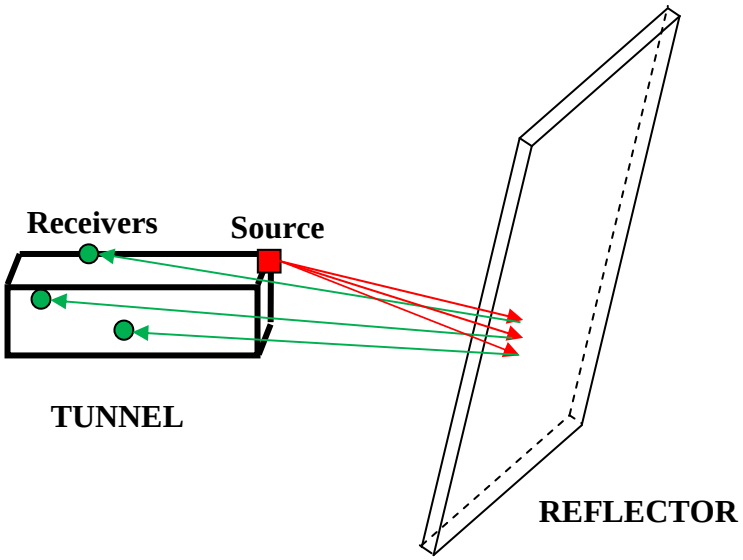

Figure 3.1. The reflection of the seismic waves generated by the source (red square) is produced by the reflector (or discontinuity), and the reflected waves are recorded by the sensors placed on the tunnel walls (green circles).

3.2. Geometric idea

Let's start by analyzing the equations from the simplest case, in two dimensions, while the 3-D case will be presented successively.

3.2.1. 2D representation

In Figure 3.2, the representation of a 2D investigation is depicted. The discontinuity, indicated with the thick brown line, is inclined respect to the vertical axis of an angle α. The source point S is the point in which the waves are generated. Typical experimental excitations are hammer strokes, blasting or magneto-strictive sources.
The wave reaches the discontinuity in the reflection point P, where it is reflected back with an angle ϑ which depends both on the discontinuity inclination and on the relative position between P and S. The reflected wave reaches the tunnel at the sensor placed in the point R. For a different sensor, placed in R_1, the reflection point is P_1, and it is different from P.
The parameter d has the meaning of the distance between the tunnel front and the discontinuity: in other words it indicates the number of missing meters before meeting the discontinuity, by supposing that the tunnel is constructed on a straight line.

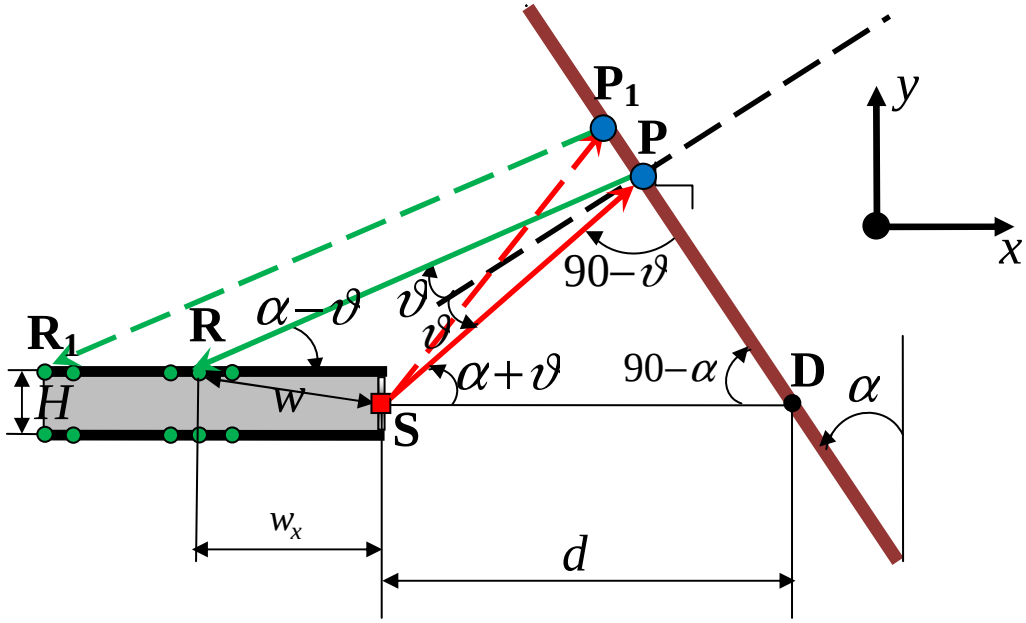

Figure 3.2. Geometric illustration of the problem in two dimensions. The tunnel is colored in grey, while the discontinuity is indicated with the thick brown line. The red line represents the direct wave, while the green line represents the reflected wave.

The purpose of this approach is to find both the angle α and the distance d, which are the two parameters characterizing the discontinuity.

The position of the source can be either on the tunnel face or on the tunnel walls, but often it is located on the tunnel wall for reasons of convenience and simplicity, since the tunnel face is filled by explosives (drilling and blasting technique) or by the cutter head of the TBM. The typical case in which the source is on the tunnel front is when monitoring during the excavation of the TBM (Petronio and Poletto, 2002; Poletto et al., 2007; Bruckl et al., 2008). In this case, however, since the cutter head is in contact with the rock in many points, a punctual source cannot be assumed.

3.2.2. Relationships among the parameters in the 2D case

In this subsection, the governing equations for the two-dimensional problem are extracted. By using the law of sines on the triangle SRD,

$$\frac{d}{\sin(90-\vartheta)} = \frac{\overline{SP}}{\sin(90-\alpha)} \tag{3.1}$$

$$\overline{SP} = d\frac{\cos\alpha}{\cos\vartheta} \tag{3.2}$$

and, equivalently, on the triangle RPD, with the approximation of the source S on the same side of the receiver considered,

$$\frac{d + w_x}{\sin(90 + \vartheta)} = \frac{\overline{PR}}{\sin(90 - \alpha)} \tag{3.3}$$

$$\overline{PR} = (d + w_x)\frac{\cos\alpha}{\cos\vartheta} \tag{3.4}$$

The total distance L travelled by the seismic wave observed at the sensor R is

$$L = \overline{SP} + \overline{PR} = (2d + w_x)\frac{\cos\alpha}{\cos\vartheta} \tag{3.5}$$

and so it depends on three unknowns: d, α and ϑ. Using again the law of sines, but on the triangle RSP,

$$\frac{w_x}{\sin(2\vartheta)} = \frac{\overline{PR}}{\sin(180 - \alpha - \vartheta)} \tag{3.6}$$

and therefore

$$\frac{w_x}{\sin(2\vartheta)} = \frac{(d + w_x)\frac{\cos\alpha}{\cos\vartheta}}{\sin\alpha\cos\vartheta + \cos\alpha\sin\vartheta} \tag{3.7}$$

$$\frac{w_x}{2\sin\vartheta} = \frac{(d + w_x)\cos\alpha}{\sin\alpha\cos\vartheta + \cos\alpha\sin\vartheta} \tag{3.8}$$

$$\frac{w_x}{2} = \frac{d + w_x}{\tan\alpha\cot\vartheta + 1} \tag{3.9}$$

$$d + w_x = \frac{w_x}{2}\left(\frac{\tan\alpha}{\tan\vartheta} + 1\right) \tag{3.10}$$

and finally

$$d = \frac{w_x}{2}\left(\frac{\tan\alpha}{\tan\vartheta} - 1\right) \tag{3.11}$$

Now, by using together Eq. (3.5) and Eq. (3.10), it is possible to write

$$L = (2d + w_x)\frac{\cos\alpha}{\cos\vartheta} = d\,\frac{\cos\alpha}{\cos\vartheta} + \frac{w_x}{2}\left(\frac{\tan\alpha}{\tan\vartheta} + 1\right)\frac{\cos\alpha}{\cos\vartheta} \tag{3.12}$$

$$L = \left(d + \frac{w_x}{2}\right)\frac{\cos\alpha}{\cos\vartheta} + \frac{w_x}{2}\,\frac{\sin\alpha}{\sin\vartheta} \tag{3.13}$$

$$(2d + w_x)\frac{\cos\alpha}{\cos\vartheta} = \left(d + \frac{w_x}{2}\right)\frac{\cos\alpha}{\cos\vartheta} + \frac{w_x}{2}\,\frac{\sin\alpha}{\sin\vartheta} \tag{3.14}$$

$$\frac{w_x}{2}\,\frac{\sin\alpha}{\sin\vartheta} = \left(d + \frac{w_x}{2}\right)\frac{\cos\alpha}{\cos\vartheta} \tag{3.15}$$

$$w_x\,\frac{\sin\alpha}{\sin\vartheta} = 2\left(d + \frac{w_x}{2}\right)\frac{\cos\alpha}{\cos\vartheta} = L \tag{3.16}$$

and finally the relationship about the distance travelled is

$$L = w_x\,\frac{\sin\alpha}{\sin\vartheta} \tag{3.17}$$

Since the medium is supposed to be homogeneous, the velocity v of the seismic wave is supposed to be constant. Then, since $L = vt$, where t is the time in which the wave passes from S to P to R. The set of independent equations is given by

$$\begin{cases} t = \dfrac{w_x}{v}\,\dfrac{\sin\alpha}{\sin\vartheta} \\ d = \dfrac{1}{2}\,w_x\left(\dfrac{\tan\alpha}{\tan\vartheta_i} - 1\right) \end{cases} \tag{3.18}$$

where there are three unknowns, therefore the system cannot be solved. The unique way to obtain a solution is to use the relationships also for other receivers or sources, to have more information. This is the main subject of the successive chapters, where a solution of the problem is proposed.

3.2.3. 3D representation

The extension to the three dimensional case implies that the seismic waves can propagate in the space and the discontinuity is no more a line but a plane. Therefore a second angle, which is indicated by γ, is necessary to take the additional direction into account.

In Figure 3.3 the 3D reflection is represented and, for clarity, the most important parameters are here listed:

- S : source point
- P : reflection point, indicated by the coordinates x_P, y_P and z_P
- R : position of the sensor considered
- α : inclination of the discontinuity respect to the axis z
- γ : inclination of the discontinuity respect to the axis x

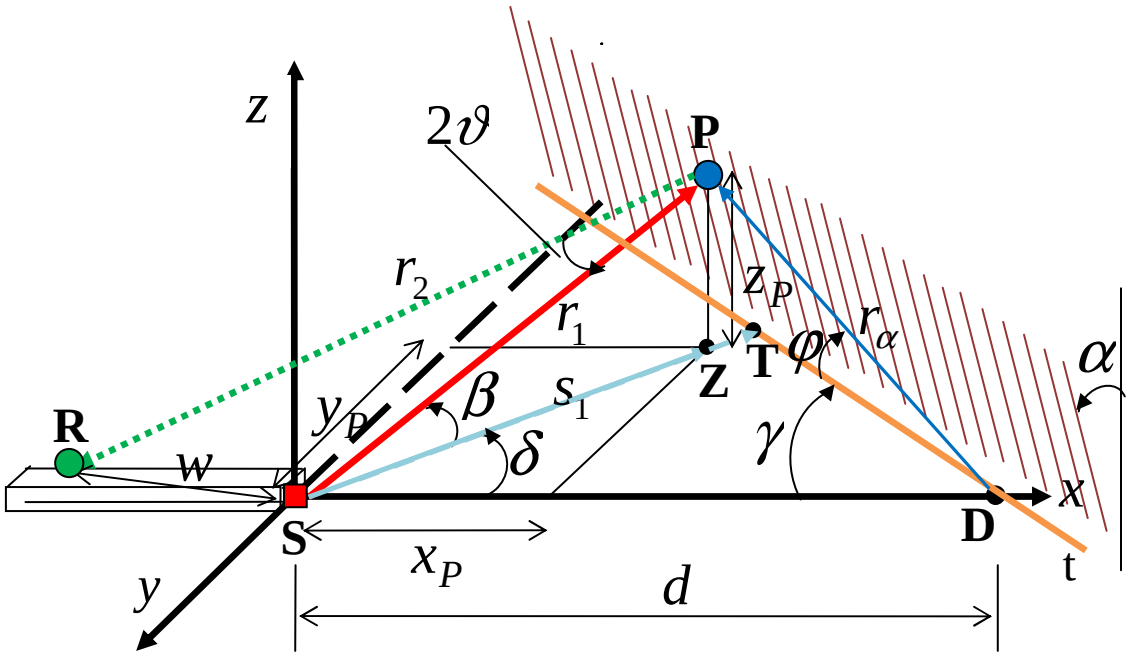

Figure 3.3. Geometric illustration of the problem in three dimensions. The discontinuity plane is indicated with thin brown lines. The red line represents the direct wave, while the green dotted line represents the reflected wave.

- r_1: direction of the wave generated in S
- r_2: direction of the wave reflected in P
- D: point in which the tunnel will cross the discontinuity
- d: distance between the tunnel face and the discontinuity
- ϑ: wave incident angle (equal to the reflection angle)
- w: distance between the sensor and the source point.

3.2.4. Characterization of the discontinuity

Since the discontinuity is a plane, then it can be expressed as:

$$a_1 x + a_2 y + a_3 z + a_4 = 0 \tag{3.19}$$

where a_i, $i = 1,...,4$ are constant coefficients.

If intersecting the discontinuity with the planes $z = 0$ and $y = 0$, it is possible to find the distance d as

$$d = -\frac{a_4}{a_1} \tag{3.20}$$

Now, we have to find a similar relationships for the angles γ and α. To do this, some geometrical relationships must be reminded.

The angle φ between the line r and the line s whose equation are, respectively,

$$y = mx + q \qquad y = m'x + q' \tag{3.21}$$

can be calculated by means of the following formula:

$$\tan\varphi = \frac{m - m'}{1 + mm'} \tag{3.22}$$

Coming back to the problem, if intersecting the discontinuity with the XY plane, the line t is obtained and the angle between the x-axis and t is calculated:

$$\tan(\gamma) = \frac{a_1}{a_2} \tag{3.23}$$

Moreover, the angle between the line obtained by intersecting the discontinuity with the YZ plane and the z-axis, is exactly the angle α:

$$\tan(\alpha) = \frac{a_3}{a_1} \tag{3.24}$$

Since Eq. (3.19) can be re-written as

$$x + \frac{a_2}{a_1} y + \frac{a_3}{a_1} z + \frac{a_4}{a_1} = 0 \tag{3.25}$$

then conclusively the discontinuity is of the form

$$x + \frac{1}{\tan(\gamma)} y + \tan(\alpha) z - d = 0 \tag{3.26}$$

3.3. Construction of the ellipsoids

Instead of considering all the relationships among the variables expressed in Subsection 3.2.2., it is better to introduce the concept of ellipsoids, which is basilar in these kinds of reflection seismology and it allows to simplify the equations defining the problem under analysis. Let's consider a source S, a receiver R and a reflection point P, respectively defined by

$$S = (x_S, y_S, z_S) \qquad R = (x_R, y_R, z_R) \qquad P = (x, y, z) \tag{3.27}$$

The sum of the distance between S and P and between P and R is equal to L, which corresponds to the total path travelled by the wave:

$$\sqrt{(x - x_S)^2 + (y - y_S)^2 + (z - z_S)^2} + \sqrt{(x - x_R)^2 + (y - y_R)^2 + (z - z_R)^2} = L \tag{3.28}$$

Actually, the constant L is the given by

$$L = v t_R \tag{3.29}$$

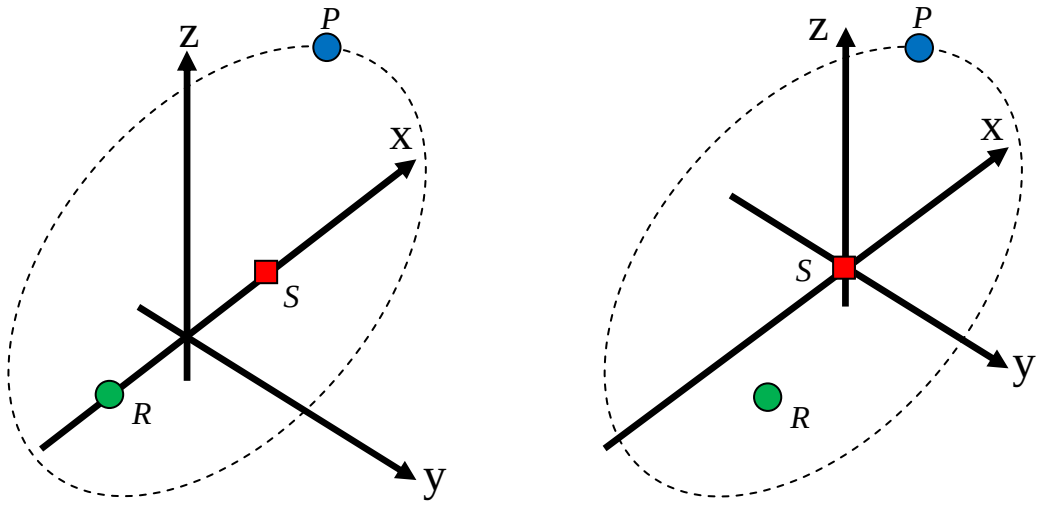

Figure 3.4. Choice of the Cartesian coordinates for the Ashida's moving approach (a) and for the static approach (b).

where v is the velocity of the wave and t_R is the recorded travel time. The velocity is supposed to be constant since the rock is assumed as a homogeneous material.

The ellipsoids are built by considering one source and one receiver as the two foci. Successively, they can be obtained in two ways:

- by fixing the origin of the axes in the middle point between the source and the receiver, as indicated in Figure 3.4a
- by imposing the source in the origin of the axes, as indicated in Figure 3.4b

In the first case, according to the Ashida's approach (Ashida and Koichi, 1993; Ashida *et al.*,2001), the axes change for each source-receiver pair and the equation of the ellipsoid is

$$\frac{x^2}{L^2 - 4x_s^2} + \frac{y^2}{L^2 - 4x_s^2} + \frac{z^2}{L^2} = \frac{1}{4} \tag{3.30}$$

where the dependence is only on the x-coordinate of the source and on the total path L, therefore the construction of the ellipsoids is very simple. For the same reason, the first two axes of the ellipsoid are equal.

In the second case, the axes are fixed but the equations of the ellipsoids are simply comparable. Let us consider separately the cases in which the receivers have one and two non-null coordinates, respectively.

3.3.1. Sensors aligned with the source

If the sensors have only one coordinate different from the source (i.e. the x-coordinate) then it is possible to define the source S, a generic receiver R and the corresponding reflection point P as

$$S=(0,0,0) \qquad R=(x_R,0,0) \qquad P=(x,y,z) \tag{3.31}$$

The distance source - reflection point – receiver is

$$\sqrt{x^2+y^2+z^2}+\sqrt{(x-x_R)^2+y^2+z^2}=L \tag{3.32}$$

$$\sqrt{(x-x_R)^2+y^2+z^2}=L-\sqrt{x^2+y^2+z^2} \tag{3.33}$$

$$x^2-2xx_R+x_R^2+y^2+z^2=L^2+x^2+y^2+z^2-2L\sqrt{x^2+y^2+z^2} \tag{3.34}$$

$$-2xx_R+x_R^2=L^2-2L\sqrt{x^2+y^2+z^2} \tag{3.35}$$

$$2L\sqrt{x^2+y^2+z^2}=L^2+2xx_R-x_R^2 \tag{3.36}$$

$$4L^2\left(x^2+y^2+z^2\right)=L^4+4x^2x_R^2+x_R^4+4L^2xx_R-2L^2x_R^2-4xx_R^3 \tag{3.37}$$

$$L^2\left(x^2+y^2+z^2\right)=\frac{L^4}{4}+x^2x_R^2+\frac{x_R^4}{4}+L^2xx_R-\frac{L^2x_R^2}{2}-xx_R^3 \tag{3.38}$$

Now, let us assume that $p=\frac{x_R}{2}$.

$$L^2\left(x^2+y^2+z^2\right)=\frac{L^4}{4}+4x^2p^2+4p^4+2L^2xp-2L^2p^2-8xp^3 \tag{3.39}$$

$$L^2\left(x^2-2xp+p^2\right)+L^2y^2+L^2z^2=\frac{L^4}{4}+4x^2p^2+4p^4-8xp^3-L^2p^2 \tag{3.40}$$

$$L^2(x-p)^2 + L^2y^2 + L^2z^2 = \frac{L^4}{4} + 4p^2\left(x^2 + p^2 - 2xp\right) - L^2p^2 \tag{3.41}$$

$$L^2(x-p)^2 + L^2y^2 + L^2z^2 = \frac{L^4}{4} + 4p^2(x-p)^2 - L^2p^2 \tag{3.42}$$

$$L^2(x-p)^2 - 4p^2(x-p)^2 + L^2y^2 + L^2z^2 = \frac{L^4}{4} - L^2p^2 \tag{3.43}$$

$$\left(L^2 - 4p^2\right)(x-p)^2 + L^2y^2 + L^2z^2 = \frac{L^2}{4}\left(L^2 - 4p^2\right) \tag{3.44}$$

$$\frac{(x-p)^2}{\frac{L^2}{4}} + \frac{y^2}{\frac{\left(L^2 - 4p^2\right)}{4}} + \frac{z^2}{\frac{\left(L^2 - 4p^2\right)}{4}} = 1 \tag{3.45}$$

Conclusively, the equation extracted is an ellipsoid of the form

$$\frac{(x-p)^2}{a^2} + \frac{y^2}{b^2} + \frac{z^2}{b^2} = 1 \tag{3.46}$$

$$p = \frac{x_R}{2} \qquad a = \frac{L}{2} \qquad b = \sqrt{\frac{L^2 - 4p^2}{4}} = \sqrt{a^2 - p^2} \tag{3.47}$$

where a and b are the semi-axes of the ellipsoid. It is possible to see that Eq. (3.46) is equivalent to the Ashida's formula expressed in Eq. (3.30).

3.3.2. Sensors not aligned with the source

If the receivers have also the y-coordinate different from the source, then the source and a generic receiver can be written as

$$S = (0,0,0) \qquad R = (x_R, y_R, 0) \tag{3.48}$$

Considering the corresponding reflection point $P = (x, y, z)$, the sum of the distance source-reflection point and reflection point-receiver is given by

$$\sqrt{x^2+y^2+z^2}+\sqrt{(x-x_R)^2+(y-y_R)^2+z^2}=L \tag{3.49}$$

Now, let us manipulate the equations as in the previous subsection

$$\sqrt{(x-x_R)^2+(y-y_R)^2+z^2}=L-\sqrt{x^2+y^2+z^2} \tag{3.50}$$

$$x^2-2xx_R+x_R^2+y^2-2yy_R+y_R^2+z^2=L^2+x^2+y^2+z^2-2L\sqrt{x^2+y^2+z^2} \tag{3.51}$$

$$-2xx_R+x_R^2-2yy_R+y_R^2=L^2-2L\sqrt{x^2+y^2+z^2} \tag{3.52}$$

$$2L\sqrt{x^2+y^2+z^2}=L^2+2xx_R-x_R^2+2yy_R-y_R^2 \tag{3.53}$$

$$\begin{aligned}4L^2\left(x^2+y^2+z^2\right)=&L^4+4x^2x_R^2+x_R^4+4L^2xx_R-2L^2x_R^2-4xx_R^3+4y^2y_R^2+\\&+y_R^4-4yy_R^3+2\left(L^2+2xx_R-x_R^2\right)\left(2yy_R-y_R^2\right)\end{aligned} \tag{3.54}$$

Let us impose $p=\frac{x_R}{2}$ and $q=\frac{y_R}{2}$, then

$$\begin{aligned}L^2\left(x^2+y^2+z^2\right)=&\frac{L^4}{4}+4x^2p^2+4p^4+2L^2xp-2L^2p^2-8xp^3+\\&+4y^2q^2+4q^4-8yq^3+\left(\frac{L^2}{2}+2xp-2p^2\right)\left(4yq-4q^2\right)\end{aligned} \tag{3.55}$$

$$\begin{aligned}\left(L^2-4p^2\right)(x-p)^2+L^2y^2+L^2z^2=&\frac{L^4}{4}-L^2p^2+4q^2(y-q)^2+2L^2yq+\\&-2L^2q^2+8xypq-8xpq^2-8yp^2q+8p^2q^2\end{aligned} \tag{3.56}$$

$$\begin{aligned}\left(L^2-4p^2\right)(x-p)^2+\left(L^2-4q^2\right)(y-q)^2+L^2z^2-8(x-p)(y-q)pq=\\=\frac{L^4}{4}-L^2p^2-L^2q^2\end{aligned} \tag{3.57}$$

Renaming some parameters as

$$s_p=L^2-4p^2 \tag{3.58}$$

$$s_q = L^2 - 4q^2 \tag{3.59}$$

$$A = \frac{L^4}{4} - L^2 p^2 - L^2 q^2 \tag{3.60}$$

Then it is possible to obtain

$$a = \sqrt{\frac{A}{s_p}} = \sqrt{\frac{\frac{L^4}{4} - L^2 p^2 - L^2 q^2}{L^2 - 4p^2}} = \frac{L}{2}\sqrt{1 - \frac{4q^2}{L^2 - 4p^2}} \tag{3.61}$$

$$b = \sqrt{\frac{A}{s_q}} = \sqrt{\frac{\frac{L^4}{4} - L^2 p^2 - L^2 q^2}{L^2 - 4q^2}} = \frac{L}{2}\sqrt{1 - \frac{4p^2}{L^2 - 4q^2}} \tag{3.62}$$

$$c = \sqrt{\frac{A}{L^2}} = \frac{L}{2}\sqrt{1 - 4\frac{p^2 + q^2}{L^2}} \tag{3.63}$$

$$k = \frac{A}{8pq} = \frac{\frac{L^4}{4} - L^2 p^2 - L^2 q^2}{8pq} \tag{3.64}$$

With this new parameters, the equation of the ellipsoid becomes

$$\frac{(x-p)^2}{a^2} + \frac{(y-q)^2}{b^2} + \frac{z^2}{c^2} - \frac{(x-p)(y-q)}{k} = 1 \tag{3.65}$$

This equation is equal to Eq. (3.30) only if $q = 0$, i.e. when only the x-coordinate of the sensor is different from zero.

3.3.3. How to do in a real investigation?

It is very difficult to obtain the general equation, by considering a receiver with three components different from zero, because a cube of a polynomial of seven terms should be calculated.

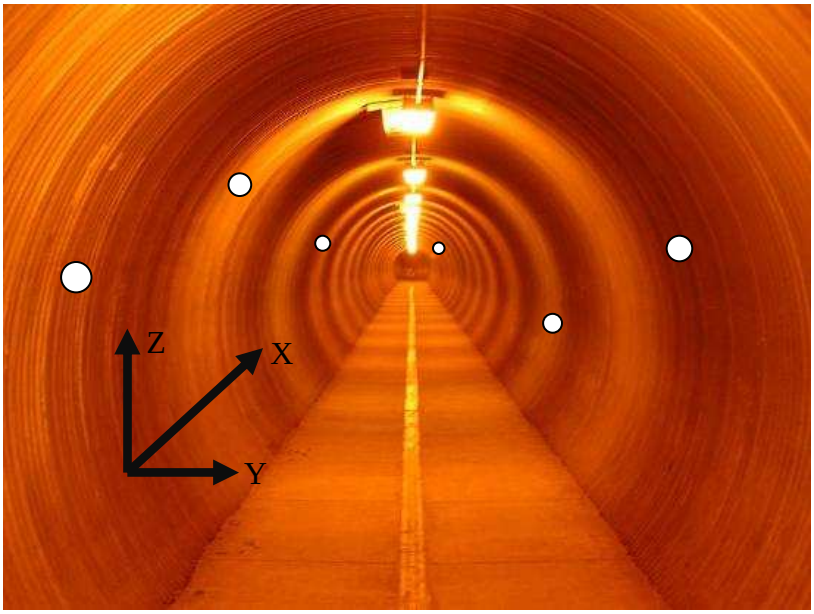

Figure 3.5. Schematic representation of the receiver positions in a tunnel investigation. The white circles represent accelerometers placed on the tunnel walls.

Anyway, in real tunnel investigations, the x-coordinate of the sensors is the predominant one. This is due to the fact that the sensors are disposed on the tunnel walls, and this is the unique direction which can be exploited to have significant distances among the receivers.

At the same time, the y-coordinate of the sensors is not equal to that of the source but is practically assumes two values (one positive and one negative).

Finally, the z-coordinate of the receivers should be chosen such that the variation respect to the z-coordinate of the source is minimum. In this case, the proposed approach can find good results.

Figure 3.5 shows a typical sensor configuration in a tunnel monitoring. The receivers are at different heights but the variation in the z-coordinate is inferior than the variation in the y-coordinate, since the tunnel width usually varies from 4 to 10 meters. The worst case is when some sensors are placed at the top of the tunnel, but this is practically less convenient because a special machine is needed to lift one person for the installation.

3.4. Characterization of the discontinuity

In this section, all the equations involving the different parameters present in the problem are listed, especially about the tangent plane, the positions of sources and receivers and the reflection points.

3.4.1. Tangent plane

Once extracted the equation of the ellipsoids, it is necessary to calculate the tangent plane in the reflection point which represents the discontinuity that generated the reflection. The tangent plane of a function $f = f(x, y, z)$ in the reflection point $P_0 = (x_0, y_0, z_0)$ is given by

$$\frac{\partial f}{\partial x}|_{P_0}\,(x - x_0) + \frac{\partial f}{\partial y}|_{P_0}\,(y - y_0) + \frac{\partial f}{\partial z}|_{P_0}\,(z - z_0) = 0 \tag{3.66}$$

Therefore, from Eq. (3.46), it is possible to write

$$\frac{2(x_0 - p)}{a^2}(x - x_0) + \frac{2y_0}{b^2}(y - y_0) + \frac{2z_0}{b^2}(z - z_0) = 0 \tag{3.67}$$

If the plane is in the standard form of the type

$$a_1 x + a_2 y + a_3 z + a_4 = 0 \tag{3.68}$$

then the coefficients are expressed by

$$a_1 = \frac{(x_0 - p)}{a^2} - \frac{(y_0 - q)}{2k} \tag{3.69}$$

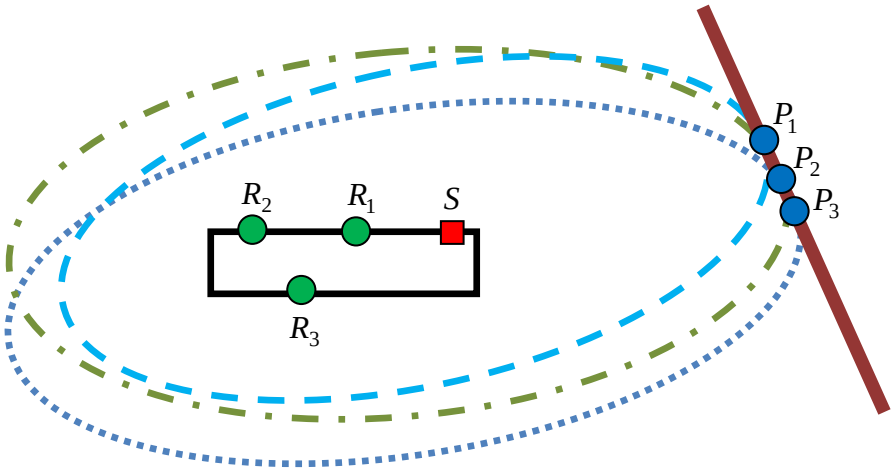

Figure 3.6. Geometric interpretation of the ellipsoids, whose common tangent plane is the discontinuity (the reflector).

$$a_2 = \frac{(y_0 - q)}{b^2} - \frac{(x_0 - p)}{2k} \tag{3.70}$$

$$a_3 = \frac{z_0}{c^2} \tag{3.71}$$

$$a_4 = -a_1 x_0 - a_2 y_0 - a_3 z_0 \tag{3.72}$$

When considering several sources and receivers, then from each source-receiver pair it is possible to build an ellipsoid and later to calculate the tangent plane. All the tangent planes are theoretically equal and they correspond to the reflector.

In Figure 3.6, three ellipsoids are constructed starting from three sensors and one common source. For each case, the reflection point is different from the other cases, but the tangent is the same and it is equal to the discontinuity.

3.4.2. Generic discontinuity

If the discontinuity is not a straight line, then some observations should be done on the problem.

First of all, as can be seen in Figure 3.7, the reflection point is depending on the tangent to the curve. Consequently it is not possible to have a direct connection between every point and its reflection point, because the shape of curve changes instantaneously and moreover, for the same reason, it is impossible to predict the distance d .

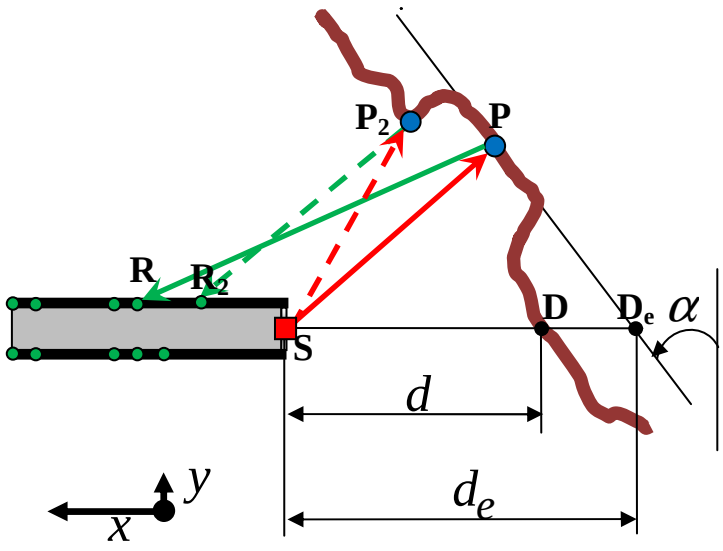

Figure 3.7. Geometric illustration of a case in which the discontinuity is not a straight line. It is represented by the thick brown line, while the tunnel is colored in red. The red lines represent the direct waves, the green lines represent the reflected waves.

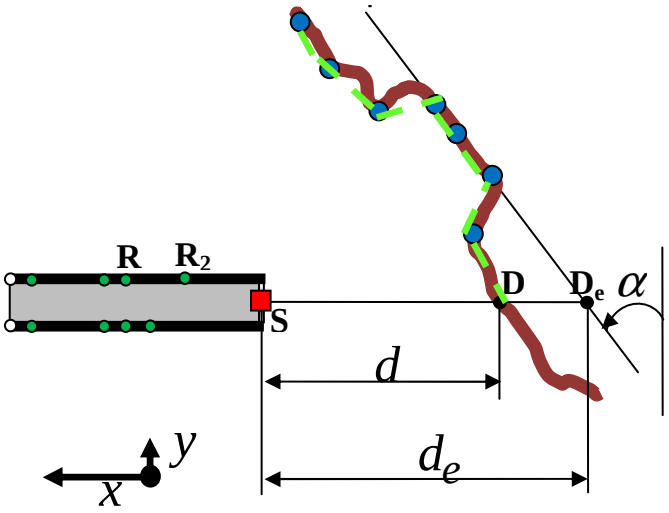

Figure 3.8. Geometric illustration of a case in which the discontinuity is not a straight line. It is represented by the thick brown line, while the tunnel is colored in red. The black dots represent some reflection points, while the dashed green line indicates the reconstruction of the discontinuity.

Indeed, by looking at Figure 3.7, the reflection in the point P leads to estimate the distance tunnel front-discontinuity as d_e instead of d. Because of the curve shape, the reflection point is not directly linked to the position of the receiver.

In order to have a complete map of the lithological variation, infinite sensors should be theoretically placed on the tunnel walls. Since in practice the number of sensors n is limited to the maximum of few tenths, the reflection points obtained should be considered zone by zone in order to create a continuous line given by different segments connecting the different reflection points estimated. Practically, a map like that in Figure 3.8 will be obtained.

Due to this facts, in order to avoid complications and long processing times, the discontinuity will be always considered as a straight line in the 2D analyses and as a plane in the 3D analyses.

3.4.3. Source and receiver position

In the previous section, it has been discussed about the case with all the sensors aligned or not to the source. This is a crucial point not only for the construction of the equations but also for the estimation of the discontinuity.

Let us analyze the configuration of Figure 3.9. Four sensors and four different sources are considered, therefore sixteen ellipsoids can be built. Actually, in this 2D case they are simply ellipses, but since the validity is general, they are called ellipsoids.

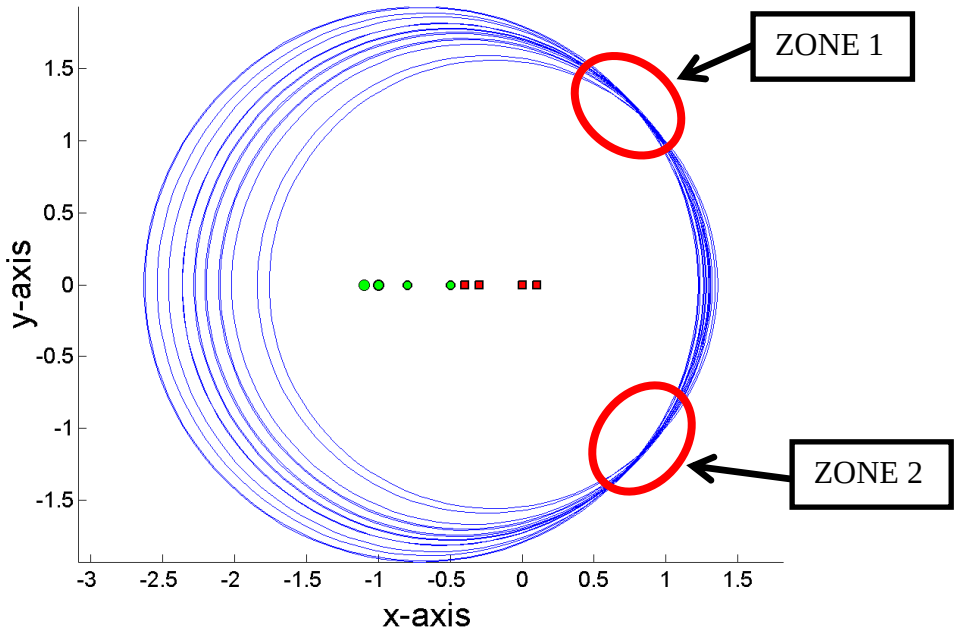

Figure 3.9. Ellipsoids built from a configuration with the sources and receivers aligned. The sources are indicated with red squares while the receivers with green circles.

There are two zones (called respectively 1 and 2) in which the ellipsoids are very close, while they are quite distinguishable in the other parts of the domain. This means that the discontinuity is tangent in one of the two zones but it is impossible to known which is the correct one, because they are completely equal. Indeed, the ellipsoids are symmetric respect to the line including the sources and the sensors.

Due to this fact, the position of the sources and of the receivers must follow a simple rule:

For the identification of a reflector, at least one element (source or receiver) must be not aligned with the other ones.

In Figure 3.10, instead, a configuration with a source not aligned with the other elements is depicted. In this case, the two zones are no more specular: the first one is similar to the previous case, with all the ellipsoids superposing in a small region, while the second one is completely different, because there is not a total superpositions of the curves. In particular, the ellipsoids created by considering the source not aligned with the other elements do not cross the reflection region identified by the other ellipsoids. This fact causes a simple interpretation: the unique part of the domain in which all the ellipsoids are crossing each other is zone 1, and then this is the reflection zone.

Moreover, the discontinuity can be detected as the tangent line to the ellipsoids in that region.

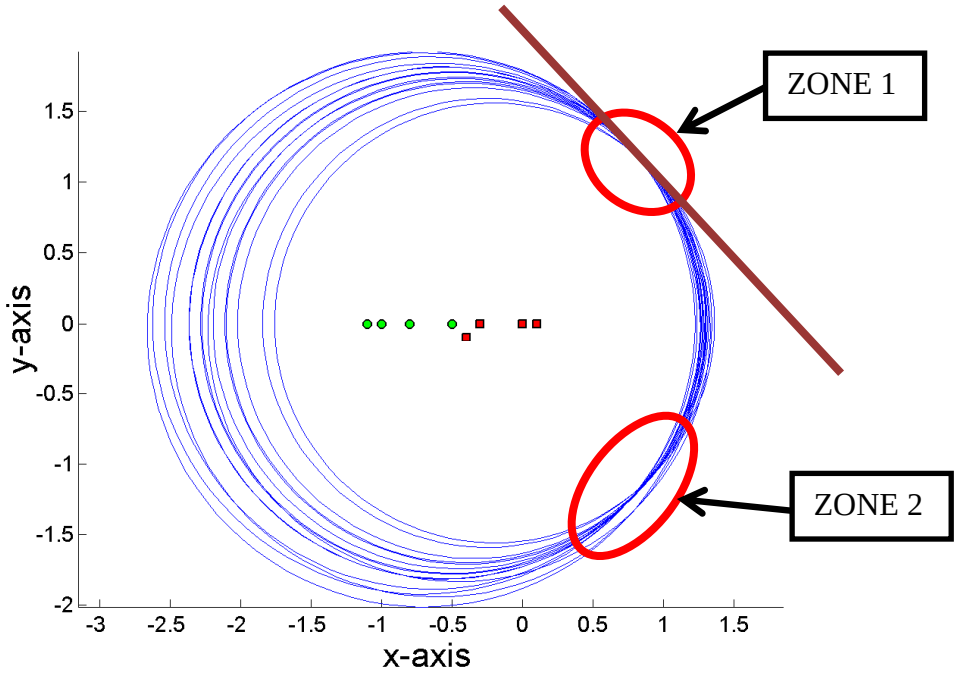

Figure 3.10. Ellipsoids built from a configuration with sources and receivers not aligned. The sources are indicated with red squares while the receivers with green circles. The discontinuity is the thick brown line.

3.5. Relationships among the receivers and reflection point

The discontinuity is defined by the parameters d, γ and α according to Eq. (3.20), (3.23) and (3.24), respectively.

If considering only one coordinate of the receiver different from zero, and starting from

$$a_4 = -a_1 x_0 - a_2 y_0 - a_3 z_0 \tag{3.73}$$

and by using the relationships expressed by Eq. (3.69)-(3.72), since the reflection point belongs to the ellipsoid, it is possible to obtain

$$\begin{aligned} a_4 &= -\frac{x_0(x_0-p)}{a^2} - \frac{y_0^2}{b^2} - \frac{z_0^2}{b^2} = -\frac{x_0(x_0-p)}{a^2} + \frac{(x_0-p)^2}{a^2} - 1 = \\ &= \frac{(x_0-p)}{a^2}(-x_0 + x_0 - p) - 1 = \\ &= -\frac{(x_0-p)}{a^2} p - 1 \end{aligned} \tag{3.74}$$

$$a_4 = -a_1 p - 1 \tag{3.75}$$

Now, the whole system involving all the relationships is therefore:

$$\begin{cases} a_1 = \dfrac{x_0 - p}{a^2} \\ a_2 = \dfrac{y_0}{b^2} \\ a_3 = \dfrac{z_0}{b^2} \\ \dfrac{a_3}{a_1} = \tan(\alpha) \\ \dfrac{a_1}{a_2} = \tan(\gamma) \\ -\dfrac{a_4}{a_1} = d \\ a_4 = -a_1 p - 1 \\ a^2 = b^2 + p^2 \end{cases} \tag{3.76}$$

In the case of two coordinate different from zero, the equations are:

$$\begin{cases} a_1 = \dfrac{(x_0 - p)}{a^2} - \dfrac{(y_0 - q)}{2k} \\ a_2 = \dfrac{(y_0 - q)}{b^2} - \dfrac{(x_0 - p)}{2k} \\ a_3 = \dfrac{z_0}{c^2} \\ a_4 = -a_1 x_0 - a_2 y_0 - a_3 z_0 \\ a = \dfrac{L}{2}\sqrt{1 - \dfrac{4q^2}{L^2 - 4p^2}} \\ b = \dfrac{L}{2}\sqrt{1 - \dfrac{4p^2}{L^2 - 4q^2}} \\ c = \dfrac{L}{2}\sqrt{1 - 4\dfrac{p^2 + q^2}{L^2}} \\ k = \dfrac{\dfrac{L^4}{4} - L^2 p^2 - L^2 q^2}{8pq} \end{cases} \tag{3.77}$$

The solution of the system of Eq. (3.76) is discussed in the next subsections.

3.5.1. Receiver position once given the reflection point

The relationship between the reflection point and the corresponding receiver is investigated. Once given a discontinuity, it is impossible to know a priori which are the values of both the parameters, then it is more convenient to start by fixing the reflection point (which belongs to the discontinuity) and then to obtain the receiver position. The reflection points are chosen in order to have values of p similar to the reality (according to the TRT scheme of Subsection 2.4.3), i.e. included between -5 m and -25 m, approximately.

If a reflection point is given, then the other parameters characterizing the equations can be calculated.

Firstly, a value for z_0 is chosen, then y_0 is calculated by considering the second, the third, the fourth and the fifth equations of the system of Eq. (3.76):

$$y_0 = \frac{z_0}{\tan(\alpha)\tan(\gamma)} \tag{3.78}$$

The x-coordinate x_0 is calculated by imposing that P_0 is on the tangent plane. The solution is given by manipulating the equations just written; the final relationships are:

$$p = \frac{dx_0 - d\dfrac{z_0}{\tan(\alpha)}}{d + x_0 - \dfrac{z_0}{\tan(\alpha)}} \tag{3.79}$$

$$a = \sqrt{(d-p)(x_0-p)} \tag{3.80}$$

$$a_1 = \frac{x_0 - p}{a^2} \tag{3.81}$$

$$b = \sqrt{\frac{z_0}{a_1 \tan(\alpha)}} \tag{3.82}$$

$$a_2 = \frac{y_0}{b^2} \tag{3.83}$$

$$a_3 = \frac{z_0}{b^2} \tag{3.84}$$

$$a_4 = -a_1 p - 1 \tag{3.85}$$

Let us observe that p depends only on x_0 and z_0, but not on y_0 and this is because there is only one receiver coordinate different from zero. In the same way, p could be defined by x_0 and y_0 and not by z_0. Therefore, the formula for the estimation of the reflection point is not theoretically correct but it represents a reasonable approximation.

3.5.2. Reflection point once given the receiver position

In a real application, the positions of the receivers are known. Since for the numerical examples the discontinuity is fixed, then the reflection point can be calculated by means of the following equations.

From $-\frac{a_4}{a_1} = d$ and $a_4 = -a_1 p - 1$:

$$a_1 = \frac{1}{d - p} \tag{3.86}$$

$$a_4 = -a_1 d \tag{3.87}$$

$$a_3 = a_1 \tan(\alpha) \tag{3.88}$$

$$a_2 = \frac{a_1}{\tan(\gamma)} \tag{3.89}$$

Then, since $b = \sqrt{\frac{z_0}{a_3}}$, $a^2 = b^2 + p^2$, $y_0 = a_2 b^2$, $x_0 = p + a_1 a^2$ then

$$z_0 = \frac{d - p - a_1 p^2}{\frac{a_1}{a_3} - \frac{1}{\tan(\gamma)}\frac{a_2}{a_3} + \tan(\alpha)} \tag{3.90}$$

and consequently b, a, y_0 and x_0.

3.6. A case study: frontal discontinuity

The discontinuity is said to be frontal if $\gamma = \pi/2$. Let us analyze this simplified case, by inspecting the reflection angle, the time arrivals and the positions of the reflection points, once given a configuration of sources and sensors.

3.6.1. Reflection angle

Starting from Eq. (3.90), the z-coordinate of the reflection point $P_0 = (x_0, y_0, z_0)$, related to the receiver with coordinates $R = (2p,0,0)$, is

$$z_0 = \frac{d - p - a_1 p^2}{\frac{a_1}{a_3} + \tan(\alpha)} = \\ = \frac{d - p - a_1 p^2}{\cot(\alpha) + \tan(\alpha)} \tag{3.91}$$

and then the following inequalities are obtained:

$$\frac{d}{\cot(\alpha) + \tan(\alpha)} < z_0 < \frac{d - 2p}{\cot(\alpha) + \tan(\alpha)} \qquad \text{if } p < 0 \tag{3.92}$$

$$\frac{d - 2p}{\cot(\alpha) + \tan(\alpha)} < z_0 < \frac{d}{\cot(\alpha) + \tan(\alpha)} \qquad \text{if } p > 0 \tag{3.93}$$

In Figure 3.11, the cross-sectional view of the discontinuity is represented, together with the reflection angle that allows the wave generated in S to be recorded in R.
The y-coordinate of the points under analysis is no more considered because $\gamma = \pi/2$.
From the figure, it is possible to understand that:

$$\overline{HD} = z_0 \tan(\alpha) \tag{3.94}$$

$$\overline{SH} = z_0 \cot(\alpha) \tag{3.95}$$

$$\overline{GD} = z_0 (\tan(\alpha) + \cot(\alpha)) \tag{3.96}$$

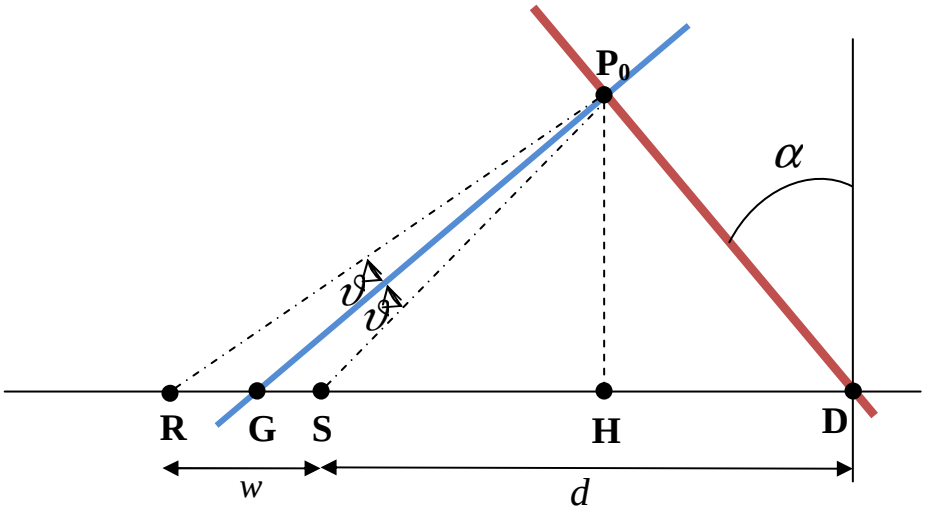

Figure 3.11. Geometric representation of a frontal discontinuity, seen in two dimensions (cross-sectional view).

$$\overline{GS} = | -p - a_1 p^2 | \tag{3.97}$$

By using the theorem of sines on the triangle P_0-G-S,

$$\frac{| -p - a_1 p^2 |}{\sin(\vartheta)} = \frac{\sqrt{x_0^2 + z_0^2}}{\sin(\alpha)} \tag{3.98}$$

and then the reflection angle is extracted:

$$\vartheta = \sin^{-1}\left(\frac{| -p - a_1 p^2 |}{\sqrt{x_0^2 + z_0^2}} \sin(\alpha) \right) \tag{3.99}$$

3.6.2. Investigation on the reflection point

All the relationships written up to now can be visualized through the numerical example here proposed. The case under study is a discontinuity with $\gamma = \pi / 2$ and the purpose is to verify if the reflection point can be considered unique. This topic is very important not only for the modeling but for the two methodologies proposed in the thesis: the forward method (Chapter 4) and the backward method (Chapter 5).

If the reflection point can be approximately considered as unique, then all the relationships connecting the different parameters can be simplified because it is no more necessary to calculate each single reflection point.
In the simulation created in *Matlab*®, the given data are the discontinuity and the reflection point. The parameters of the discontinuity are taken directly from a simulation produced previously in *Comsol Multiphysics*®:

$$d = 216.84 \tag{3.100}$$

$$\alpha = 38° \tag{3.101}$$

$$\gamma = 90° \tag{3.102}$$

Table 3.1. Coordinates of reflection points and corresponding receivers, for the simulation with the discontinuity indicated by Eq. (3.100)-(3.102).

Coordinates of P_0			Coordinates of R		
124.0000	0	118.8318	-64.5615	0	0
124.3000	0	118.4479	-62.4808	0	0
124.6000	0	118.0639	-60.4175	0	0
124.9000	0	117.6799	-58.3712	0	0
125.2000	0	117.2959	-56.3419	0	0
125.5000	0	116.9119	-54.3292	0	0
125.8000	0	116.5279	-52.3330	0	0
126.1000	0	116.1439	-50.3530	0	0
126.4000	0	115.7599	-48.3891	0	0
126.7000	0	115.3759	-46.4411	0	0
127.0000	0	114.9919	-44.5087	0	0
127.3000	0	114.6079	-42.5919	0	0
127.6000	0	114.2240	-40.6903	0	0
127.9000	0	113.8400	-38.8039	0	0
128.2000	0	113.4560	-36.9324	0	0
128.5000	0	113.0720	-35.0757	0	0
128.8000	0	112.6880	-33.2336	0	0
129.1000	0	112.3040	-31.4059	0	0
129.4000	0	111.9200	-29.5924	0	0
129.7000	0	111.5360	-27.7931	0	0
130.0000	0	111.1520	-26.0076	0	0
130.3000	0	110.7680	-24.2360	0	0
130.6000	0	110.3840	-22.4779	0	0
130.9000	0	110.0001	-20.7333	0	0

The abscissa of the reflection point is varying from 124 to 130.9 m, the ordinate is null and the z-coordinate is calculated by imposing the reflection point on the discontinuity. In Table 3.1, the positions of the sensors (only the x-coordinate is different respect to the source) are listed. Even if the reflection points are quite close each other, the receivers have a significant distance among them, since they lie on a line which is about 45 meters long.

This result is obviously depending on the inclination of the discontinuity, but this can be seen a representative example, since it is impossible to compare the coordinates of the receivers for different inclinations, once given the reflection points.

If the coordinates of the receivers are more distant from the source, then the reflection points would be closer among each other and this means that the approximation of considering a unique P_0 is sufficiently good.

This is a useful practical indication for the sensor placement in a real tunnel survey: if they are close to the source then the reflection point cannot be considered as unique, otherwise the approximation is valid. However, the study of an optimum configuration of both sensors and sources is still a challenge.

3.6.3. Time arrivals

In Figure 3.12, the time arrivals of the reflected waves are presented, for the case under analysis. The trend is slightly nonlinear, even if it is difficult to understand from the figure.

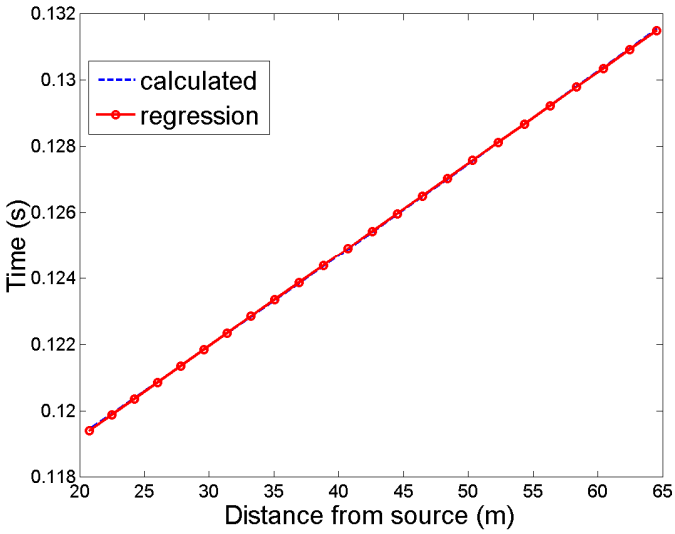

Figure 3.12. Time arrivals of the reflected waves as function of the receiver positions, for the simulation with the discontinuity indicated by Eq. (3.100)-(3.102).

This is due to the fact that :

$$t = \frac{L}{v} = \frac{\sqrt{x_0^2 + y_0^2 + z_0^2} + \sqrt{(x_0 - x_R)^2 + y_0^2 + z_0^2}}{v} \tag{3.84}$$

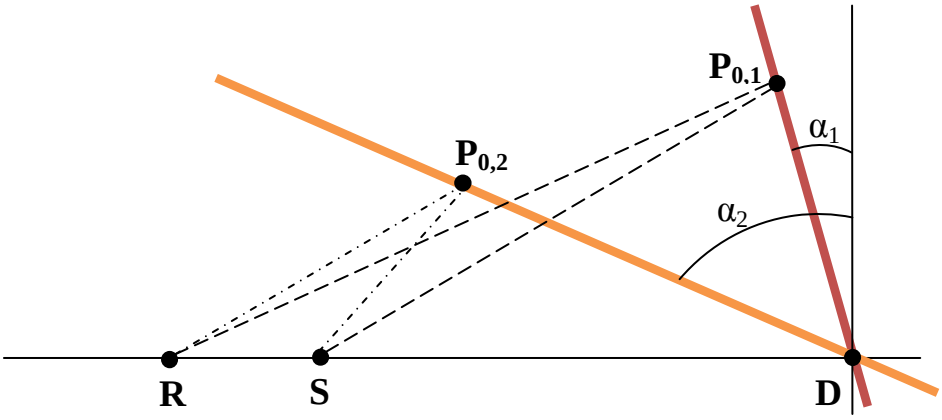

Figure 3.13. Graphical representation of reflection with discontinuities with different inclinations.

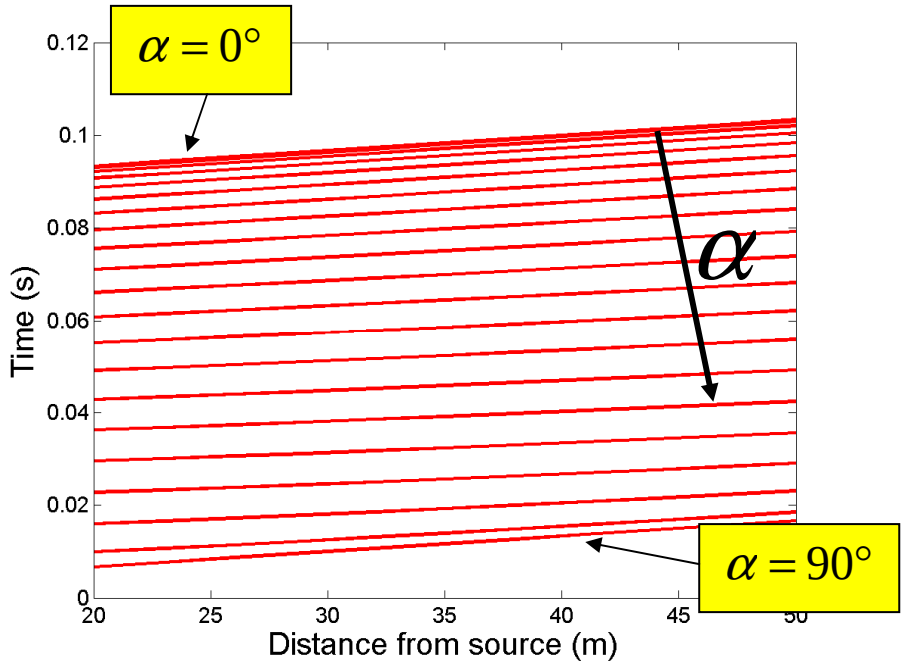

Figure 3.14. Time arrivals of the waves, as function of the receiver positions and for different values of the angle α.

and, since the velocity is constant, then the time arrivals has the same trend of the distance $\overline{SP} + \overline{PR}$. The time arrivals are disposed on a line only if the angle α is equal to zero, which corresponds to the case when z_0 and y_0 are equal to zero.

To better highlight this fact, another simulation where α is varying from 0 to 90° is created, with the distance $d = 216.84$ and the angle $\gamma = 90°$, as for the previous simulation. The receiver positions varies within the range $(-50,-20)$ m, with step equal to 3.

If α is small (with the same d), then more time is need to reach the receiver because the reflection point is farther from the source, as can be clearly seen in Figure 3.13, where $\alpha_1 < \alpha_2$.

In Figure 3.14, the time arrivals of the waves, for the different positions of the receivers and for the different inclinations are shown. In particular, α has been chosen within the interval $(0°, 90°)$, in order to treat all the possible configurations.

The final case $\alpha = 90°$ is unexpected because it has a different tendency respect to the other cases. In order to understand the reason of this result, a polynomial regression of order 2 is applied on each time arrivals and the three coefficients p_0, p_1 and p_2 (related to order zero, one and two respectively) obtained are plotted against α, as can be seen in Figure 3.15. To build this figure, many intermediate cases between $\alpha = 0°$ and $\alpha = 90°$ are considered.

From Figure 3.15a, it follows that the constant term is monotonically decreasing until to reach the zero value for $\alpha = 90°$. In Figure 3.15b and 3.15c, the trend is monotone until about 80°, then there is apparently an inexplicable inversion. More deeply, this is not an incongruence, because when the inclination of the discontinuity is very high, the reflection points are close to the sensors and this fact can cause some strange trends due to the geometric relationships involving the different variables.

Moreover, the coefficient p_2 is equal to zero if $\alpha = 0$ and then it increases monotonically: this means that only when $\alpha = 0$ the trend is a line, as already said about Figure 3.12.

Conclusively, the time arrivals of the reflected waves are always increasing with the distance source-receivers and the trend is given according to the inclination of the discontinuity and the positions of the receivers.

The last parameter that can be shown is the reflection angle ϑ, visible in Figure 3.16. It is equal to 0 when $\alpha = 0$, and equal to 90° if $\alpha = 90°$, because in that cases the reflection is in the same direction of the wave direction. In all the other cases, $\vartheta < \alpha$.

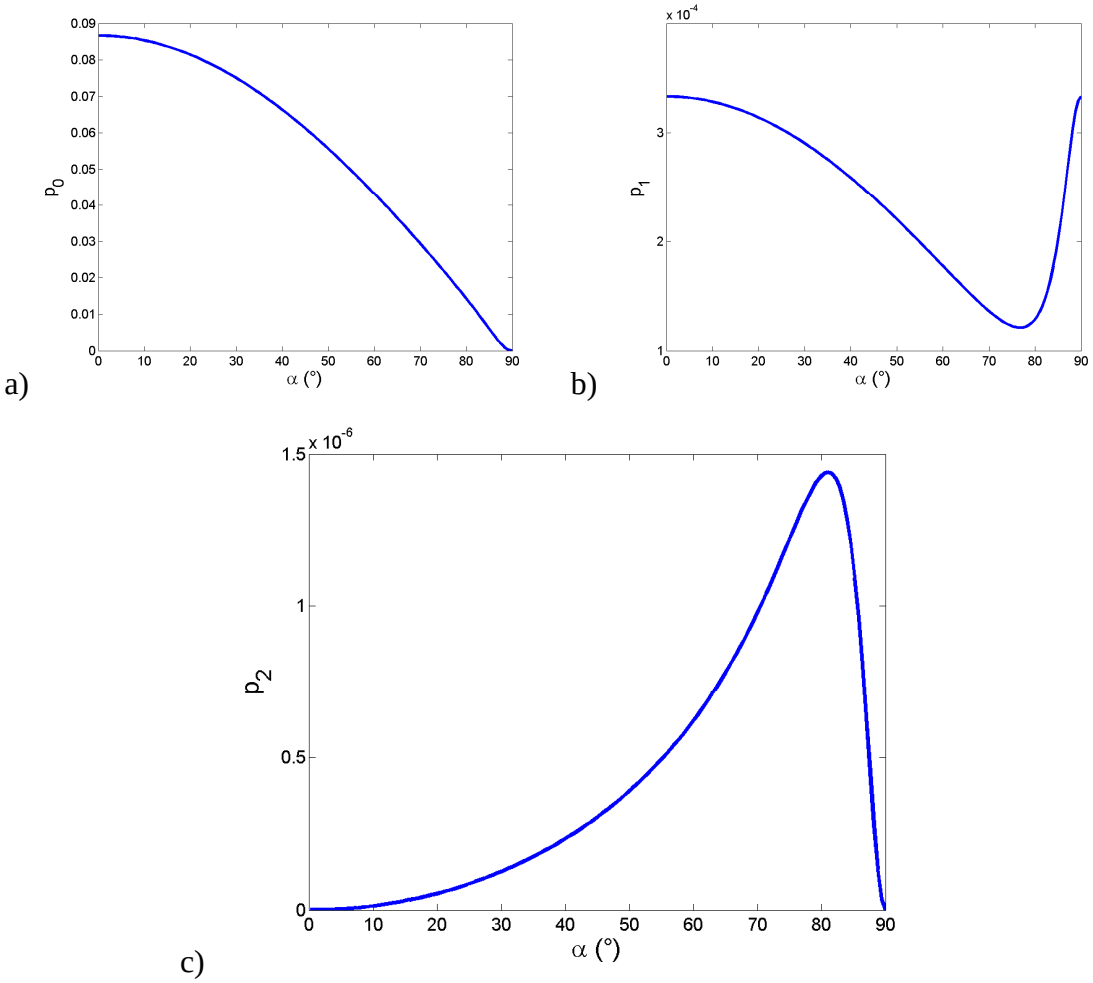

Figure 3.15. Trend of the three coefficients p_0, p_1 and p_2 in function of the angle α.

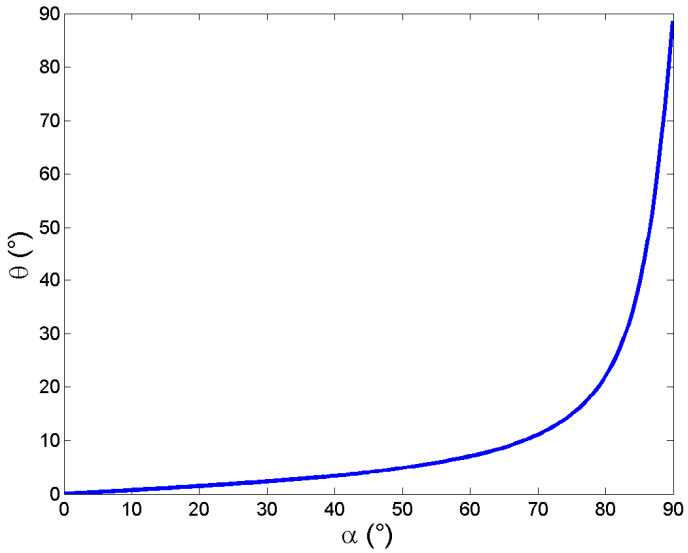

Figure 3.16. Reflection angle as function of α.

Chapter 4

The ellipsoid method for the estimation of discontinuities

The direct consequence of the studies presented in the previous chapter is the definition of a method which is able to identify the discontinuities by knowing the positions of receivers and sources, and the traces recorded by the sensors.
Let us define in general what an inverse problem is and then let us present the forward method, followed by some numerical examples.

4.1. The meaning

In general, an inverse problem is a problem where the purpose is to identify some unknown characteristics of the system under analysis by knowing only some quantities that have been measured or recorded. This concept can be adopted in many engineering and science fields and often it assumes a different denomination according to the specific field of study.
The method presented in this chapter is called ellipsoid method and it is basically a "forward method". This denomination means that the identification is conducted starting from the knowledge of the basilar quantities available and then the estimation is done by using the relationships presented in Chapter 3. In this sense, "forward" means that there are no iterations or *predictor-corrector* approaches inside the methodology, therefore it can be interpreted as a direct estimation method.
Our goal is to detect rock discontinuities ahead of the tunnel front, by knowing only three sets of parameters:

- the positions of the source points
- the positions of the receivers

- the time arrivals corresponding to the reflected waves

Clearly, both the positions of sources and receivers are measured manually, while the first time arrivals must be extracted from the traces recorded by the sensors.

4.2. The ellipsoid method

The idea of the ellipsoid method begins with Figure 3.9 and Figure 3.10, where many ellipsoids created from each source-receiver pair are depicted. The zone of larger concentration of ellipsoids is the reflection zone. This is the base of the procedure presented: the critical zone must be estimated automatically and then the discontinuity can be reconstructed by calculating the tangent plane.

This modus operandi has been chosen in order to find a solution for the problem expressed by Eq. (3.18) since the analytical approach is not sufficient.

Let's now analyse the different parts of the methodology.

4.2.1. Construction of the ellipsoids

This is the first part of the algorithm, where the data obtained from the analyses of the recorded traces are collected and then used to construct the ellipsoid. Let's consider a configuration with n_S sources and n_R receivers.

First of all, an approximation of the medium velocity v must be given, by inspecting the first time arrivals of the direct waves. Successively, the values of the first arrivals of the reflected waves are collected. They are indicated by t_i, $(i = 1,..., n_S \times n_R)$ meaning that they come from all the combinations sources-receivers.

Both the arrival times related to direct and reflected waves are extracted manually from the seismogram including all the traces. This operation usually requires a certain geophysical experience because it is not always simple to detect and distinguish the different events.

The total amount of meters covered by the wave is given by

$$L_i = vt_i \tag{4.1}$$

The ellipsoids can be now constructed, by using the Ashida's formula:

$$\frac{x^2}{L_i^2 - 4x_s^2} + \frac{y^2}{L_i^2 - 4x_s^2} + \frac{z^2}{L_i^2} = \frac{1}{4} \tag{4.2}$$

where x_S is the x-coordinate of the source, according with the reference system of Figure 3.4a.

If the ellipsoids are rewritten in the classical form

$$\frac{x^2}{a^2}+\frac{y^2}{a^2}+\frac{z^2}{b^2}=1 \tag{4.3}$$

Then, it is possible to highlighting that the axes are defined respectively by:

$$a^2=\frac{L_i^2-4z_{S_i}^2}{4} \qquad b^2=\frac{L_i^2}{4} \tag{4.4}$$

4.2.2. Search of the reflection point

The most important part of the algorithm is the search of the reflection point for each ellipsoid, and of the reflection zone because after that the discontinuity is easily detected by calculating the tangent plane in that point.

The basic idea on which the forward method proposed is built is that the ellipsoids intersect not in a zone but in a single point, which is the reflection point. As already studied in Subsection 3.6.2, this approximation can be considered valid when the discontinuity is sufficiently away from the receivers.

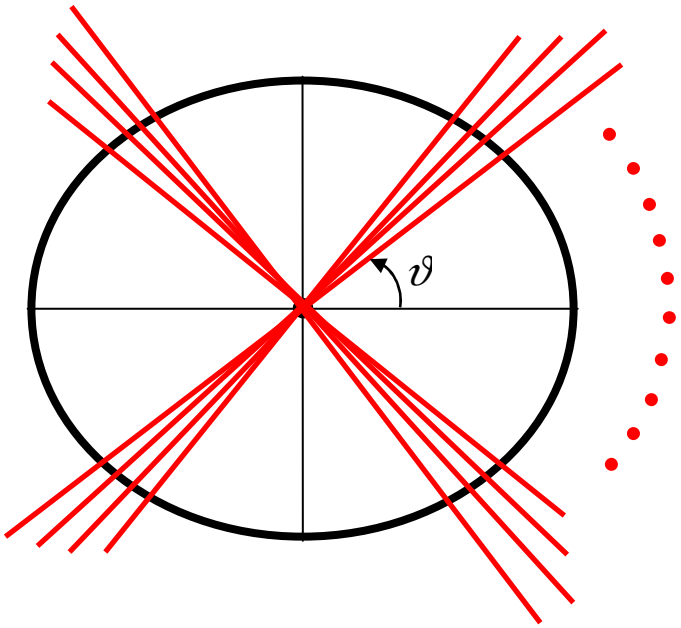

Figure 4.1. Intersection of the lines with different angles with the ellipsoids.

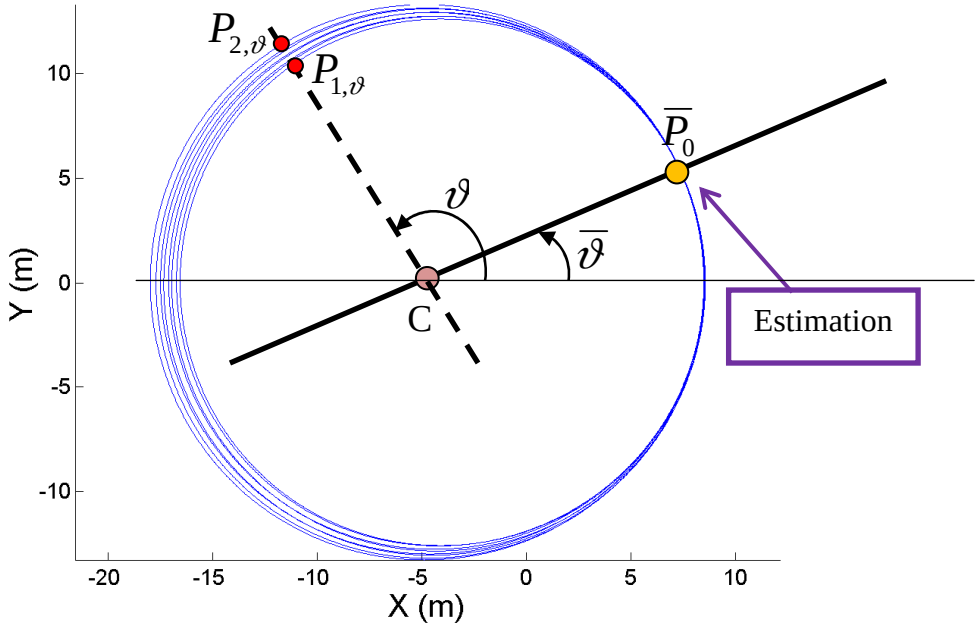

Figure 4.2. Representation of the procedure for the search of $\overline{P}_0$, together with the points $P_{1,\vartheta}$ and $P_{2,\vartheta}$, which indicate the closest and the farther point belonging to the ellipsoids, for the line with angle ϑ.

The search of the reflection point is divided in two parts:

1. a first indication of its position
2. estimation of the precise location

The first part takes the entire space into account, and tries to identify where the reflection zone is.

Consider a set of angles included in the interval $(0,\pi]$, where the generic angle is called ϑ (see Figure 4.1). These angles form different lines that intersect each ellipsoid in two opposite points. Moreover, as represented in Figure 4.2, two points can be detected for each slope:

- $P_{1,\vartheta}$: the point closest to C
- $P_{2,\vartheta}$: the point farthest from C

The center point C in which all the lines intersect is the center of the smallest ellipsoid. The intersection between the lines and the ellipsoids is implemented in the software *Matlab*® by means of the symbolic calculus, to easily deal with 2D and 3D problems.

The best angle $\overline{\vartheta}$ is found as that who minimizes the distance between $P_{1,\vartheta}$ and $P_{2,\vartheta}$. After that, $\overline{\vartheta}$ is inserted in the analytical relationships of the ellipsoids, and the coordinates of the point are obtained by averaging among the values obtained:

$$\overline{P}_0 = (\overline{x}_0, \overline{y}_0, \overline{z}_0) \tag{4.5}$$

The result obtained represents only an initial estimation of the real location of the reflection point, because of computational efforts that should be spent in 3D if a high definition of the region is desired. For this reason, the set of the angles ϑ is usually chosen quite small, with few tenths of angles.
Successively, the second part of this step tries to improve the initial approximation.
Here, a small neighbor of $\overline{P}_0$ is considered and this domain is finely discretized. The zone is simply determined by two constants K and n_p representing the domain size and the number of x, y and z points in which the zone is discretized, respectively:

$$x_{adm} = [\overline{x}_0(1 \pm K)] \qquad y_{adm} = [\overline{y}_0(1 \pm K)] \qquad z_{adm} = [\overline{z}_0(1 \pm K)] \tag{4.6}$$

For all points of the zone, the sum of the distances from the closest point of every ellipsoid to each point of the domain must be calculated and successively the reflection point P_0 is extracted as the point that minimizes this function.

4.2.3. Calculation of the tangent plane

To identify the discontinuity, the tangent plane must be calculated after having considered the point $P_i = (x_i, y_i, z_i)$ on each ellipsoid which is the closest to P_0:

$$\frac{\partial f_i}{\partial x}|_{P_i}\,(x - x_i) + \frac{\partial f_i}{\partial y}|_{P_i}\,(y - y_i) + \frac{\partial f_i}{\partial z}|_{P_i}\,(z - z_i) = 0 \tag{4.7}$$

where $f_i(x, y, z) = 0$ indicates the ellipsoid equation.
The equation of the plane, after having applied Eq. (4.2) and Eq. (4.7)

$$\frac{x_i}{L_i^2 - 4x_s^2}(x - x_i) + \frac{y_i}{L_i^2 - 4x_s^2}(y - y_i) + \frac{z_i}{L_i^2}(z - z_i) = 0 \tag{4.8}$$

This equation can be rewritten as:

$$a_1 x + a_2 y + a_3 z + a_4 = 0 \tag{4.9}$$

where the constant coefficients are expressed by:

$$a_1 = \frac{x_i}{L_i^2 - 4x_s^2} \tag{4.10}$$

$$a_2 = \frac{y_i}{L_i^2 - 4x_s^2} \tag{4.11}$$

$$a_3 = \frac{z_i}{L_i^2} \tag{4.12}$$

$$a_4 = -\frac{x_i}{L_i^2 - 4x_s^2} x_i - \frac{y_i}{L_i^2 - 4x_s^2} y_i - \frac{z_i}{L_i^2} z_i \tag{4.13}$$

Now, by intersecting the tangent plane with the horizontal line representing the tunnel axis, the distance d_i between the cutter head and the discontinuity is estimated.

$$d_i = -\frac{a_4}{a_1} \tag{4.14}$$

The angle α_i is calculated as

$$\alpha_i = \tan^{-1}\left(\frac{a_3}{a_1}\right) \tag{4.15}$$

while the angle γ_i is computed as

$$\gamma_i = \tan^{-1}\left(-\frac{a_1}{a_2}\right) \tag{4.16}$$

4.2.4. Estimation of the discontinuity

In the last part, the results of the previous step are averaged to obtain the final estimation d_S, α_S and γ_S.

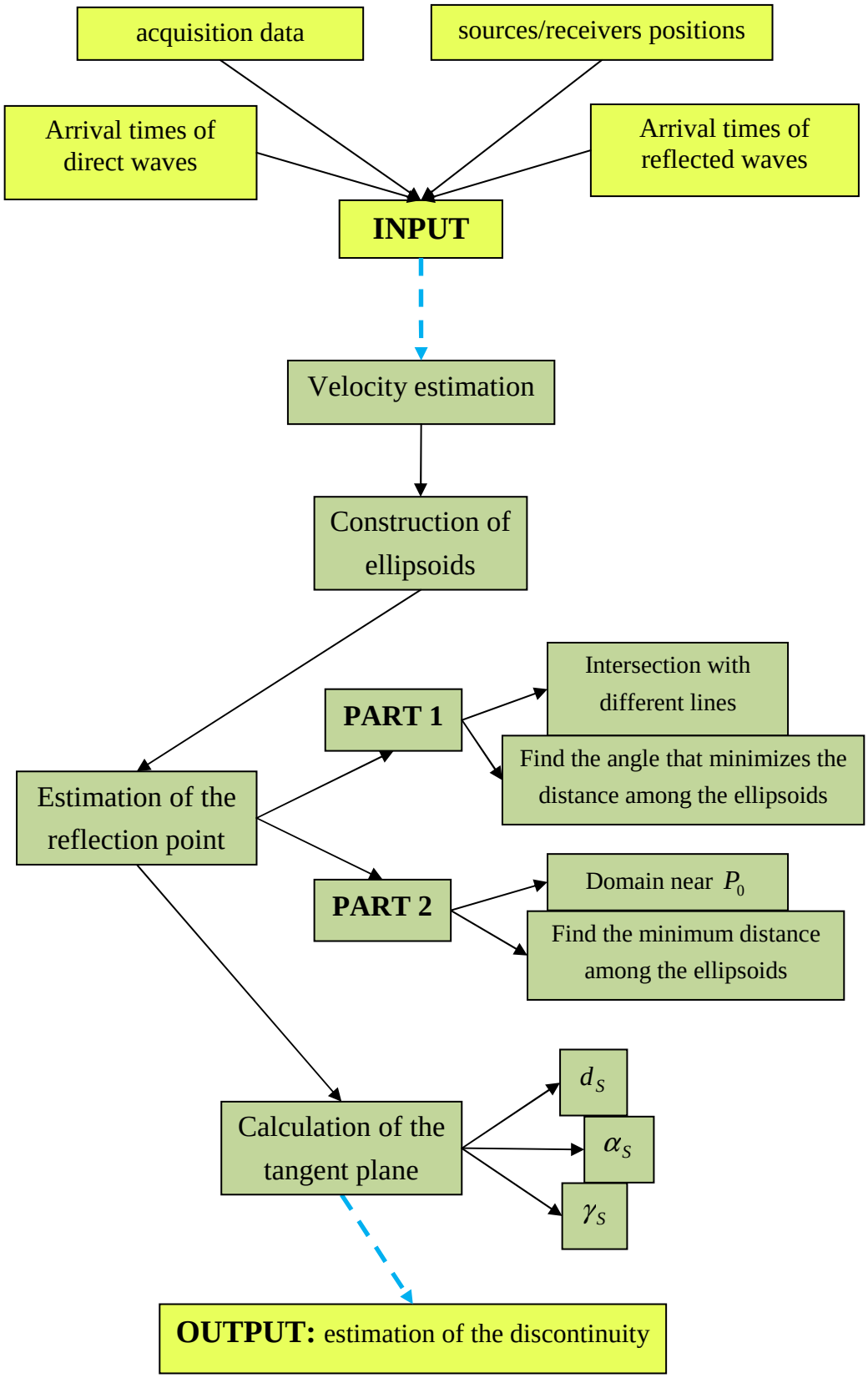

Figure 4.3. Scheme of the ellipsoid method.

These three parameters allow to completely identify the discontinuity.
All the steps of the procedure are listed in the Figure 4.3.

4.3. Numerical simulations in Matlab®

The first examples created in order to test the reliability of the method are developed by means of the software *Matlab*®.
The first configuration analyzed is characterized by 10 receivers disposed on a straight line and 3 aligned sources. The parameters characterizing the discontinuity are listed in Table 4.1, together with the results of the ellipsoid method in presence of 0% and 3% of white noise, added to the space travelled by the reflected wave.
In Figure 4.4 and 4.5, instead, the representations of the estimations, together with the ellipsoids, is depicted.

Table 4.1. Real parameters of the simulation compared with the result obtained with 0% and 3% of noise.

Parameters	Results for 0% of noise	Results for 3% of noise
$d = 45$ m	46.33 m	44.36 m
$\alpha = -36°$	-37.07°	38.50°

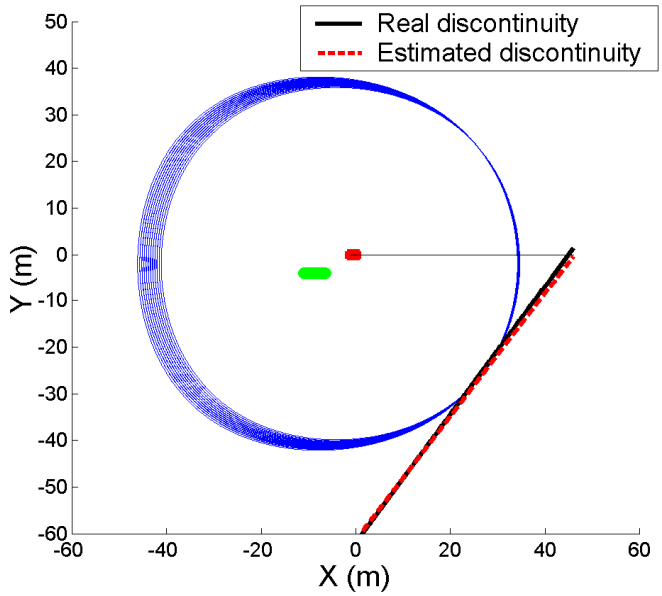

Figure 4.4. Estimation of the discontinuity by means of the ellipsoid method, for the case under analysis, with no added noise.

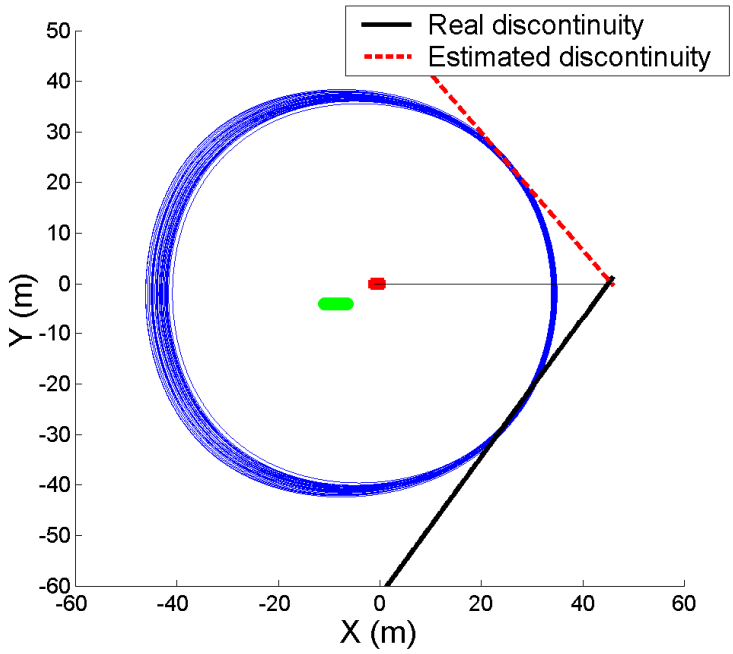

Figure 4.5. Estimation of the discontinuity by means of the ellipsoid method, for the case under analysis, with 3% of added noise.

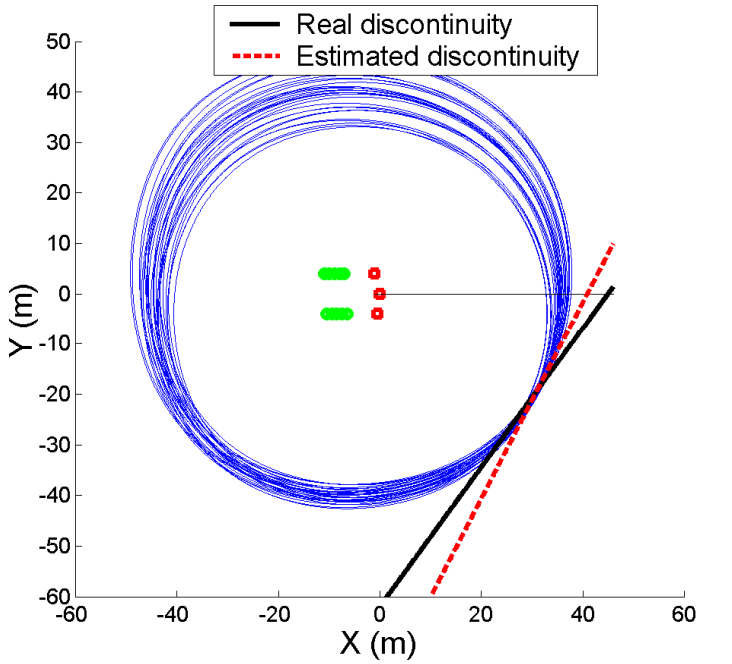

Figure 4.6. Estimation of the discontinuity by means of the ellipsoid method, for the case with the sensor and sources as in a real TRT tunnel survey, with 3% of added noise.

In absence of noise, the results are very good but in presence of a realistic percentage of noise (3%) the estimated angle is opposite to the real value, because in this case the algorithm is no more able to understand where the reflection zone is, but anyway the estimation of distance d is very accurate.

Successively, another simulation is proposed, with a configuration of sensors and sources similar to a real TRT tunnel survey (see Subsection 2.4.3). A 3% of white noise is added to the space travelled by the reflected wave, as in the first two examples. In this case, the results are represented in Figure 4.6. The dispositions of sensors and sources allow to construct different ellipsoids which are close to each other only in a precise region that correspond to the reflection zone. However, the estimation is not so accurate, since the angle estimated is $\alpha_S = -27.23°$ and $d_S = 40.90\,\text{m}$.

This example is useful to understand that is the sensors and the sources are more distributed in the domain, then the reflection zone is identified with minor ambiguity.

4.4. A numerical simulation in Reflex

This section is dedicated to the analysis of the data simulated with the software named *Reflex*. The purpose is to distinguish the different wave phenomena in the seismogram and to estimate the discontinuity inserted in the model.

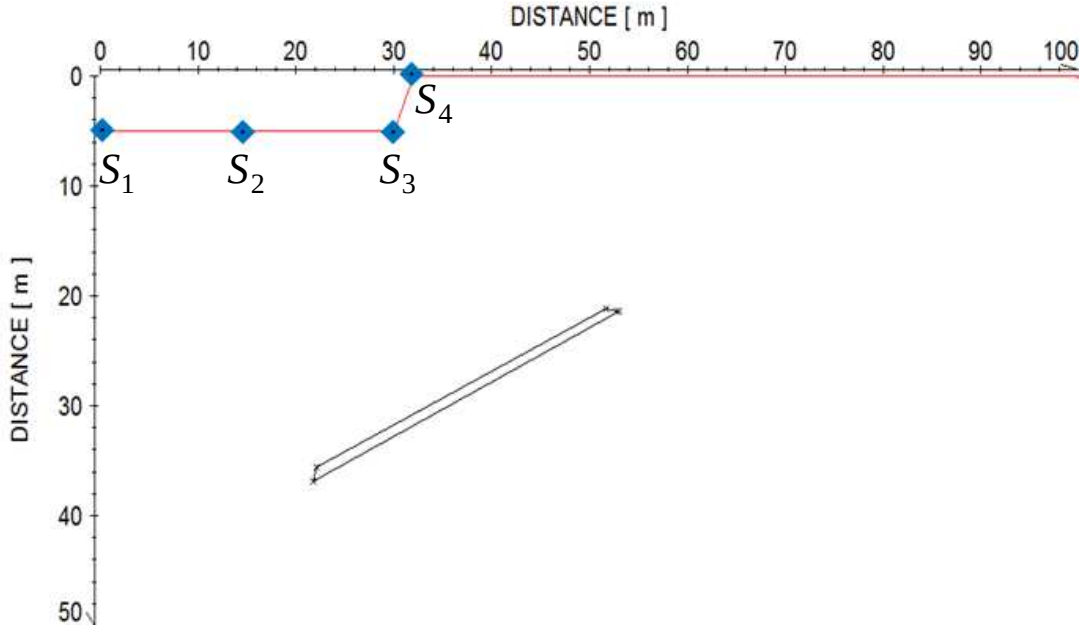

Figure 4.7. Geometric description of the numerical simulation created with *Reflex*, in which the sources and the discontinuity are represented.

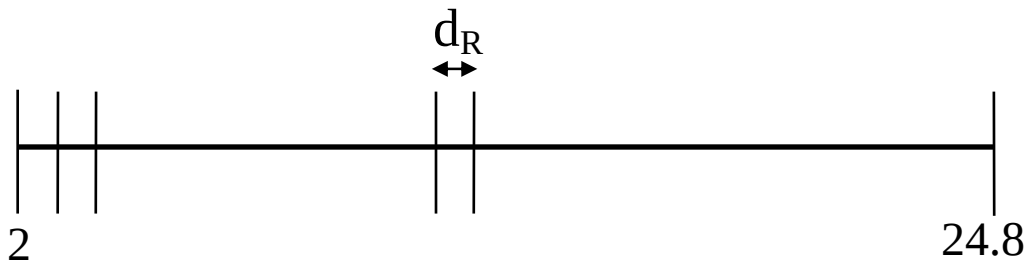

Figure 4.8. Disposition of the receivers along the tunnel.

4.4.1. Physical description

Four acquisitions have been simulated based on the geometry represented in Figure 4.7, where:

- The red line indicates the tunnel, from the beginning ($x = 0$) to the end ($x = 32$)
- The blue rhombi represent the sources considered in each acquisition
- The black line indicates the discontinuity

The simulation reproduces a configuration of a real tunnel survey. Here, the tunnel is five meters large and 58 sensors are placed on the right wall, with an abscissa varying from 2 m to 24.8 meters, in agreement with Figure 4.8. The spatial interval between two successive receivers is equal to $d_R = 0.4$ m.

The entire domain have been discretized with a spatial resolution of $\Delta x = 0.4$ m, while the sampling frequency is equal to 5000 Hz. The medium is characterized by

- P-wave velocity: $v_P = 2000$ m/s
- S-wave velocity: $v_S = 1200$ m/s
- material density: $d = 2500$ kg/m^3

The fracture is embedded by water and debris ($v_P = 1500$ m/s, $v_S = 500$ m/s, $d = 1000$ kg/m^3).

Table 4.2. Characteristics of the different simulations.

Source	Source position
S_1	$S_1 = (1,5)$
S_2	$S_2 = (15,5)$
S_3	$S_3 = (30,5)$
S_4	$S_4 = (32,0)$

The source was simulated using a Kuepper wavelet, centered at the frequency of 150 Hz. The source is able to generate both P-waves and S-waves.
The characteristics of the four files generated can be seen in Table 4.2. The analysis procedure is composed by different parts:

- Identification of the wave phenomena
- Estimation of the velocity of the waves by looking at the direct waves
- Extraction of the first time arrivals of the reflected waves
- Application of the ellipsoid method
- Interpretation of the results

4.4.2. Identification of the wave phenomena

The first step is based on the interpretation of the seismogram. In particular, it is necessary to distinguish:

- the wave nature (direct wave, reflected wave, refracted wave, diffracted wave).
- the type of wave (P-wave, S-wave, superficial wave)

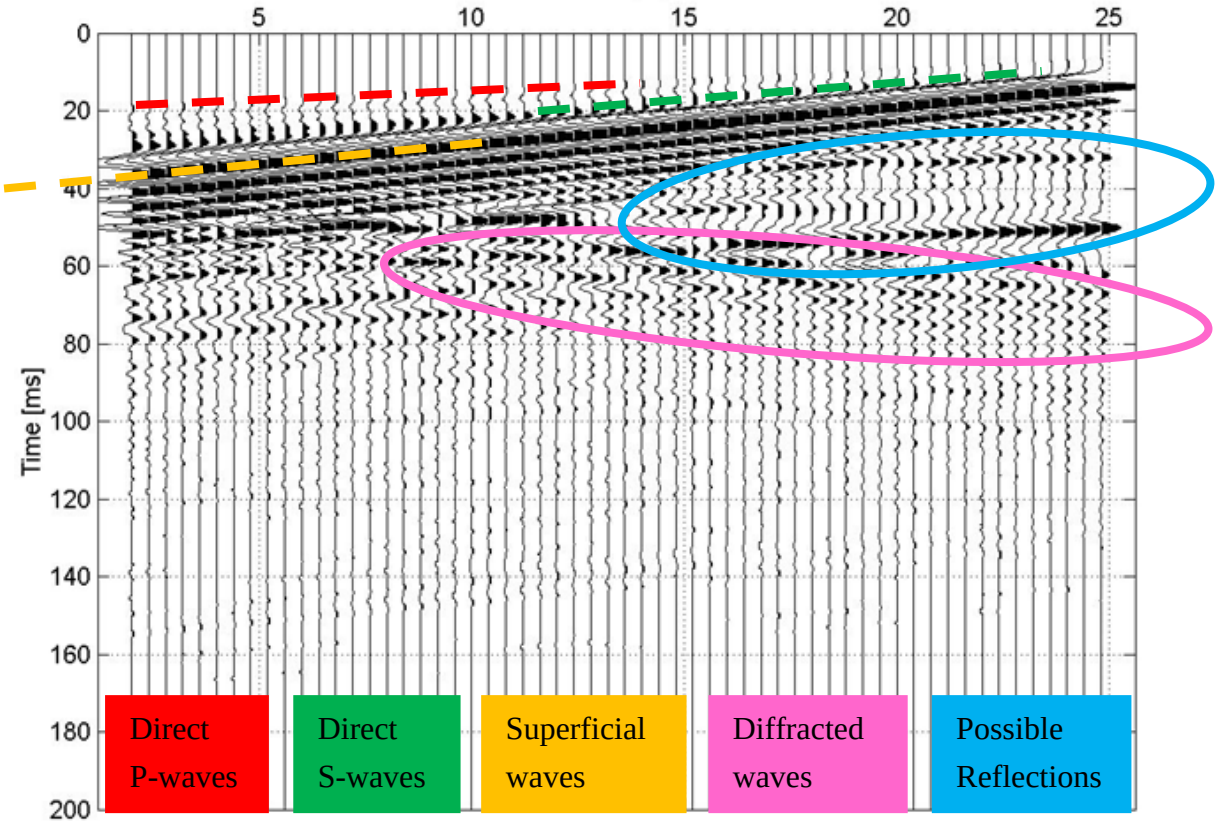

Figure 4.9. Seismogram relative to the numerical simulation created with *Reflex*, considering source S_4, and relative interpretation of the wave phenomena.

In Figure 4.9, the seismogram of the first file is analysed. As expected, the P-waves are responsible for the first variation of the signals; moreover, they have small amplitudes. The S-waves, instead, are slower but more energetic. The superficial waves, finally, are the most energetic and their presence can be easily detected.
Below the zone dominated by the direct waves, some reflective phenomena can be distinguished, but a more accurate analysis is needed in order to select the real reflections and to associate them to the correct type of waves.
The diffracted waves add lots of disturb to the seismogram.

4.4.3. Estimation of the velocity

The estimation of the velocity is based on the extracted direct waves.
In Figure 4.10, the time arrivals of the direct waves are represented for the source S_3. The velocity obtained from the linear regression is equal to $v_{P,3} = 1858.8$ m/s, with a relative error of 7.06%.
For source S_1 and S_4 the estimated velocity is equal to $v_{P,d} = 1813.2$ m/s and $v_{P,d} = 1894.9$ m/s, respectively. The case with S_2 has not be considered.
The estimation of the velocity of the P waves was not so satisfying as expected, since the relative error calculated with the real value varies from 5% to 9%. A possible explanation is the interaction with other types of wave.

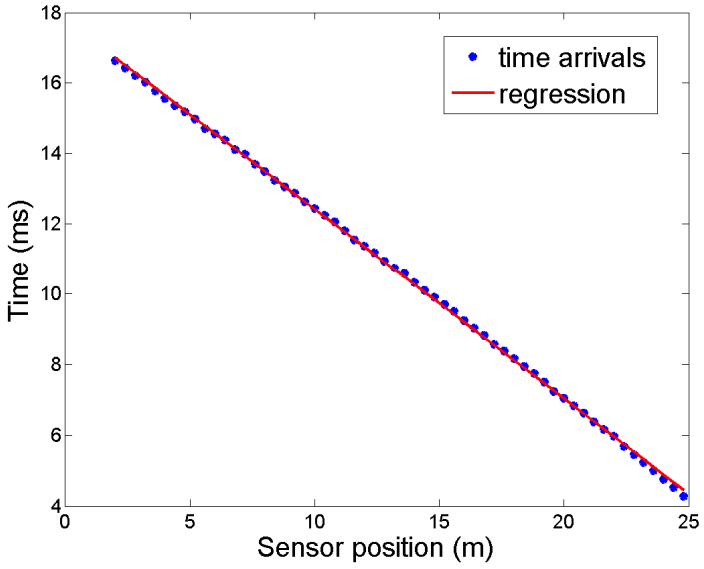

Figure 4.10. Time arrivals of the direct P-waves, for the source S_3.

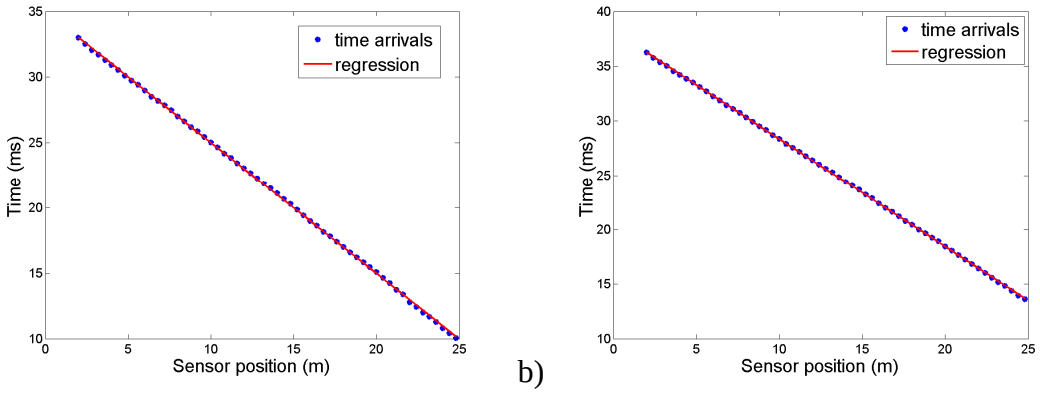

a) b)

Figure 4.11. Time arrivals of the superficial waves, for the source S_3 and S_4.

Let's analyze the S-waves of the cases S_1, S_3 and S_4. The combined velocity estimated is equal to 1180.1 m/s, with a relative error of 1.16%. In this case, the results are very accurate.

There is another type of waves which is very important in this simulation as well as in tunnel surveys: the superficial waves. They are the most energetic waves and therefore they are very simply identified. According to the theory, the velocity of the superficial waves is about the 90% the velocity of the S-waves, as already seen in Eq. (2.10). In this case, the values expected will be therefore around 1000 m/s.

In Figure 4.11 the time arrivals of the superficial waves for the source S_1 and S_2 are shown. The velocities extracted are equal to 1010.1 m/s and 997.4 m/s, respectively.

4.4.4. Reflected waves

The analysis of reflected waves is much more difficult than respect of the analysis of the direct waves. In particular, it is difficult to distinguish the reflections among all the peaks, especially because of the interferences of other waves and the dissipation of energy during the wave travel time. Moreover, the precise time instants in which the wave crosses each receiver (not the positive or negative peak) are needed.

The procedure for the extraction of the reflected waves is composed by four steps:

1. Identify a possible reflection.
2. Consider, for each receiver, the positive or the negative peaks belonging to the reflection event considered.
3. Subtract a fix value (chosen from the traces with higher signal-to-noise ratio), such that the final value corresponds to the real arrival time of the wave.
4. Identify the type of wave corresponding to the reflection (P-wave or S-wave).

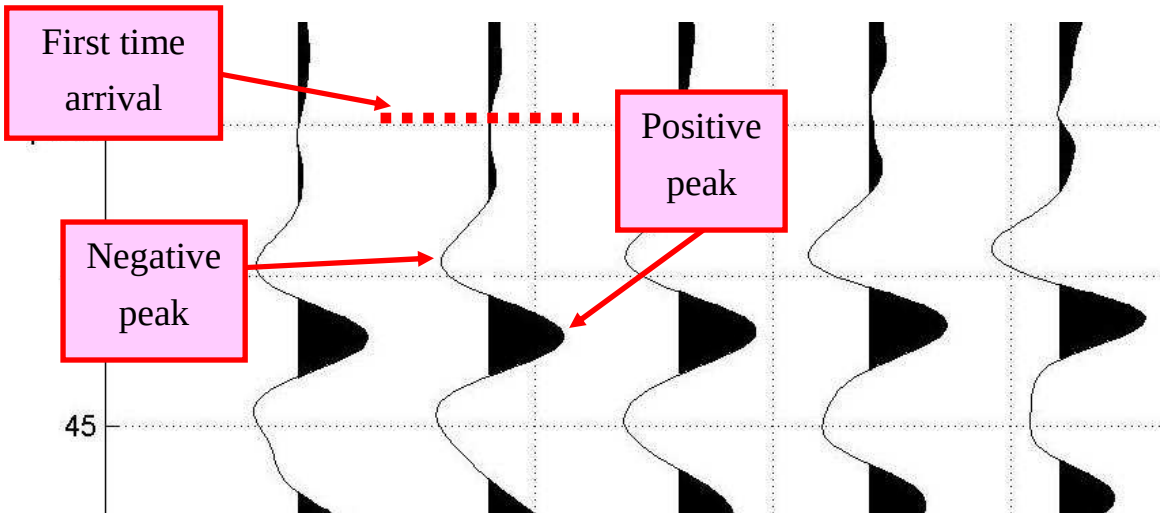

Figure 4.12. Zoom of the seismogram with the peaks relative to the reflected P-waves, for the source S_1.

A practical example of this procedure can be seen in Figure 4.12, where the different positive and negative peaks are detected, and successively the first time arrival is determined.

4.4.5. Discontinuity estimation

Once completed this procedure, the temporal values extracted can be inserted in the ellipsoid method, which will provide an estimation of the discontinuity.

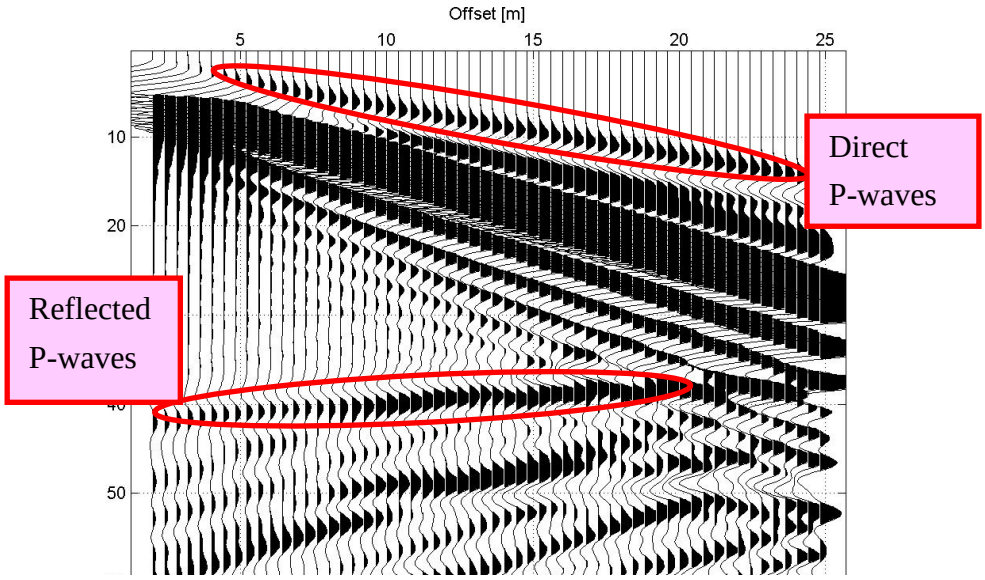

Figure 4.13. Seismogram with peaks relative to P-waves, for the source S_1.

Let us concentrate on the case with the source S_1, because it is the source farther from the discontinuity and then it is the most suitable for the its detection, since the arrival times due to the reflection are easier to be detected.

The seismogram is shown in Figure 4.13, with both direct and reflected P-waves. The amplitudes of the peaks are very similar in both the cases and so this is a confirmation of the fact that it is a reflection of the P-waves.

The result of the ellipsoid method is depicted in Figure 4.14. The discontinuity is estimated as the tangent to the curves in the intersection point. When the receiver considered is close to the source, then the corresponding ellipse is similar to a circle.

The results and the relative errors of the estimation process are represented in Table 4.3. The results are satisfying for the angle, since the inclination is very similar to the real one, but the distance has not well predicted. This is mainly due to the velocity estimation that is not so accurate.

If the velocity is assumed to be equal to 2000 m/s, as the real value used for the simulation, then the results are in Figure 4.15 and in Table 4.4.

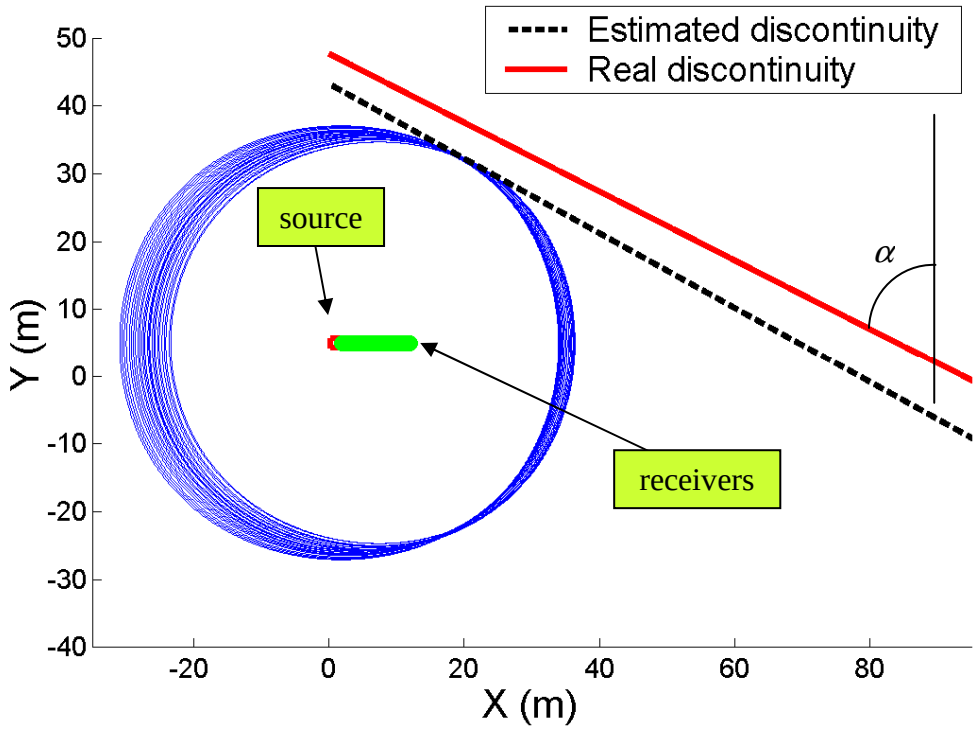

Figure 4.14. Ellipsoids and discontinuity estimation for the source S_1.

Table 4.3. Parameters extracted for the analysis with the source S_1.

Parameter	Real value	Estimated value	Relative error
Angle α	$\alpha = 27\,°$	$\alpha = 28.86\,°$	6.89 %
Distance d	$d = 93.8$ m	$d = 78.44$ m	16.39 %

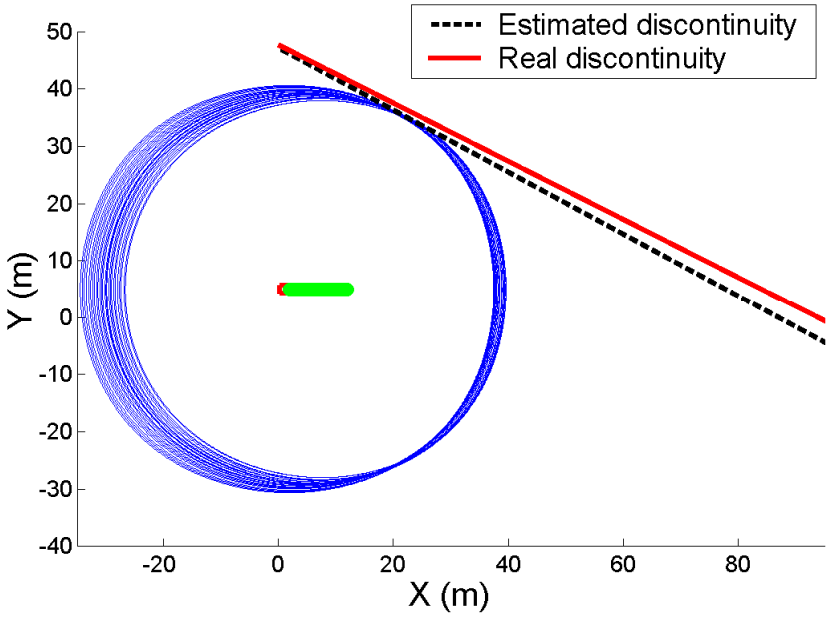

Figure 4.15. Ellipsoids and discontinuity estimation for the source S_1, with velocity assumed equal to the real one.

Table 4.4. Parameters extracted for the analysis with the source S_1, with velocity assumed equal to the real one.

Parameter	Real value	Estimated value	Relative error
Angle α	$\alpha = 27\,°$	$\alpha = 28.47\,°$	5.67 %
Distance d	$d = 93.8$ m	$d = 86.95$ m	7.33 %

In this case, both the angle and the distance between the source and the discontinuity are estimated with a sufficient accuracy.

4.5. Simulations in 3D

In this section, a numerical example in three dimensions is proposed, in order to simulate a case closer to a real tunnel survey.
Let us consider the following characteristics for the discontinuity:

$$d = 130 \text{ m}, \quad \alpha = 49°, \quad \gamma = 90° \tag{4.17}$$

Two receivers are chosen with an abscissa varying from -50 m to -20 m, every 2 meters, while the y-coordinate is always equal to -4 and the z-coordinate is null. The source is in the origin of the axes. The theoretical time arrivals of the reflected waves are calculated and then modified by adding random noise.
In Figure 4.16, the discontinuity estimation, for the case with no added noise, is represented, together with two ellipsoids: the first and the last one. The ellipsoids are quite different but they have a common tangent plane.

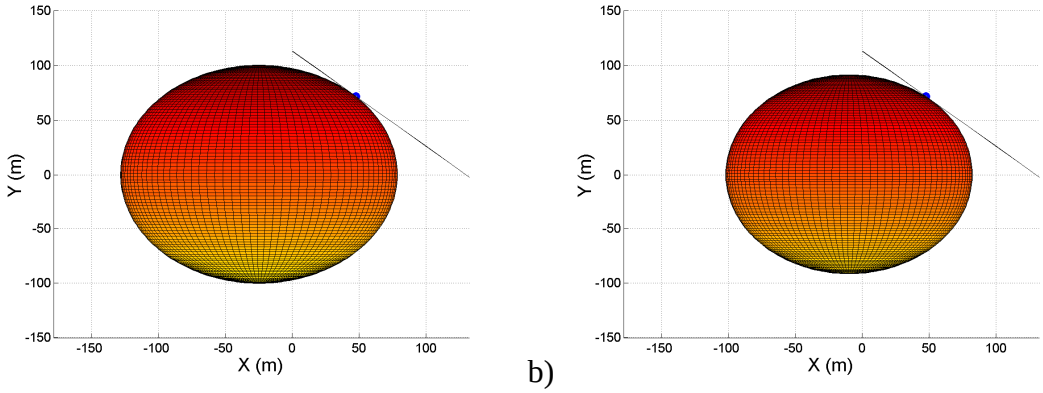

a) b)

Figure 4.16. Ellipsoids and estimation of the discontinuity, without added noise: a) first ellipsoid, b) last ellipsoid. The blue point is the estimated reflection point.

Table 4.5. Results of the simulation, for the simulation without added noise.

Data	Estimation	Error/difference
$P_0 = (47.23,0,71.95)$ (average)	$P_0 = (47.45,0,71.73)$	--
$d = 130$ m	$d_S = 129.73$ m	0.21 %
$\alpha = 49°$	$\alpha_S = 48.87°$	0.13°
$\gamma = 90°$	$\gamma_S = 90°$	0°

The results of the estimation are given in Table 4.5: all the parameters are well estimated, and in particular the reflection point.

The starting value for the search of the reflection point is quite far from the real value (considered as unique), which can be taken as the average of the theoretical reflection points, since it is equal to $P_t = (35.47,0,48.26)$.

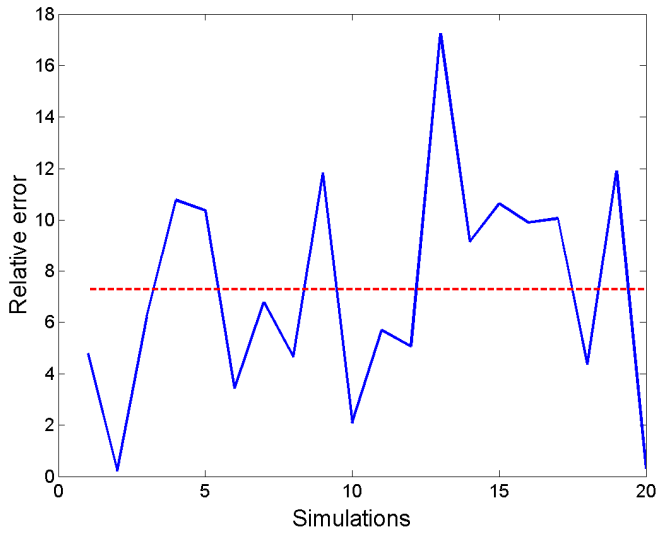

Figure 4.17. Relative errors on the distance source-discontinuity for 20 simulations, with a 2% of added noise.

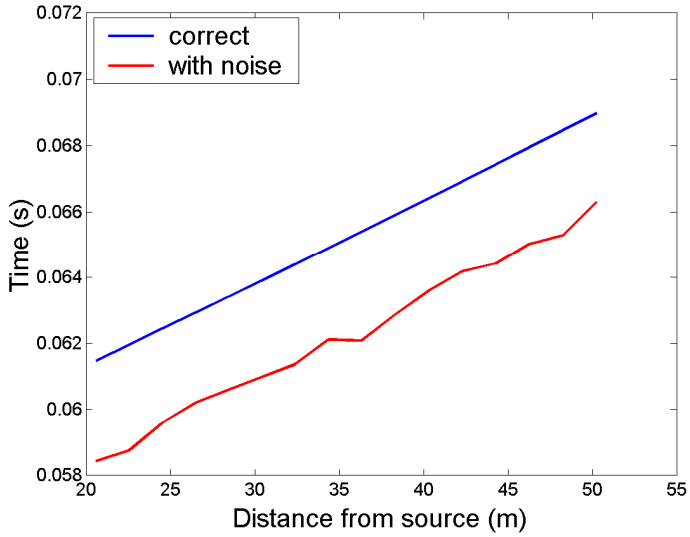

Figure 4.18. Example of time arrivals of the reflected waves, with 1% of noise and 5% of shift.

Now, let us add 2% of random noise to the time arrivals and collect the results of 20 simulations. The relative errors on the estimation of the distance source-discontinuity are shown in Figure 4.17, together with the average value.
The results are not very good because the average error is about 7% and the maximum is 17%, but actually these are not large errors in practice, meaning only a difference of few meters. Indeed, in tunnels, there is the possibility to acquire data at different excavation fronts and then to reduce the error.
In Figure 4.18, in order to simulate a more realistic sequence of first arrival times, they are corrupted with only 1% of random noise but with a shift of 5% of the real values.

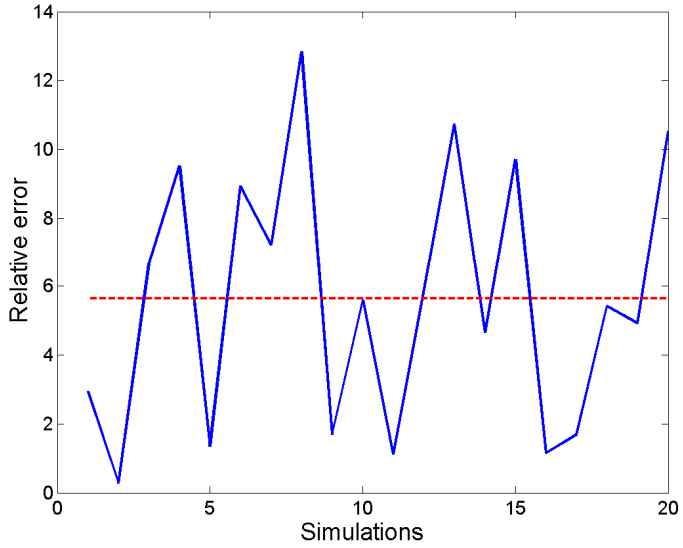

Figure 4.19. Relative errors on the distance source-discontinuity for 20 simulations, with 1% of added noise and 5% of delay.

In Figure 4.19, the relative errors on the distance, for 20 simulations, are shown. The average error is smaller than in the previous case and this is a good indication because this is referred to a case more similar to real applications in tunnels.

4.6. Multiple ellipsoid method

The main idea of the multiple ellipsoid method is to perform the estimation of the discontinuity given by the ellipsoid method not only one time, but different times, by considering groups of ellipsoids per each investigation.

In general, this method can be applied in different ways:

- Fixing one source, then use some or all the receivers to construct the ellipsoids; successively, consider another source and repeat the operations.
- Fixing one receiver, then use some or all the sources to construct the ellipsoids; successively, consider another receiver and repeat the operations.

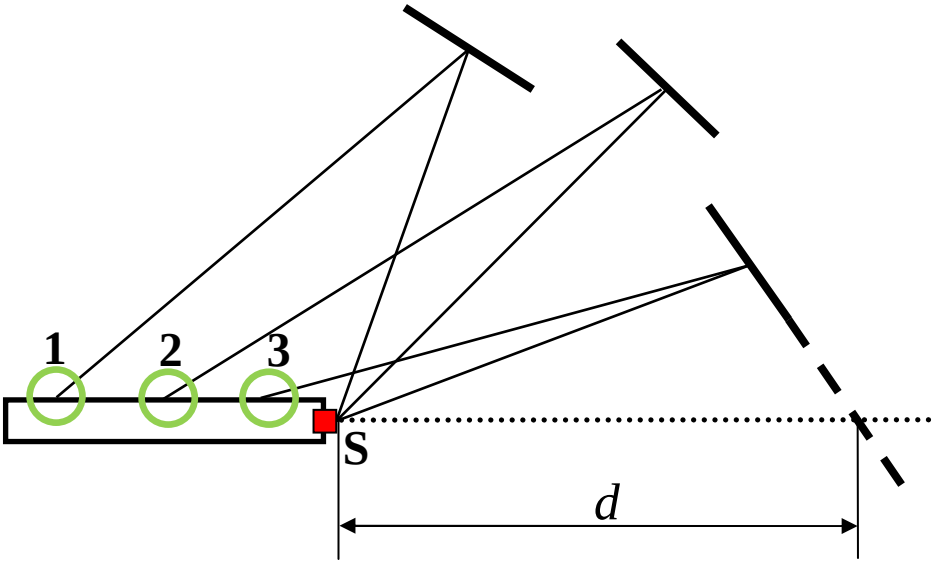

Figure 4.16. Idea of the multiple ellipsoid method. Some groups of sensors, indicated with green circles, are distributed along the tunnel walls, and they generate many ellipsoids that can intercept more than one reflectors.

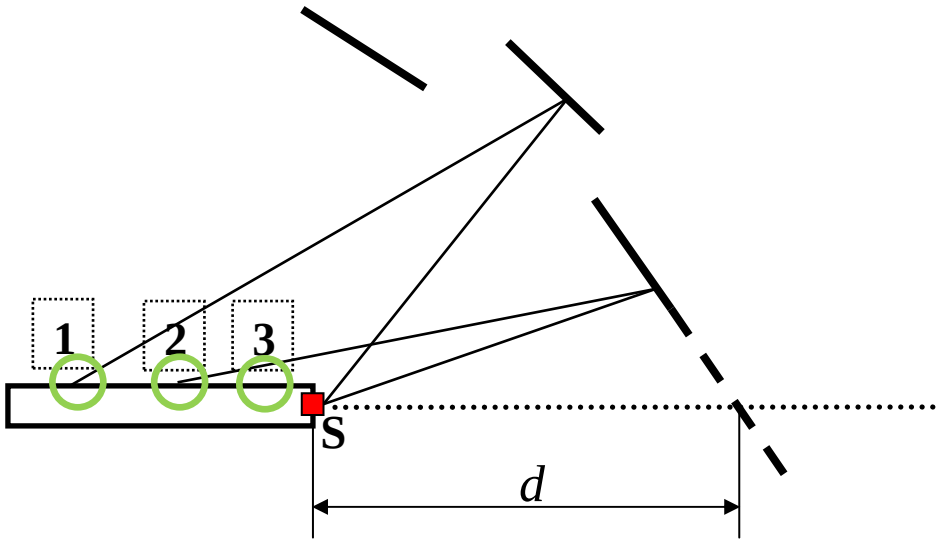

Figure 4.17. Estimation of the discontinuity at a successive step, based on the idea of the multiple ellipsoid method.

To obtain good results, it is advisable to have as many ellipsoids as possible. Moreover, sources and receivers must be placed in such a way to have a high coverage of the domain.
In Figure 4.16, there are three groups of receivers and three different discontinuities are estimated. For this reason, the validity of the method is only local, in the sense that the estimation is valid only in a small region around the reflection point extracted.
During a successive investigation, new ellipsoids can be built and new applications of the method can be performed in order to confirm the previous estimates (see Figure 4.17). In general, the discontinuities can be identified by different receiver sets respect to the previous case.

4.7. Limitations of the forward methods

The ellipsoid method has been used for the estimation of discontinuities in 2D and 3D examples. In many cases, the results are satisfying but, as can be noted from all the examples proposed, the ellipsoid method has the following disadvantages:

- The peaks related to the reflections must be detected manually, by an expert geophysicist. This operation can be long and difficult, because the peaks corresponding to reflections (if present) must be recognized and selected.
- It is difficult to find the reflection point, because the procedure can fail in presence of a low signal-to-noise ratio and, consequently, the discontinuity (identified as the tangent plane) is not estimated in its real location. Even in presence of a high signal-to-noise ratio, the procedure could extract a discontinuity which is not coincident with the real one, because a small error in the reflection point (or in the velocity) can lead to a significant error in the estimation of the tangent plane, especially for those cases in which the reflection points are far from the tunnel axis.
- The method is deterministic, in the sense that it does not quantify the probability of finding the discontinuity in a certain zone. For example, in Figure 4.5 it would be better to indicate that it could be placed on the other side of the tunnel.

For all these reasons, a new method able to overcome these problems is needed. A possible solution is given in the next chapter where the backward method is presented.

Chapter 5

The backward method

The method proposed in this chapter is the most important issue of the thesis. The automatic procedure for the prediction of discontinuities ahead of the tunnel front is described in all its parts, starting from the concept and the pre-processing until to the final representation.

5.1. The concept

The name of the method has been obviously chosen in contrast with the forward techniques presented in the previous chapter. Actually, this means that this procedure is based on a fundamental idea that is completely opposite from those already shown: the time arrivals are not considered as known quantities and therefore they are additional unknowns to the system, which needs a special algorithm to be solved.
In the following subsections, the idea of the method, the peculiarities of the algorithm and the differences respect to the forward approaches are proposed.
As already said in the Section 4.7, the forward methods are not satisfying mainly because of the difficulties in recognizing the times due to reflections and in identifying the reflector in presence of poor signal-to-noise ratio.
For this reasons, the backward method is suggested, in a way similar to TRT (Descour *et al.*, 2012; Yamamoto *et al.*, 2006), described in Subsection 2.4.3.
More in details, the proposed procedure has the following characteristics:

- it is completely automatic;
- it obtains a map of all the discontinuities present in a specified domain.

As a matter of fact, the method is able to get the results without any human intervention except for inserting the positions of sources and receivers (i.e. the general geometry of the test); in particular the manual identification of the peaks corresponding to the

reflections in the seismogram is avoided, since it is a long and difficult operation. The peaks are identified automatically among all the peaks of the seismograms recorded by the receivers.

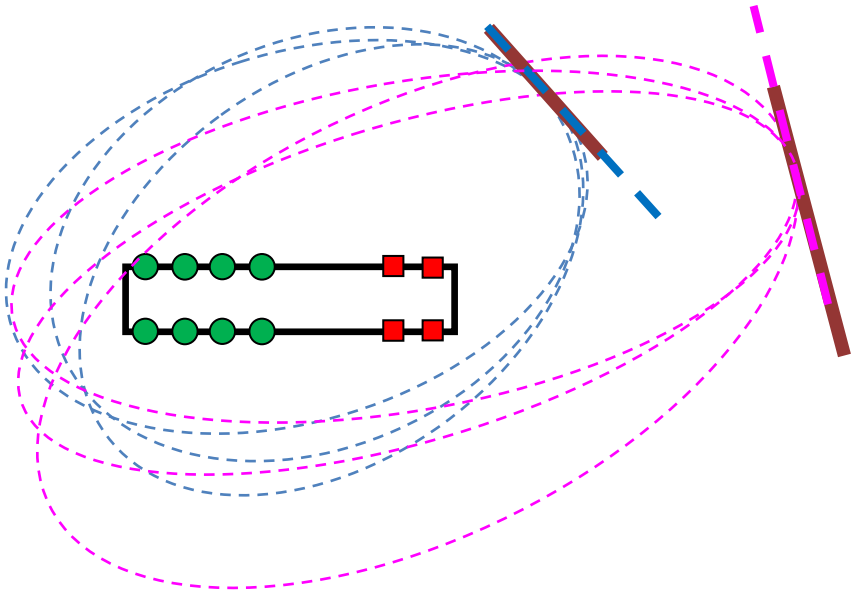

a)

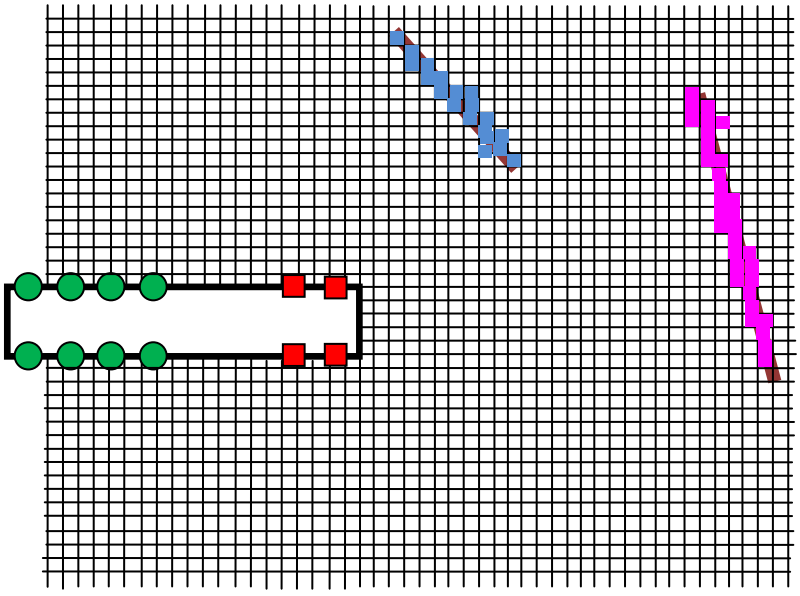

b)

Figure 5.1. Representation of the basic idea of the two most important approaches: a) forward method, where the estimations of the discontinuities are obtained by means of the tangent planes in the intersection of the ellipsoids; b) backward method, where the estimations are highlighted by coloured cells, identified as reflection points.

Firstly, a space domain of some tenths of meters in front and on the side of the tunnel is considered. Usually, the prediction required is about 100-150 meters ahead of the tunnel face, while only 30-40 meters around the tunnel for the other directions are sufficient.
Successively, the domain is divided in a fixed number of cells, and each node is considered as a reflection point. Then, the method automatically checks if there are some peaks on the seismograms compatible with a reflector placed in that position; if the response is positive, that node is highlighted and a successive node is considered.
At the end of the process, only the reflection zones are emphasized: this is the final image of the lithological discontinuity around the tunnel.
The different ideas of the forward and backward method are shown graphically in Figure 5.1a and in Figure 5.1b, respectively. The estimation of the forward method is done in four steps:

1. estimation of the wave velocity;
2. extraction of the travel times that can correspond to the reflections events;
3. construction of the ellipsoids;
4. estimation of the tangent plane.

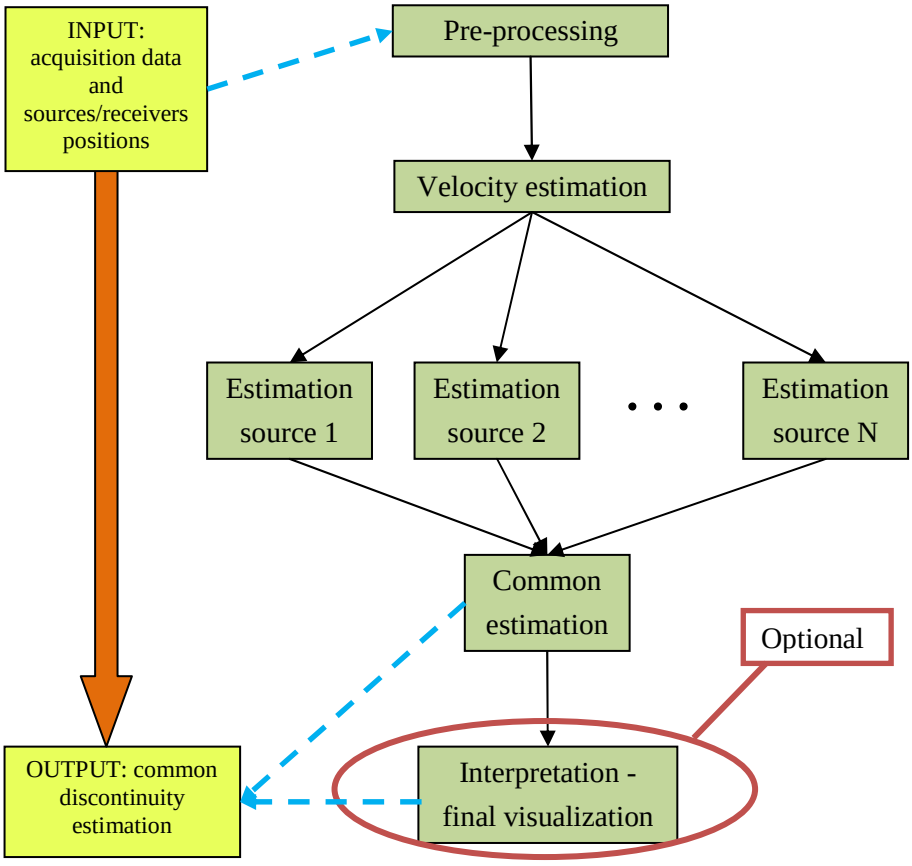

Figure 5.2. Schematic representation of the backward method.

In Figure 5.1b, the backward method visualization is sketched, by evidencing the coloured nodes correspond to the estimated reflectors. The final result is obtained by following these three major steps:

1. estimation of the wave velocity;
2. detection of the discontinuities for each source;
3. common discontinuity estimation.

The simplified scheme of the algorithm proposed is depicted in Figure 5.2.
The steps of the backward methods are analyzed separately, in order to well understand each operation of the whole procedure.

5.2. Pre-processing

In this section, the actions that must be done before applying the method are illustrated. When a disposition of n_S sources and n_R sensors has been chosen for the investigation, it is important to choose a reference system and to determine the Cartesian coordinates of the principal points.
The section of the tunnel is represented in Figure 5.3 as a circle truncated by an horizontal line, together with some parameters:

- h : tunnel height

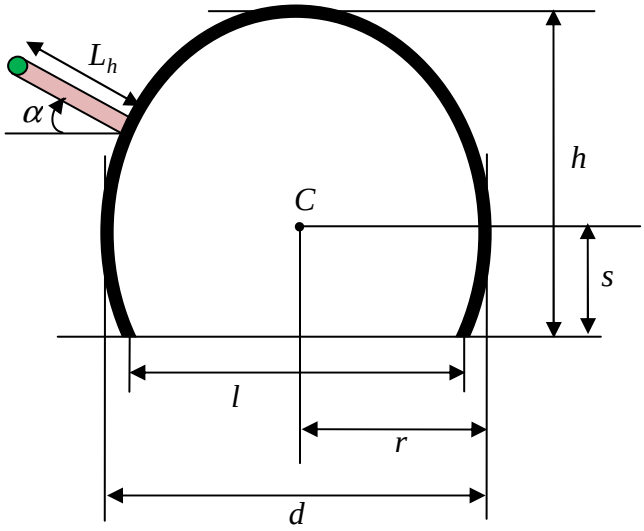

Figure 5.3. Tunnel section with the main quantities useful for the placement of sensors and sources.

- r : tunnel radius

- d : tunnel maximum width
- l : tunnel width at the ground level
- $s = h - r$: length of the segment between the center of the circle C and the ground
- L_h : length of the hole in which a sensor or a source is placed (it is equal to zero if it is placed on the tunnel wall)
- α : angle of the hole respect to the ground.

When positioning a sensor (or a source) on the tunnel wall, its x- and z-coordinates are simply measured. In order to obtain the y-coordinate a simple operation must be done:

$$y_R = \pm\sqrt{r^2 - (z_R - s)^2} \tag{5.1}$$

In the case that a sensor (or a source) is placed inside the rock, then the z-coordinate z_M taken at the beginning of the hole is not the real z-coordinate of the sensor (or the source) but it is necessary to first obtain the y-coordinate:

$$y_R = \pm\left(\sqrt{r^2 - (z_M - s)^2} + L_h \cos\alpha\right) \tag{5.2}$$

$$z_R = \pm(z_M + L_h \sin\alpha) \tag{5.3}$$

In Figure 5.4, the reference system for the Cartesian coordinates of sources and receivers is visualized. The origin of the axes is placed on the tunnel front, in the middle of the section width, at the ground level. The orientation of the axes is the following:

- x-axis: positive in the sense of tunnel excavation
- y-axis: positive towards the right, if the tunnel front is behind the back
- z-axis: positive in the opposite direction of the gravity force.

The choice of the positive direction of the y-axis seems to be strange, but it is connected to the final visualization proposed by the method (Section 5.4 and 5.5). Indeed, if representing a map view by means of a figure created in Matlab, the positive values are on the side indicated by the positive part of the y-axis.

Before starting the analysis of the data coming from the sensors, the first goal is to measure all the positions of sources and receivers, according to the reference system.

The other fundamental information that are needed are:

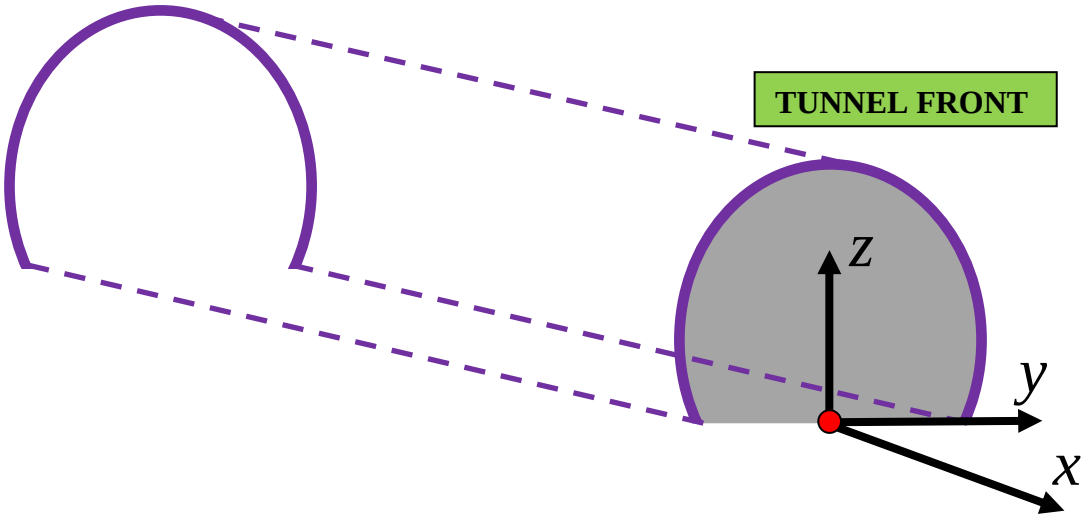

Figure 5.4. Reference system adopted for the determination of the Cartesian coordinates.

- the chainage, which indicates the number of meters that have been already excavated in the tunnel under analysis
- the sampling frequency f_s

The data acquired are first truncated after a fraction of a second, in order to consider reflections up to maximum 150-200 meters ahead of the tunnel face.

The final time t_{fin} should be correlated to the supposed wave velocity v and to the maximum distance $d_{\max}$ we want to inspect with the technique:

$$t_{fin} \cong 2\frac{d_{\max}}{v} \tag{5.4}$$

The factor 2 indicates that the wave have to come back to the receivers and then the travel time is roughly doubled.

5.3. Velocity estimation

In Section 4.3, the velocity has been estimated with the time arrivals related to the direct waves identified directly on the seismogram. This operation can be very long if the total number of signals (equal to the number of sensor times the number of sources) is high, consequently an automatic approach must be introduced.

5.3.1. Spectral analysis

Before starting the velocity estimation process, the spectral analysis of the traces recorded by the receivers must be performed. This is useful for:

- find the range of the most significant frequencies of the signals, in order to filter from f_1 to f_2
- find the fundamental frequency
- check if there exist some anomalous frequencies.

The last operation can be done manually or avoided. The presence of strange peaks is directly connected to problems in the acquisition: in that case, the signals must not be considered.

Once performed the spectral analysis, the traces are filtered with a Chebyshev filter, with minimum and maximum frequencies equal to f_1 and f_2, respectively.

5.3.2. The method of successive eliminations

Let's consider a single source. The first step is to calculate the distances D between the receivers and the source. Then, for each trace that has been recorded, the maximum peak is identified. This value is theoretically more evident for the receivers closer to the source, because for the others the signal-to-noise ratio could be lower.

For this reason, the process start by collecting the maxima of the two traces corresponding to the two receivers with minor D, while the successive eliminations method is applied only to the other signals.

For each remaining signals, the two most relevant peaks are collected. The two peaks should not be too close because otherwise they could belong to the same event. Once extracted the values for the third and the fourth traces, four combinations are built together with the two already fixed values coming from the first two traces (see Figure 5.5). A linear regression is performed for the four cases and the combination which minimizes the error from its regression line is chosen as the right one. In Figure 5.5, the case 1 minimizes the error and therefore the two circles near the red curve are inserted in the final list of the times of the direct waves.

The process goes on up to the last trace by considering one trace at a time and by choosing the value minimizing the error with its regression line (including also the values already calculated). This step is represented in Figure 5.6a, where it is clear the distinction between the first part, with all the values already selected, and the second part, where the procedure decides which elements must be eliminated.

In Figure 5.6b, a critical case is proposed, where the selected points are close but the method is able to choose the right value.

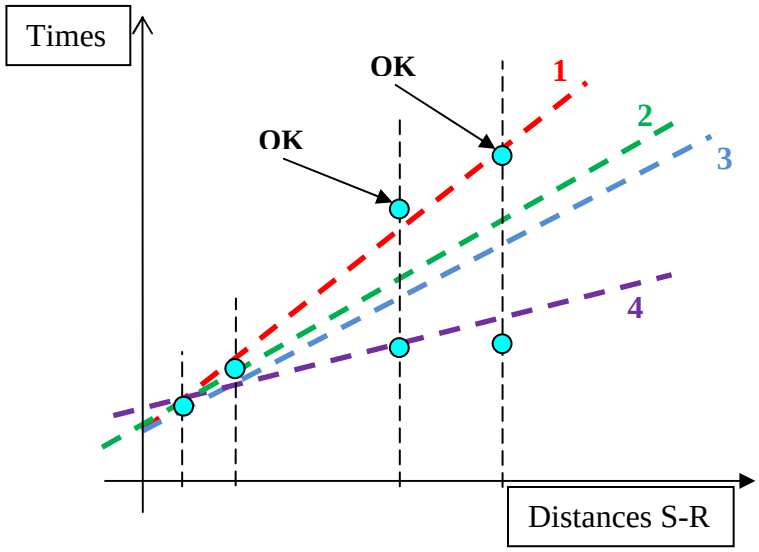

Figure 5.5. Representation of the first part of the method of successive eliminations. The cyan points are the times corresponding to the maximum peaks identified.

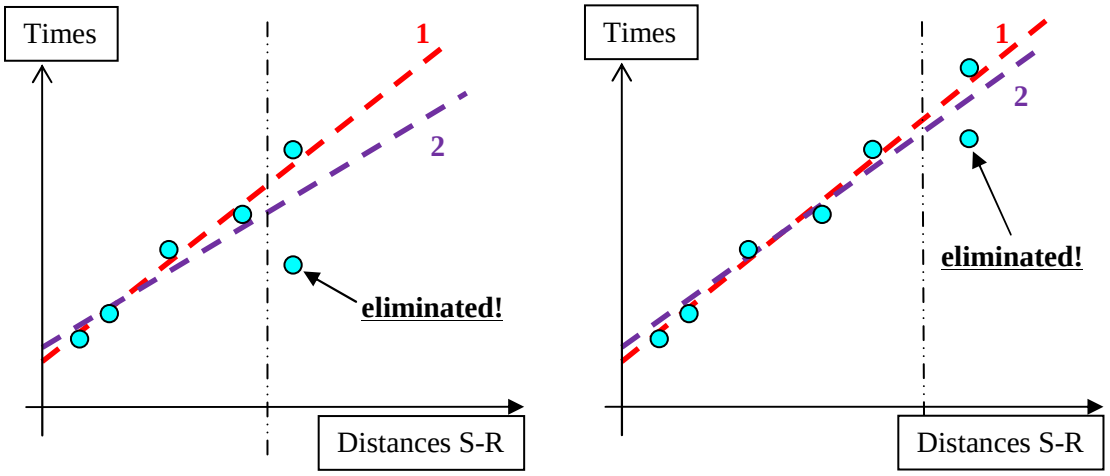

a) b)

Figure 5.6. Second part of the successive eliminations method: a) simple elimination b) critical case because the selected points are quite close each other.

In practical investigation in tunnels, for the estimation of the velocity, as well as for the identification of the discontinuities, only the accelerometers located on the same tunnel side of the source are considered. This is done because the tunnel curvature is not negligible and this cause a delay in the arrival times of the wave, both direct and reflected.

5.3.3. Estimation of velocity and delay time

Once obtained all the times due to the direct waves, it is possible to calculate the velocity by simply performing a linear regression. This operation is repeated for all the acquisitions and then at the end the values are averaged in order to obtain the final estimate.

The estimation of the velocity is directly connected to the estimation of the delay time t_D, which represents the time of the maximum amplitude of the wave generated at the source, and it is actually the intercept of the regression line in the distance-time graph. Analogously to the velocity, this value is obtained by averaging all the values obtained at the different sources.

5.3.4. The admissible times

Another important step is to gather all the maxima and minima of the signals recorded by the sensors, because these are all the possible times related to the reflected waves. They are simply called “admissible times”.

Since the method does not include the manual extraction of the peaks referred to the reflections, it selects automatically those values. Within this operation, only the peaks successive to the direct wave travel-times are considered. Actually, if the peaks of the direct waves and those referred to its decay are considered, then wrong estimations of the discontinuity can be obtained, because the times considered do not correspond to a reflection but only to a decay. Therefore, it is advisable to neglect these values and start from the first peak that is no more smaller respect to the previous one.

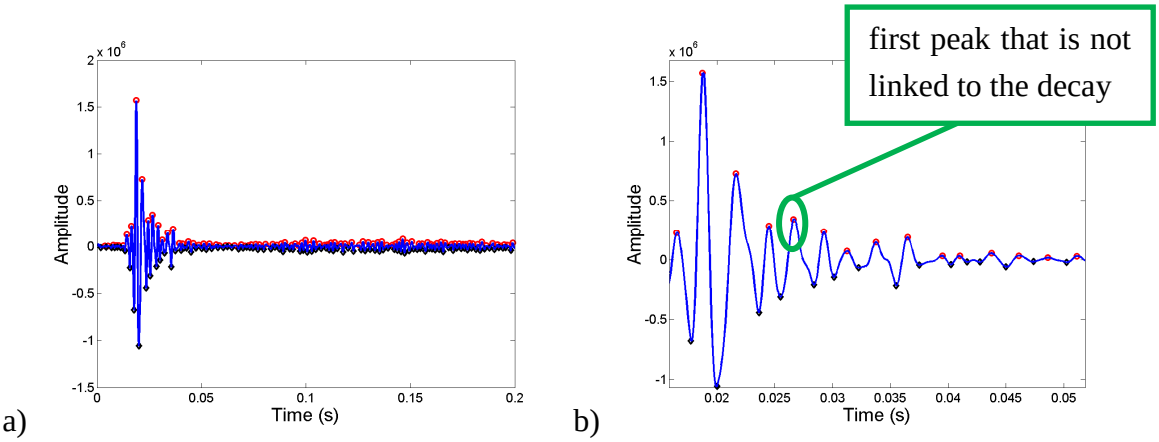

a) b)

Figure 5.7. Signal recorded by an accelerometer, coming from a survey on a tunnel under construction: a) the signal considered, truncated at 0.2 s; b) magnification in the zone near the peak of the direct wave and choice of the first admissible time.

Let‘s present in Figure 5.7 a signal coming from a real investigation on a tunnel under construction. At first, the signal is limited to 0.2 s, which is given by a wave velocity around 3000 m/s and by a maximum prediction of 300 m (Figure 5.7a). Successively, the first admissible time is easily detected as the first one that has a larger amplitude respect to its previous one (Figure 5.7b).

5.3.5. Summary of the first part

The first part of the algorithm can be summarized by the scheme proposed in Figure 5.8. Actually, the results of this part are the estimates of the velocity and the delay time, and moreover the admissible times, which are essential information for the following part dedicated to the discontinuity estimation.

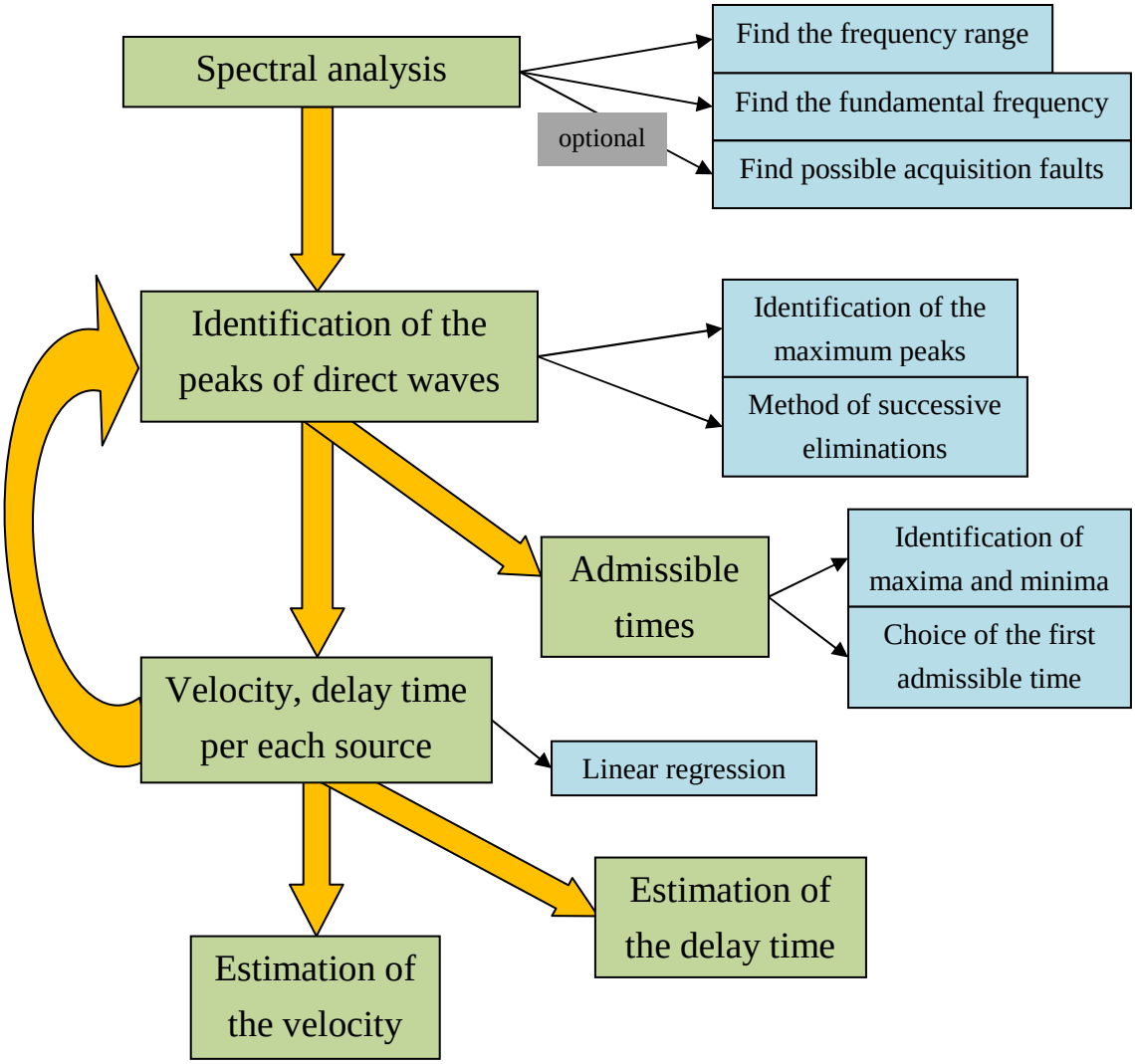

Figure 5.8. Summarizing scheme of the first part of the method.

5.4. Single estimation of the discontinuities

Once estimated the wave velocity, the prediction of discontinuities is explained, which is the real core of the procedure. In this part, the data are treated separately for each source.

The main idea is to assume that each point produces a reflection, due to a contrast of acoustic impedance. In this way, it is possible to evaluate all the points independently and to analyze whatever part of the domain, something that is not possible with a forward approach. Moreover, since the methodology is fully automatic, many discontinuities can be identified, even if the related peaks have a small amplitude and could be at first associate to noise.

5.4.1. Choice of the domain

As said in the Section 5.1, the method is based on the backward estimation, and therefore the first thing to do is to choose the domain of investigation. This step is more important than the expected because a wrong choice can lead to a large computational time or to low-definition results.

In particular, there are two parameters that must be chosen per each axis:

- the limits
- the resolution

Each source is considered in the origin of the axes, therefore the positions of the receivers are changed according to the source considered, at every investigation.

Because of this choice, the minimum value of the x-axis of the domain must be zero, i.e. the estimation is forward, from the source to a value that is chosen by the user. Usually, in real applications, the requested forward prediction is about 100-150 meters, in order to excavate some day before starting a new survey (considering a excavation rate of about 15-20 m/day in favourable conditions).

About the y- and z-axis, a fixed interval should be considered, for example 30-40 meters above and below the source, and the same for the lateral direction.

The resolution is the other fundamental parameter. For significant predictions as expected in real tests, it is advisable to consider one meter of resolution in every direction, in order to have a good accuracy and avoid long calculation times.

For simplicity, the results of the method are represented in two dimensions:

- XY plane (plan view)
- XZ plane (cross-section view).

This means that the domain of investigation considered is only two-dimensional, but all the calculations are done by considering the three spatial coordinates.

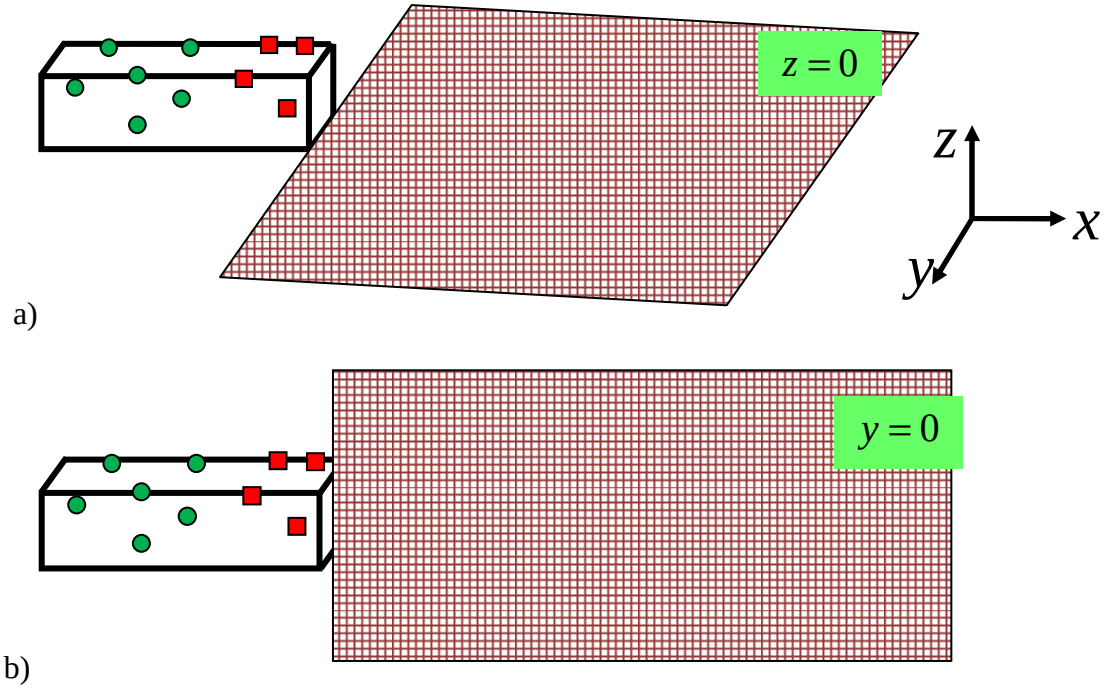

Figure 5.9. Domain of investigation of the method: a) for the analysis on the XY plane (plan or map view); b) for the analysis on the XZ plane (cross-section view).

The two representations are depicted in Figure 5.9a and 5.9b, showing that the area of exploration is given by two planes which are representative for the whole tunnel, since the dimensions of the tunnel face are limited to few meters. This approach permits to significantly reduce the computational time.

The map view consists in considering $z = 0$, i.e. it is the prediction at the ground level; the cross-sectional view, instead, is for $y = 0$, that is for the centre of the tunnel section.

The combination of both the views allows to have a quite accurate idea of the rock discontinuity ahead of the tunnel face.

5.4.2. Calculation of the reflection points

Since the domain has been already defined, now let's consider only one source and the relative sensors and admissible times.

The procedure is mainly divided in three parts:

- each point of the domain is considered a reflection point
- the theoretical times due to the reflection can be easily calculated because the positions of sources and receivers are known
- these times are compared with the admissible times to check if there is a correspondence; if yes, the point is defined as a reflection point.

As studied in Subsection 4.2.2, the reflected waves recorded by the accelerometers are generated in a specific zone of the discontinuity, that in real cases can be often supposed only a point. This approximation is valid mainly when the source and the receivers are sufficiently far from the discontinuity, therefore for the points immediately after the source the estimation could be not so accurate.

Once chosen the node P to analyze, the theoretical time of arrival at the sensor R is

$$t_P = \frac{d(S,P) + d(P,R)}{v} + t_D \tag{5.5}$$

where S is the source considered and $d(\cdot)$ indicates the distance between two points. The value is shifted of the quantity t_D because this is the theoretical time of the peak of the wave in the source signal.

The method, after the computation of the theoretical times t_P, finds the sequence $\bar{t}_P$ of times, among all the admissible times, closer to t_P. The times $\bar{t}_P$ must satisfy the following conditions:

1. they must be chosen one per receiver;
2. the corresponding amplitudes must have the same polarity for all the values;
3. the vector formed by all the times $\bar{t}_P$ should be the closest vector to the theoretical values t_P.

The statistical check of the solution is given by the standard deviation σ_P between the two times series t_P and $\bar{t}_P$:

$$\sigma_P = std\left(\bar{t}_P - t_P\right) \tag{5.6}$$

This step detects automatically the nodes with σ_P close to 0, identified as reflection points, from the others with a very large standard deviation, labelled as non-reflection points. It is not necessary to fix a threshold to distinguish the low values from the high values, because the algorithm is able to identify the time series $\bar{t}_P$ and, when not, random values are inserted as $\bar{t}_P$, such that the standard deviation is very large. This will be more clear in the numerical examples of the next chapter.

The selected nodes point out the identification of the discontinuities for the source under analysis. We repeat the operation n_S times to produce n_S different estimations of the discontinuities. In the next subsection, the discontinuities are gathered to form a unique estimation.

5.4.3. Summary of the second part

The second part of the method is summarized through Figure 5.10.

5.5. Common discontinuity estimation

The method is able to obtain n_S different estimations of the discontinuities, but a common map of reflectors should be given as a final result.

5.5.1. Change of coordinates

At first, since every source has been considered in the origin of the axes for every estimation of the discontinuity, the sources, the sensors and the single estimates are re-collocated in order to reflect the real survey configuration.
The single estimates of the discontinuities are not very indicative mainly because they don't have the right placement, then this step re-organizes the positions in order to have a unique final visualization.

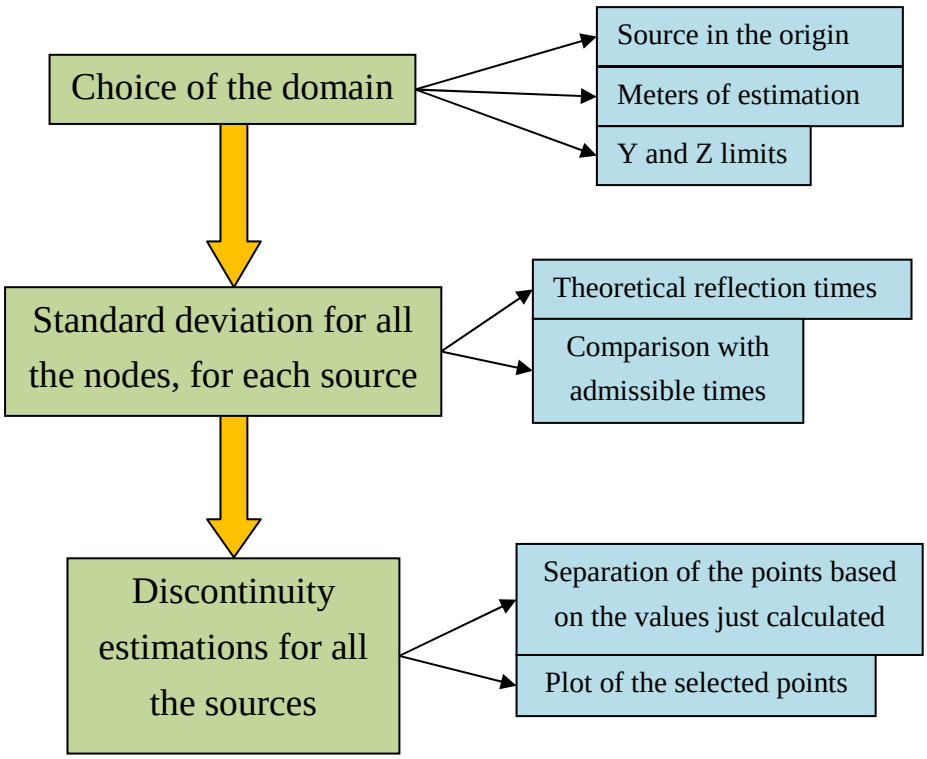

Figure 5.10. Summarizing scheme of the second part of the method: discontinuity estimation from a single acquisition (one source).

5.5.2. Visualization of common points

Now, the visualization of the common points requires a criterion which defines when the reflected points, coming from different sources, can be considered part of the common estimation.

The idea is to consider each node of the domain and to count the reflection points close or coincident with it. We didn't apply any cluster algorithm but define a square centered in the node; as a good compromise we select the half-side R as a quarter of the wavelength:

$$R = \frac{1}{4}\lambda = \frac{1}{4}\frac{v}{f} \tag{5.7}$$

where v is the wave velocity and f the fundamental frequency.

However, in order to insert a certain tolerance in the process, a distance R is introduced, with the meaning of neighbourhood of the point P considered. In Figure 5.11, it is possible to see that actually R does not represent a circle around the point P but a square because is less time-consuming during the automatic calculation.

The number of sources with a reflection point in the neighbourhood of a node P is called N_P. The concept of superposition of the reflection points coming from different acquisitions can be seen in Figure 5.12. The two different estimations have a clear common zone where N_P is equal to 2, while for the other coloured zones $N_P = 1$ and in the white parts $N_P = 0$.

For this reason, the final representation shows the number of sources N_P for each node of domain. In this way, by using a pseudo-colour scale from the light to the dark colours, we emphasize the nodes where the number of superposed estimations is higher.

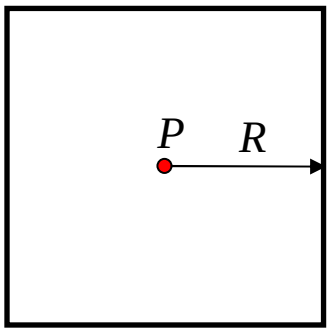

Figure 5.11. Explanation of the concept of the parameter R.

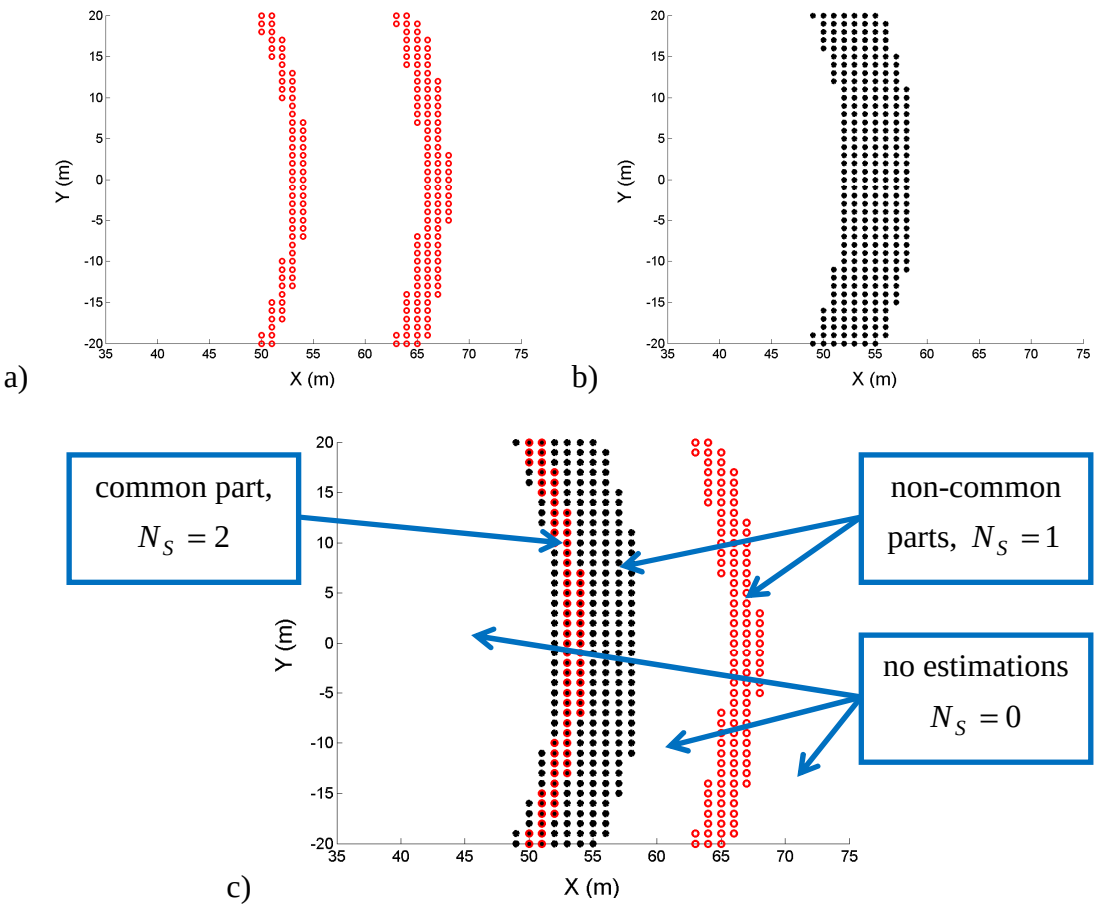

Figure 5.12. Overlaps of reflection points coming from different acquisitions: a) estimation coming from the first source; b) estimation coming from the second source; c) common estimation with highlight on the common part.

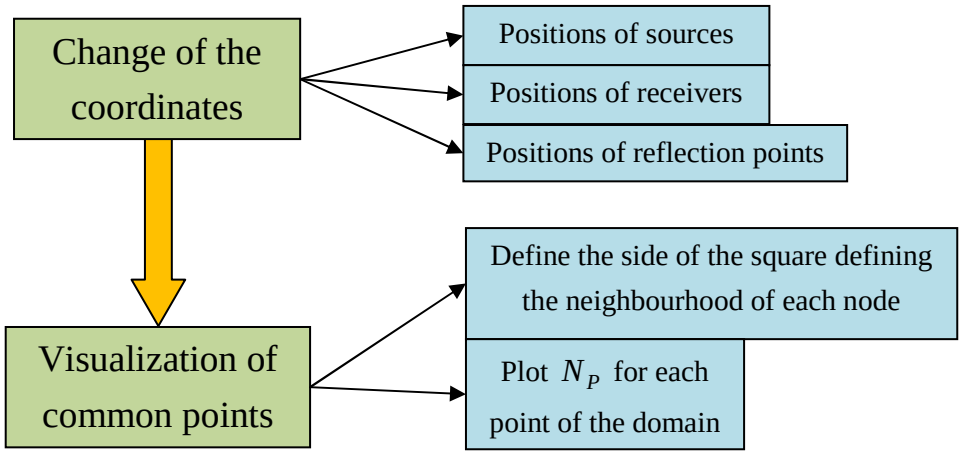

Figure 5.13. Summarizing scheme of the third part of the method: common discontinuity estimation.

This result can be interpreted as a map of probability to detect a discontinuity in a certain node of the domain.
This approach is in some sense statistical and it is in contrast with all the other methods present in literature which give a deterministic result in terms of velocity field or reflection coefficient.

5.5.3. Summary of the third part

In Figure 5.13 a scheme of the third part of the methodology is represented. This is the last automatic step and gives the final results, except for the successive interpretation done by an expert, which is very important in the experimental tests.

5.6. Interpretation and final visualization

The final part of the method is dedicated to the interpretation done by the analyzer. This step is neither easy nor standard, in the sense that the results given in the previous step cannot be always clear. In this case, an expert can propose a personal analysis of the results in order to provide a comprehensible final visualization.
The interpretation is very important in real experiments, where the noise and others technical imperfections (non-exact measurement of the sensor positions, unknown type of discontinuities) affect significantly the quality of the results.
However, by looking at common estimation figure, the expert can recognize which of the critical zones can effectively be considered a discontinuity and which is the degree of criticality. The final visualization should be very simple and easy to understand, with only inclined lines and/or brief comments.

Chapter 6

Numerical simulations

The numerical simulations proposed in this chapter are the first test for the backward method, which has been described in the previous section. They are created both in *Reflex*, a dedicated program for geophysical applications, and in *Comsol Multiphysics*®, one of the most used programs in the field of modelling, based on finite element method (FEM).

6.1. A tutorial example

The first example proposed is a numerical simulation using the software *Reflex (Sandmeier trademark).*

6.1.1. The configuration

The configuration is two-dimensional, with six source points (whose positions are listed in Table 6.1) and an array of 30 receivers disposed on a straight line, with the x-coordinate varying from 19 to 47.5, at a fixed interval of 1.5 m.
The excitation is simulated by means of a Ricker Wavelet, with a main frequency equal to 200 Hz, while the rock mass discontinuity is herein simulated by a triangular inclusion (see Figure 6.1). The mechanical properties of the media involved are listed in Table 6.2.

Table 6.1. Positions of the sources.

	S_1	S_2	S_3	S_4	S_5	S_6
Coordinates	(50,1)	(50,5)	(40,5)	(30,5)	(20,5)	(30,1)

Table 6.2. Characteristics of the media involved in the numerical simulation.

	Medium in the domain	Medium in the discontinuity
P-wave velocity	2000 m/s	1000 m/s
S-wave velocity	1200 m/s	500 m/s
Density	2700 kg/m^3	1500 kg/m^3

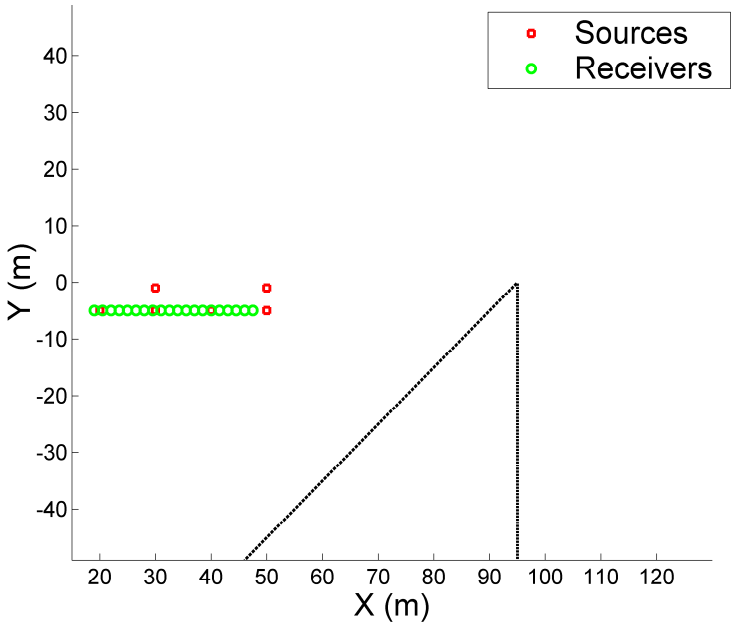

Figure 6.1. Configuration of the numerical example proposed. The black dashed line indicates the triangular discontinuity.

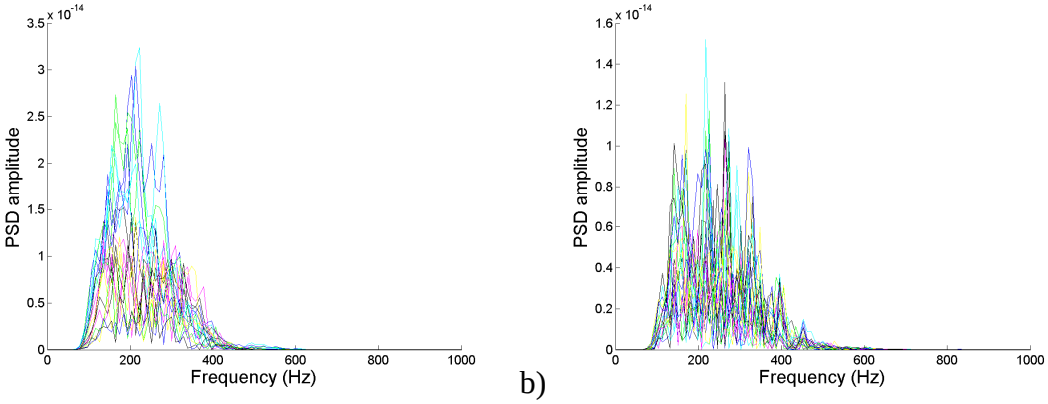

a) b)

Figure 6.2. Power Spectral Density of the recorded traces: a) for the first source; b) for the second source.

S-waves have been mainly generated, in order to simulate a real tunnel survey, where usually the S-waves are preferred respect to the P-waves, because of their larger amplitude. In Figure 6.2, the Power Spectral density of the recorded traces of the first and the second source are depicted. The frequency contents is included from 80 to 500 Hz, approximately, while the fundamental frequency is about 200 Hz, analogously to the frequency of the wavelet chosen as seismic source.

6.1.2. Velocity estimation

The seismogram relative to the first source is depicted in Figure 6.3. The direct waves are clearly identifiable, particularly the shear waves which are more energetic. About the reflection events, different peaks can be found, but a priori it is not always simple to know exactly the wave types and to discriminate the peaks due to noise or to a discontinuity. This observation is valid especially in real cases, where the signal-to-noise ratio can be quite small.

The advantage of the backward method respect to the forward approaches is then to avoid both the manual extraction of the peaks related to the reflected waves and every kind of signal analysis except for the calculus of the spectra, for the check of the frequency content. This is very convenient because it allow to save a lot of time and avoid the presence of a geophysicist in the data analysis.

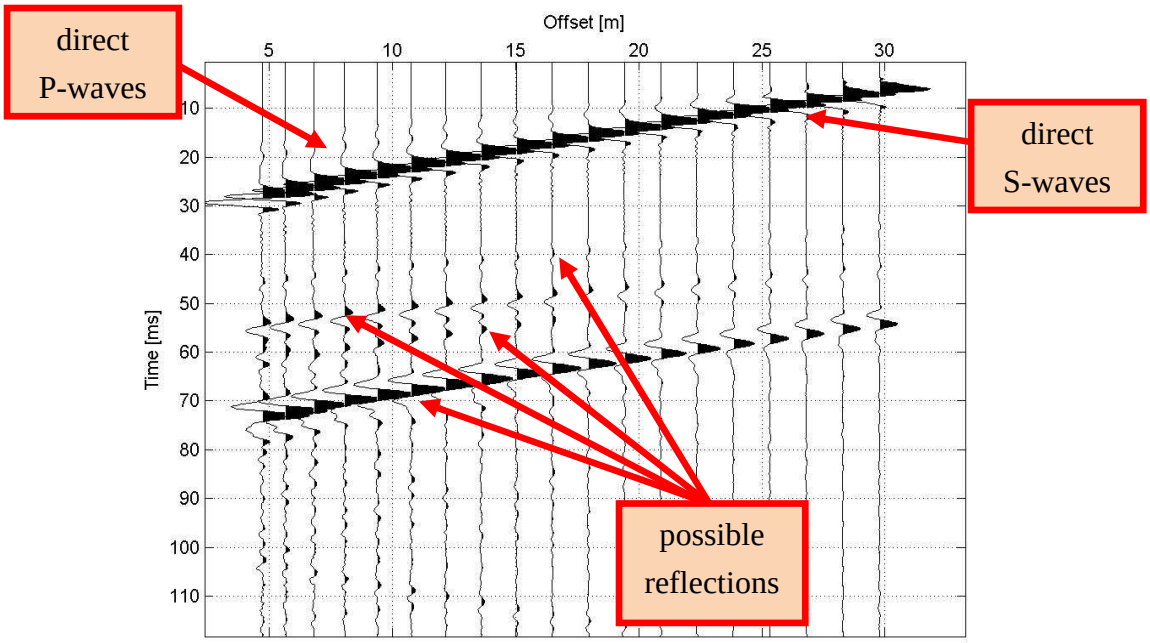

Figure 6.3. Spectrogram related to the first source, together with the interpretation of the different wave phenomena.

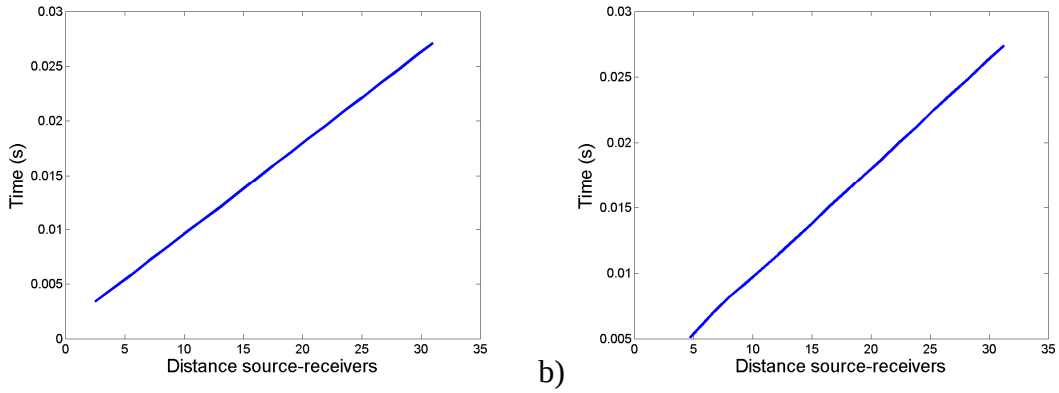

a) b)

Figure 6.4. Estimation of the velocity: a) for the first source; b) for the second source.

Once analysed the seismogram, according to the procedure explained in the previous chapter, the estimation of the velocity is firstly done on each source separately (see Figure 6.4) and successively the values obtained are averaged in order to obtain the final result. In this case, the S-wave velocity is estimated equal to 1197.3 m/s with a relative error of 0.23%.

6.1.3. Single estimates of the discontinuities

After the velocity estimation, the method collects all the admissible times, for the detection of the reflection points. In particular, as written in Subsection 5.4.2, the process searches a sequence of times that should be as close as possible to the theoretical times created by considering a point of the domain as a reflection point, and with the same polarity for corresponding amplitudes. This operation is shown in Figure 6.5, for the numerical model under analysis, for the first source.

In Figure 6.5a, the point $P_1 = (20,-25)$ is taken into account. This is not referred to the general domain (Figure 6.1) but to the domain defined by the first source. The theoretical times $t_R^{(1)}$ associated, indicated with the red line, are very close to the sequence $\bar{t}_R^{(1)}$ identified as the peaks in the traces corresponding to the reflection. If the point $P_2 = (0,-40)$ is considered, then the results are represented in Figure 6.5b: in this case, the method understands that there is not an admissible sequence of times and then it automatically generates a random succession of numbers that leads to a very high value of the standard deviation. On the contrary, in Figure 6.5a, the sequence created is close to the red line and then the standard deviation is small. This is the explanation why the method find the reflection points without inserting a threshold (that would be arbitrary) on the values of standard deviation.

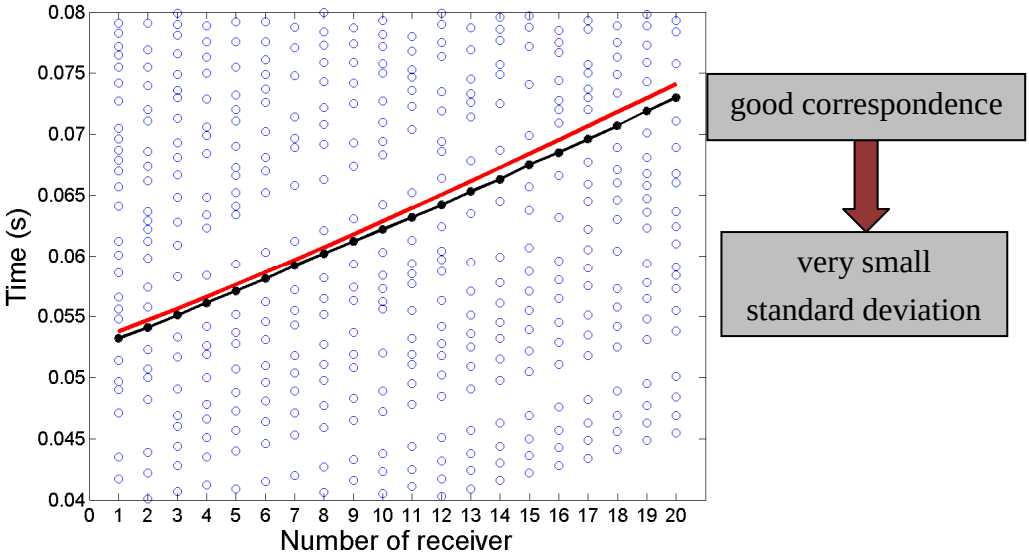

a)

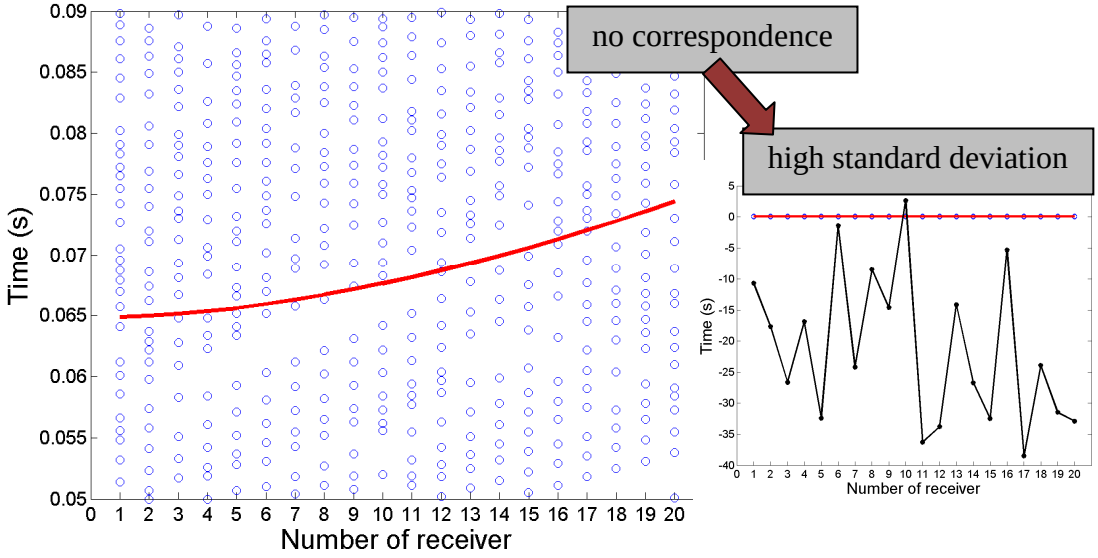

b)

Figure 6.5. Comparison between the theoretical times t_R, calculated by considering a point of the domain in the analysis conducted on the first source, and the time sequence $\bar{t}_R$ obtained by the method: a) for a reflection point; b) for a point not belonging to a reflector.

Once solved the identification of the time sequence $\bar{t}_R$, the method calculates the standard deviation for all the nodes of the domain. In Figure 6.6a the quantity $1-\sigma$ is depicted for one source, together with a magnification in order to highlight the zones close to one. In these regions, the points are recognized as reflection points.

The same thing can be noted in Figure 6.6b, where the plane X-Y is represented. The brown zones corresponds to the peaks of Figure 6.6a.

The six different estimations (each for source) are gathered according to the data processing described in Section 5.4, and they are directly derived from the previous process.

In Figure 6.7, for example, the estimation coming from the third and the sixth source are represented.

As can be seen in Figure 6.5b, the domain has been chosen in this way:

- x-coordinate varying from 0 to 100 meters
- y-coordinate varying from -40 to 40 meters

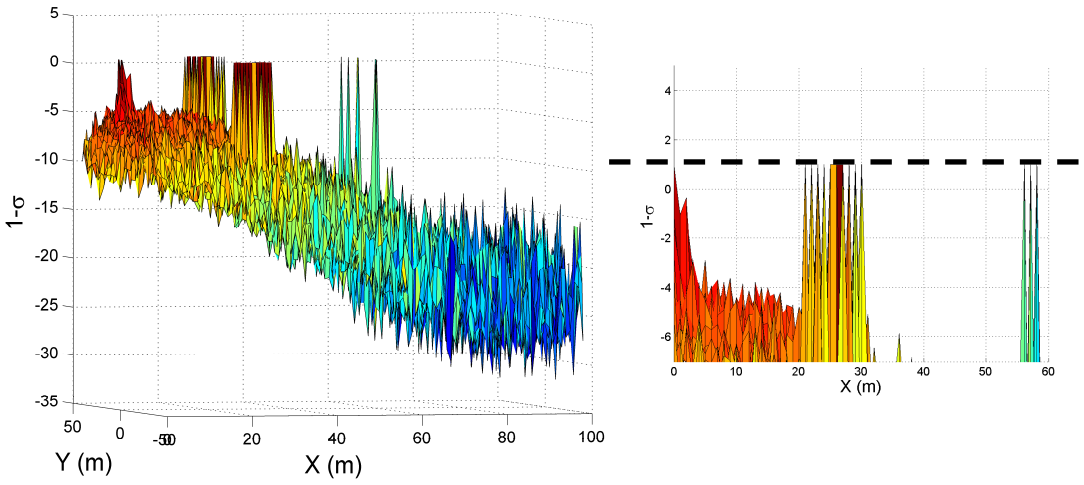

a)

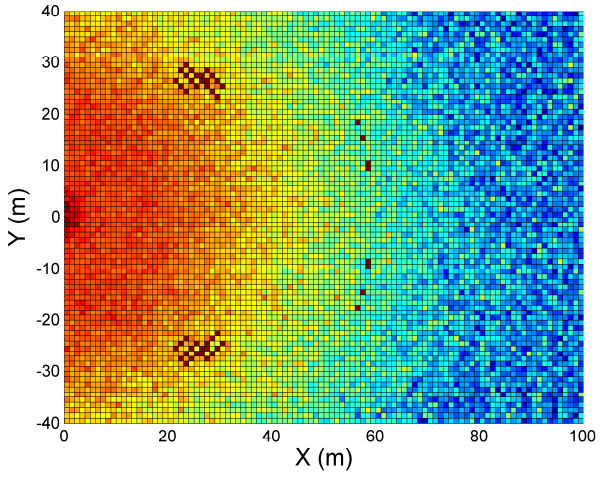

b)

Figure 6.6. Representation, for the third source, of the quantity $1-\sigma$, which is at the base of the statistical check for the discontinuity identification: a) in three-dimensional way and with a magnification in the X-σ plane; b) in X-Y plane.

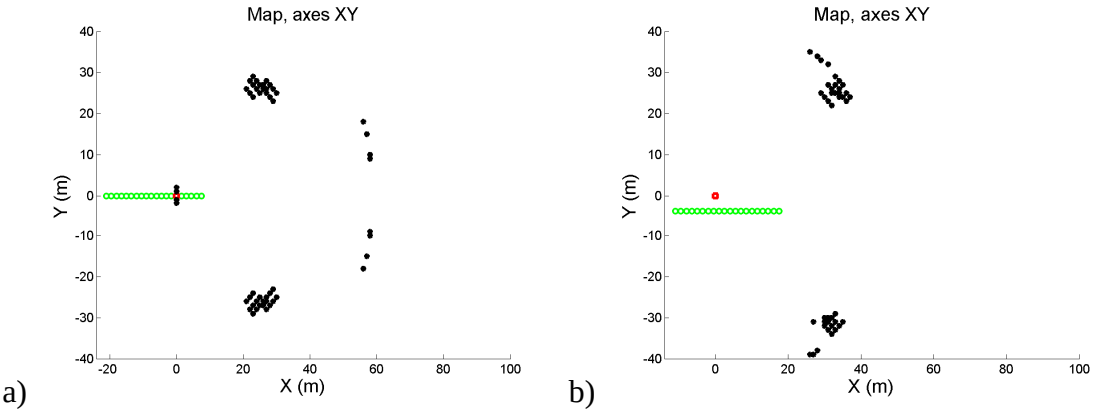

a) b)

Figure 6.7. Estimations of the reflection zones: a) for the third source; b) for the sixth source.

It is immediate to note that Figure 6.7a reflects exactly the brown regions of Figure 6.6b. Furthermore, in Figure 6.7a two reflection regions can be noted, but there is an ambiguity because they are specular to the tunnel axis. This is due to the fact that the receivers are disposed on a line, and moreover the source is also aligned with them. This topic has been already studied in Subsection 3.4.3 about the ellipsoids. Here it is important to note that the basilar principles are the same, even the ellipsoids are not explicitly created. On the contrary, in Figure 6.7b, only a reflector zone is identified and it is not exactly specular, since the source is not aligned with the sensors.

6.1.4. Final representation

For the final representation, the automatic procedure selects $R = 2$, since actually $R = \lambda/4 = v/4f \cong 1.5$.

The result given by the automatic procedure is represented in Figure 6.8, where the number of estimations N_P for each node is depicted. The colour scale has been set based on N_P: since there are six sources, the colours are seven, from white (no superposition) to black (total superposition). If in a node the colour is darker, then there is a larger probability to cross a discontinuity in that node.

In the figure there are many coloured zones, but two main regions can be identified. The most highlighted zone corresponds to the inclined side of the discontinuity, where all the estimates coming from the different sources superpose (black colour). However, a similar region is present in the superior part of the domain, but in this case there is not a total superposition (only blue colour). As already said in the previous subsection, this ambiguity happens because of the configuration of sensors and source points.

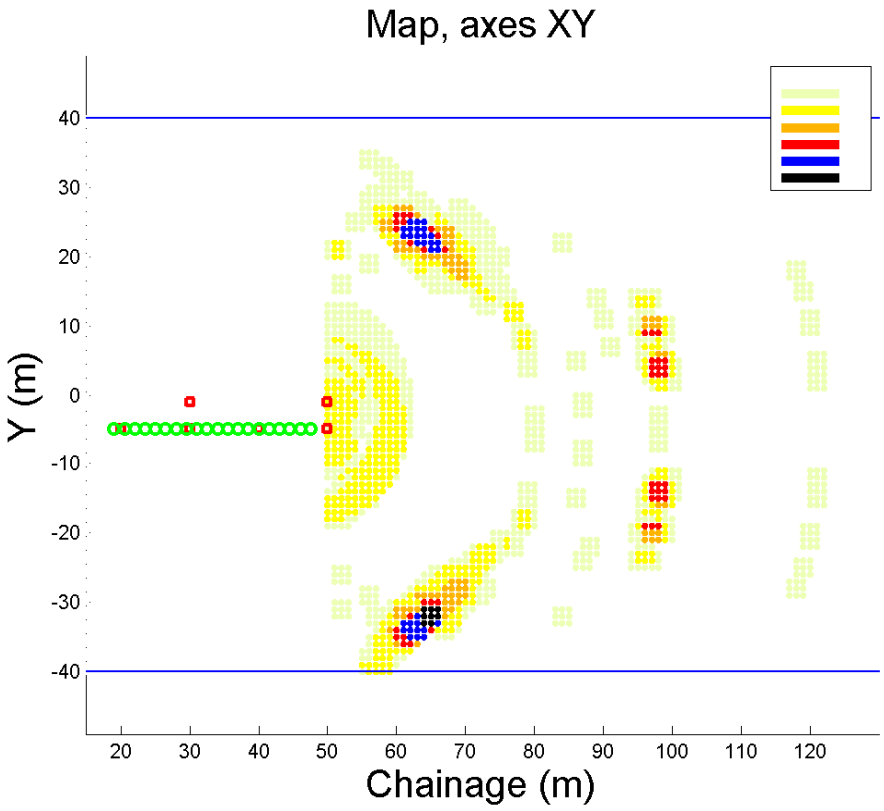

Figure 6.8. Final result obtained by the proposed method. The different colours indicate the probability to find a reflector in a certain point. The red squares point out the source locations, while the green circles reveal the receiver positions.

The example reflects a possible configuration in a tunnel survey, which is very limited spatially, and then it is difficult to well distinguish the estimates on both the tunnel sides. For this reason, the probability map helps us to understand that the reflector can be either on the right side or on the left side, and in this case it is more probable to find it on the right side.

The same annotation is valid for the second discontinuity, corresponding to the vertical side of the triangle, where the estimates are specular respect to the tunnel axis.

All the other zones of the domain are characterized by light colours, meaning that there is a very small probability to find a reflector.

6.1.5. Observations

All the visible zones in Figure 6.8 have a circular form. This is intrinsic to the problem: the reflections can be identified only in circular zones, with the radius increasing with the distance from the source.

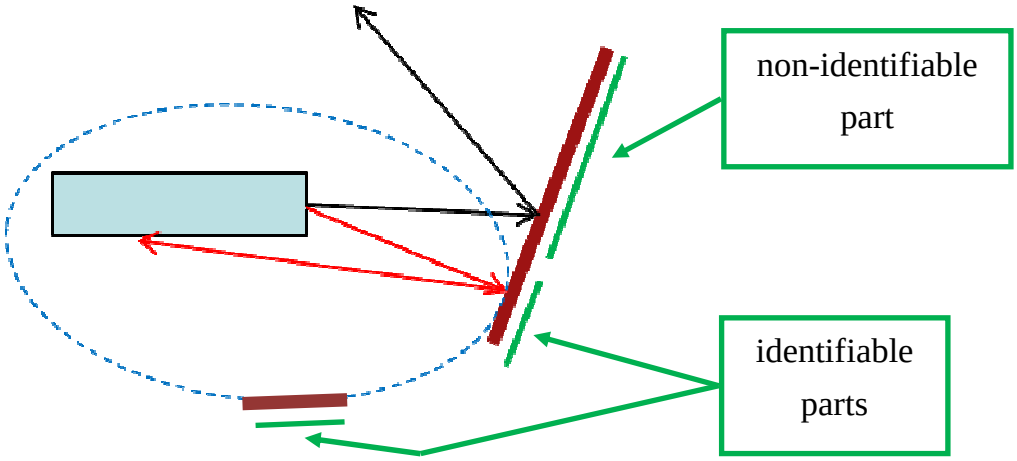

Figure 6.9. Scheme of the regions of the domain identifiable by an approach based on seismic reflection, in a tunnel survey.

Actually, they are not circles but ellipses, according with the theory introduced in Chapter 3. It is impossible to obtain other shapes, because the wave would be reflected in another part of the domain.

In Figure 6.9, this concept is explained by showing a tunnel with two discontinuities. The first one is almost completely identifiable, while the second one can be detected only in a small part. This is due to the fact that the reflections cannot be recorded by the receivers placed on the tunnel walls.

The computational time is very small, about 100 s to obtain the results of Figure 6.8, for a computer Intel Core 2 Duo CPU, 2.76 GHz, 1.87 GB RAM. The velocity in the computation is one of the most important aspect of the methodology, and therefore it is suitable for data processing of real investigations, especially for those tunnels in which the excavation is very quick.

6.1.6. Interpretation of the results

Once obtained the visualization given by the automatic method, the expert analyzing the data can add a personal interpretation of the results, such that they become clearer.

In particular, the discontinuity slopes can be approximated with a line crossing the most highlighted zones of the darker regions: this corresponds to the final interpretation of the survey and it is useful to understand where the tunnel axis will reach the discontinuity.

In Figure 6.10, two lines are drawn:

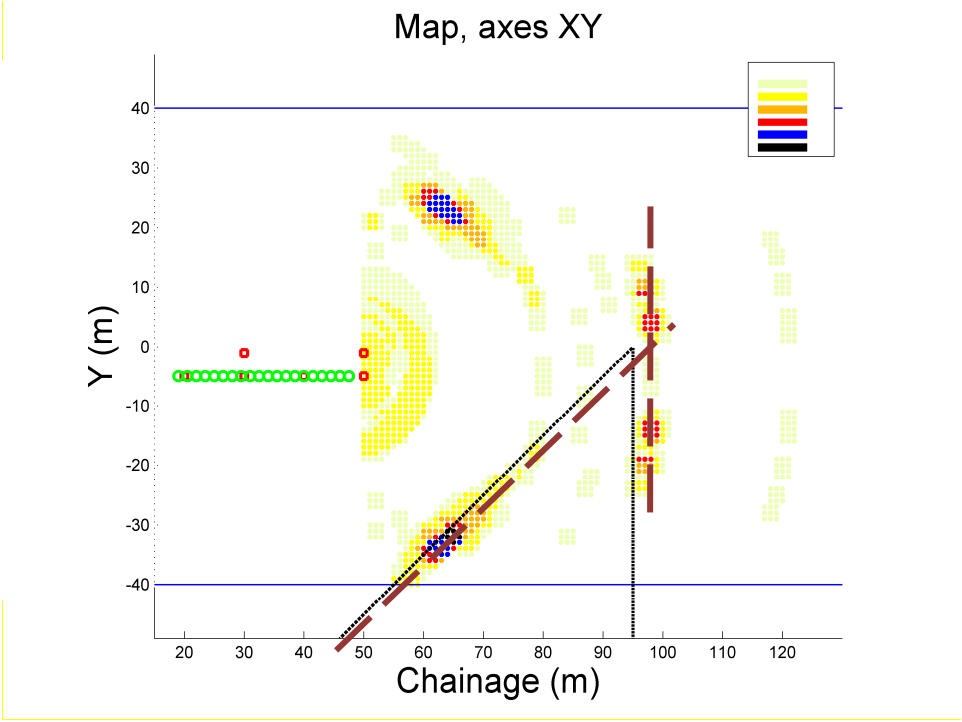

Figure 6.10. Final interpretation of the results obtained automatically by the method proposed. The thin black dashed line indicates the real discontinuity inserted in the numerical simulation, while the thick brown dashed lines indicate the interpretation.

1. The first line is designed over the identified reflection zone and prolonged in order to understand where the tunnel axis will cross the discontinuity. This line, compared with the inclined side of the reflector, shows that the estimation obtained is very good.
2. The second line is sketched over the two symmetric zones, meaning that the discontinuity is vertical. The result little overestimates (2-3 meters) the real location of the reflector because in the discontinuity zone the velocity is much smaller with respect to the estimated one.

The interpretation of the results is fundamental in a real survey where the estimations are not so clear, and therefore the expert can suggest the physical version of the results, maybe in collaboration with a geologist.

6.2. Simulation in Comsol Multiphysics®

The second numerical simulation has been created in *Comsol Multiphysics*®, in order to simulate a real tunnel configuration, i.e. with sensors disposed on two parallel lines, and with many different source points.

6.2.1. The configuration

In Figure 6.11, the configuration of the simulation is depicted, showing the presence of two materials: the granite and the brick. The latter is obviously impossible to find during a tunnel survey, but it has been chosen to simulate a rock softer than the granite. In this case, the reflection caused by the difference of impedance between the two materials can be estimated by the automatic method. The characteristics of the two media are listed in Table 6.3, where the velocities relative to the S-waves are also inserted, since the P-waves are not considered in the simulation.

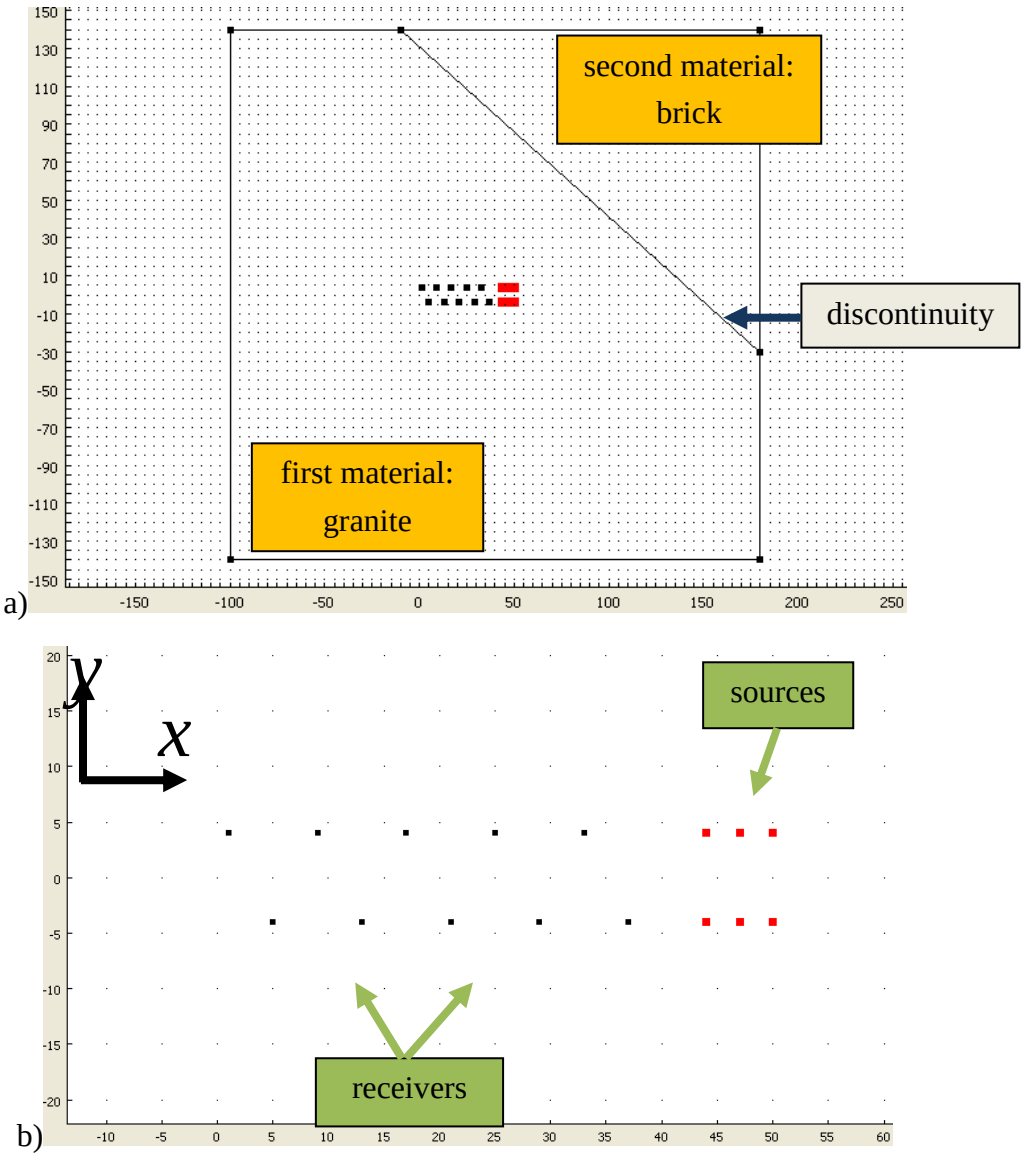

Figure 6.11. Configuration of the second numerical simulation: a) general view; b) magnification in correspondence of the zone including sources and receivers.

The positions of sources and receivers is listed in Table 6.4 and 6.5. In particular, there are six sources, three per each side, with three meters between two of them. About the receivers, they are disposed on two sides, spanned 8 meters each. This configuration allows both to simulate a real tunnel investigation and to have a sufficient misalignment to reduce the uncertainties in the estimation of the discontinuities.

Table 6.3. Characteristics of the media involved in the numerical simulation.

	First material: Granite	Second material: Brick
Young modulus	6×10^{10} N/m^2	1.7×10^{10} N/m^2
Poisson ratio	0.25	0.3
Density	2700 kg/m^3	1500 kg/m^3
S-wave velocity	3038.2 m/s	1808.1 m/s

Table 6.4. Positions of the source points.

	S_1	S_2	S_3	S_4	S_5	S_6
Coordinates	(50,4)	(50,-4)	(47,4)	(47,-4)	(44,4)	(44,-4)

Table 6.5. Positions of the receivers.

Number of receiver	Position
R_1	(1,4)
R_2	(5,-4)
R_3	(9,4)
R_4	(13,-4)
R_5	(17,4)
R_6	(21,-4)
R_7	(25,4)
R_8	(29,-4)
R_9	(33,4)
R_{10}	(37,-4)

The source is a Ricker wavelet with frequency equal to 200 Hz. Let us suppose that the receivers are geophones and therefore the velocity (in the y-direction) is estimated.

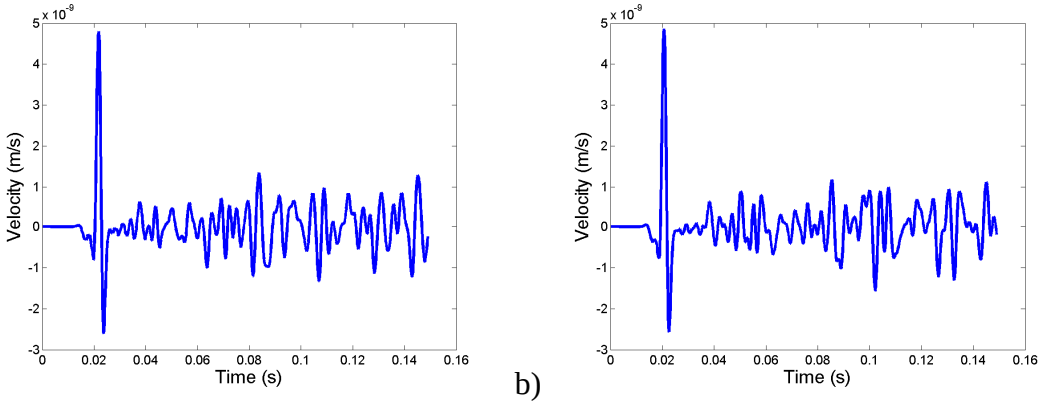

Figure 6.12. Representation of two signals extracted by the numerical simulation about the first source: a) signal relative to the first receiver, b) signal relative to the second receiver.

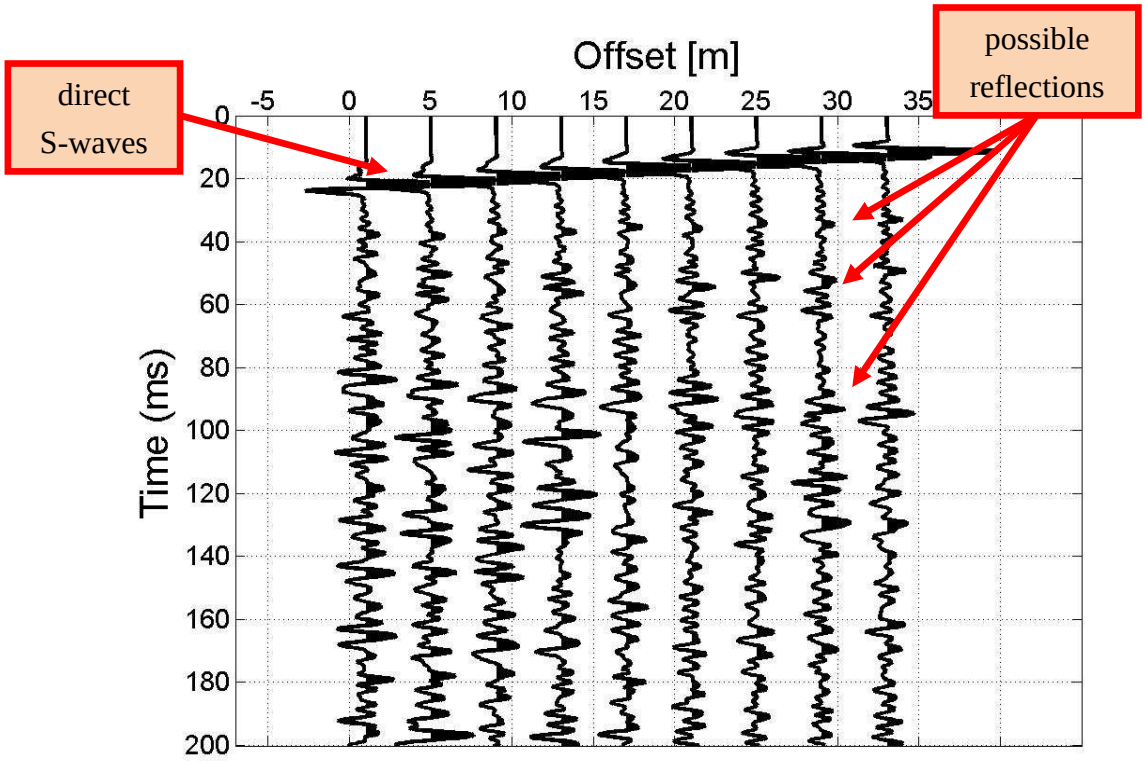

Figure 6.13. Seismogram relative to the first source, together with the interpretation of the different wave phenomena.

6.2.2. The signals and the velocity estimation

Once generated the numerical simulation, it is advisable to examine the signals extracted from the program. Two examples are proposed in Figure 6.12, where the signals coming from the first and the second receiver, relative to the first source S_1, are represented. In both the images, the direct wave is clearly identifiable, while the second part of the signal shows many peaks but a priori it is almost impossible to say which of these will correspond to the discontinuity between the two materials.

To have a more precise idea, in Figure 6.13 let us analyse the seismogram relative to the first source. Analogously to Figure 6.12, the peaks relative to the direct waves are easily detected, while the peaks connected to the reflection due to the change of material cannot be clearly distinguished, as happen in a real survey.

The velocity estimated is equal to 3047.6 m/s, with a relative error equal to 0.31%.

6.2.3. The estimation of discontinuities

After estimated the wave velocity, the automatic method is applied to obtain the final representation of Figure 6.14. The parameter R is equal to 4.

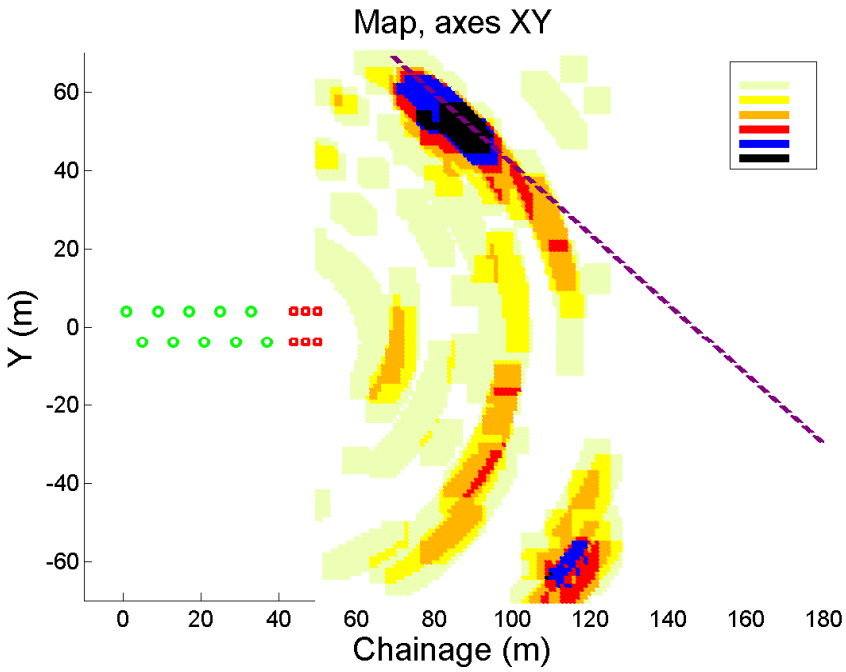

Figure 6.14. Representation of the discontinuity obtained by the automatic method. The red squares indicate the source points, while the green circles indicate the receivers. The violet line indicates the discontinuity.

In the figure, only one critical zone is identified, with black colour. This actually corresponds to the reflection zone given by all the sources and receivers. It lies perfectly on the real discontinuity and therefore the prediction can be considered very accurate. Moreover, there is not a specular estimation, as seen in Figure 6.10, this because the configuration is more spatially distributed and the sensors are not aligned. Every other zone cannot be considered as critical, except for a small region on the right side of the tunnel.

This example, simulating an experimental case in a real tunnel, is useful to demonstrate the performance of the method even in presence of a seismogram which is not particularly clear. Indeed, the method is able to automatically select the peaks referred to the reflection, in order to avoid the manual intervention of a geophysicist, which can be both a long and not accurate operation. Finally, the method produces very accurate results, avoiding also ambiguities connected with the sensor placement.

Chapter 7

Experimental tests in the Brenner Base Tunnel

All the experimental tests done for the verification of the algorithm have been performed in the Mules site, within the Brenner Base Tunnel.
Let's first explain the global project of the Brennero tunnel and the Mules site, then the acquisitions with the TRT and TRUST schemes are presented and finally some tests are analyzed by means of the backward method.

7.1. The Brenner Base Tunnel

7.1.1. The project

The Brenner Base Tunnel (in Italian: "Galleria di base del Brennero", in German: "Brennerbasistunnel", but often abbreviated in BBT), is a railway tunnel connecting Italy with Austria, exactly from Fortezza (Italy) to Innsbruck (Austria), through the base of the Brenner massif. The tunnel will be 55 km long, but if the final part is considered, the total length will be 62.7 km, and then it will be longest railway tunnel in the world.
The idea of the project is to improve the connection along one of the most important commerce ways between the south and the north of Europe. In particular, the BBT represents a central element of the AV/AC way (Berlin-Munchen-Verona-Bologna-Palermo) which is around 2.200 km long.
Since the existing railway reaches the maximum slope of 26%, it is not possible to easily transport a big amount of wares. In order to allow high-speed trains to quickly transport wares from Italy to Austria, the new tunnel will have two main advantages:

- the railway length from Fortezza to Innsbruck is significantly reduced

Figure 7.1. General scheme of the BBT project (Font: Google Maps, http://maps.google.it).

- the maximum slope is equal to 5%

In Figure 7.1, the project of the tunnel is indicated, together with the connections to the most important cities interested by the project.

Analogously to the system adopted for the Gotthard tunnel (Switzerland), the BBT is constituted by two separated tunnels. The works started in 2008 with the Aica tunnel, in the Italian part. This tunnel is about 10 km long.

7.1.2. The Mules site

The objective of our work is to monitor one of the most problematic rock zones, interested by the so-called Periadriatic seam, which is supposed to be close to the Mules site, which is situated at the end of the Aica tunnel, in the Italian part, as can be seen in Figure 7.2. The Periadriatic seam is a distinct geologic fault in Southern Europe, running S-shaped about 1000 km from the Canavese (in the north of Piemonte) to Carnic Alps (in Friuli Venezia Giulia). It forms the division between the Adriatic plate and the European plate. Actually, this is a very interesting zone from a geological point of view; therefore the main objective of the work is to estimate the lithological

variations ahead of the tunnel face and to understand when the Periadriatic seam is located. From some rough geological inspections, it is situated some tenths of meters ahead of the end of the Aica tunnel.

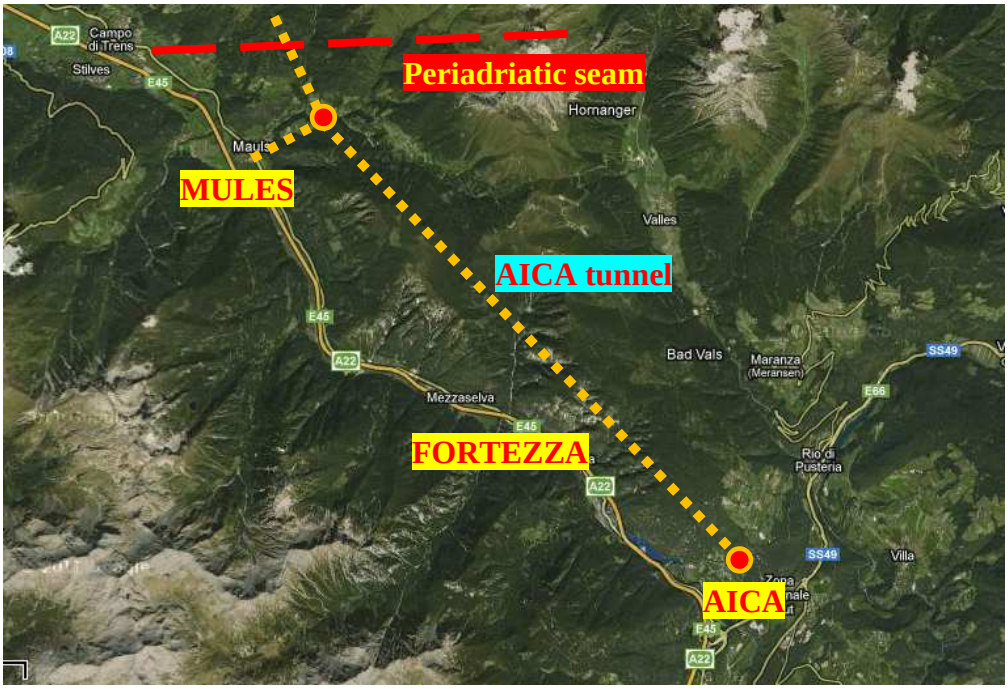

Figure 7.2. Map of the first zone of the Italian part (Font: Google Maps, http://maps.google.it).

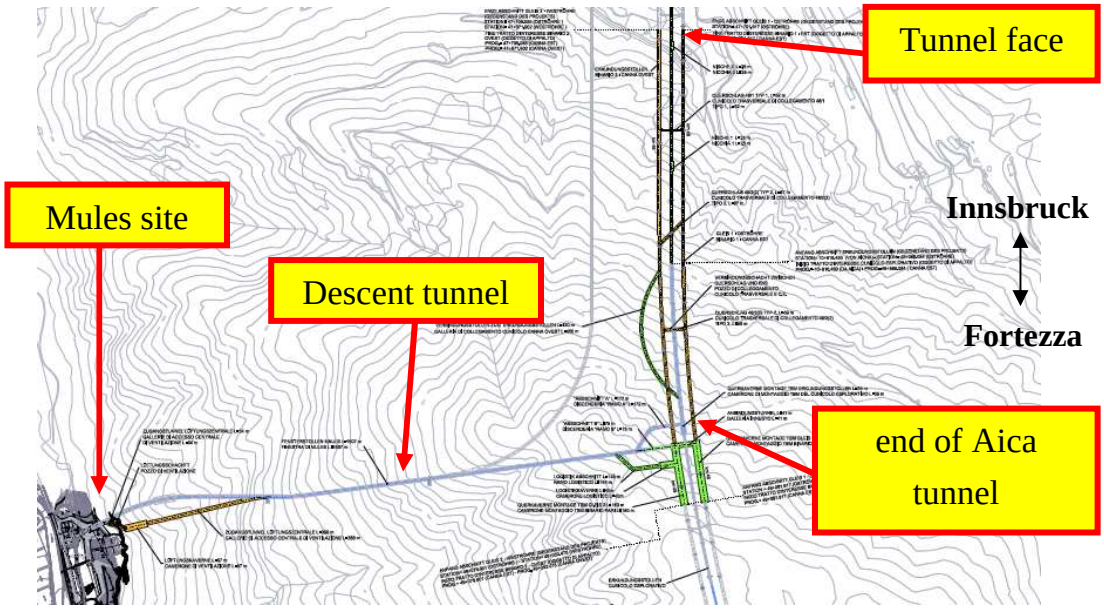

Figure 7.3. Map of Mules site.

In the Mules tunnel, like in Aica tunnel, the granite and the tonalite are the dominant rocks. If an abrupt change in the rock characteristics will be identified, probably that discontinuity will correspond to the Periadriatic seam. Due to this fact, once completed the Aica tunnel, the excavation technique has been changed from TBM to the classical drilling and blasting.
In Figure 7.3, the map of the Mules site is visualized. It is characterized by a descent tunnel that allows to reach the end of the AICA tunnel.

7.2. The experimental survey

The data acquired on the tunnel are based on two configurations:

1. TRT scheme (Subsection 2.4.3)
2. TRUST scheme (Subsection 2.4.4).

7.2.1. TRT scheme

According to the TRT scheme (Descour *et al.*, 2012; Aoki K. *et al.*, 2007; Yamamoto et al., 2006), the waves are generated in 12 points by hammer strokes, and ten receivers are placed on the tunnel walls. The source points are on two sections, while the accelerometers are disposed on four sections, alternating two and three sensors per each section, analogously to Figure 2.15.
In each source point, five hammer stroke are applied, and successively the tracks recorded have been stacked to increase the signal-to-noise ratio. A sensor has been placed on the hammer to have a representation of the source signal and to automatically get the initial acquisition time (see Figure 7.4).

Figure 7.4. Hammer used for the excitation against the tunnel walls. A pilot sensor is mounted on it and connected to the acquisition system.

a)  b) 

Figure 7.5. Examples of source locations: a) near the ground level; b) close to the top of the tunnel. They are always highlighted by means of a red marker.

From a practical point of view, the excitations produced near the ground level, as in Figure 7.5a, can be performed in a convenient position, contrarily to the case when the sources are close to the top of the tunnel, as in Figure 7.5b.

The accelerometers are mounted at the top of small fiberglass bars (see Figure 7.6), after having first mounted a small screw to fix the sensors. Successively, they are inserted in small holes inside the tunnel walls, as shown in Figure 7.7. During this operation, first a square hole of about 30 cm of side is excavated and then, once made the small holes, the fiberglass bars are inserted in, together with the accelerometers. This process assures a good rock-sensor coupling.

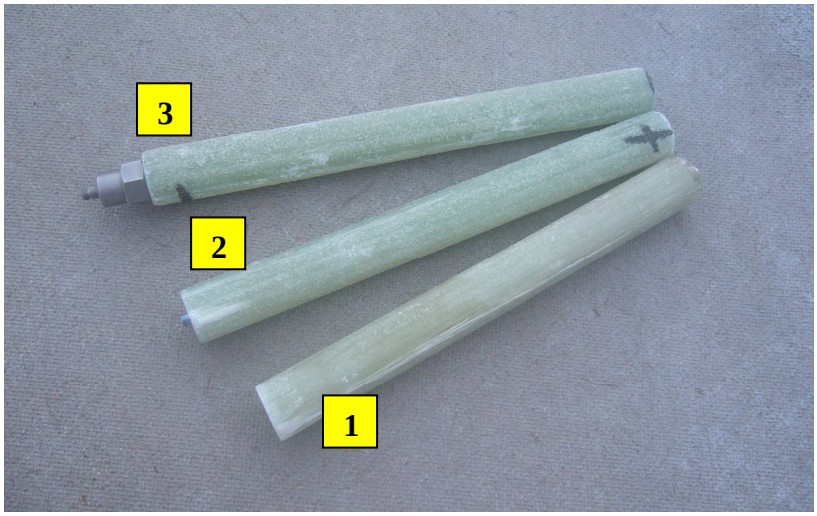

Figure 7.6. Fiberglass bars used for the coupling rock-sensors. The numbers indicate the sequence for connecting the sensor to the bar.

Figure 7.7. Placement of the sensor and the fiberglass bar in the tunnel wall.

a)  b) 

Figure 7.8. (a) Acquisition system and (b) seismograph for the signal visualization.

The signals coming from the sensors are recorded with the acquisition system of Figure 7.9a, while they are visualized by means of the seismograph of Figure 7.9b.
The sampling frequency is chosen equal to 8000 Hz, and the traces are truncated to 0.2 s to consider reflections up to 250-300 meters ahead of the tunnel face. These settings are valid also for the TRUST scheme.

7.2.2. The TRUST scheme

The TRUST scheme is completely different from the TRT scheme. It has been planned by the German company DMT (Benecke *et al.*, 2008).

The main difference is that the excitation is produced by blasting. Moreover, the sources are usually disposed on the same tunnel side, at a fix distance of five meters one from another, as already seen in Figure 2.16. Obviously, in this case the excitations are not repeated and then the stack procedure is not applied.

The sensors are disposed on four sections, with three sensors per each section.

The process for the preparation of the acquisition is based on different points, which are shown in Figure 7.9:

a) The sensors are mounted at the end of special wood supports, which have rigid springs able to obtain a good coupling with the rock; after that, they are inserted in the holes previously excavated.
b) The blasting is prepared, by means of a collaboration between the people devoted to the acquisition and the blasting experts
c) The explosives are inserted in holes previously excavated, with the aid of a long plastic bar.

Figure 7.9. Sequence of operations for the TRUST investigation: a) fixing the accelerometer on the support; b) preparation of the explosive; c) insertion of the explosive in the hole previously excavated in the tunnel wall; d) connecting all the cables to start the acquisition.

d) All the cables coming from sensors and explosives are connected with the acquisition system.

The initial time of the acquisition is given by the sudden change in voltage occurring when the explosion is detonated, because it breaks the cable connected to the acquisition system.

7.2.3. Evaluation of the results

The unique way to evaluate the results of an analysis is to compare them with the results coming from the excavation. This can obtained in two ways:

- with a pilot probe, drilled into the rock to obtain punctual information for some tenths of meters ahead of the tunnel face
- with a front survey (or evaluation), by inspecting the rock quality and the presence of discontinuities.

The two approaches can be seen as complementary, because the first one is along the tunnel axis, while the second is a survey along the tunnel face, i.e. on the y- and z-coordinate.

About the pilot probe, the most important parameter obtained is the RQD (Rock Quality Designation), which is one of the most important classification index for rocks, introduced by D. U. Deere in 1964. It is based on the percentage of rock fragments whose lengths is larger than 10 cm, get back from the drilling operation. The mathematical definition is given by:

$$RQD = \frac{\sum_{l>10} l}{L} \tag{7.1}$$

where l indicates the length of an extracted sample, and L the total length of the drilling operation. If $RQD < 25\%$ then the rock mass quality is considered very poor, if $RQD < 90\%$ then it is considered excellent.

Every time a drilling and blasting technique is applied for the tunnel excavation, a front survey is performed. It includes a photography of the tunnel face, information about the presence of water and the visible fractures, even if they are very small. For simplicity, in the thesis, the information is summarized by associating simple colours to the rock quality:

- no colour: absence of reflectors
- grey colour: weak or not much visible discontinuity
- black colour: strong or evident discontinuity

7.3. First test

The first test in the Brennero tunnel is based on the TRT scheme (Figure 2.15), with the 12 sources and the 10 receivers placed in the positions listed in Table 7.1.
Let us first analyze the signals and then the backward method is applied to obtain the prediction of the lithological discontinuities.

Table 7.1. Positions of sources and receivers, for the first test.

Source	Position		Receiver	Position
S_1	(-2.00, 2.34, 0.50)		R_1	(-20.00, 2.78, 3.50)
S_2	(-2.00, 2.98, 2.70)		R_2	(-20.00, -2.86, 3.30)
S_3	(-2.00, 2.31, 4.30)		R_3	(-25.00, 2.66, 1.00)
S_4	(-2.00, -2.38, 4.20)		R_4	(-25.00, 0.00, 5.38)
S_5	(-2.00, -2.97, 2.80)		R_5	(-25.00, -2.66, 1.00)
S_6	(-2.00, -2.34, 0.50)		R_6	(-30.00, 2.78, 3.50)
S_7	(-6.00, 2.34, 0.50)		R_7	(-30.00, -2.82, 3.40)
S_8	(-5.50, 3.00, 2.30)		R_8	(-35.00, 2.66, 1.00)
S_9	(-5.50, 2.82, 3.40)		R_9	(-35.00, 0.00, 5.38)
S_{10}	(-6.00, -2.53, 4.00)		R_{10}	(-35.00, -2.66, 1.00)
S_{11}	(-6.00, -3.00, 2.50)			
S_{12}	(-6.00, -2.34, 0.50)			

7.3.1. Signals and spectra

Before applying the backward method, it is advisable to analyze the recorded signals and their spectrum.
In Figure 7.10 the signal recorded by the sensor mounted on the hammer is visualized. The peak due to the hammer stroke is clearly identifiable, while the remaining part is only due to noise.
In Figure 7.11, instead, the signal recorded by the first accelerometer, for the second source, is considered. Its time history (shown in Figure 7.11a), in the first part, is similar to the corresponding signal source, but it contains some reflective events in the second

part, after the peak corresponding to the direct wave. In Figure 7.11b, the power spectral density of the signal under analysis reveals that the frequency content is included mainly between 350 and 500 Hz. This will be useful also for the extraction of the parameter R.

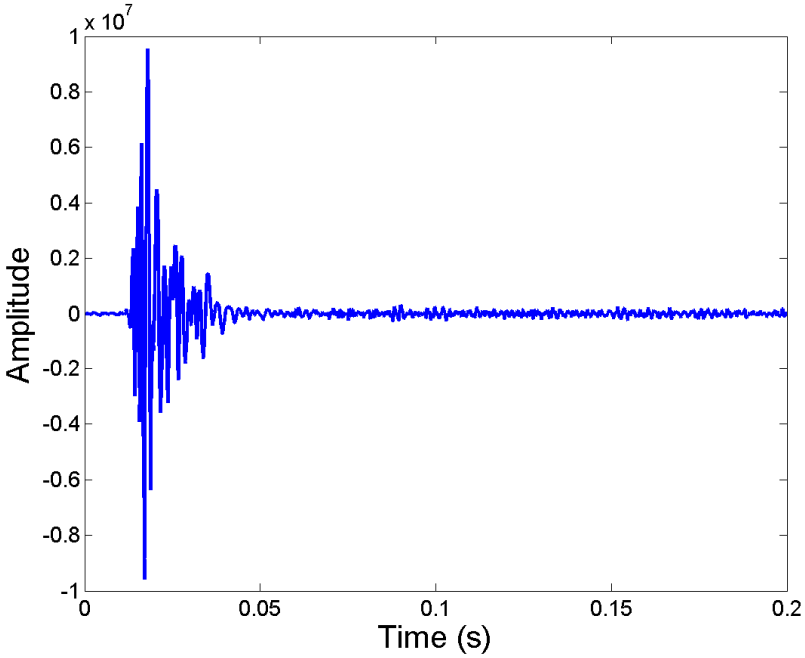

Figure 7.10. Signal representing the source signal, given by an hammer stroke, for the second source.

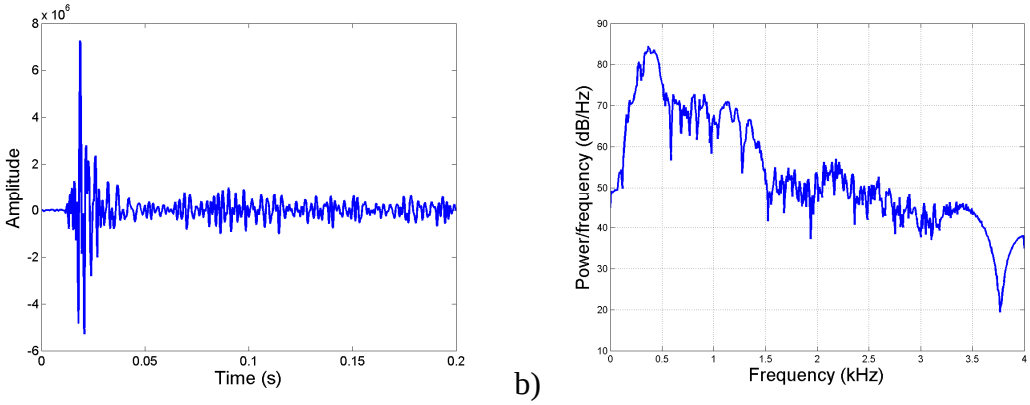

a) b)

Figure 7.11. Signal recorded by the first accelerometer, for the source n°2: a) time history; b) power spectral density.

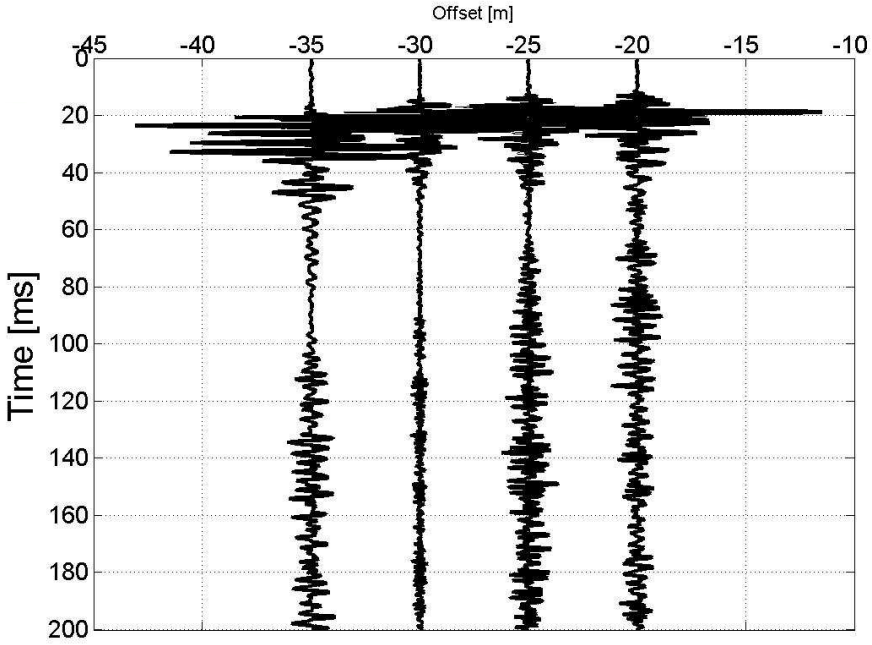

Figure 7.12. Seismogram relative to the source n°2, including four traces recorded by the accelerometers.

Coming back to the reflective events, at a first sight they are very difficult to be estimated, even if collected with others coming the same acquisitions, as shown in the seismogram of Figure 7.12, where four traces are collected. No evident peaks indicating a reflection can be seen.

For this reason, the method created is applied to automatically identify the peaks related to a discontinuity, without “manually” analyzing all the traces.

7.3.2. Estimation of the discontinuities

The estimation of the reflectors begins with the estimation of the wave velocity. For this purpose, as well as for the identification of discontinuities, only the accelerometers placed on the same tunnel side of the source are considered. This is done because the tunnel curvature is not negligible and this causes a delay in the arrival times of the wave, both direct and reflected. This annotation is valid in general for each type of configuration in a tunnel.

In Figure 7.13, the values obtained for the different sources are depicted. A value is calculated for each source and then the values outside the interval defined by the standard deviation are eliminated. Finally, the velocity is calculated as the average of the remaining values, and the value obtained is 2611.9 m/s.

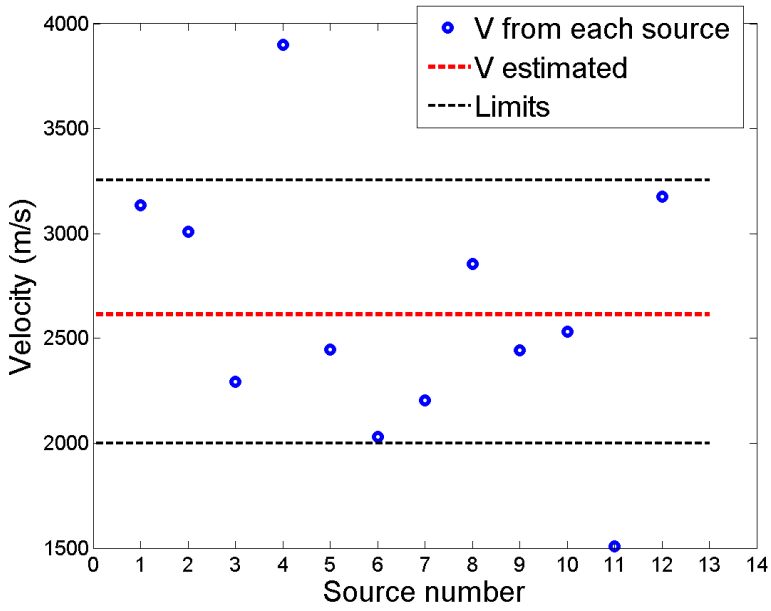

Figure 7.13. Estimation of the velocity for the first test under analysis.

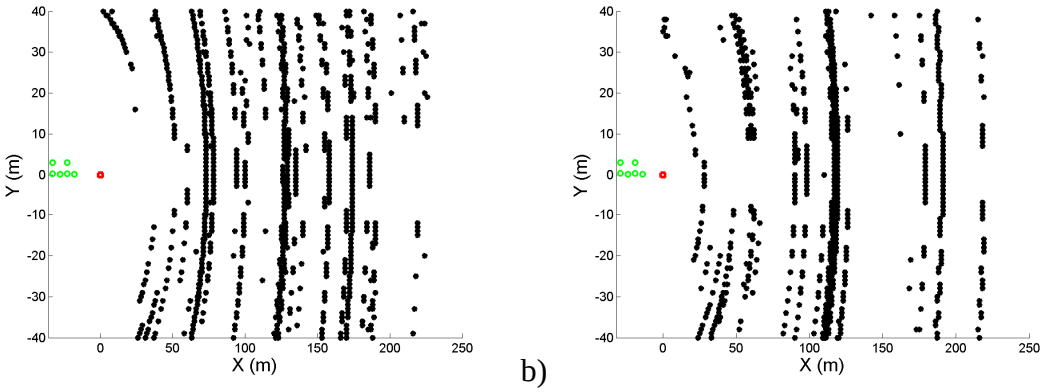

a) b)

Figure 7.14. Estimations coming from the analysis on a single source (map view): a) for the fifth source; b) for the eleventh source.

Successively, a domain of (-40,40) m has been chosen both for the Y and the Z direction, while 250 meters of forward prediction are considered for the X-axis.

In Figure 7.14a and 7.14b, two estimations coming from the fifth and the eleventh source are shown, for the analysis on the XY plane.

As described in Subsection 5.4.1, the source, indicated by a red square, is in the origin of the axes, while the accelerometers, defined by green circles, are behind the source point. Moreover, the forward prediction has been extended up to 250 meters ahead of the tunnel face. Apparently, the estimations do not have a high degree of similarity but

effectively they have many common points, which can be seen in better way in the common representation of Figure 7.15, by compacting all the partial results into a unique final result.

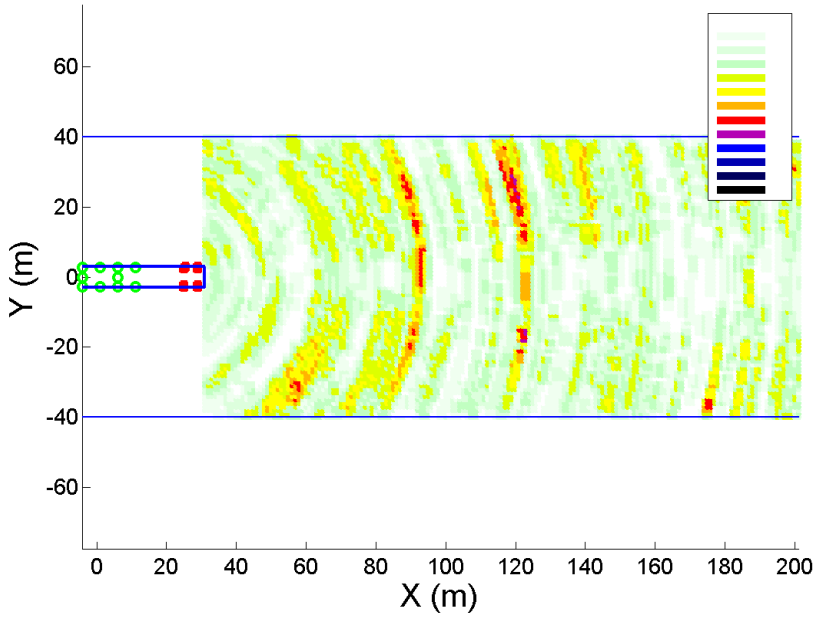

a)

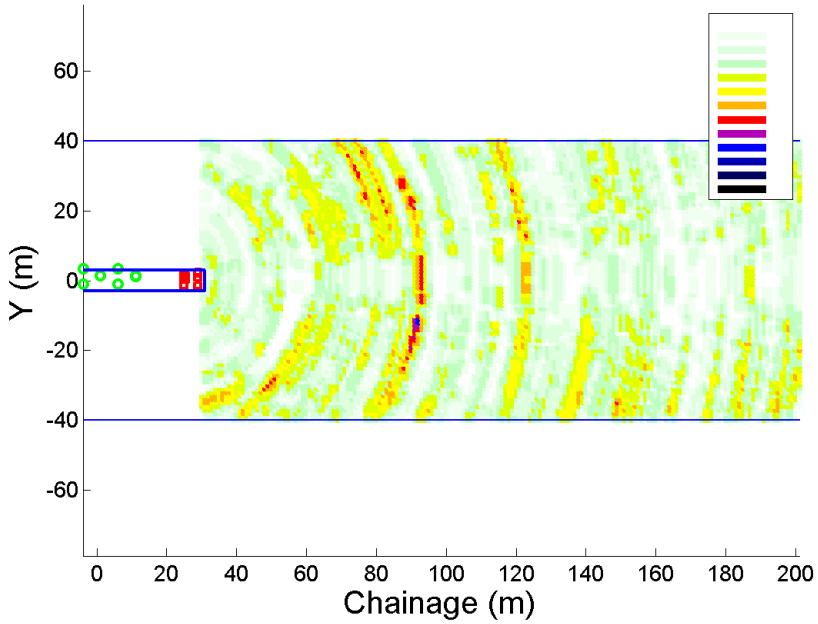

b)

Figure 7.15. Final representation given by the automatic method for the first test, depicting the number of common estimations for each point of the domain: a) map view; b) cross-sectional view. Source points are indicated with red squares, receivers with green circles.

To build the figure, the parameter R has been automatically chosen equal to 2, and the domain has been slightly reduced. In Figure 7.15a the map view is shown, while in Figure 7.15b the cross-section view is depicted. In Figure 15.a, two evident reflection zones are distinguishable, while other small reflectors can be seen at the beginning and at the end of the domain. As already said, the method does not identify the entire region of a certain rock or material but only the reflectors, i.e. the boundary zones between two media having different impedances. That's the reason why in the final representation only some curves are depicted, instead of coloured zones. In Figure 7.15b, the cross-sectional view (X-Z plane) is depicted, showing results similar to those of the X-Y plane. In particular, the most evident discontinuities are close to the chainage 95 m and 120 m, but there is not any indication about the critical zone close to the chainage 60 m in Figure 7.15a.

7.3.3. Final interpretation and evaluation of the results

Once obtained the final representations by means of the automatic method both for the map and for the cross-sectional view, the analysis ends with the interpretation of the results: an indication of the number and the inclination of the discontinuities must be given, such that the figures are more understandable for the people who just want to know how to set the excavation in the tunnel.

In Figure 7.16, the interpretation of the results is presented, by superposing some blue dashed lines to the results of the automatic procedure, both for the map and the cross-sectional view. Moreover, the results of the excavation are expressed by grey and black colours, as described in Subsection 7.2.3. In this case, these colours indicate the presence of a zone with characteristics slightly or significantly different from the tonalite (respectively), which is the rock taken as reference within this part of the Brennero tunnel. In this analysis, only this qualitative information about the lithology is available, because no pilot probes are drilled into the rock.

About the interpretation, the dashed lines are drawn over the zones with darker colours and prolonged until to reach the tunnel axis. This operation allows to approximately identify the angles α and γ characterizing the discontinuity (see Subsection 3.2.3 for more details). The lines must be compared with the coloured zone given by the excavation results. There are some different critical zones, especially at the beginning of the domain of analysis. This is a reason why the velocity value (2611.9 m/s) is smaller respect to the expected one (around 3000 m/s).

The automatic method identifies three major discontinuities, correspond to rock change. In particular, the beginning of the critical zone starting close to the chainage 90 m has been perfectly detected. Moreover, the previous rock change (close to chainage 80 m)

has been underestimated by the X-Y analysis and overestimated by the X-Z analysis. An average value of the two predictions is a good estimation of the discontinuity. The last discontinuity predicted roughly estimates the beginning of the last critical zone.
The fact that the map and the cross-sectional analyses give very similar results, in terms of intersection with the tunnel axis, is another indication of the reliability of the method.

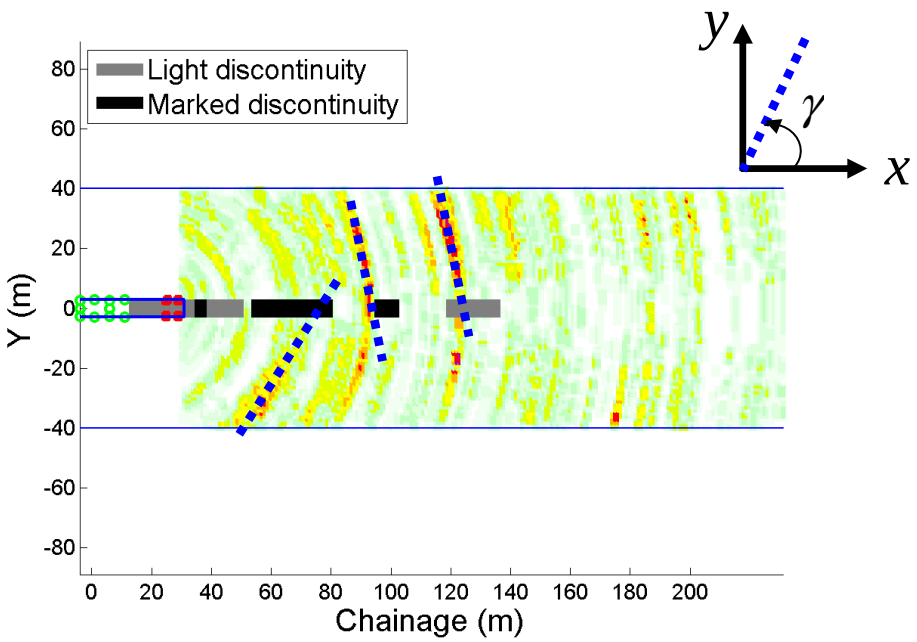

a)

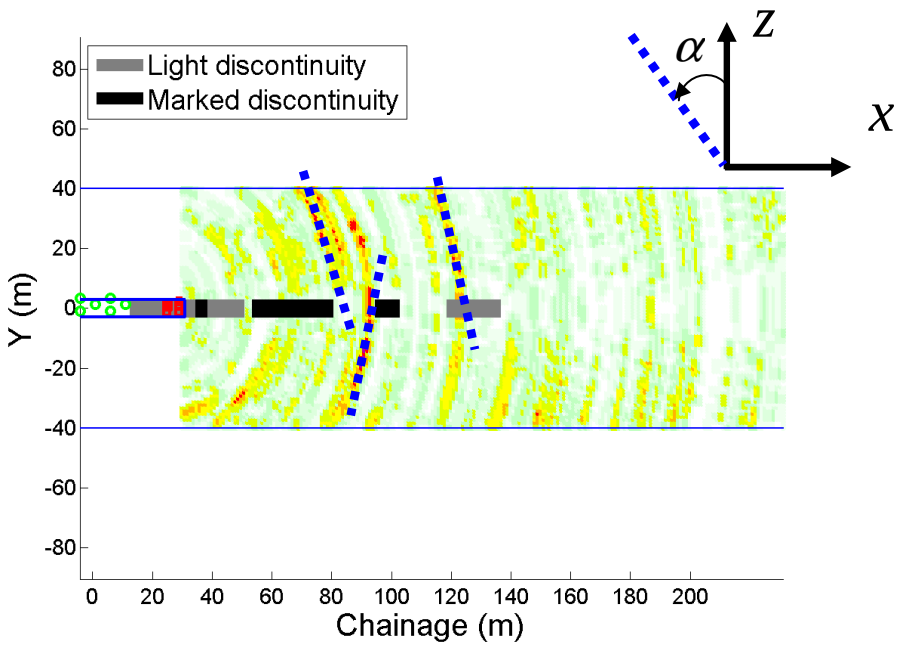

b)

Figure 7.16. Results of the automatic method for the first test compared with the results of the front survey (grey and black rectangles), and with the personal interpretation (blue dashed lines): a) map view; b) cross-sectional view.

7.4. Second test

The second test, analogously to the first one, is based on the TRT scheme. The location of the source points and of the receivers are listed in Table 7.2. Analogously to the previous test, there are 12 sources and 10 receivers.

Table 7.2. Positions of sources and receivers, for the second test.

Source	Position		Receiver	Position
S_1	(-6.00, 4.74, 0.50)		R_1	(-20.00, 4.27, 5.80)
S_2	(-6.00, 5.10, 4.00)		R_2	(-20.00, -4.27, 5.80)
S_3	(-6.00, 3.96, 6.20)		R_3	(-25.00, 5.22, 2.20)
S_4	(-6.00, -4.34, 5.70)		R_4	(-25.00, 0.00, 8.30)
S_5	(-6.00, -5.10, 4.00)		R_5	(-25.00, -5.22, 2.20)
S_6	(-6.00, -4.74, 0.50)		R_6	(-30.00, 4.12, 6.00)
S_7	(-10.00, 4.74, 0.50)		R_7	(-30.00, -4.41, 5.60)
S_8	(-10.00, 4.74, 4.20)		R_8	(-35.00, 5.22, 2.20)
S_9	(-10.00, 3.57, 6.60)		R_9	(-35.00, 0.00, 8.30)
S_{10}	(-10.00, -3.67, 6.50)		R_{10}	(-35.00, -5.22, 2.20)
S_{11}	(-10.00, -5.10, 4.00)			
S_{12}	(-10.00, -4.74, 0.50)			

The velocity is estimated equal to 3080 m/s, and this is consistent with typical values of the S-waves of sound granite.

In this case, $R = 3$ because the most evident frequency is around 250 Hz.

In Figures 7.17a and 7.17b, different critical zones can be identified, especially around chainage 170 m. The interpretation is depicted in Figures 7.18a and 7.18b, together with the results coming from the excavation, showing six critical zones for the X-Y analysis and four critical zones for the X-Z analysis. There is a good agreement between the results of the automatic method and the geological results obtained with a front survey after the excavation. In particular, the first, the third and the fourth boundary zones are well detected, while the second and the fifth are not precisely identified.

Although the velocity is assumed to be constant, the estimates obtained by the automatic procedure are close to the real discontinuities: this is probably due to the presence of rather homogeneous rock mass with local discontinuities that slightly affect the average wave velocity values.

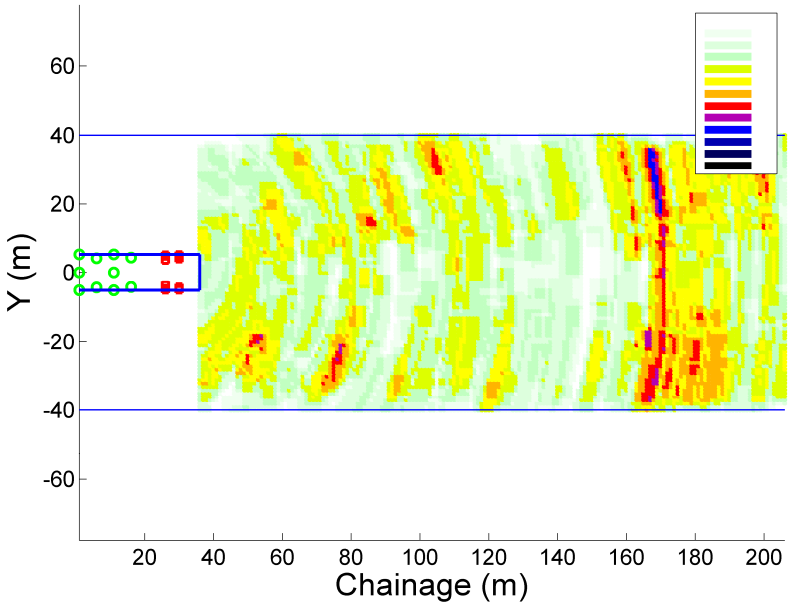

a)

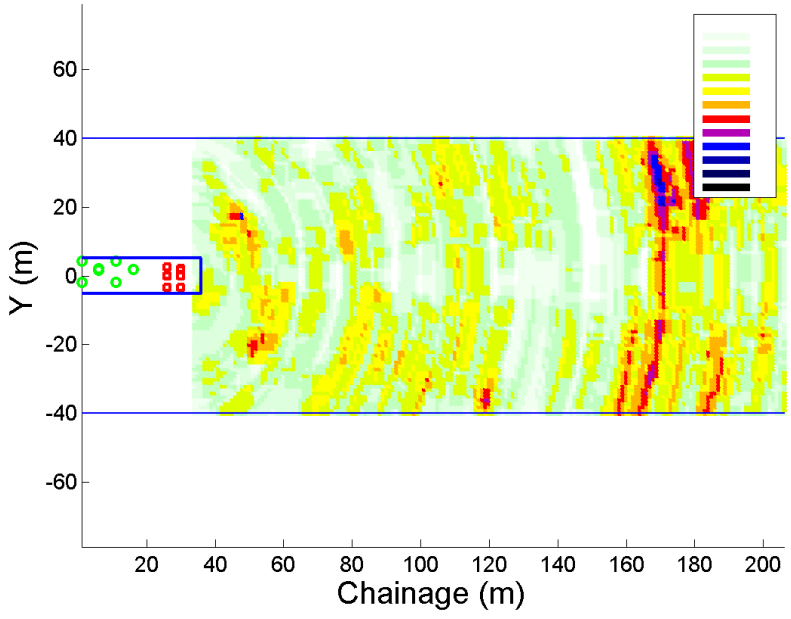

b)

Figure 7.17. Final representation given by the automatic procedure for the second test, depicting the number of common estimations for each point of the domain: a) map view; b) cross-sectional view.

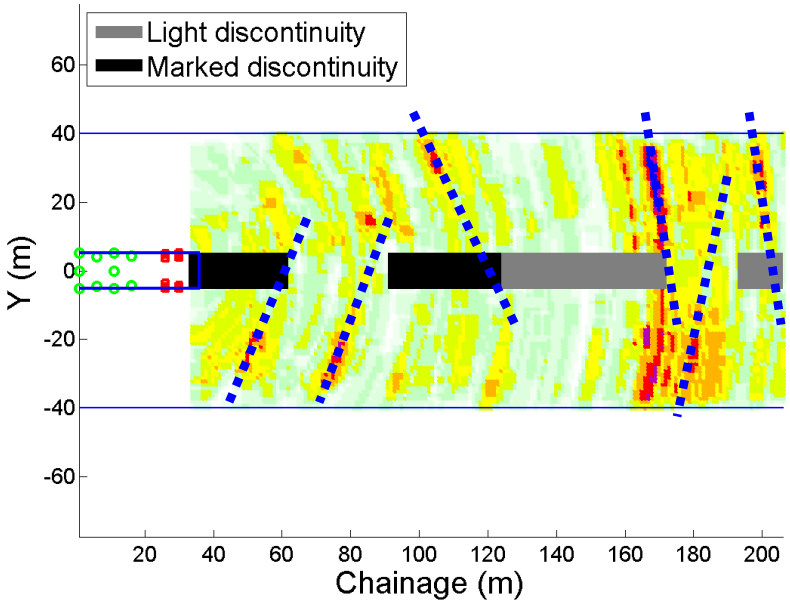

a)

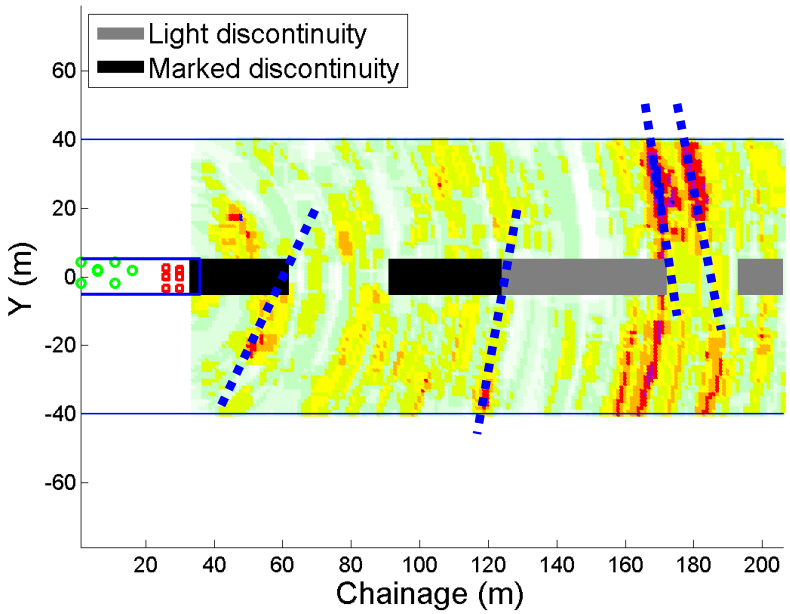

b)

Figure 7.18. Final representation compared with the interpretation and the data coming from the lithological analyses after the excavation, for the second test: a) for the map view; b) for the cross-sectional view.

7.5. Third test

The third test is based on the TRUST scheme (Figure 2.16). In the survey, 15 sources are adopted, included from 50 to 155 meters away from the tunnel face. The distance

between two successive sources is not constant, but it is equal either to 5 or 10 meter. The receivers are disposed based on the second configuration of Figure 2.16b, i.e. at 8-, 12- and 4-hours positions. The distance between two consecutive sensor sections is 50 meters.

Since a pilot sensor cannot be placed too close to the blasting, it is not possible to have a graphical representation of the excitation source,. The typical signal recorded is like that depicted in Figure 7.19a for the first accelerometer, for the first source. The frequency content is mainly included between 100 and 800 Hz, as can be seen from Figure 7.19b.

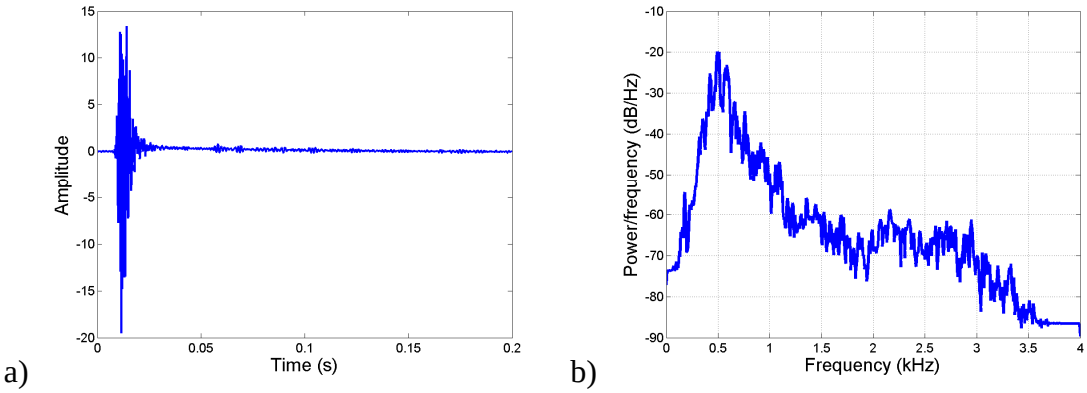

a) b)

Figure 7.19. Signal recorded by the first accelerometer, for the first source: a) time history; b) power spectral density.

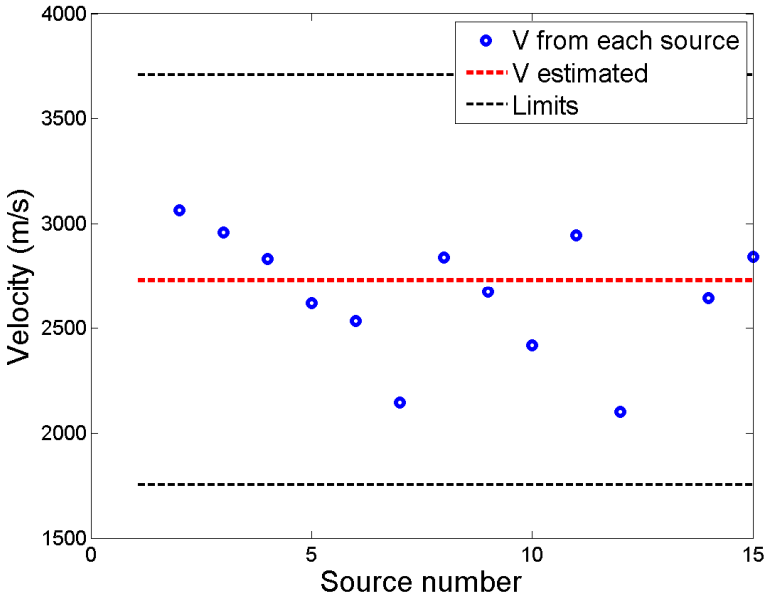

Figure 7.20. Estimation of the velocity for the third test under analysis.

In Figure 7.20, the velocities estimated from each source are depicted, together with the threshold within which the values can be considered reliable and the average value, which corresponds to 2731.4 m/s.

In Figure 7.21, the prediction of discontinuities is shown. The parameter R is equal to 2 because the most evident frequency is around 430 Hz.

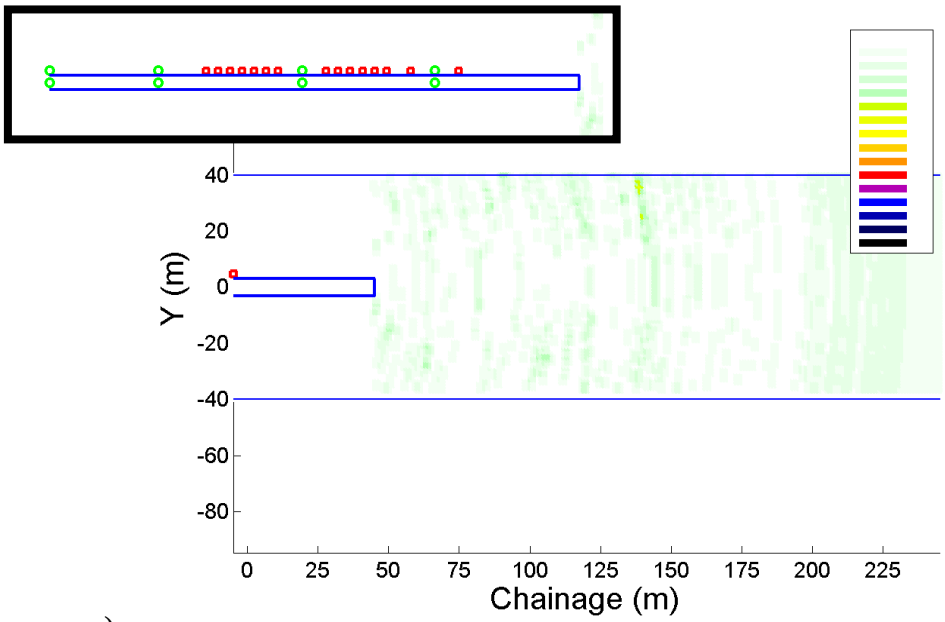

a)

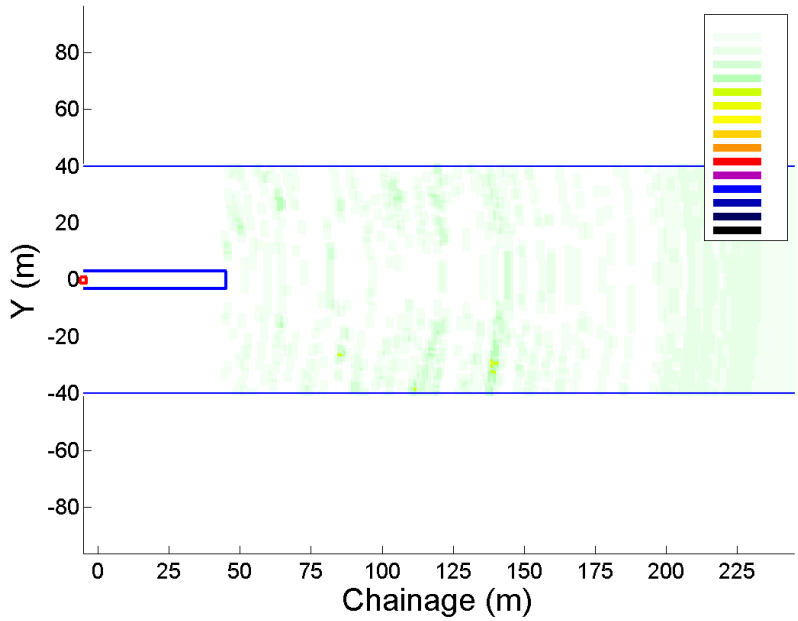

b)

Figure 7.21. Final representation given by the automatic procedure for the third test, depicting the number of common estimations for each point of the domain: a) map view; b) cross-sectional view.

At the top of Figure 7.21a, the entire configuration of sources and receivers is depicted, since for space reason it is not represented in the estimations. Differently from the previous results, both the map view and the cross-sectional view show very light colours, meaning that the probability to cross a discontinuity is very low, except in a zone close to the centre of the domain of investigation.

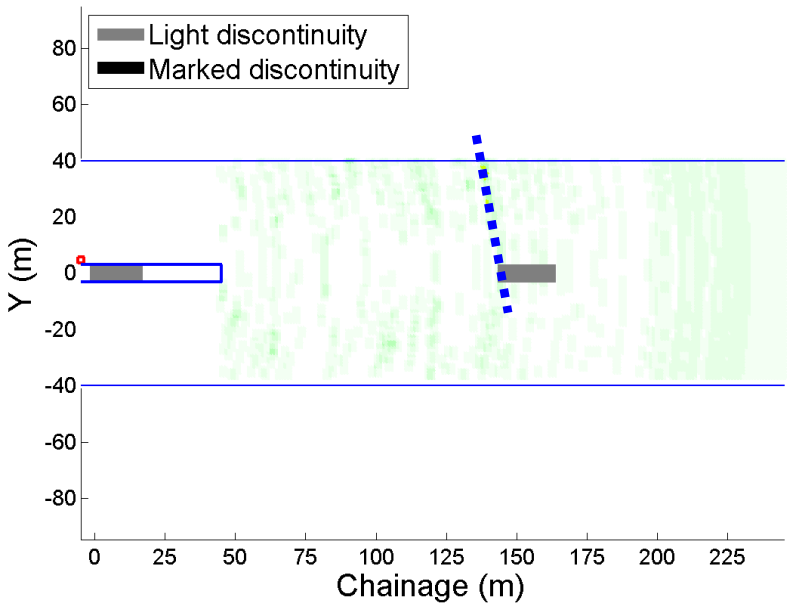

a)

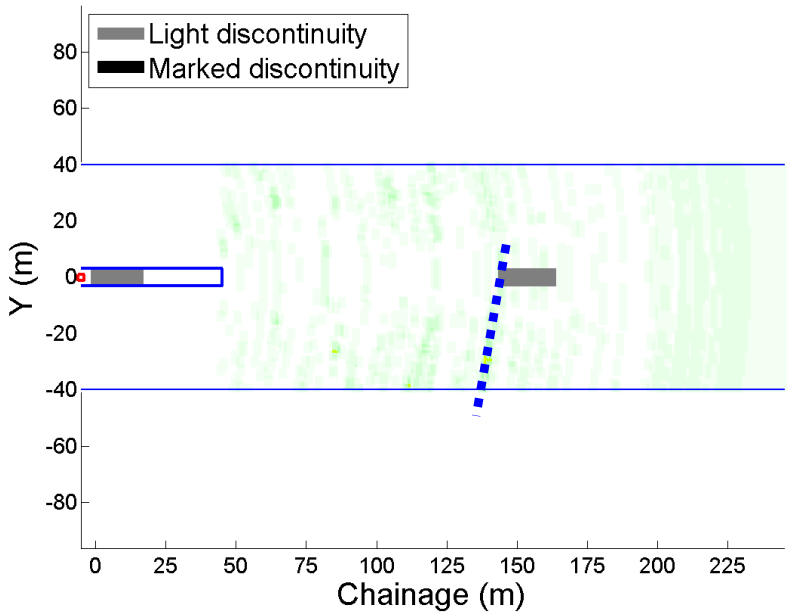

b)

Figure 7.22. Final representation compared with the interpretation and the data coming from the lithological analyses after the excavation for the third test: a) for the map view; b) for the cross-sectional view.

In Figure 7.22, the interpretation of the analysis is depicted. The weak discontinuities estimated by the automatic method actually correspond to a real change of material inside the Brennero tunnel. This confirms the accuracy and the reliability of the methodology.

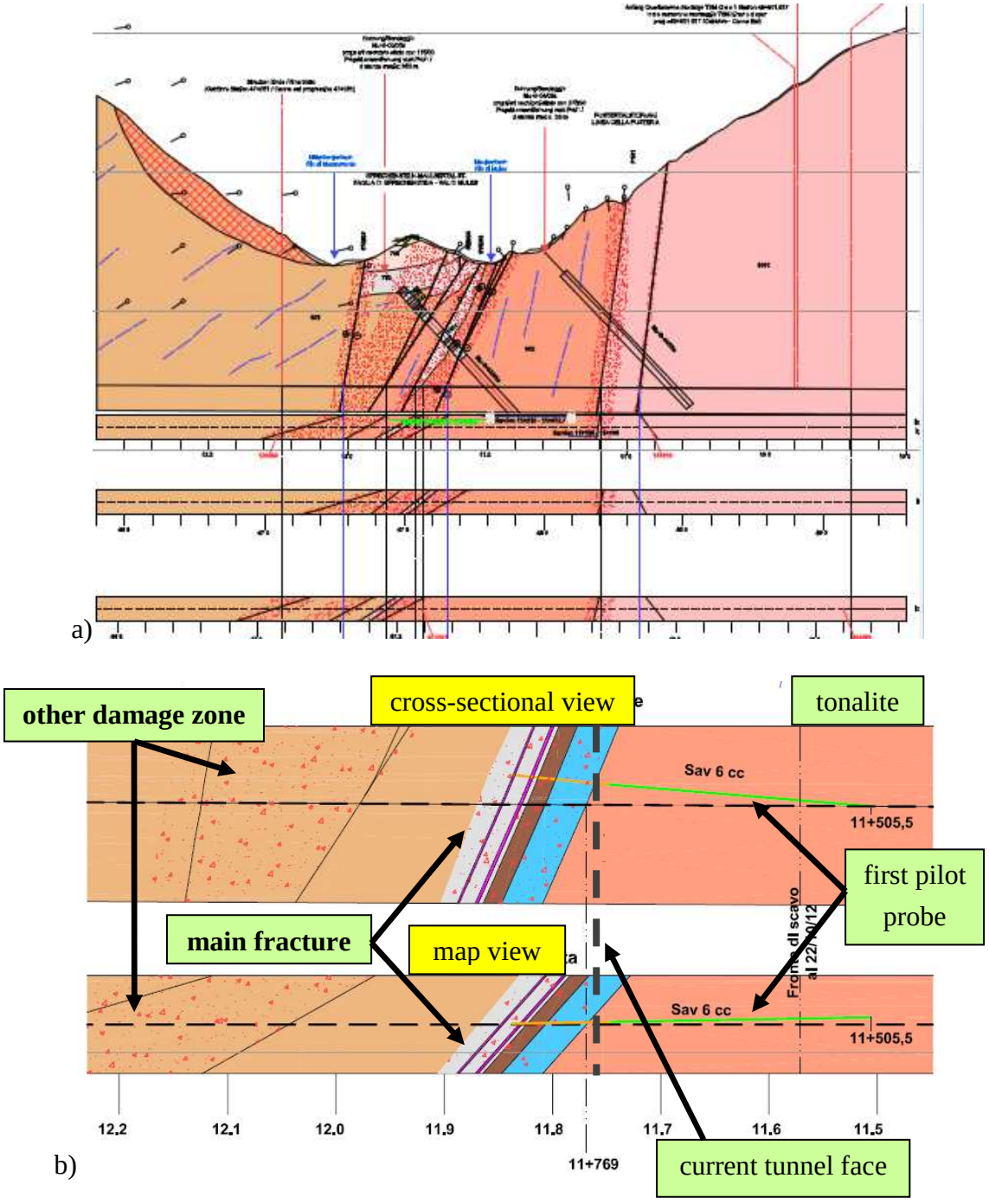

Figure 7.23. Rock profile of the zone around the Periadriatic seam: a) general three-dimensional view; b) two dimensional view (cross-sectional and map).

7.6. Identification of the Periadriatic seam

The identification of the Periadriatic seam is the real objective of the thesis, because it is actually the most important geologic fault affecting the construction of the Brennero tunnel.

7.6.1. Planning of the survey

In Figure 7.23, the rock profile of the zone around the Periadriatic seam, coming from some geological studies, is depicted. Moreover, two pilot probes, starting respectively at chainage 11505 m and 11732 m, are used to know the lithology for about 300 m ahead of the tunnel face. These investigations can be considered only as an indication of the exact location and spatial distribution of the discontinuity, because the geological surveys cannot be considered too accurate as well as the pilot probes cannot be considered too representative of the rock composition. As highlighted in Figure 7.23, the chainage is no more specified by numbers starting from 0 but they are expressed by the distance from the beginning of the Aica tunnel. In this case, the tunnel face is at chainage 11744 m.

The objective of the seismic survey is to compare the results obtained by the automatic method to those given by the other techniques, both in terms of distance from the current tunnel face and in terms of inclination.

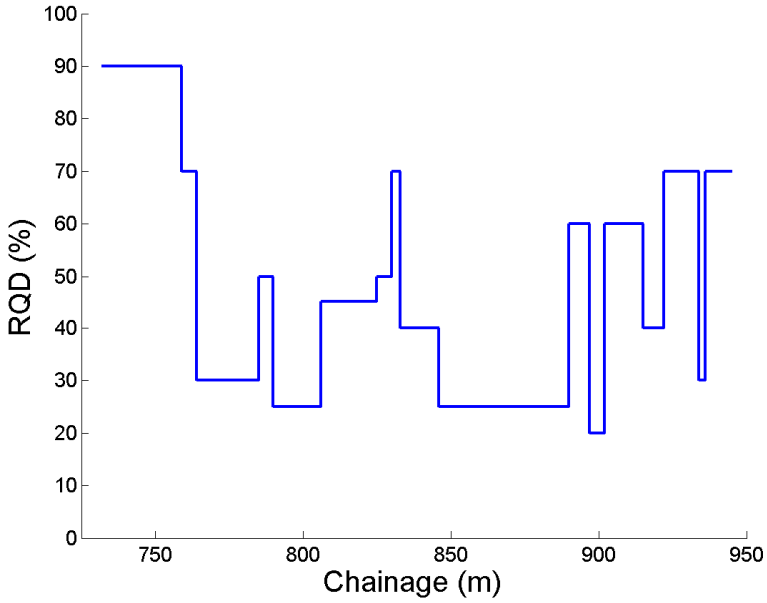

Figure 7.24. RQD obtained by one of the pilot probe drilled into the rock, from chainage 11732 to 11950.

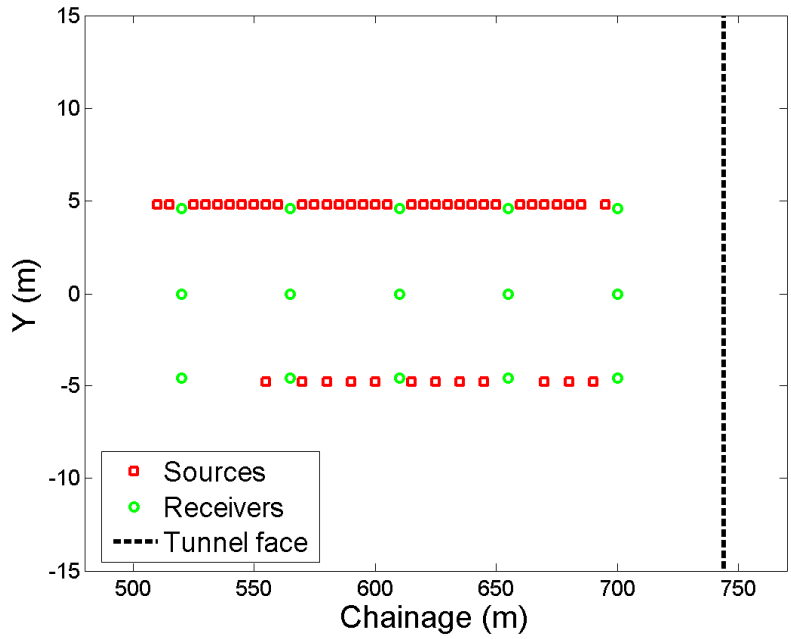

Figure 7.25. Configuration of sources and receivers during the analysis for the prediction of the Periadriatic seam.

In Figure 7.24, the RQD extracted by means of the second pilot probe is depicted. The most critical zones are around the chainage 11800 and between 11850 and 11900. No discontinuities should appear before the chainage 11760 m.

The work supervisors chose to adopt the TRUST configuration for the survey but I suggested to modify the classical TRUST scheme in order to have more sources, especially close to the tunnel face, and to place them on both the tunnel sides, to have more information. The acquisitions were therefore performed with 45 source points and fifteen receivers, disposed on five sections, with a distance of 55 m between two consecutive sections (see Figure 7.25). The typology of section is that expressed in the second image of Figure 2.16b.

7.6.2. Results about the Periadriatic seam

In some cases, (see for example Figure 2.8), the estimation provided by the method could be very different from the reality. This happens because the "hidden" discontinuities cannot be identified, since a notably increase of the domain is needed to reach their identifiable part. This is the starting point of this analysis: the domain must be significantly increased (especially on the X-axis and on the Y-axis) to be sure to estimate the exact location and inclination of the Periadriatic seam.

The velocity has been estimated equal to 2903.2 m/s and the parameter R is equal to 3.

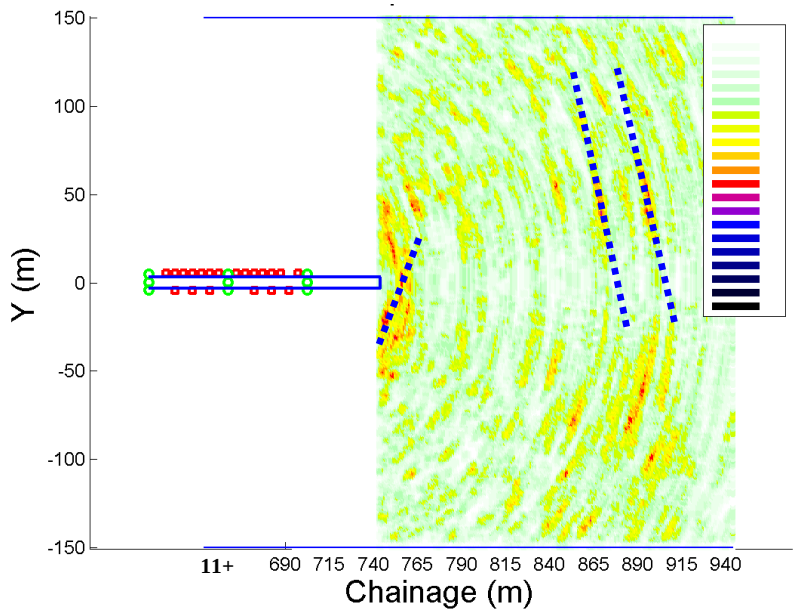

Figure 7.26. Discontinuity map referred to the analysis of the Periadriatic seam, together with the interpretation of the results, for the analysis with three receiver sections and 20 sources.

As will be described in details in the next section, it is preferable to consider only the sensors and the sources which are not too far from the tunnel face. For this reason, only the three first sections of accelerometers are used in the first analysis, represented in Figure 7.26, while the 20 sources closest to the tunnel face are taken into account. The analysis shows a critical zone very close to the tunnel face and moreover two discontinuities, with a similar inclination, crossing the tunnel axis around the chainages 11880 m and 11905 m, respectively.

In order to have another proof, only the two first sections of receivers and the first 12 sources are considered. In this case, only 4 sensors are taken into account for each source: the two lateral and the two placed at the top of the tunnel. In Figure 7.27, the map and the cross-sectional views are depicted. Contrarily to the previous cases, the probability to find a discontinuity is very high, especially in the second part of the domain. There are two main discontinuities:

1. the first is found at the first appearance of the blue colour, near the chainage 11840 m
2. the second crosses the tunnel axis around the chainage 11890

These results appear to be in accord with those presented in Figure 7.24. The two angles α and γ, defining the inclination of the discontinuities appear to be always positive for both the reflectors.

After the second discontinuity, a critical zone, with many change of material, is estimated, probably corresponding to the most evident region of the Periadriatic seam. This fact could demonstrate that the Periadriatic seam has been well detected but, in order to be sure of that, it is necessary to wait the progress of the excavation, which will be set up accordingly with the results of all the surveys (geological and geophysical).

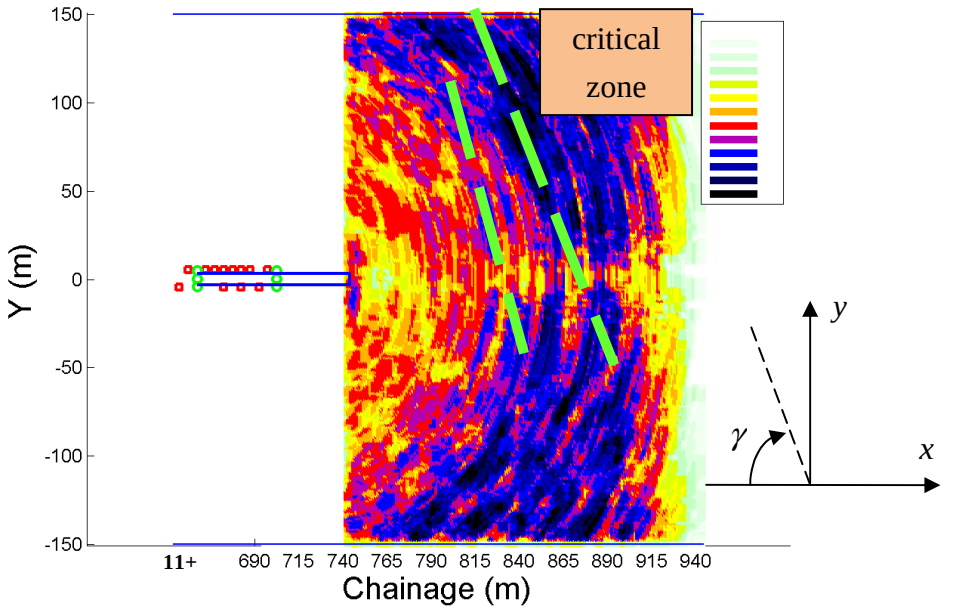

a)

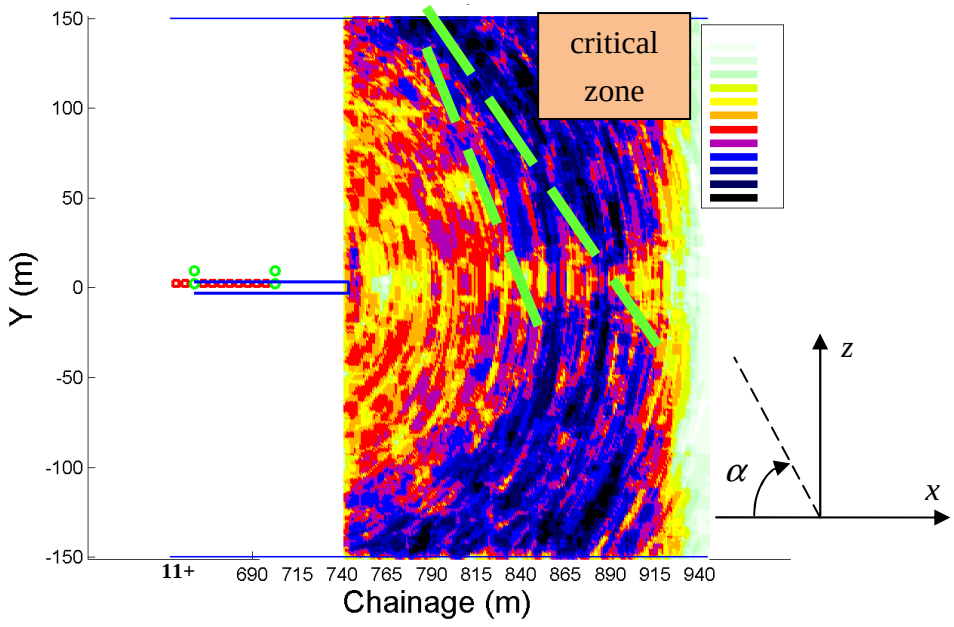

b)

Figure 7.27. Final representation compared with the interpretation for the analysis on the Periadriatic seam: a) for the map view; b) for the cross-sectional view.

7.7. Final observations

In this section, some comments about the results of the experimental tests in the Brennero tunnel are presented.

7.7.1. Computational time

One of the most important characteristics of the automatic method is to obtain reliable results in a small time interval. Considering the experimental surveys, the procedure takes between 10 and 15 minutes for a TRT analysis and between 20 and 40 minutes for a TRUST analysis, including both the map and the cross-sectional views. This time must be added to the time due to the manual insertion of the positions of sensor and sources. Conclusively, if no additional checks on the signals are needed, a result can be obtained in less than one hour.

7.7.2. Differences between TRT and TRUST approach

The two main differences between the TRT and the TRUST approach are:

- the configuration of sources and sensors
- the type of excitation

In particular, the configuration is completely different: in the TRT scheme, the sensors and the sources are quite close to the tunnel face, while in the TRUST scheme they have a large distribution along the tunnel axis. This aspect is fundamental when applying the backward method, which is based on the assumption that the reflection point can be considered unique for all the sensors.

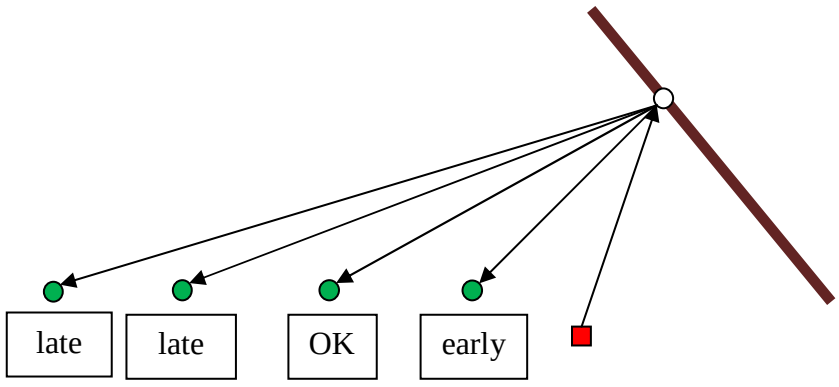

Figure 7.28. Schematic representation of the error committed by considering a unique reflection point. The red square indicates the source, the green circles indicate the receivers and the white circle indicates the reflection point.

Actually, this is not true when dealing with a configuration having sources and receivers very far from the tunnel face, like the TRUST. In Figure 7.28, indeed, a simple representation of this problem is sketched. In particular, if a source and a node of the domain (reflection point), corresponding to a real discontinuity, are taken into account, then there is certainly at least one receiver for which this approximation can be considered valid. For the other sensors, instead, this assumption cannot be applicable and then some significant errors could be introduced in the estimation. Two consequences are obtained:

- the best configuration for the application of the backward method is the TRT scheme or another similar configuration which has sources and receivers concentrated in 20-30 meters from the tunnel face;
- the results obtained on the experimental tests characterized by the TRUST scheme cannot be too reliable.

In particular, the two tests presented with such a configuration are characterized by light colours (see Figure 7.21, 7.22 and 7.26), meaning that the use of receivers far from the tunnel face reduces the probability to detect a discontinuity. For this reason, the results about the third test can be considered accurate, even if the probability is lower than the reality. About the test on the Periadriatic seam, the results expressed in Figure 7.27 are more reliable because only the first sensors are taken into account.

Chapter 8

Rockburst monitoring

Parallel to the estimation of the rock discontinuities ahead of the tunnel front, another important phenomenon characterizing the tunnel excavation must be considered: the rockburst. See Subsection 2.4.7 for other details.
The monitoring of the rockburst is fundamental to ensure safety for workers and machinery, analogously as the prediction of lithological discontinuities.
The monitoring is based on three operations:

- estimate the position of the source, given a certain array of sensors
- calculate the magnitude of the seismic event
- check the frequency of the event

This means that it is not sufficient to estimate the position of the rockburst source but also to verify the intensity of the event and moreover its frequency, because it is fundamental to identify the critical zones, which will be analysed more accurately by geologists.

8.1. Estimation of the rockburst source

Let's start with the estimation of the rockburst source, which is a problem similar to the identification of the location of an acoustic source (Ali *et al.*, 2007). In this field, however, some modifications to the classical algorithms are applied, in order to obtain the best results as possible.

8.1.1. The idea

The basic idea is represented in Figure 8.1, where many receivers record the wave (seismic, acoustic or whatever type) generated in the source point. The objective is to

estimate the location of the source from the known positions of the sensors and from the signals recorded.

Since the rockburst is a seismic event, an idea would be to use the techniques adopted for the earthquakes. In that case, since long distances are covered by the seismic waves before being recorded by a geophone, it is possible to clearly distinguish the P-wave and the S-wave. Successively, the times elapsed from the epicentre to the seismic stations are identified and then, by means of the difference between the P and S arrivals, the distance between the recording stations and the epicentre is calculated. By constructing a circle and considering at least other two circles, it is possible to estimate the epicentre, as done for the figure below.

The rockburst is a seismic phenomenon but the distance between the epicentre and the tunnel axis is small (some tenths of meters, at maximum), because it is an alteration of the rock near the excavation zone. Consequently, it is difficult to identify the two types of waves, in particular the P-waves (the energy is low). For this reason, different approaches are proposed in the prosecution of the article.

8.1.2. The problem

Let us suppose that the source is located in $S=(x_0, y_0, z_0)$ and the receivers are in $R=(x_i, y_i, z_i)$, $i=1,2,...,N$. The matrix collecting the positions of the accelerometers is called Q:

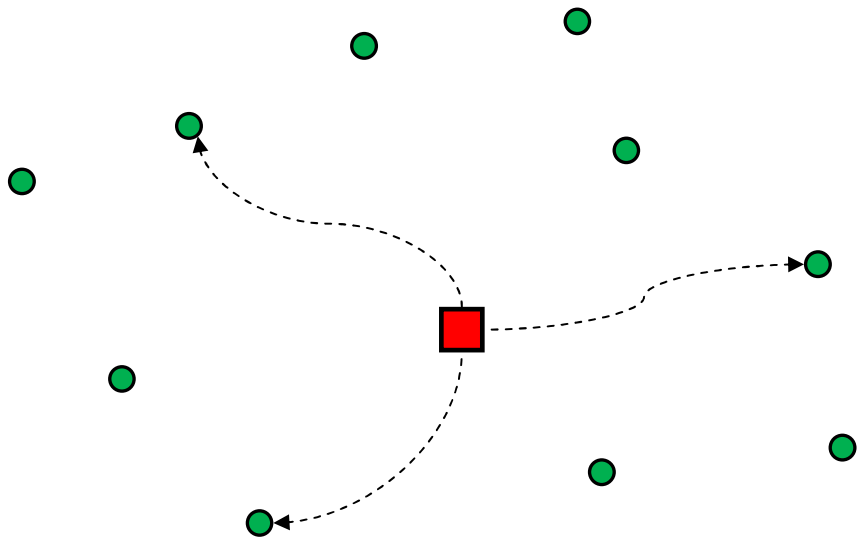

Figure 8.1. Idea of the identification of the source location from a set of receivers. The source is indicated by a red square, while the receivers are indicated by green circles.

$$Q = \begin{bmatrix} x_1 & y_1 & z_1 \\ x_2 & y_2 & z_2 \\ \vdots & \vdots & \vdots \\ x_N & y_N & z_N \end{bmatrix} \tag{8.1}$$

The relationships expressing the distance between the source and a generic receiver is:

$$d_{i0} = \sqrt{(x_0 - x_i)^2 + (y_0 - y_i)^2 + (z_0 - z_i)^2} = v(t_i - t_0) \tag{8.2}$$

where v is the medium velocity (supposed to be constant) and t_i is the time corresponding to the first arrival of the direct wave. The constant t_0 is called origin time and it indicates the instant in which the wave has been generated, which is not the zero-time.

In this problem there are four unknowns and therefore four independent equations are needed because, in addition to the source coordinates, also the origin time must be calculated to solve the problem.

Some methods for the identification of the rockburst source position will be presented in the following. For all the methods, the velocity is supposed to be known. In a real survey, it is sufficient to give an hammer stroke in a known point and to apply the first part of the backward method to obtain the wave velocity.

8.1.3. 4CM method

The first method presented is called 4CM, which stands for 4-Columns Matrix method, which is the most classical approach, involving the construction of a matrix with four columns, in order to solve a linear problem with the Least-Square method.

Let us start from Eq. (8.2). By considering the square:

$$(x_0 - x_i)^2 + (y_0 - y_i)^2 + (z_0 - z_i)^2 = v^2 t_i^2 - 2v^2 t_i t_0 + v^2 t_0^2 \tag{8.3}$$

Then, by using two generic receivers

$$\begin{aligned} &(x_0 - x_i)^2 - (x_0 - x_j)^2 + (y_0 - y_i)^2 - (y_0 - y_j)^2 + (z_0 - z_i)^2 - (z_0 - z_j)^2 = \\ &v^2 t_i^2 - v^2 t_j^2 - 2v^2 t_0 (t_i - t_j) \end{aligned} \tag{8.4}$$

$$x_0^2 - 2x_0x_i + x_i^2 - x_0^2 + 2x_0x_j - x_j^2 + y_0^2 - 2y_0y_i + y_i^2 - y_0^2 + 2y_0y_j - y_j^2 + z_0^2 - 2z_0z_i + z_i^2 - z_0^2 + 2z_0z_j - z_j^2 = v^2\left(t_i^2 - t_j^2\right) - 2v^2t_0\left(t_i - t_j\right) \tag{8.5}$$

and finally

$$x_0(x_j - x_i) + y_0(y_j - y_i) + z_0(z_j - z_i) + t_0\left(v^2\left(t_i - t_j\right)\right) = \frac{v^2\left(t_i^2 - t_j^2\right) + x_j^2 - x_i^2 + y_j^2 - y_i^2 + z_j^2 - z_i^2}{2} \tag{8.6}$$

In particular, by considering two successive receivers,

$$b_i = \frac{v^2\left(t_i^2 - t_{i+1}^2\right) + x_{i+1}^2 - x_i^2 + y_{i+1}^2 - y_i^2 + z_{i+1}^2 - z_i^2}{2} \tag{8.7}$$

and then it is possible to obtain a classical linear problem of the form

$$Aq = b \tag{8.8}$$

where

$$A = \begin{bmatrix} x_2 - x_1 & y_2 - y_1 & z_2 - z_1 & v^2(t_2 - t_1) \\ x_3 - x_2 & y_3 - y_2 & z_3 - z_2 & v^2(t_3 - t_2) \\ \vdots & \vdots & \vdots & \vdots \\ x_N - x_{N-1} & y_N - y_{N-1} & z_N - z_{N-1} & v^2(t_N - t_{N-1}) \end{bmatrix} \tag{8.9}$$

$$b = \begin{bmatrix} b_{1,2} \\ b_{2,3} \\ \vdots \\ b_{N-1,N} \end{bmatrix} \tag{8.10}$$

$$q = \begin{bmatrix} x_0 \\ y_0 \\ z_0 \\ t_0 \end{bmatrix} \tag{8.11}$$

8.1.4. 3CM method

The second method proposed is called 3CM (3-Columns Matrix) method, and it allows to write a matrix with only three columns because the origin time is hidden in the linear system, after some simple manipulations of the equations.
Starting again from Eq. (8.2), the information about a new receiver can be added in the term at the second member of the equation:

$$\sqrt{(x_0 - x_i)^2 + (y_0 - y_i)^2 + (z_0 - z_i)^2} = v\left(t_i - t_j + t_j - t_0\right) \tag{8.12}$$

By squaring both the terms,

$$d_{i0}^2 = d_{ij}^2 + 2d_{ij}d_{j0} + d_{j0}^2 \tag{8.13}$$

The same process can be applied by using one of the previous receivers and a new one:

$$d_{k0}^2 = d_{kj}^2 + 2d_{kj}d_{j0} + d_{j0}^2 \tag{8.14}$$

Now, Eq. (8.13) is multiplied by d_{kj} and Eq. (8.14) is multiplied by d_{ij} and the difference of this quantities is considered:

$$d_{i0}^2 d_{kj} - d_{k0}^2 d_{ij} = \left(d_{ij}^2 + 2d_{ij}d_{j0} + d_{j0}^2\right)d_{kj} - \left(d_{kj}^2 + 2d_{kj}d_{j0} + d_{j0}^2\right)d_{ij} \tag{8.15}$$

$$d_{i0}^2 d_{kj} - d_{k0}^2 d_{ij} = \left(d_{ij}^2 + d_{j0}^2\right)d_{kj} - \left(d_{kj}^2 + d_{j0}^2\right)d_{ij} \tag{8.16}$$

After some manipulations, it is possible to find

$$\begin{aligned}\left(d_{ij}^2 - x_i^2 - y_i^2 - z_i^2 + x_j^2 + y_j^2 + z_j^2\right)d_{kj} - \left(d_{kj}^2 - x_k^2 - y_k^2 - z_k^2 + x_j^2 + y_j^2 + z_j^2\right)d_{ij} = \\ = 2\left[d_{kj}\left(x_j - x_i\right) - d_{ij}\left(x_j - x_k\right)\right]x_0 + 2\left[d_{kj}\left(y_j - y_i\right) - d_{ij}\left(y_j - y_k\right)\right]y_0 + \\ + 2\left[d_{kj}\left(z_j - z_i\right) - d_{ij}\left(z_j - z_k\right)\right]z_0\end{aligned} \tag{8.17}$$

In this way, the coordinates of the source can be easily found. An estimate of the origin time for each receiver can obtained by:

$$t_{0i} = \frac{1}{v} d_{i0} + t_i \tag{8.18}$$

8.1.5. 3CMM method

The procedure just presented can be slightly modified by introducing the 3CMM (3-Columns Matrix Modified) method, which is a personal revision of the previous approach. The basic idea is to split the matrix A expressed by Eq. (8.9) in two parts called A_1 and A_2 respectively:

$$A_1 = \begin{bmatrix} x_2 - x_1 & y_2 - y_1 & z_2 - z_1 \\ x_3 - x_2 & y_3 - y_2 & z_3 - z_2 \\ \vdots & \vdots & \vdots \\ x_p - x_{p-1} & y_p - y_{p-1} & z_p - z_{p-1} \end{bmatrix} \tag{8.19}$$

$$A_2 = \begin{bmatrix} x_{n_C-p+2} - x_{n_C-p+1} & y_{n_C-p+2} - y_{n_C-p+1} & z_{n_C-p+2} - z_{n_C-p+1} \\ x_{n_C-p+3} - x_{n_C-p+2} & y_{n_C-p+3} - y_{n_C-p+2} & z_{n_C-p+3} - z_{n_C-p+2} \\ \vdots & \vdots & \vdots \\ x_{n_C} - x_{n_C-1} & y_{n_C} - y_{n_C-1} & z_{n_C} - z_{n_C-1} \end{bmatrix} \tag{8.20}$$

where p is an arbitrary parameter usually chosen as half the total number of sensors N. This parameter can be chosen from 3 to $N-1$.

Parallel, the vector b is split in b_1 and b_2

$$b_1 = \frac{v^2\left(t_i^2 - t_{i+1}^2\right) + x_{i+1}^2 - x_i^2 + y_{i+1}^2 - y_i^2 + z_{i+1}^2 - z_i^2}{2} \qquad i = 1,2,\ldots, p \tag{8.21}$$

$$b_2 = \frac{v^2\left(t_i^2 - t_{i+1}^2\right) + x_{i+1}^2 - x_i^2 + y_{i+1}^2 - y_i^2 + z_{i+1}^2 - z_i^2}{2} \qquad i = N - p + 2,\ldots, N-1 \tag{8.22}$$

The equations can be written as

$$A_1 q = b_1 + k_1 \tag{8.23}$$

$$A_2 q = b_2 + k_2 \tag{8.24}$$

where the vectors k_1 and k_2 are expressed by:

$$k_1 = t_0 v^2 (t_i - t_{i+1}) \qquad i = 1,2,..., p \tag{8.25}$$

$$k_2 = t_0 v^2 (t_i - t_{i+1}) \qquad i = N - p + 2,..., N - 1 \tag{8.26}$$

Then, new matrices and vectors are built:

$$\tilde{A}_1 = \left[\frac{x_{i+1} - x_i}{t_i - t_{i+1}}; \frac{y_{i+1} - y_i}{t_i - t_{i+1}}; \frac{z_{i+1} - z_i}{t_i - t_{i+1}} \right] \qquad i = 1,2,..., p \tag{8.27}$$

$$\tilde{A}_2 = \left[\frac{x_{i+1} - x_i}{t_i - t_{i+1}}; \frac{y_{i+1} - y_i}{t_i - t_{i+1}}; \frac{z_{i+1} - z_i}{t_i - t_{i+1}} \right] \qquad i = N - p + 2,..., N - 1 \tag{8.28}$$

$$\tilde{b}_1 = \frac{b_1}{t_i - t_{i+1}} \qquad i = 1,2,..., p \tag{8.29}$$

$$\tilde{b}_2 = \frac{b_2}{t_i - t_{i+1}} \qquad i = N - p + 2,..., N - 1 \tag{8.30}$$

The equations obtained are:

$$\tilde{A}_1 x = \tilde{b}_1 + t_0 v^2 \tag{8.31}$$

$$\tilde{A}_2 x = \tilde{b}_2 + t_0 v^2 \tag{8.32}$$

and then the term due to the origin time t_0 can be cancelled by considering the new linear system:

$$\left(\tilde{A}_1 - \tilde{A}_2\right) x = \tilde{b}_1 - \tilde{b}_2 \tag{8.33}$$

8.1.6. Iterative method

In the fourth method presented, the origin time t_0 is determined by using the following iterative algorithm:

- Impose some values to t_0, in the interval included from 0 to the maximum values of the time arrivals

- Consider the times $t_i + t_0$.
- Calculate the solution by using a simplified approach respect to the 4CM method, by considering the matrix

$$A = \begin{bmatrix} x_2 - x_1 & y_2 - y_1 & z_2 - z_1 \\ x_3 - x_2 & y_3 - y_2 & z_3 - z_2 \\ \vdots & \vdots & \vdots \\ x_N - x_{N-1} & y_N - y_{N-1} & z_N - z_{N-1} \end{bmatrix} \tag{8.34}$$

and the vector

$$b_i = \frac{v^2\left(t_i^2 - t_{i+1}^2\right) + x_{i+1}^2 - x_i^2 + y_{i+1}^2 - y_i^2 + z_{i+1}^2 - z_i^2 - 2t_0\left(v^2\left(t_i - t_{i+1}\right)\right)}{2} \tag{8.35}$$

instead of that of Eq. (8.7), in order to take the term with the velocity into account.

- Calculate the distance $d_{xR} = d(x, R)$ between the solution and the sensors.
- If the relative error between d_{xR} and $v\left(t_i + t_0\right)$ is minor than respect to a fixed threshold then that value of t_0 is the real origin time.

8.2. Condition number and optimal sensor configuration

The methods proposed in the previous section try to estimate the coordinates of the source, once known the velocity of the seismic waves and the positions of the receivers. For this reason, at least 5 sensors are necessary for a rockburst identification, since differences among the coordinates are calculated.

The first two methods proposed in the previous section has been taken directly from the literature, while the latter two ones have been developed by me, in order to be as more accurate as possible when dealing with real data coming from a rockburst monitoring, with a sensor configuration which is conditioned by the tunnel shape.

The most important aspects for the selection of the best method are:

- the condition number of the matrix present in the linear system (see Appendix B for details)
- the configuration of sensors (number and disposition)

These two aspects are however strictly connected. In particular, if considering Eq. (8.9), it is clear that the differences among the coordinates of the same type are those who determine the condition number of A.

If the x-coordinates of the sensors vary on a large range of values (since they can be placed along the tunnel axis), then the matrix A has a first column which is dominant respect to the others. This situation usually leads to a high condition number, which can mean difficulties in finding the numerical solution of the linear equation.

In order to avoid this situation, pre-conditioners could be used, but they are built only for square matrices, and therefore the unique way is to build the matrix A such that the condition number is as small as possible. To do this, the sensors must be chosen in the most convenient position.

Another important observation is that if the column is dominant then the correspondent coordinate of the source will be well estimated, contrarily to the other coordinates. This is the reason why the matrix A should have numbers as uniform as possible, and this must be obtained by placing the sensors in convenient positions. The problem of an optimal configuration for sensors is studied in the next subsections.

8.2.1. Estimation of the x-coordinate

The positions of the sensors cannot be chosen in an arbitrary way, or without particular criteria, as happens for all the surveys studied in a tunnel, therefore some additional studies must be done about this topic.

Let us simulate a real case, being inspired by the experimental test that will be presented at the end of the chapter. In particular, let's see in Table 8.1 three different sets for the x-coordinate of the sensors, while the other two coordinates are fixed and simulating a real case, and they are expressed in Table 8.2.

The three configurations have 4, 5 and 10 sections, respectively. For each case, a 3% of Gaussian noise is added on the first time arrivals, created by considering the source in $S = (72,-21,15)$ and by imposing a velocity of 3000 m/s.

Table 8.1. List of the three cases considered, with the x-coordinates of the sensors and the relative error on the estimation of the x-coordinate x_S of the rockburst source.

TYPE	X-COORDINATE	ERROR ON x_S
5 sections	[0 0 30 30 60 60 90 90 120 120]	0.13 %
4 sections	[0 0 0 40 40 40 80 80 120 120]	0.40 %
10 sections	[0 30 60 90 120 15 45 75 105 135]	0.25 %

Table 8.2. Coordinates y and z used for the three configurations under study.

TYPE	X-COORDINATE
5 sections	[-2.2 2.5 -2 2.1 -2.3 2.4 -2.8 2 -2.2 2.9]
4 sections	[2 1.6 1.2 0.8 0.4 0.4 0.8 1.2 1.6 2]

The estimation, performed with the classical 4CM method, of the x-coordinate of the source is slightly better for the first case, which is also the configuration planned to use for the rockburst monitoring in the Brennero tunnel, but it is very satisfying also for the other configurations.

This initial example is useful to understand that a good estimation of the x-coordinate is possible with different configurations, because if the sensors cover a large range of values of a coordinate, then the estimation of the same coordinate of the source will be very accurate.

8.2.2. Estimation of the other coordinates

Contrarily to what has been just shown about the x-coordinate, it is not possible to have an equal disposition of the sensors in all the directions, and moreover it is almost impossible to obtain a small condition number with sensors disposed as described in Table 8.1.

For these reasons, let us create new simulations, with the source again in the point $S = [72 \ -21 \ 15]$ m and three following configurations listed in Table 8.3, about the x-coordinate. The three cases represent some possible choices for a real survey:

1. “concentrated” configuration: the sensors are very close each other, in two meters;
2. “intermediate” configuration: the receivers are quite close each other, in 28 meters;
3. “distributed” configuration: the sensors are more distributed along the tunnel axis, in 120 meters.

In Table 8.4, instead, the y- and z-coordinates of the sensors are presented. They are equal for all the configurations. The y-coordinates are calculated from the z-coordinates supposing that the tunnel has the same dimensions of the Brennero tunnel, in order to have realistic cases, based on Eq. (5.1).

Now, let’s inspect the relative errors between the exact source position and the estimations produced by the method, for the three configurations.

In this regard, 30 simulations are created for each of the three cases, with a 2% of Gaussian noise added to the first time arrivals.

Table 8.3. List of the x-coordinates of the sensors for the three configurations under study.

Configurations	x-coordinates
CASE 1: concentrated	[0 2 1.6 0.4 1.8 0.7 1.4 0.2 1.4 0.4]
CASE 2: intermediate	[0 10 28 21 19 13.5 37 12 17 22]
CASE 3: distributed	[0 0 30 30 60 60 90 90 120 120]

Table 8.4. Coordinates y and z of the sensors used for the three configurations under study.

y-coordinates	[2.9976 -2.9758 2.8680 -2.6638 2.9976 -2.9758 2.8680 -2.6638 2.9976 -2.9758]
z-coordinates	[2.5 2 1.5 1 2.5 2 1.5 1 2.5 2]

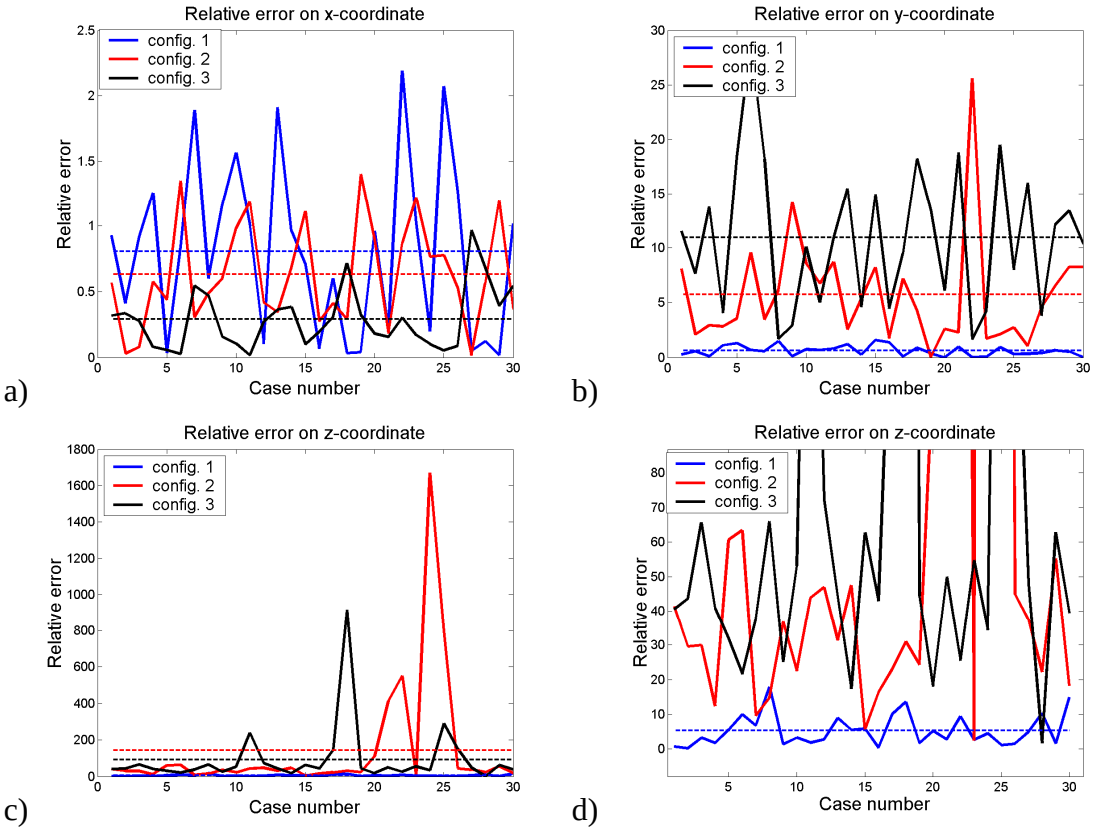

Figure 8.2. Relative error on the different coordinates for the three configurations: a) x-coordinate; b) y-coordinate; c) z-coordinate; d) magnification of the previous figure.

Firstly, the errors on the estimation of the single coordinates of the source are depicted in Figure 8.2.

About the x-coordinate of the source, the best estimation is obtained by the third configuration, and this confirms, analogously to Table 8.1, that having a large distribution of sensors in a direction allows a very good estimation of the corresponding coordinate of the source.

However, when considering the y-coordinate, the errors are larger for the second and third configurations, and this fact is significantly more evident for the z-coordinate. This happens because if the matrix A has non-uniform values (i.e. higher in the first column, corresponding to the x-coordinate, respect to the other columns), then the condition number is higher, as can be seen in the Table 8.5. Even if the second and the third configurations seem to be very different, their condition number is not so dissimilar, meaning that only the first configuration can be considered a good choice.

In Figure 8.3, the total relative error is depicted, confirming that only the first configuration is suitable for a recognition of the rockburst source. Moreover, even if the source is distant from the sensors, the results are very good.

Table 8.5. Condition number of the matrix A for the three cases analyzed.

Configurations	Condition number
CASE 1: concentrated	9.77
CASE 2: intermediate	25.09
CASE 3: distributed	30.44

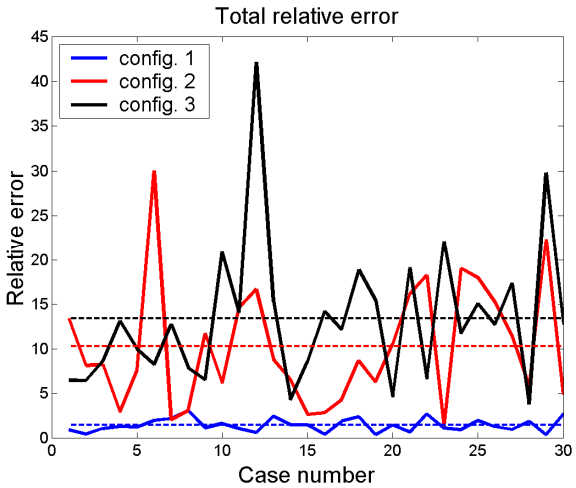

Figure 8.3. Total relative error in the estimation of the source location, for the three configurations.

8.2.3. Minimization of the condition number

If exchanging two rows of a matrix, its condition number does not change. In this case, however, it is possible to exchange two or more rows of the sensor matrix Q in order to modify the condition number of the matrix A, because it is based on differences on the values of the sensor coordinates. Consequently, it is important to set the matrix Q such that the matrix A has the condition number as smaller as possible. Actually, this operation can take a very long computational time because the permutation of the rows includes $n!$ cases (for $n=10$ → 3628800 cases). Therefore, a simpler thing can be done: only the rows of the matrix Q containing a negative value for the y-coordinate are permuted in order to find a case with a lower condition number.

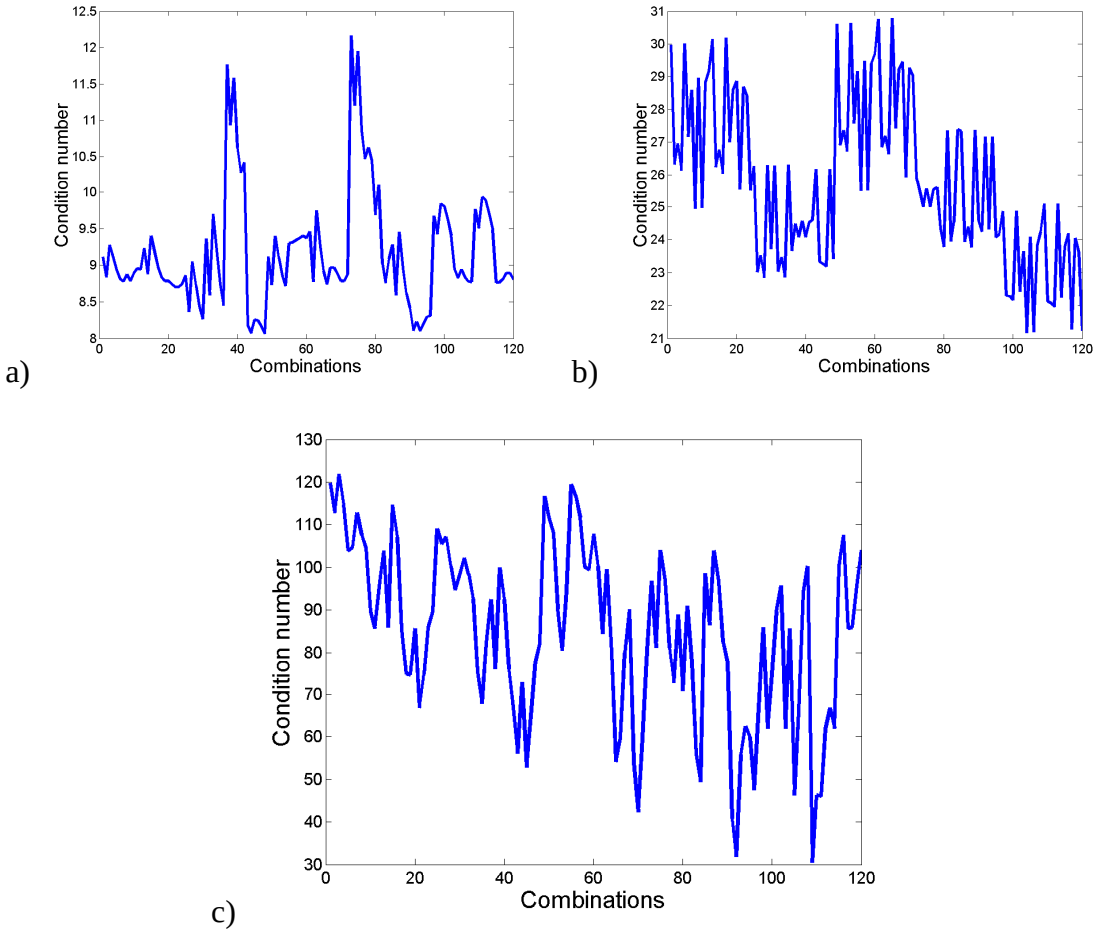

Figure 8.4. Condition number of the matrix A in function of the permutations of the rows of the matrix Q: a) for the first configuration; b) for the second configuration; c) for the third configuration.

In this case, since only half of the rows have negative values, the number of combinations is significantly reduced (for $n = 5$ → 120 cases). For each case, the matrix A is built and its condition number is calculated.

Figure 8.4 represents the condition number for the different combinations, based on the coordinates expressed in Table 8.2 and 8.3, about the three configurations. For the first one (Figure 8.4a), the minimum value of the condition number is 8.07 against the original value of 9.77, therefore the improvement is not so evident.

In Figure 8.4b, it is shown that the second configuration can have condition numbers from 21 to 30, while in Figure 8.4c, for the third case, they vary from 30 to 120.

To directly see the effect of selecting the minor condition number, it is advisable to check what happens to the total relative error on thirty numerical cases created analogously to Figure 8.2 and 8.3. Looking at Figure 8.5a, the improvement in the estimation of the source location, for the first configuration, is very small. This is due to the fact that the condition number is slightly changed and therefore the enhancement cannot be too large.

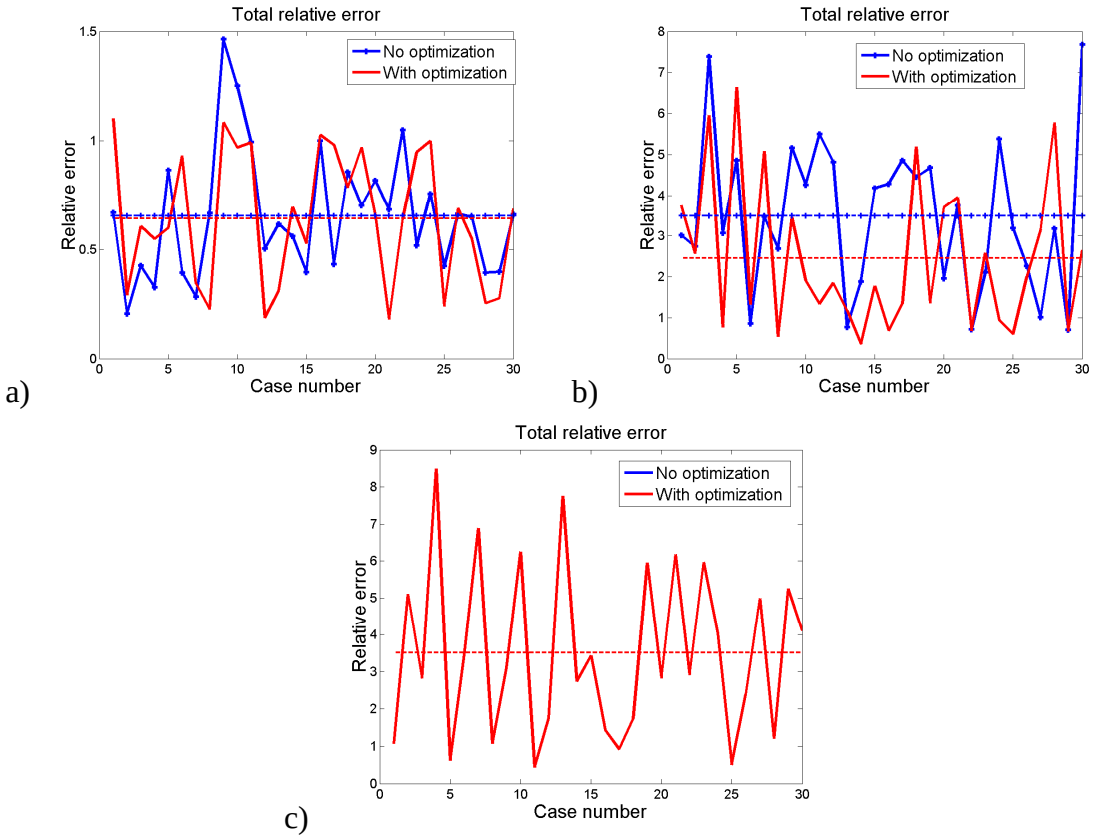

Figure 8.5. Total relative error, before and after the minimization of the condition number for the matrix A: a) for the first configuration; b) for the second configuration; c) for the third configuration.

A higher improvement occurs in Figure 8.5b, for the second configuration, because the condition number decreases from 25.09 to 21.16. For the last case, represented in Figure 8.5c, no improvements can be seen because the value expressed in Table 8.5 (30.44) is the minor condition number as possible, and therefore the results cannot be better respect to those depicted in Figure 8.3.
Except this lucky case, it has been shown the importance to reduce the condition matrix, because a low value leads to obtain a more accurate solution of the problem.

8.2.4. Optimal configuration of sensors

Now, let us to study an optimal placement of the sensors on the tunnel walls in order to have a smaller condition number as possible. Let us consider 10 sensors and a simple proposal is the configuration represented in Figure 8.6. Its characteristics are:

- X-coordinate: 5 sections with 2 sensor per each section, distributed in 10-15 meters. This choice is done to obtain small values for the differences between different x-coordinates.
- Y-coordinate: 2 sensors for each section, one on the left wall and one on the right wall. The choice allows to have values similar to those of the X-coordinate.
- Z-coordinate: 4 different heights. They are called H_1, H_2, H_3 and H_4 respectively, starting from the bottom up to the top. H_1 and H_3 are associated to the left wall, H_2 and H_4 to the right wall.

With this configuration, it is possible to have both a quite simple scheme for the workers (no holes at the top of the tunnel) and a matrix with a quite low condition number.

8.3. Procedure of analysis

Now, let's summarize the procedure for the identification of a rockburst source. The procedure is mainly divided in two parts: the sensor placement and the source estimation. Then, additional information about the rockburst can be given with the magnitude estimation and the monitoring of the event frequency.

8.3.1. Sensor placement

The sensor placement is the most important topic in a rockburst monitoring, because it is fundamental for the condition number of the matrix of the linear system whose solution is the source location.

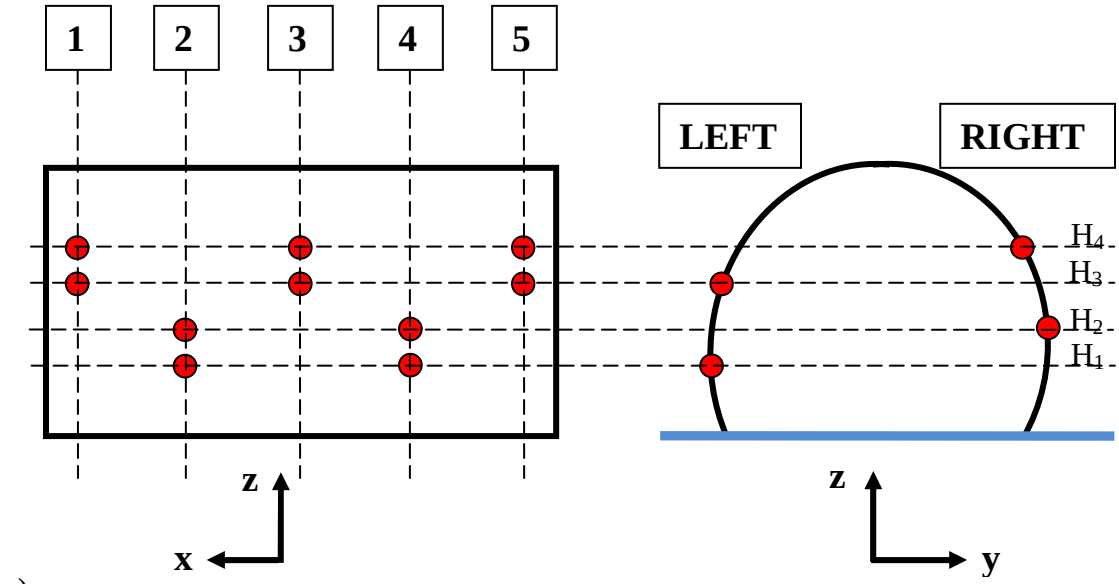

a)

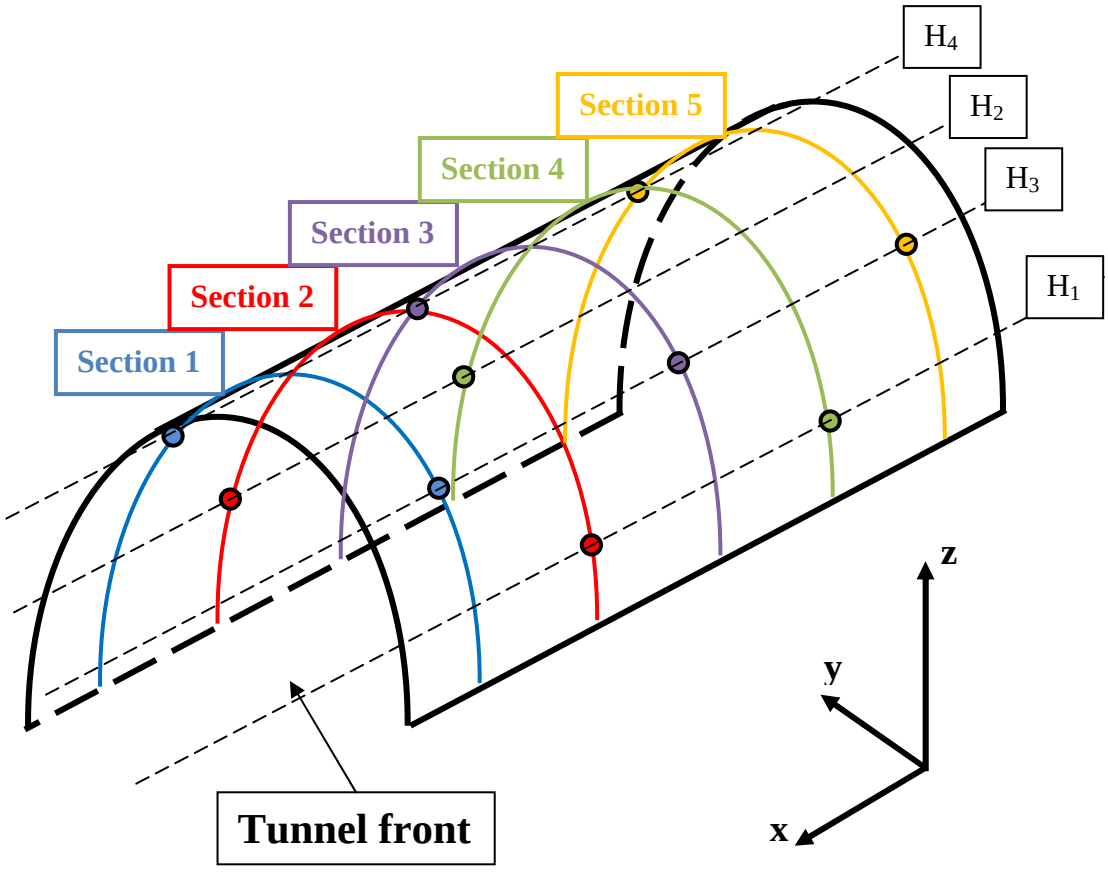

b)

Figure 8.6. Proposal for an optimal configuration of sensors for the rockburst monitoring: a) map and frontal view; b) three-dimensional view. The circles indicate the receivers.

What is really important is to build the matrix Q of Eq. (8.1) in order to have a low condition number of the matrix of the linear system. For this reason, the configuration presented in Figure 8.6 is advisable.

8.3.2. Estimation of the source location

The estimation of the source location is mainly divided in four parts:

1. Estimate the wave velocity
2. Identify the first time arrivals of the direct waves from the recorded signals
3. Reduce the condition number of the matrix of the linear problem
4. Estimate the source position by solving the linear problem

The estimation of the velocity is necessary in a real survey, because otherwise any method can be applied. The simplest way to solve this problem is to give an hammer stroke against one of the tunnel walls, in a known position, and then to apply the first part of the backward method (see Subsections 5.3.2 and 5.3.3) to find the velocity.

After that, the first time arrivals of the direct waves are extracted by geophysists, or, if the excitation is strong enough, by re-using the automatic approach.

In Section 8.1, many methods have been presented for the estimation of the rockburst source. After some simple tests, in my opinion, the third approach (3CMM method), described in Subsection 8.1.5, has been demonstrated to be the most reliable. For this reason, it has been chosen to analyse the numerical and experimental data.

The method is divided in two parts: the first one is dedicated to a rough estimation of the possible values for the source coordinates, while the second part is dedicated to the operations allowing to obtain the final result.

At first, different vectors are defined in order to have all the combinations of $n_C = N - 3$ elements over the total number N of sensors:

$$N_C = \frac{N!}{(N - n_C)! n_C!} \tag{8.36}$$

These process permits to build many cases, by creating different combinations of the rows of the matrix Q and to study the problem in a statistical sense. The choice of $n_C = N - 3$ is arbitrary but it has been proven to be satisfying. For example, with 10 sensors, the combinations of 7 elements over a 10-element vectors are 120.

Now, the method requires the definition of two matrices in the same manner as in Eq. (8.19) and (8.20).

Each of the two matrices A_1 and A_2 have $p-1$ rows. Successively, the procedure explained in Subsection 8.1.5 is followed to obtain N_C estimations of the source location. For each estimation k, the condition number $c_A^{(k)}$ of the matrix $A^{(k)} = \tilde{A}_1^{(k)} - \tilde{A}_2^{(k)}$, defined in Eq. (8.33), is collected. This is the end of the first part of the methodology.

The second part is focused on eliminating the outliers of the first estimation and then on finding the final solution, by averaging the values obtained, but weighted by the inverse of their condition number. In this way, the estimations coming from the cases with a low condition number matrix are more incident on the final result, which represents the estimation of the source position.

8.3.3. Estimation of the intensity

Analogously to the earthquakes, a magnitude can be defined also for the rockburst, which is a particular seismic event. For the earthquakes, as well known, there are two scales defining the intensity:

- The Mercalli scale: it measures the effects of the earthquake on structures, humans and whatever natural element.
- The Richter scale: it is a base-10 logarithmic scale, and the magnitude is defined as the logarithm of the ratio of the wave amplitude recorded by a seismograph respect to an arbitrary small amplitude (referred to a distance of 100 km).

In the rockburst case, it is fundamental to find a definition similar to the Richter scale. The procedure is:

1. Estimate the arrival times of the direct waves and collect the relative amplitudes A_i, for $i = 1,...,N$ where N is the number of receivers used in the survey;
2. Estimate the source location;
3. Estimate the amplitude relative to the source point A_S and the attenuation coefficient α, from the relationship

$$A_i = \frac{A_S e^{-\alpha r_i}}{r_i} \tag{8.37}$$

   where r_i is the distance between the source point S and the i-th receiver;
4. Calculate the magnitude as

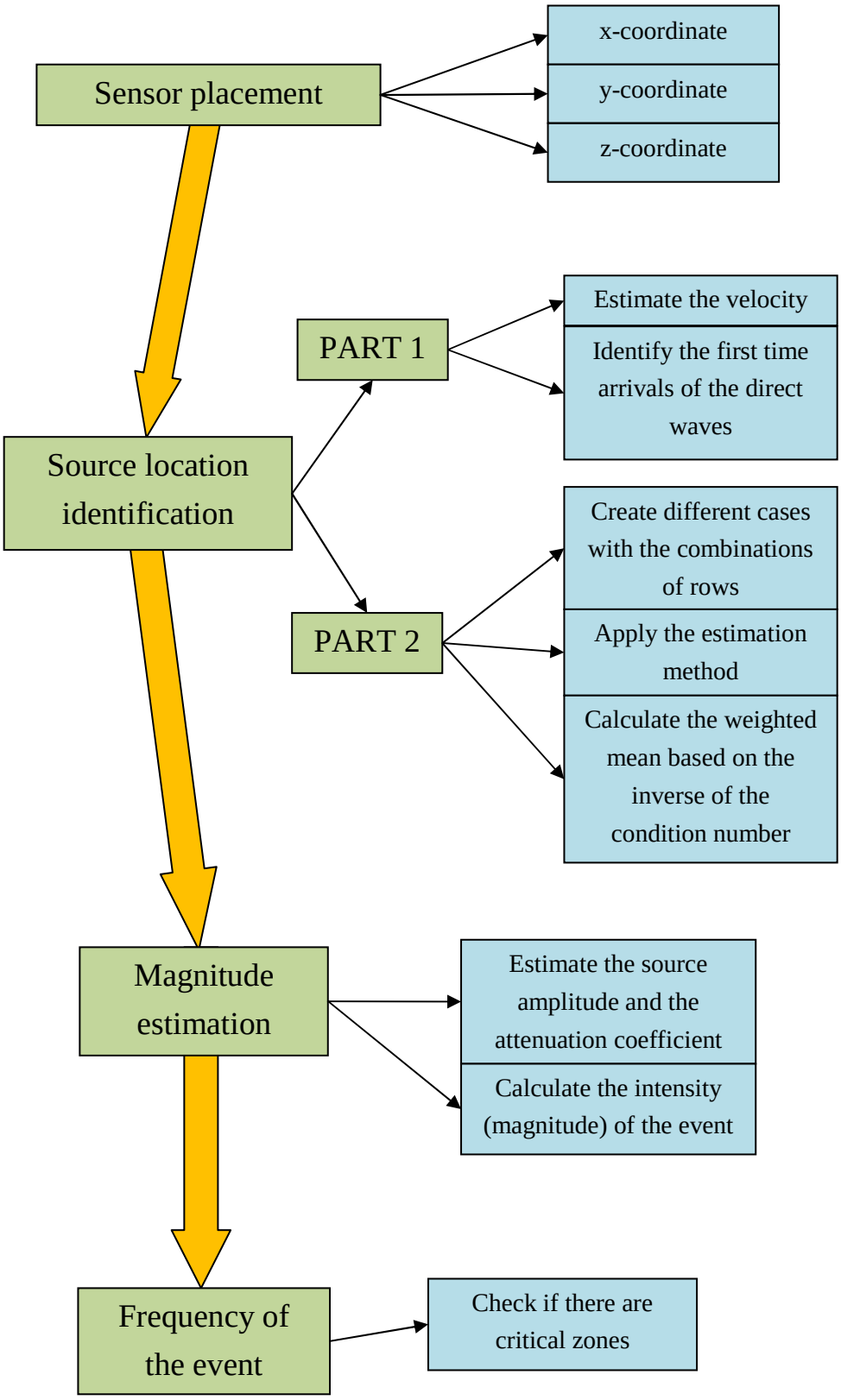

Figure 8.7. Scheme of the rockburst monitoring.

$$M = Log \frac{A_S}{A_r} \tag{8.38}$$

where A_r is called reference amplitude.

The choice of the reference amplitude could seem difficult but actually, in practical investigations, it is straightforward, as will be explained in Section 8.5.

8.3.4. Frequency of the event

The frequency of the event is simply determined by counting the events of a certain intensity that have been localized in a certain zone. In this way, it is possible to distinguish the critical zones from those which do not present many estimations in a well-confined region.

Geologists will deeply study the critical zones in order to understand the causes and the possible effects on the tunnel construction of successive rockbursts.

8.3.5. Scheme of the analysis

The summarizing scheme of the procedure is represented in Figure 8.7.

8.4. Numerical example

In this section, two numerical examples are created and analysed with the procedure presented in the previous section. At the end, a practical indication on the reliability of the estimation is proposed.

8.4.1. First simulation

In this section, let's analyse the numerical simulation whose characteristics are listed in Table 8.6. The disposition of the sensors is similar to what has been presented in Subsection 8.2.4, with a distribution on the tunnel axis (x-coordinate) that ranges in 11.6 m. The source has been placed in $S = [15, -2, 15]$, because in real cases the rockburst events originate quite close to the tunnel. The velocity, equal to 5000 m/s, is typical for P-waves in hard rock as the granite.

The time arrivals are built with the parameters just described, adding 2% of Gaussian noise.

The methodology described in the previous section is applied to the numerical example under analysis, by using $p = 5$.

Table 8.6. Characteristics of the first numerical case under study.

Parameter	Value
Source	$S = [15, -2, 15]$
X-coordinate of receivers	$x_R = [0, 10, 11.6, 4.4, 2.8, 9.7, 5.4, 8.2, 7.4, 3.4]$
Y-coordinate of receivers	$y_R = [2.9976, -2.9758, 2.8680, -2.6638, 2.9976, -2.9758, 2.8680, -2.6638, 2.9976, -2.9758]$
Z-coordinate of receivers	$z_R = [2.5, 2, 1.5, 12.5, 21.5, 1, 2.5, 2]$
Velocity	$v = 5000$ m/s
Percentage of added noise	2%

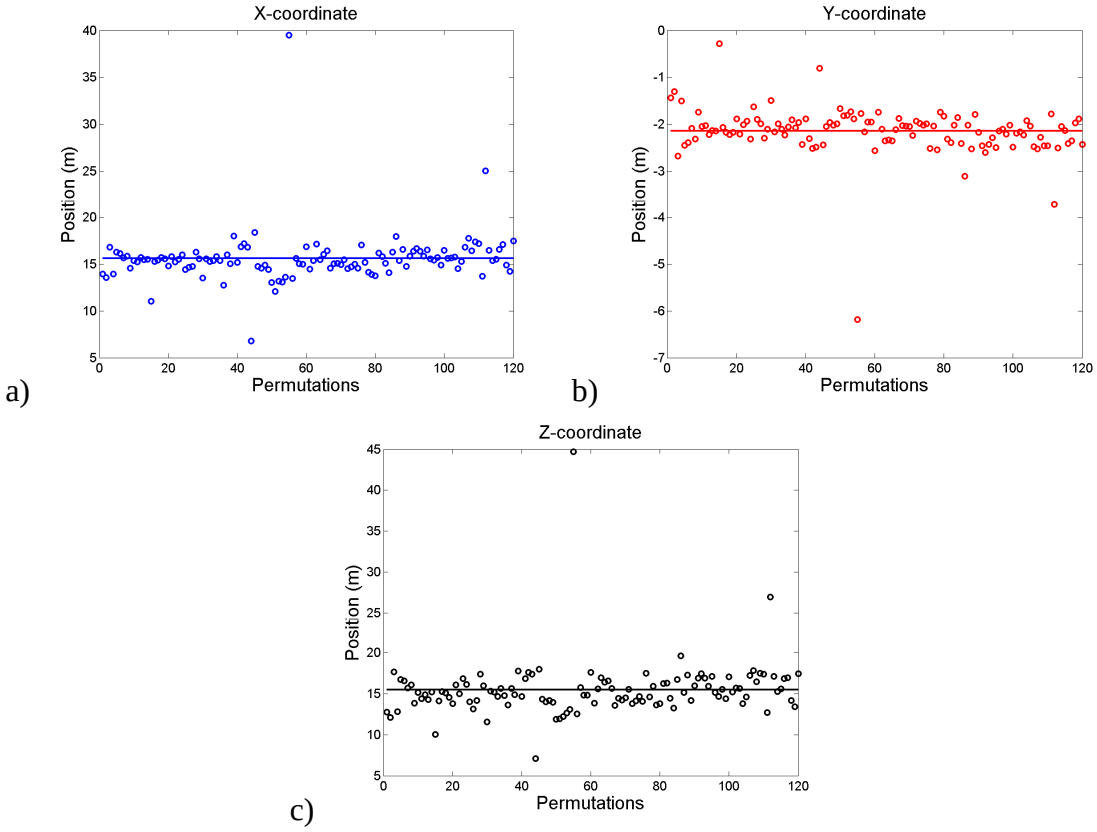

Figure 8.8. First estimations of the coordinates of the source, for the first numerical case: a) x-coordinate; b) y-coordinate; c) z-coordinate.

In Figure 8.8, the estimations of the three coordinates of the source, coming from the first analysis, are depicted. In all the cases, the estimations is very precise, meaning that almost all the values are close to the average, with few outliers. In Figure 8.9, the same values represented in Figure 8.8 are visualized, but without the outliers and then with

new average values, which still do not represent the final estimation, because the weighted mean must be applied.

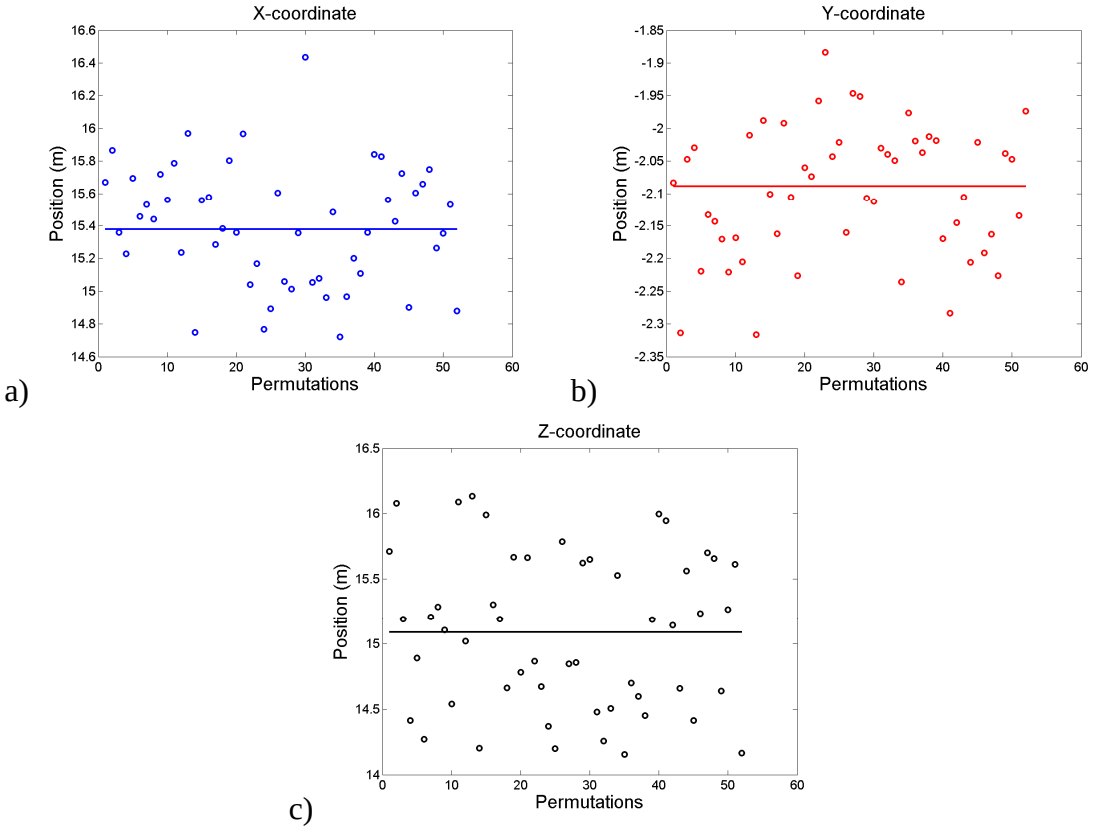

Figure 8.9. Estimations of the coordinates of the source after the elimination of the outliers, for the first numerical case: a) x-coordinate; b) y-coordinate; c) z-coordinate.

In Figure 8.10, the estimation of the three coordinates is depicted in function of the condition number of the matrix A, in order to highlight where the more significant estimations (corresponding to small condition numbers) lie. The figure shows that the condition number is quite high, and the best zone shows values from 5 to 50, approximately.

The weighted average gives the the final estimation of the rockburst source location, which is $S_e = (15.38, -2.09, 15.09)$, with a relative error of 1.86%. It is represented in Figure 8.11, together with the sensors used for the identification.

If the sensor configuration would be chosen more compact, then the condition number would be smaller but the zone of identification will be reduced, because the sensors have a minor spatial coverage.

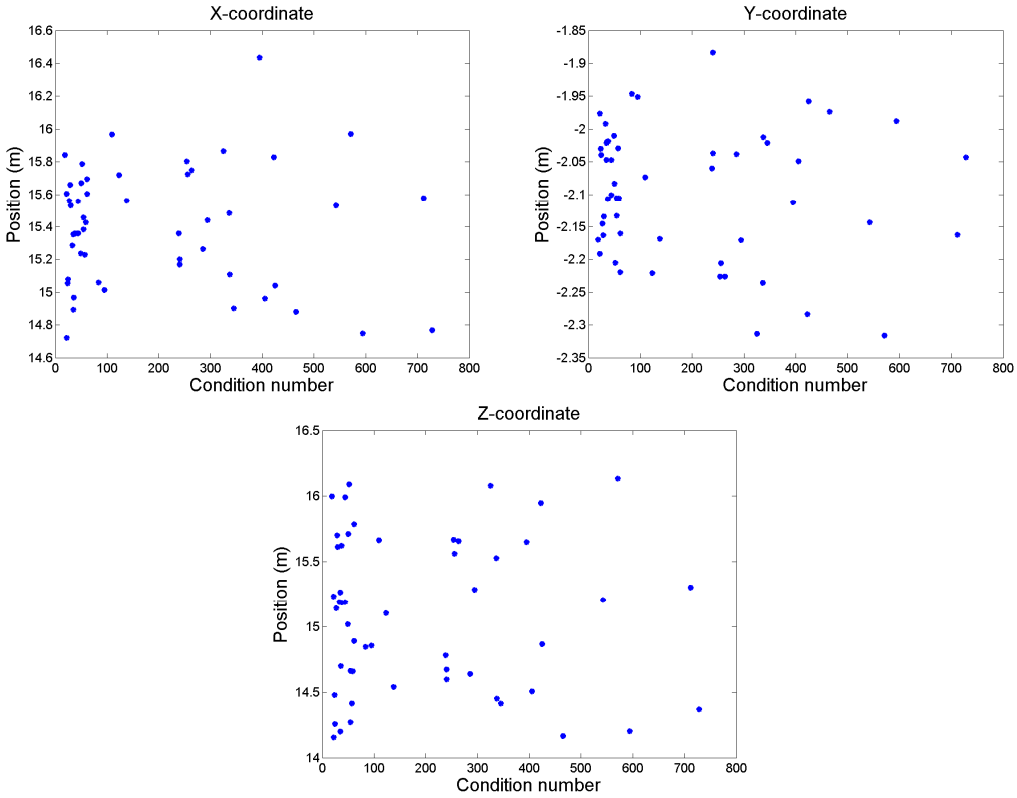

Figure 8.10. Estimations of the source in function of the condition number of the matrix *A*: a) x-coordinate; b) y-coordinate; c) z-coordinate.

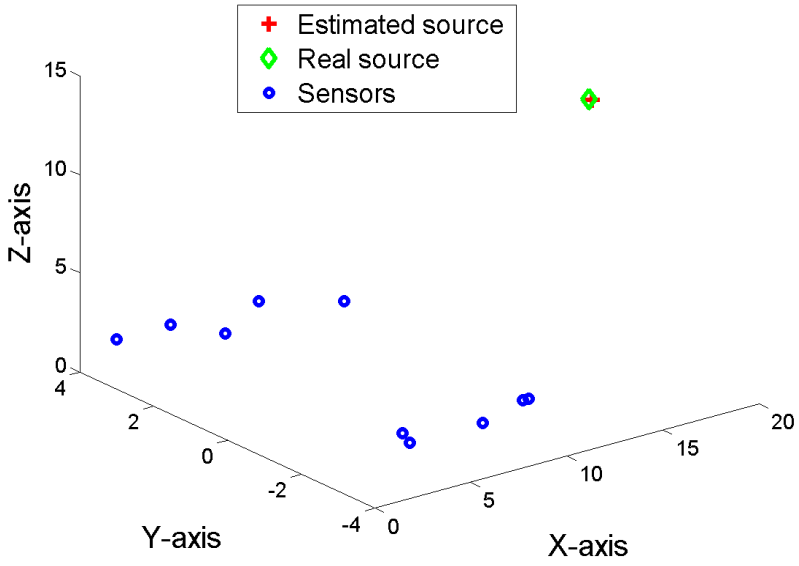

Figure 8.11. Final estimation of the source location.

Table 8.7. Characteristics of the numerical case under study.

Configurations	Condition number
Source	$S = [72, -21, 15]$
X-coordinate of receivers	$x_R = [0, 0, 30, 30, 60, 60, 90, 90, 120, 120]$
Y-coordinate of receivers	$y_R = [-2.2, 2.5, -2, 2.1, -2.3, 2.4, -2.8, 2, -2.2, 2.9]$
Z-coordinate of receivers	$z_R = [2, 1.6, 1.2, 0.8, 0.4, 0.4, 0.8, 1.2, 1.6, 2]$
Velocity	$v = 5000$ m/s
Percentage of added noise	2%

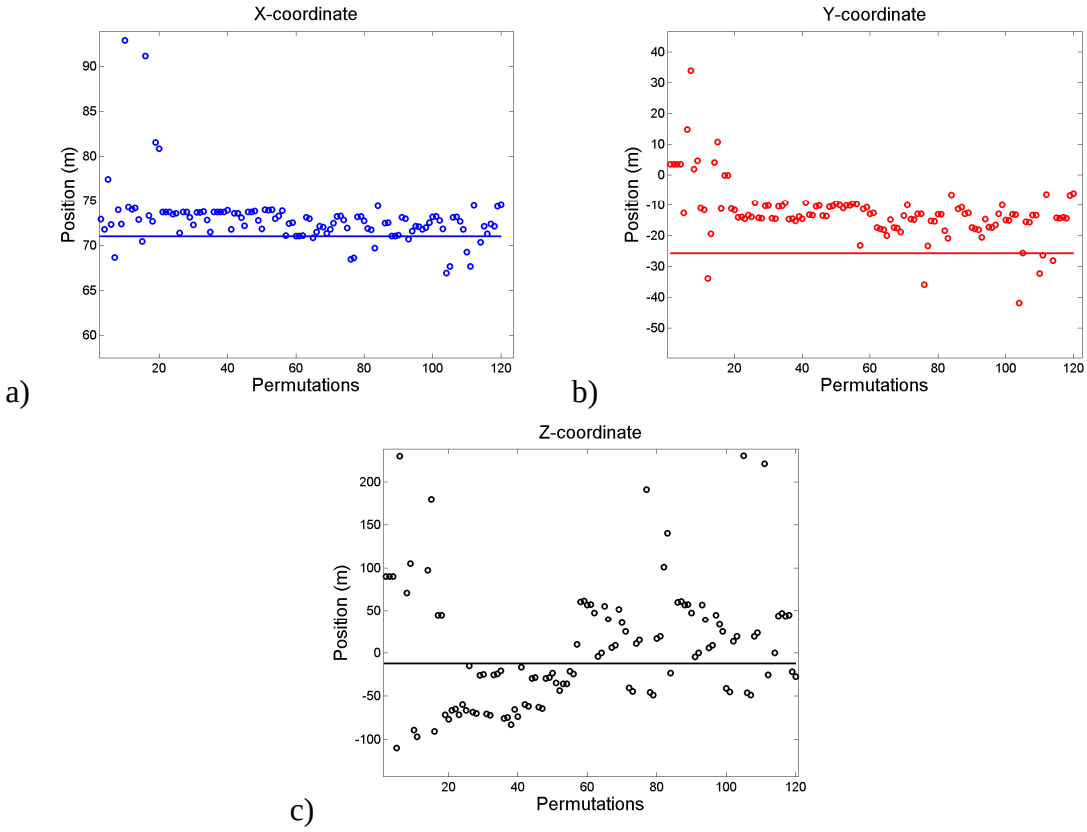

Figure 8.12. First estimations of the coordinates of the source, for the second numerical case: a) x-coordinate; b) y-coordinate; c) z-coordinate.

8.4.2. Second simulation

The second simulation is based on a configuration similar to a real rockburst investigation in a tunnel, where the sensor configuration is often the same of the seismic methods for the prediction of discontinuities. In this case, there are ten sensors

distributed over 5 sections, with 30 meters between two consecutive of them. The velocity is 5000 m/s, as in the previous case. All these characteristics are listed in Table 8.7.

The first estimation is depicted in Figure 8.12. Respect to the previous numerical case, the values have a significant larger dispersion, especially for the z-coordinate. This is due to the fact that the sensor configuration is very different and leads to high condition numbers, as can be seen in Figure 8.13, since the values exceed even 2000 in some cases.

The weighted mean leads to find the final estimation of the rockburst source location, which is $S_e = (72.77, -13.54, -22.85)$, with a relative error which is:

- small for the x-coordinate, since the sensors cover a large zone along the tunnel axis;
- quite large for the y-coordinate
- very large for the z-coordinate

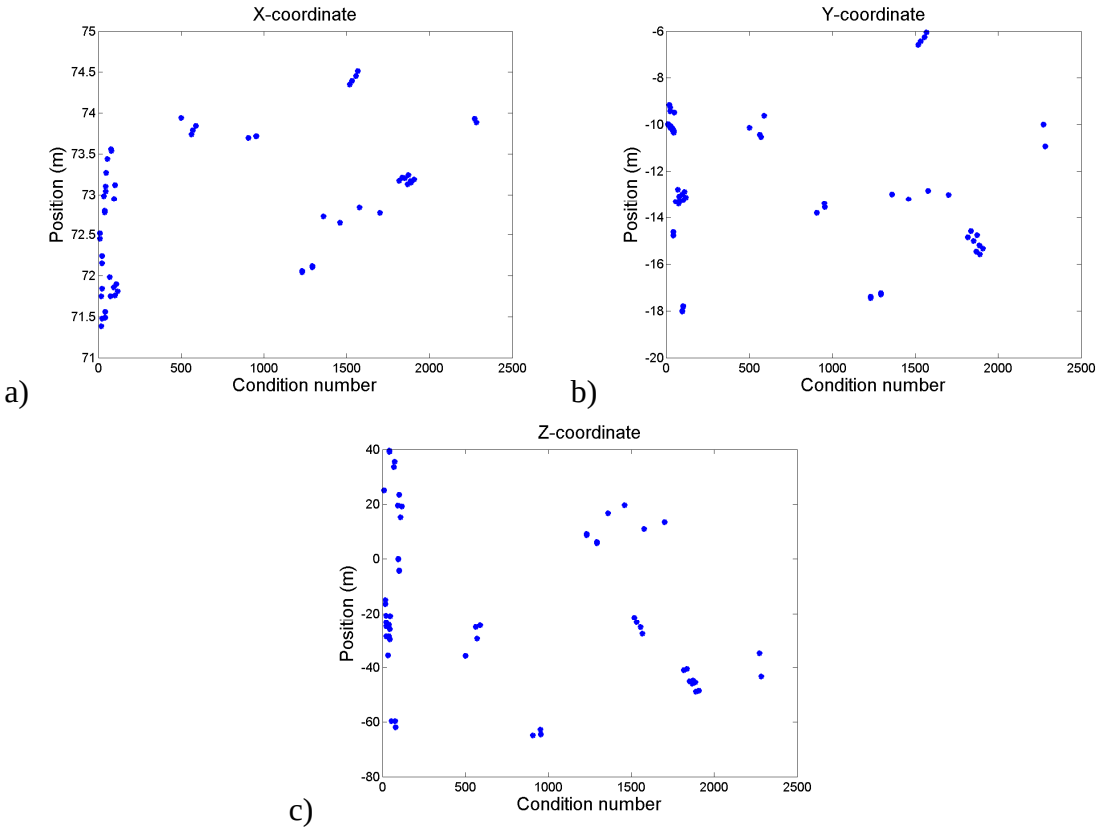

Figure 8.13. Estimations of the source in function of the condition number of the matrix A: a) x-coordinate; b) y-coordinate; c) z-coordinate.

In the last two cases, the disposition very concentrated respect to the x-coordinate prevents the possibility to obtain an accurate estimation.

8.4.3. Reliability of the estimation

The estimation of the source, for many reasons like noise, sensor configuration and others, could not be very accurate, as just seen in the second numerical example. Consequently, a reliability indicator is useful to understand how much the estimation is reliable.

First of all, the reliability of the estimation must not be considered in a general sense, but singularly on the three spatial coordinates of the source. This signifies that, in general, it is meaningless to compare the distance between the real and the identified source, because it is more important to evaluate the error committed in each of the three components.

As already said, in tunnel investigations, if the configuration is similar to a TRUST scheme, probably the condition number will be large and an accurate estimate will be obtained only on the x-coordinate of the source. Vice versa, for a TRT configuration, the estimation will be more reliable but only if the source is close to the zone in which the sensors are placed.

A simple indicator of the reliability of the estimation is the standard deviation of the second estimations (those obtained by the method, after having eliminated the outliers). If it is inferior to 5, then the estimation can be considered sufficiently reliable.

In Table 8.8, the reliability indicators for both the numerical simulations are listed. For the first one, the values are very small and correspondingly the estimation is very accurate. On the contrary, for the second simulation, while the reliability indicator is small only for the x-coordinate (good estimation), it is borderline for the y-coordinate (estimation not so accurate), and it is very large for the z-coordinate (bad estimation).

Table 8.8. Reliability indicators for the three coordinates of the source, for both the numerical simulations presented.

Coordinate	First simulation	Second simulation
X-coordinate	0.50	1.64
Y-coordinate	0.09	7.19
Z-coordinate	0.41	36.78

8.5. Test in the Brennero tunnel

Up to now, no experimental tests have been conducted in the Brennero tunnel about the rockburst monitoring, with the described methodologies. The unique investigation available is a test during an excavation with drilling and blasting technique, done in a tunnel some meters away from the tunnel considered. Indeed, when constructing long tunnels, many galleries are excavated both for accessing the principal tunnel and both for the security of the train passengers, once the work is finished.

8.5.1. The acquisition

In a rockburst monitoring, the acquisition is different from a seismic survey because it is a passive monitoring, meaning that the sensors start recording only when the accelerations overcome a fixed threshold. Otherwise, it would be impossible to acquire and process all the data available. Moreover, a pre-trigger is always present, usually equal to one second, while the acquisition lasts three seconds.

The threshold for the recording is fixed arbitrarily based on the acceleration levels recorded during preliminary analyses. The selection of this parameter is very important because if it is too large, some important events cannot be recorded, on the contrary too much data must be examined.

Coming back to Subsection 8.3.3, the threshold is also used as the reference amplitude in the magnitude estimation of the rockburst event. In this way, it is possible to well quantify the intensity of the seismic event, by comparing the source amplitude with a fixed value.

The configuration adopted for the survey under analysis is based on the TRUST scheme (Figure 2.16), since it was used also for a seismic investigation ahead of the tunnel front. The coordinates of the sensors are listed in Table 8.9, where it is possible to note that nine sensors are available, on four sections, with large distances between two successive sections. About the z-coordinates, there are only two values different from zero.

Table 8.9. Sensor coordinates for the experimental test under analysis.

Coordinate	Value
X-coordinate	$x_R = [0, 0, 0, 48, 48, 48, 98, 98, 146]$
Y-coordinate	$y_R = [3.2, -3.4, -3.2, 3.2, 0, -3.2, 3.2, -3.2, -3.2]$
Z-coordinate	$z_R = [0, 1.8, 0, 0, 4.8, 0, 0, 0, 0]$

8.5.2. The data analysis

As suggested in Subsection 8.3.2, the velocity is estimated by performing a quick test with an hammer stroke in a known point and by considering the peaks referred to the first time arrivals of the P-waves. In this case, the velocity estimated (average of the values obtained for each trace) is 4854 m/s, value that has been inserted in the algorithm for the source localization.

The data relative to the acquisition are not accessible; therefore only the first time arrivals are available. They have been detected by an expert geophysicist.

The real source is considered in the middle of the excavation front since its area is about 20-30 m^2. The value is $S = (7, 30, 14.5)$.

The first estimations given by the methodology proposed are depicted in Figure 8.14. The figures shows that the uncertainty on the different coordinates is quite large and moreover the average lines are not close to the real source coordinates.

In Figure 8.15, the source coordinates are shown as function of the condition number of the matrix A.

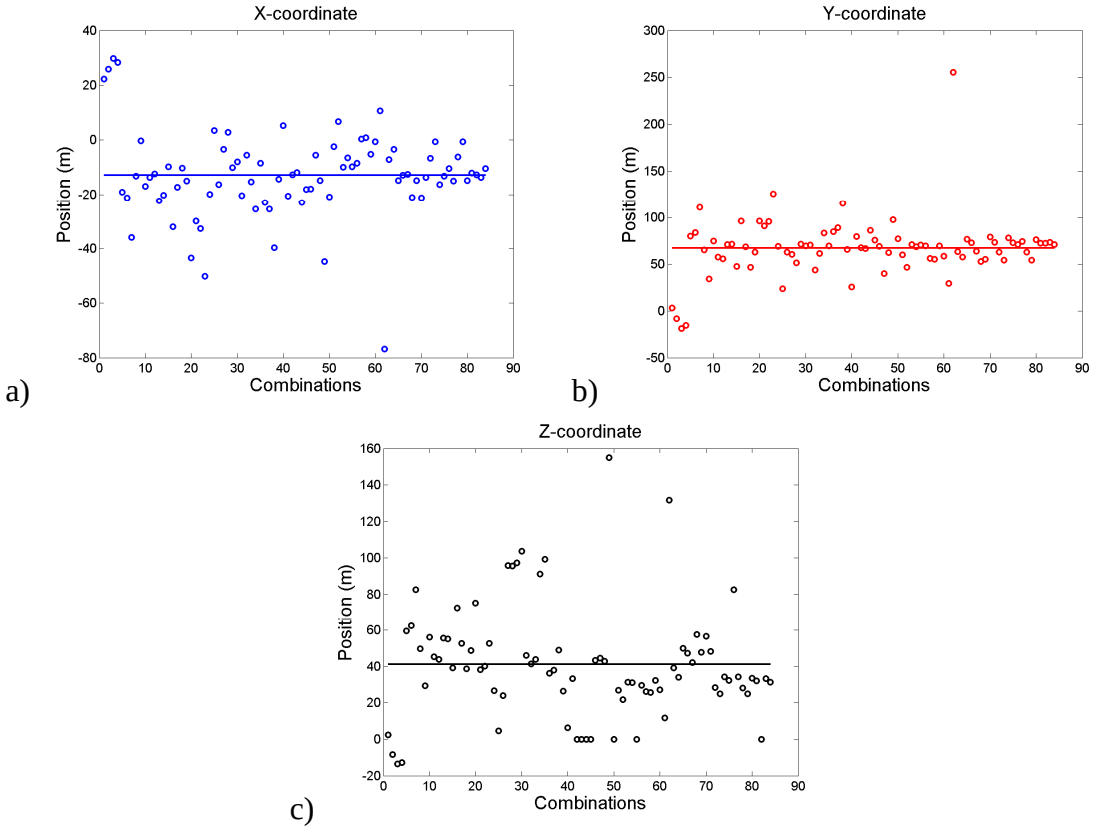

Figure 8.14. First estimations of the coordinates of the source, for the experimental case under analysis: a) x-coordinate; b) y-coordinate; c) z-coordinate.

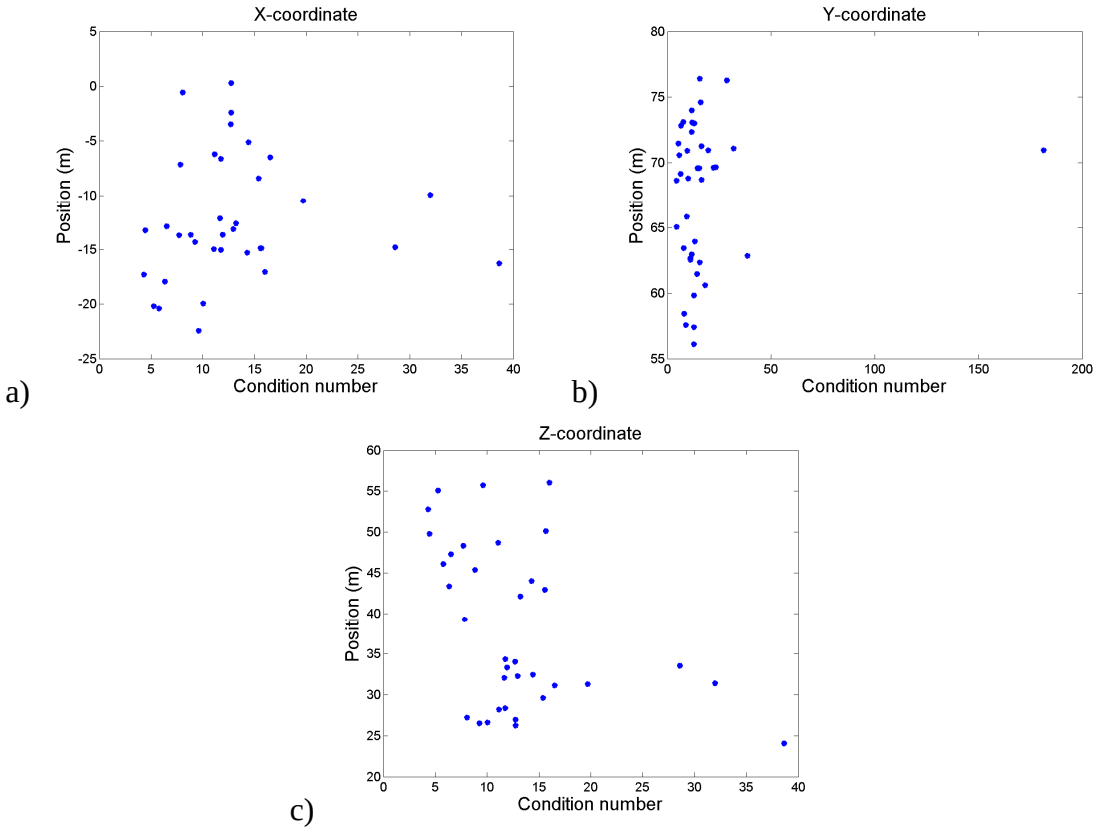

Figure 8.15. Estimations of the source in function of the condition number of the matrix *A*: a) x-coordinate; b) y-coordinate; c) z-coordinate.

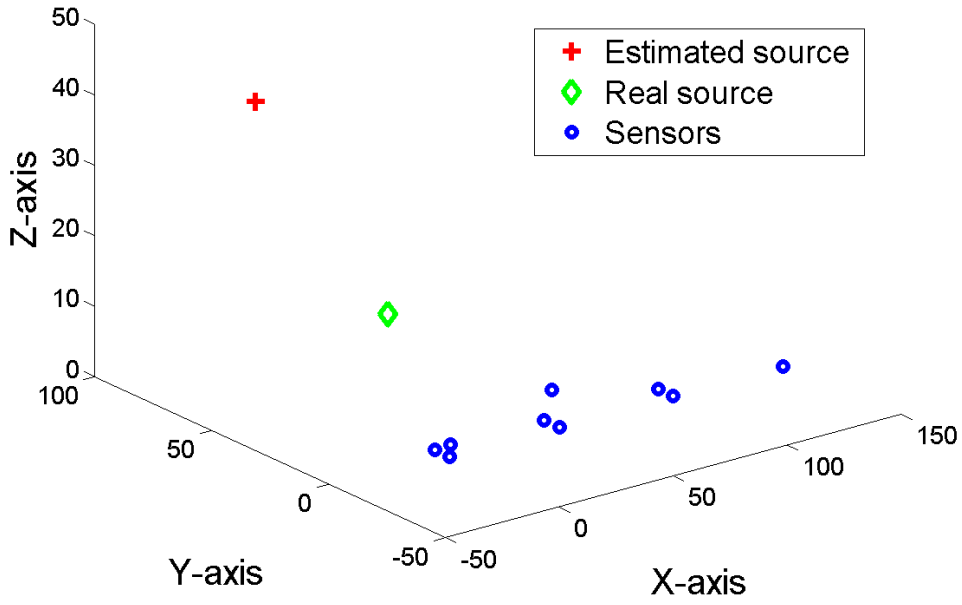

Figure 8.16. Final estimation of the source location.

Respect to the numerical simulations presented in the previous section, the condition numbers involved are smaller, but the reliability factors do not foretell an accurate estimation, since they are equal to 5.73 (x-coordinate), 5.77 (y-coordinate) and 9.95 (z-coordinate). This is exactly what happens, because the estimation of the source location is $S_e = (-13.01, 67.35, 40.76)$, with non-negligible errors for every coordinate. This can be seen graphically in Figure 8.16.

In a real survey, what is actually important is to estimate not the exact position of the rockburst but the region in which it actually is. In this way, it is possible to affirm that the method has roughly identified the critical zone and this is fundamental for the rockburst detection. Moreover, since many small seismic events can happen in a tunnel under construction, many consecutive events are monitored and then finally a map with the critical zones (and also the amplitudes) can be drawn.

In the next months, the rockburst monitoring will be analyzed in the Brennero tunnel and the algorithm proposed will be fundamental for its detection.

Chapter 9

Conclusions and future works

9.1. Final comments

The thesis presents two fundamental issues about the monitoring of a tunnel under construction, i.e. the estimation of rock discontinuities ahead of the tunnel front and the rockburst monitoring.

About the first topic, the work starts by describing the seismic methods present in literature and by extracting the main relationships involving the physical parameters. The major difference with the classical seismic reflection methods is the configuration of receivers and source points, which is strongly conditioned by the particular shape of the tunnel. This fact obliges to locate those elements on the tunnel walls or on the tunnel face.

Referring to the discontinuity prediction, two methods are proposed to process the data using a random array of receivers and sources: the first one is based on the intersection of the ellipsoids, built from each source-receiver pair; the second one is a fully automated method, based on a sort of “cluster analysis” of all the reflection events that can be back-projected on the space domain close to the tunnel. With this approach, the results are considered in terms of probability to point out discontinuities of rock mass, indicating lithological changes, faults or fractures. This is one of the most innovative characteristics of the methodology: the final illustration is a probability map where the critical zones are represented by dark colours. Darker the colour, larger the probability to meet a reflector in that point. Another interesting aspect is the tuneable sensitivity of the method, which can be settled on the basis of noise measurements and data acquisition quality.

Many tests have been performed on synthetic signals and on real data coming from the Brennero tunnel, pointing out the performances of the proposed methodology in terms

of accuracy in the identification of discontinuities. In some experimental cases, no information about the lithology is available and then the results cannot be completely evaluated.
The computational time for the data processing is very small: it lasts only few minutes for the experimental tests presented. In other words, it means that, after a simple re-organization of the gathered data set, a preliminary interpretation can be available almost in real time, i.e. in few minutes after the data acquisition.
Referring to the rockburst phenomenon, an optimal configuration for the sensor placement and some techniques for the estimation of the source location have been proposed. The procedure has been applied mainly on numerical data showing the reliability and the peculiarities of the algorithm, which is a modification of the classical approaches used to find the position of an acoustic source.
Both the seismic reflection techniques and the rockburst monitoring have been developed not only from a theoretical and numerical point of view but also with a constant attention to the experimental and practical problems. This means that the experimental works done in the Brennero tunnel have been very important to give indications about the feasibility of the conducted study and how to tune the parameters during the different kinds of analyses.

9.2. Improvements of the automatic method

In the following, some ideas are proposed for the improvement of the automatic method for the estimation of rock discontinuities.

9.2.1. Reflection not in a single node

The backward method, as demonstrated in Section 7.7, is not the best suitable technique when sources and receivers are placed far from the tunnel face, because the hypothesis of common reflection point cannot be considered valid, like for the TRUST configuration. For this reason, the method should be slightly modified to be applied in most of the real cases, without requiring a specific disposition of sources and receivers.
A weaker condition for the determination of the discontinuities is to take into account not only one node per time, but also those in a specified neighbourhood of that node, such that the reflections can come also from near nodes, as theoretically happens. In this way, even considering sources and receivers very far from each other, the method could obtain more reliable results.

9.2.2. Velocity in the domain

Another critical point of the method is the velocity estimation. When analysing cases where there are different types of rocks, the backward method can fail, as demonstrated in the numerical example presented in Section 6.1. In this case, the value of velocity estimated in the first medium cannot be supposed valid also for the second medium, because its characteristics are very different. Even if in real situations this event happens only few times, the creation of a velocity field could be a significant improvement.

Practically, there are some methods in literature which are based on a velocity model, meaning that the starting point is to define a domain and to associate a velocity value to each node instead of considering it as a reflection point. However, in the algorithm proposed in the thesis, it is difficult to combine the two aspects, therefore this topic should be analysed more in details to find a good compromise between the two approaches.

An additional improvement about the velocity could be the method for its estimation: the successive elimination technique could be substituted by more common approaches as the STA/LTA (Short Time Average over Long Time Average).

9.2.3. Application in the case of excavation with TBM

The work presented in this thesis has been successfully applied to the seismic sources produced with the blasting and with the hammer. Successively, some tests will be done with the magneto-strictive source, where the main problem will be to obtain a satisfying cross-correlation among the pilot signal (characterizing the source) and the signals recorded by the receivers.

However, since almost the tunnels under construction are excavated with the TBM, the automatic method must be adapted in order to be used in this situation. In presence of TBM, as already noted in the introduction and in Section 2.4.5 and Section 2.4.6, the monitoring of the discontinuities can be done either by exploiting the noise produced by the cutter head or by exciting the tunnel walls by means of magneto-strictive sources placed on the grippers.

The method presented in the thesis is able to work only with the second case, because in presence of noise of the cutter head the following incompatibilities hold:

- the source is not a unique point
- the excitation is continuous

About this topic, a partial solution is given by correlating the signal coming from the pilot accelerometer with those coming from the other accelerometers.

Actually, the unique way to apply the backward method is to follow the procedure of Luth et al. (2008), because in this case there are source points on both the sides. The

accelerometers should be placed in a convenient position, in the open spaces of the TBM. Furthermore, they should be preferably wireless, because it is almost impossible to use cables with such a machine. About this point, the wireless accelerometers are an interesting solution for this kinds of applications in tunnels: they are connected to the acquisition system via a wireless communication and then the wiring operations are avoided. This will be a significant improvement not only in presence of a Tunnel Boring Machine, but in general for different environmental and civil applications.

9.2.4. Characterization of the discontinuities

Further implementation of the proposed method will consider the analysis of the reflection coefficient, to provide information about the properties of the materials after the discontinuities estimated by the automatic method.

The reflection coefficient must be estimated after having corrected the amplitudes of the waves. Indeed, referring to Figure 9.1, where a schematic representation of the seismic reflection in tunnels is sketched, the amplitudes of the reflected waves follow a simple formula:

$$A = A_0 \frac{1}{r_1 + r_2} e^{-\alpha(r_1+r_2)} \tag{9.1}$$

where A_0 is the wave amplitude at the source, α is the attenuation coefficient, and r_1 and r_2 are the path travelled by the wave, according to Figure 9.1.

The correction of the amplitudes should be done in two steps:

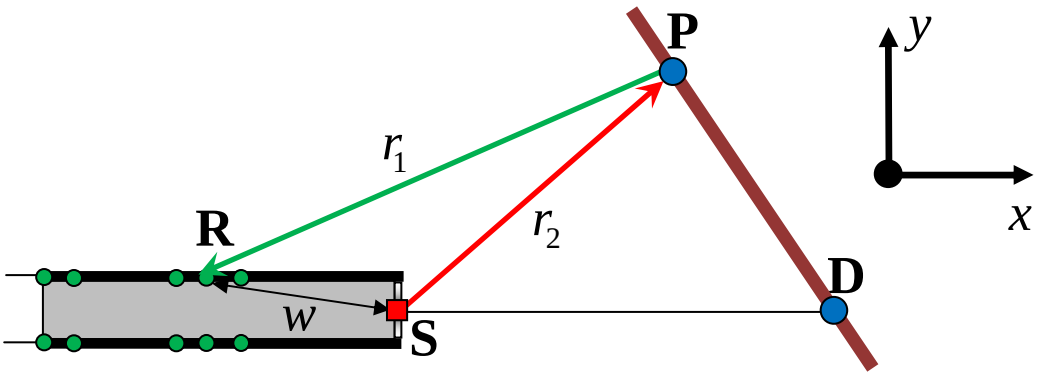

Figure 9.1. Scheme of the reflection in a tunnel investigation.

1. Correction of the geometric dispersion
2. Correction of the intrinsic attenuation

The geometric correction is dedicated to the first part of Eq. (9.1) while the correction of the attenuation should be done iteratively, by considering many sensors to estimate the coefficient α.

Once corrected the traces, and after having identified the peaks corresponding to the discontinuities, the reflection coefficient is obtained by dividing the amplitudes of the reflected waves by those of the incident waves.

As expressed in Section 2.2, the reflection coefficient is directly connected to the difference of impedance between two successive materials (or rocks), therefore an indication of the rock types corresponding to the estimated discontinuities is provided. This represents the final prediction of the lithology ahead of a tunnel face.

9.3. Backward method for the rockburst

Since the backward method for the estimation of the discontinuities ahead of the tunnel face has been demonstrated to be reliable, quick and automatic, the rockburst monitoring can be improved by adopting the same ideas. In particular, the main advantage would be the elimination of the manual selection of the peaks due to the first time arrivals.

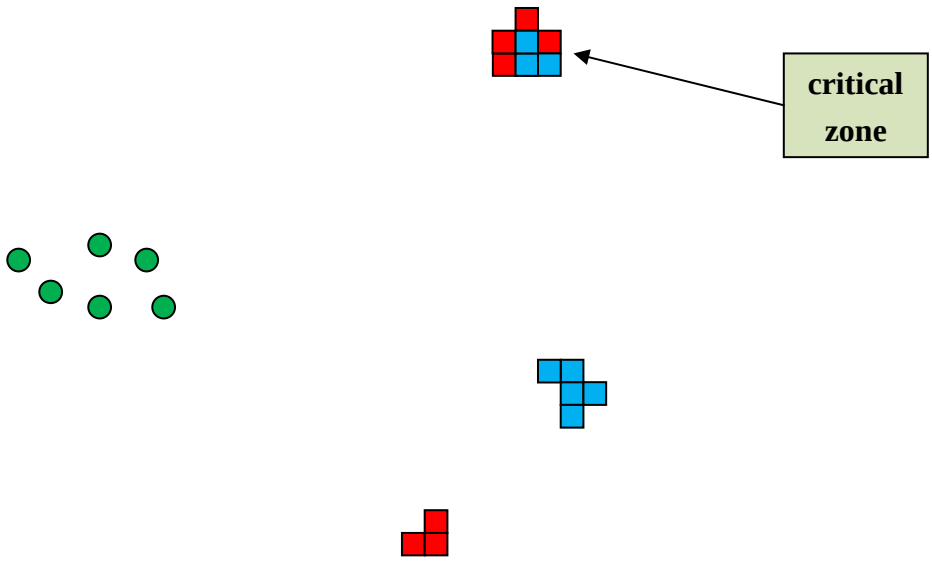

Figure 9.2. Representation of the idea of the backward method for the rockburst monitoring. The green circles indicate the receivers, while the squares indicate the estimation produced by a first estimation (red) and by a second one (blue).

Indeed, this long operation is necessary to run the procedure presented in Section 8.3. Moreover, another improvement is the possibility to analyze a big amount of data recorded by the receivers placed on the tunnel walls. This fact allows to understand if there are some repetitions in the results, meaning that a critical zone has been detected.
The idea of the method is represented in Figure 9.2, where two estimations coming from different analyses are shown. The value extracted cannot be unique, but it can be compared with successive estimations to find recurrences and critical zones.
Respect to the method introduced in Chapter 5, the most significant differences are:

- the domain must be three-dimensional,
- only the peaks related to the direct waves are considered.

Consequently, even if the computational time could increase due to the 3D domain, on the other hand there are less operations respect to the previous case and therefore probably the results will be obtained in few minutes.

Appendix A

The ellipsoid

The ellipsoid is a closed quadric surface, representing the direct extension of the ellipse in three dimensions (see Figure A.1). Indeed, it has the same fundamental properties of the ellipse, which has two special points on the major axis, called foci, which are equidistant from the centre point O and such that the sum of the distances from any point P on the ellipse to those two foci is constant.

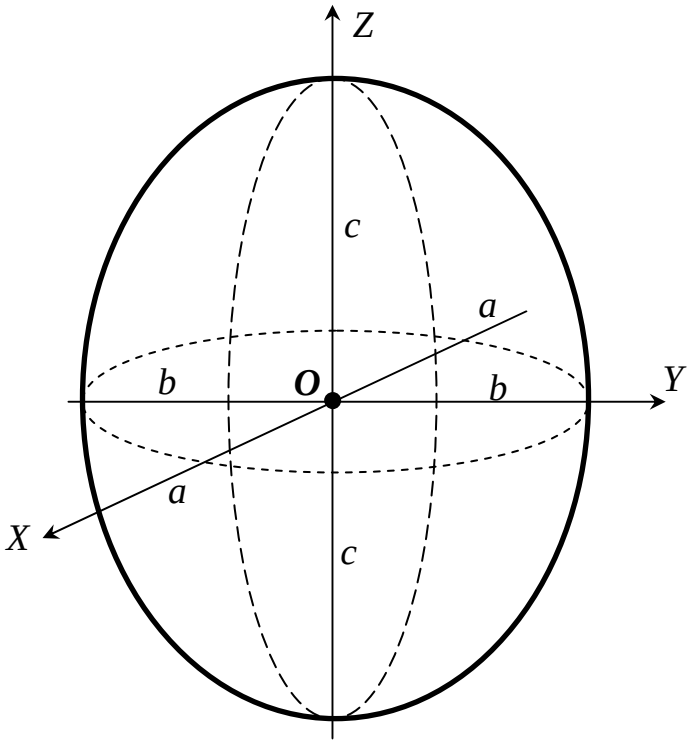

Figure A.1. Representation of a generic ellipsoid.

The general equation of an ellipsoid is

$$\frac{x^2}{a^2}+\frac{y^2}{b^2}+\frac{z^2}{c^2}=1 \tag{A.1}$$

where a, b and c are positive constant parameters indicating the semi-axes of the ellipsoid.

If the lengths of two axes of an ellipsoid are the same, the figure is called a spheroid, and if all three are the same, it is called a sphere.

In two dimensions, the equation if the ellipse is simply:

$$\frac{x^2}{a^2}+\frac{y^2}{b^2}=1 \tag{A.2}$$

The distance from the centre O to a focus is

$$f=\sqrt{a^2-b^2} \tag{A.3}$$

while the eccentricity is defined by

$$e=\frac{f}{a} \tag{A.4}$$

where a is the semi-major axis.

Appendix B

The condition number

Let us consider a linear system of the type

$$Ax = b \tag{B.1}$$

where A is a $n \times m$ matrix, x and b are m and n-dimensional vectors, respectively. It can be demonstrated that the relative error in x is $k(A)$ times the relative error in A and b, where $k(A)$ is the condition number of the matrix A.

From a practical point of view, the condition number quantifies the accuracy of the solution. If it is very large, the matrix is said to be ill-conditioned and consequently it is impossible to expect a good solution from such a system. Even, for some extremely ill-conditioned systems it is not possible to obtain any solution.

There is not a unique mathematical definition of the condition number; here three common definitions are listed:

1. ratio between the maximum and the minimum singular value

$$k(A) = \frac{\sigma_{MAX}}{\sigma_{MIN}} \tag{B.2}$$

2. ratio between the maximum and the minimum eigenvalue

$$k(A) = \frac{\lambda_{MAX}}{\lambda_{MIN}} \tag{B.3}$$

3. multiplication of the maximum sum of the rows for the matrix and the same quantity for its inverse matrix

$$k(A) = \max_j \sum_{i=1}^{n} | a_{ij} | \times \max_j \sum_{i=1}^{n} | a_{ij}^{-1} | \qquad \text{(B.4)}$$

Note that the permutation of the rows of the matrix is not a useful operation because the change does not reduce the condition number.

In every kind of linear problem, it is advisable to have a small condition number, such that the estimation of the vector of unknowns x is more accurate. If the condition number is too high, it can be reduced by specific techniques of preconditioning.

References

Ali A., Yao K., Collier T., Taylor C. E., Blumstein D. T., Girod L., 2007. An empirical study of collaborative acoustic source localization, IPSN 07.

Anderson N., Akingbade A., 2011. Overview of the shallow seismic reflection technique.

Antoni J., 2005. Blind separation of vibration components: Principles and demonstration. Mechanical System and Signal Processing 19, 1166-1180.

Aoki K., Mito Y., Yamamoto T., Shirasagi S., 2007. Geostatistical evaluation of the mechanical properties of rock mass for TBM tunneling by seismic reflection method, Rock Mechanics and Rock Engineering 40 (6), 591-602.

Ashida Y., Koichi S., 1993. Depth Transform of Seismic Data by Use of Equi-Travel Time Planes, Exploration Geophysics 24, 341-346.

Ashida Y., 2001. Seismic imaging ahead of a tunnel face with three-component geophones, International Journal of Rock Mechanics and Mining Sciences 38, 823-831.

Akazawa T., 2004. A technique for automatic detection of onset time of P- and S-phases in strong motion records, 13th World Conference on Earthquake Engineering, Vancouver.

Baldi A.M., Fuoco S., De Luca J., 2006. Application of new seismic methodologies for the solution of geomechanic problems connected to the excavation of tunnels, MPES 2006, Fifteenth International Symposium on Mine Planning and Equipment Selection, Torino, September 19-22 2006.

Bellino A., Fasana A., Garibaldi L., Marchesiello S., 2010. PCA-based detection of damage in time-varying systems, Mechanical System and Signal Processing 24, 2250-2260.

Bellino A., Garibaldi L., Marchesiello S., 2011. Determination of moving load characteristics by output-only identification over the Pescara beams, Journal of Physics, Conference Series 305.

Bohlen T., Lorang U., Rabbel W., Muller C., Giese R., Luth S., Jetschny S., 2007. Rayleigh-to-shear wave conversion at the tunnel face – From 2D-FD modeling to ahead-of-drill exploration, Geophysics 72 (6), T67-T79.

Benecke N., Dombrowski B.A., Lehmann B., 2008. Trust – Exploration ahead of the tunnel face for reducing tunneling risks and supporting decision-making, World Tunnel Congress 2008 – Underground Facilities for Better Environment and Safety – India.

Bruckl E., Chwatal W., Mertl S., Radinger A., 2008. Exploration Ahead of a Tunnel Face by TSWD – Tunnel Seismic While Drilling, Geomechanik und Tunnelbau (1), 460-465.

Chang P.-S., Yu C.-W., 2005. Reliability of geological exploration methods during construction of the Hsuehshan Tunnel, World Long Tunnels.

Cosma C., Enescu N., 2001. Characterization of fractured rock in vicinity of tunnels by the swept impact seismic technique, International Journal of Rock Mechanics and Mining Sciences 38, 815-821.

Cosma C., Enescu N., Ahokas T., Heikkinen E., 2009. High resolution seismic profiling for tunnel engineering at Olkiluoto, Near Surface 2009.

Descour J. M., Morino A., Maffucci M., Pinheiro F., 2012. Ten months of ground imaging ahead of the TBM Using Seismic Reflector Tracing, American Rock Mechanics Association.

Diogo L. A., Le Diagon F. M. M., Prado R. L., 2004. Bedrock imaging using post-critical shallow seismic reflection data, Journal of Applied Geophysics 57, 1-9.

Dombrowski B., Orlowsky D., Lehmann B., Swoboda U. Combination of rockburst monitoring and seismic exploration ahead of the tunnel face: a new seismic concept for hazard reduction.

Feroci M., Orlando L., Balia R., Bosman C., Cardarelli E., Deidda G., 2000. Some considerations on shallow seismic reflection surveys, Journal of Applied Geophysics 45, 127-139.

Foti S., 2000. Multistation methods for geotechnical characterization using surface waves, PhD Thesis, Politecnico di Torino.

Fransson, A., Gustafson G., 2000. The use of transmissivity data from probe holes for predicting tunnel grouting, Tunneling and Underground Space Technology 16, 365-368.

Gelius L. J., Westerdahl H., 2002. Tunnel seismics – prediction of rock conditions ahead, European Journal of Environmental and Engineering Geophysics 7, 167-183.

Godio A., Dall'Ara A., 2012, Sonic log for rock mass properties evaluation ahead of the tunnel face – A case study in the Alpine region, Journal of Applied Geophysics 87, 71–80.

Grodner M., 2001. Delineation of rockburst fractures with ground penetrating radar in the Witwatersrand Basin, South Africa, International Journal of Rock Mechanics & Mining Sciences 38, 885-891.

Haile A. T., Le Bron K., 2001. Simulated rockburst experiment – evaluation of rock bolt reinforcement performance, Jl. S. Afr. Inst. Min. Metall. 101 (5), 247-251.

Hildyard M. W., 2007. Wave interaction with underground openings in fractured rock, Rock Mechanics and Rock Engineering 40, 531-561.

Jetschny S., Bohlen T., De Nil D., 2010. On the propagation characteristics of tunnel surface-waves for seismic prediction, Geophysical Prospecting 58, 245-256.

Kase E., Ross T., 2004. Using seismic tomography and holography ground imaging to improve site investigations, North American Society for Trenchless Technology.

Kessler D., Chan W.-K., 1993. DMO velocity analysis with Jacubowicz's dip-decomposition method, Geophysics 58 (10), 1517-1524.

Khanlari. G. R, Ghaderi-Meybodi, R., 2011. Analysis of rockburst in critical section of second part of Karaj-Tehran Water Supply Tunnel, ISGSR 2011 - Vogt, Schuppener, Straub & Bräu (eds)

Klose, 2002. Fuzzy rule-based expert system for short-range seismic prediction, Computers and Geosciences 28, 377-386.

Kneib, G., A. Kassel, and K. Lorenz, 2000, Automatic seismic prediction ahead of the tunnel boring machine, First Break 18, 295–302.

Kneib, G., and A. Leykam, 2004, Finite-difference modelling for tunnel seismology: Near Surface Geophysics, 2, 71–93.

Lee I.-M., Truong Q.-H., Kim D.-H., Lee J.-S., 2009. Discontinuity detection ahead of a tunnel face utilizing ultrasonic reflection: Laboratory scale application, Tunneling and Underground Space Technology 24, 155-163.

Liu G., Fomel S., Jin L., Chen X., 2009. Stacking seismic data using local correlation, Geophysics 74 (3), V43-V48.

Liu L., Wang X., Zhang Y., Jia Z., Duan Q., 2011. Tempo-spatial characteristics and influential factors of rockburst: a case study of transportation and drainage tunnels in Jinping II hydropower station, Journal of Rock Mechanics and Geotechnical Engineering 3 (2), 179-185.

Luth S., Giese R., Rechlin A., 2008. A seismic exploration system around and ahead of tunnel excavation – Onsite, World Tunnel Congress 2008.

Malehmir A., Juhlin C., 2010. An investigation on the effects of the choice of stacking velocities on residual statics for hard rock reflection seismic processing, Journal of Applied Geophysics 72, 28-38.

Marelli S., Maurer H. R., Manukyan E., Greenhalgh S. A., Green A. G., 2008. Monitoring changes in bentonite at the Grimsel test site using crosshole seismic tomography, Near Surface 2008, Krakow.

McKenna J., McKenna M., Yushanov S., Crompton J., Koppenhoefer K., 2008. Computational Modeling of Wavw propagation in a Geophysical domain, Proceedinings of the COMSOL Conference Boston 2008.

Mito Y., Yamamoto T., Shirasagi S., Aoki K., 2003. Prediction of geological condition ahead of the tunnel face in TBM tunnels by geostatistical simulation technique, ISRM 2003.

Petronio L., Poletto F., 2002. Seismic-while-drilling by using tunnel boring machine noise, Geophysics 67 (6), 1798-1809.

Poletto F., Petronio L., 2006. Seismic interferometry with a TBM source of transmitted and reflected waves, Geophysics 71 (4), S185-S193.

Petronio L., Poletto F., Schleifer A., 2007. Interface prediction ahead of the excavation front by the tunnel-seismic-while-drilling (TSWD) method, Geophysics 72 (4), G39-G44.

Rector J. W., Marion B. P., 1991. The use of drill-bit energy as a downhole seismic source, Geophysics 56 (5), 628-634.

Sambuelli L., Calzoni C., 2010. Estimation of thin fracture aperture in a marble block by GPR sounding, Bollettino di Geofisica Teorica e Applicata, 51 (2-3), 239-252.

Sattel, G., P. Frey, and R. Amberg, 1992, Prediction ahead of the tunnel face by seismic methods — Pilot project in Centovalli Tunnel, Locarno, Switzerland: First Break, 10, 19–25.

Sava P, Fomel S., 2006. Time-shift imaging condition in seismic migration, Geophysics 71 (6), S209-S217.

Swinnen G., Thorbecke J.W., Drijkoningen G.G., 2007. Seismic Imaging from a TBM, Rock Mech. Engineering 40 (6), 577-590.

Tang C., Wang J., Zhang J., 2010. Preliminary engineering application of microseismic monitoring technique to rockburst prediction in tunneling of Jinping II project, Journal of Rock Mechanics and Geotechnical Engineering 2 (3), 193-208.

Tzavaras J., Groß K., Buske S., Shapiro S.A., 2008. Tunnel Seismic investigations – 3D imaging, Near Surface 2008, 14th European Meeting of Environmental and Engineering Geophysics, Krakòw, Poland, September 15-17 2008.

Tzavaras J., Buske S., Groß K., Shapiro S.A., 2012. Three-dimensional seismic imaging of tunnels, International Journal of Rock Mechanics and Mining Sciences 49, 12-20.

Van Overschee P., De Moor B., 1996. Subspace Identification for Linear Systems: Theory, Implementation, Applications, Kluwer Academic Publishers, Boston / London / Dordrecht.

Widess M. B., 1973. How thin is a thin bed? Geophysics 38 (6), 1176-1180.

Yamamoto T., Shirasagi S., Murakami K., Nishioka K., Descour J., 2006. Imaging Changing Ground in Front and Above a TBM Using Seismic Reflector Tracing; A Case Study, Golden Rocks 2006, The 41st U.S. Symposium on Rock Mechanics (USRMS), June 17 - 21, 2006 , Golden, CO.

Yamamoto T., Yokota Y., Descour J., Kohlhaas, 2008. Assessing ground ahead of the TBM tunnel using low-interruption wireless seismic reflector tracing system.

Yokota T., Onishi K., Karasawa H., Ohno T., Ota A., Kaneko T., 2004. Seismic while drilling: Basic experiments using a percussion drill as an energy source, Exploration Geophysics 35, 255-259.

Yonggui Z., Jiang H., Xiaopeng Z., 2006. Tunnel seismic tomography method for geological prediction and its application, Applied Geophysics 3 (2), 69-74.

Zhu Q.-h., Lu W.-b., Sun J.-s., Luo Y., Chen M., 2009. Prevention of rockburst by guide holes based on numerical simulations, Mining Science and Technology 19, 346-351.

Vita

Andrea Bellino was born in Pinerolo (TO), in Italy, in 1984.
He achieved the Bachelor Degree at the Politecnico di Torino in March 2007 in Mathematics for the Engineering sciences, with a thesis on the crowd dynamics.
He obtained the Master Degree at the same university in October 2008, in Mathematical Engineering, with a thesis on the identification of linear time-varying systems.
From December 2008 to December 2009, he was a research fellow at the Dipartimento di Ingegneria Meccanica e Aerospaziale at the Politecnico di Torino, while in January 2010 he started the PhD in the same department.
His research interests are mainly in vibrations mechanics and geophysics. About the first theme, the main topics are the identification of time-varying and nonlinear systems, the estimation of cable tension, and the damage detection of structures under different external conditions and in presence of moving loads. The geophysical studies are concentrated on the rock discontinuities estimation in tunnelling, and they are here presented in the PhD thesis.